IMPACT OF THE COVID-19 LOCKDOWN ON THE ATMOSPHERE

EDITED BY: Suvarna Sanjeev Fadnavis, Roxy Mathew Koll, Sabine Griessbach, Bernd Heinold, Dimitris G. Kaskaoutis and Ritesh Gautam

PUBLISHED IN: Frontiers in Environmental Science

frontiers Research Topics

ISSN 1664-8714
ISBN 978-2-83250-521-2
DOI 10.3389/978-2-83250-521-2

About Frontiers

Frontiers is more than just an open-access publisher of scholarly articles: it is a pioneering approach to the world of academia, radically improving the way scholarly research is managed. The grand vision of Frontiers is a world where all people have an equal opportunity to seek, share and generate knowledge. Frontiers provides immediate and permanent online open access to all its publications, but this alone is not enough to realize our grand goals.

Frontiers Journal Series

The Frontiers Journal Series is a multi-tier and interdisciplinary set of open-access, online journals, promising a paradigm shift from the current review, selection and dissemination processes in academic publishing. All Frontiers journals are driven by researchers for researchers; therefore, they constitute a service to the scholarly community. At the same time, the Frontiers Journal Series operates on a revolutionary invention, the tiered publishing system, initially addressing specific communities of scholars, and gradually climbing up to broader public understanding, thus serving the interests of the lay society, too.

Dedication to Quality

Each Frontiers article is a landmark of the highest quality, thanks to genuinely collaborative interactions between authors and review editors, who include some of the world's best academicians. Research must be certified by peers before entering a stream of knowledge that may eventually reach the public - and shape society; therefore, Frontiers only applies the most rigorous and unbiased reviews.
Frontiers revolutionizes research publishing by freely delivering the most outstanding research, evaluated with no bias from both the academic and social point of view. By applying the most advanced information technologies, Frontiers is catapulting scholarly publishing into a new generation.

What are Frontiers Research Topics?

Frontiers Research Topics are very popular trademarks of the Frontiers Journals Series: they are collections of at least ten articles, all centered on a particular subject. With their unique mix of varied contributions from Original Research to Review Articles, Frontiers Research Topics unify the most influential researchers, the latest key findings and historical advances in a hot research area! Find out more on how to host your own Frontiers Research Topic or contribute to one as an author by contacting the Frontiers Editorial Office: frontiersin.org/about/contact

IMPACT OF THE COVID-19 LOCKDOWN ON THE ATMOSPHERE

Topic Editors:
Suvarna Sanjeev Fadnavis, Indian Institute of Tropical Meteorology (IITM), India
Roxy Mathew Koll, Indian Institute of Tropical Meteorology (IITM), India
Sabine Griessbach, Julich Research Center, Helmholtz Association of German Research Centres (HZ), Germany
Bernd Heinold, Leibniz Institute for Tropospheric Research (LG), Germany
Dimitris G. Kaskaoutis, Institute for Environmental Research and Sustainable Development, National Observatory of Athens, Greece
Ritesh Gautam, Environmental Defense Fund, United States

Citation: Fadnavis, S. S., Koll, R. M., Griessbach, S., Heinold, B., Kaskaoutis, D. G., Gautam, R., eds. (2022). Impact of the COVID-19 Lockdown on the Atmosphere. Lausanne: Frontiers Media SA. doi: 10.3389/978-2-83250-521-2

Table of Contents

frontiers | Frontiers in Environmental Science

TYPE Editorial
PUBLISHED 03 October 2022
DOI 10.3389/fenvs.2022.1034007

OPEN ACCESS

EDITED AND REVIEWED BY
Hong Liao,
University of Information Science and Technology, China

*CORRESPONDENCE
Suvarna Fadnavis,
suvarna@tropmet.res.in

SPECIALTY SECTION
This article was submitted to Atmosphere and Climate, a section of the journal Frontiers in Environmental Science

RECEIVED 01 September 2022
ACCEPTED 08 September 2022
PUBLISHED 03 October 2022

CITATION
Fadnavis S, Roxy MK, Griessbach S, Heinold B, Kaskaoutis DG and Gautam R (2022), Editorial: Impact of the COVID-19 lockdown on the atmosphere. *Front. Environ. Sci.* 10:1034007. doi: 10.3389/fenvs.2022.1034007

Editorial: Impact of the COVID-19 lockdown on the atmosphere

Suvarna Fadnavis[1]*, M. K. Roxy[1], Sabine Griessbach[2], Bernd Heinold[3], Dimitris G. Kaskaoutis[4] and Ritesh Gautam[5]

[1]Center for Climate Change Research, Indian Institute of Tropical Meteorology, Pune, India, [2]Jülich Supercomputing Centre (JSC), Forschungszentrum Jülich GmbH, Jülich, Germany, [3]Leibniz-Institut für Troposphärenforschung, Leipzig, Germany, [4]Institute for Environmental Research and Sustainable Development, National Observatory of Athens, Athens, Greece, [5]Environmental Defense Fund, Washington, DC, United States

KEYWORDS

COVID-19, pollution reduction, atmospheric chemistry, aerosols, trace gases

Editorial on the Research Topic
Impact of the COVID-19 lockdown on the atmosphere

The most dominant impact of human activities on the atmosphere is particle and gaseous pollution (Ramanathan et al., 2001). The rapidly rising trend in anthropogenic pollution levels has been evidenced for many decades in satellite and *in-situ* measurements (Akimoto, 2003). These high amounts of pollutants have impacted air quality, hydrology, and climate, posing grave risks to the ecosystem and economy (Settele et al., 2014). The economic slowdown caused by the COVID-19 pandemic measures led to a reduction in transportation, industrial emissions, and energy use (Fadnavis et al., 2021). Thus lockdowns resulted in a decline in emissions of aerosol particles and gaseous pollutants globally. These effects were more pronounced over densely populated regions e.g., South and East Asia. The remote sensing observations showed a cleaner atmosphere with a ~30% reduction in aerosol optical depth over Asia during the lockdown period between April and May 2020 (Soni, 2021). The latest research conducted on pollutants levels during the lockdown period highlights the impact of reduced pollution levels on atmospheric processes through changes in clouds, radiative forcing, atmospheric heating, and circulation. The Research Topic here explores the atmospheric impacts in response to the reduction in amounts of anthropogenic pollutants. Does reduced level of pollutants during the lockdown period provide a pathway for climate mitigation strategies?

To summarize, this Research Topic presents nine researched articles addressing the key questions raised on our Research Topic. Here, we summarize the highlights of the papers. This research will be helpful for pollution control and climate mitigation strategies for policymakers.

Mallik et al. highlight interesting effects of pollution levels. They show signatures of reduced emission on levels of atmospheric trace gases and aerosol particles contributing to air pollution over multiple sites in India's capital Delhi. A clear impact of lockdown is

observed for AOD, PM, NO_2, CO, and SO_2 as a result of emission changes while changed precursor levels led to a change in ozone chemical regimes impacting its concentrations.

Singh et al. provide a comprehensive analysis of Particulate Matter at New Delhi, India, and Riyadh, Saudi Arabia during the COVID-19 lockdown period. Their findings reveal different trends in PM10 during the pre-lockdown and the lockdown period in Riyadh, showing considerable influence from sand and anthropogenic sources during the lockdown periods.

Features of pollution parameters over an urban and adjoining rural region in India during COVID-19 are addressed by Sonbawne et al. This study reports that despite a reduction in NO_2, there is an increase in ozone amount at Delhi and Panchgaon during the lockdown. The observed enhancement in ozone may be resultant of the complex photochemical processes that involve the presence of NO_2, CO, Volatile Organic Compounds (VOCs), and water vapor.

Aerosol variations over India during the lockdown period using multiple satellite observations are reported by Bhawar et al. These observations show a 40% reduction in aerosol optical depth over the Indo-Gangetic Plain. On the contrary, central India showed ~12% AOD enhancement. This study reveals that the increase in AOD is because of transported biomass-burning aerosols. The biomass-burning aerosols forms a layer near 2–4 km that produced a heating of 3–4 K/day and a consequent negative radiative forcing at the surface of ~ −65 W/m^2 (±40 W/m^2) over the central Indian region.

Asutosh et al. report the intensification of rainfall over India during the lockdown period, the spring of 2020. The satellite data and model simulations show that the reduction in anthropogenic emissions during the COVID-19 lockdown period have enhanced the precipitation by 5–25% over India. The precipitation enhancement results from the combined effect of an enhancement in cloud cover, a reduction in aerosol-induced cloud invigoration, and dynamical changes. The paper reports an advantage of anthropogenic pollution reduction for water availability besides benefits to air quality, human health, and crop yield.

Further, Lawand et al. show the variability of aerosol and clouds over North India and Myanmar during the COVID-19 lockdown period. They study shows that aerosol particles originating from biomass burning lead to cloud dissipation/burning and precipitation reduction (−1 to −4 mm) over Myanmar. Whereas, the aerosol reduction over North India favors cloud formation, i.e., increase in cloud cover leading to precipitation enhancement indicating the anti-Twomey effect.

Wang et al. report the impact on air quality during the COVID-19 lockdown in Northeast China. They report the impacts on large-scale weather circulation patterns that affected the northeast region. They found that under the influence of the updraft in front of the trough, the ozone concentration is higher. The changes in the concentrations of $PM_{2.5}$, NO_2, CO, SO_2, and O_3 in the three cities, namely Shenyang, Changchun, and Harbin, during the lockdown period tend to first decrease and then increase, while the changes in O_3 concentration are cyclical and increased significantly during this period.

Changes in urban gas-phase persistent organic pollutants during the COVID-19 lockdown in Barcelona are reported by Prats et al. This study highlights variations in the composition of polycyclic aromatic hydrocarbons (PAHs), polychlorobiphenyls (PCBs), hexachlorobenzene (HCB), pentachlorobenzene (PeCB), and organophosphate flame retardants (OPFRs) present in the gas-phase fraction of the atmosphere of Barcelona during the lockdown and before this period.

Milićević et al. address the impact of the COVID-19 restrictive measures on urban traffic-related air pollution in Serbia. Their analysis shows a positive correlation of daily NO_2 concentrations with mobility and their significant reduction during restriction measures at all the selected monitoring stations. The O_3 concentrations were increased at all measuring stations and are negatively correlated to mobility. The findings suggest the justification for the use of traffic reduction strategies as a measure to improve air quality.

Author contributions

All authors listed have made a substantial, direct, and intellectual contribution to the work and approved it for publication.

Conflict of interest

The authors declare that the research was conducted in the absence of any commercial or financial relationships that could be construed as a potential conflict of interest.

Publisher's note

References

Fadnavis, S., Sabin, T. P., Rap, A., Müller, R., Kubin, A., and Heinold, B. (2021). The impact of COVID-19 lockdown measures on the Indian summer monsoon. *Environ. Res. Lett.* 16, 074054. doi:10.1088/1748-9326/ac109c

Ramanathan, V. Crutzen P. J., Kiehl, J. T., and Rosenfeld, D. (2001). Aerosols, climate, and the hydrological cycle. *Science* 294, 2119–2124. doi:10.1126/science.1064034

Settele, J., Scholes, R., Betts, R., Bunn, S., Leadley, P., Nepstad, D., et al. (2014). "Terrestrial and inland water systems," in *Climate change 2014: Impacts, adaptation and vulnerability. Part A: Global and sectoral Aspects.Contribution of working group II to the fourth assessment report of the intergovernmental panel on climate change*. 1. Editors C. B. Field, V. R. Barros, D. J. Dokken, K. J. Mach, M. D. Mastrandrea, T. E. Bilir, et al. (Cambridge, United Kingdom and New York, NY, US: Cambridge University Press).

Soni, P. (2021). Effects of COVID-19 lockdown phases in India: An atmospheric perspective. *Environ. Dev. Sustain.* 23, 12044–12055. doi:10.1007/s10668-020-01156-4

frontiers in Environmental Science

ORIGINAL RESEARCH
published: 13 April 2021
doi: 10.3389/fenvs.2021.650539

Changes in Urban Gas-Phase Persistent Organic Pollutants During the COVID-19 Lockdown in Barcelona

Raimon M. Prats, Barend L. van Drooge, Pilar Fernández, Esther Marco and Joan O. Grimalt*

Institute of Environmental Assessment and Water Research (IDAEA-CSIC), Barcelona, Spain

The composition of polycyclic aromatic hydrocarbons (PAHs), polychlorobiphenyls (PCBs), hexachlorobenzene (HCB), pentachlorobenzene (PeCB), and organophosphate flame retardants (OPFRs) present in the gas-phase fraction of the atmosphere of Barcelona was analyzed during the SARS-CoV-2 coronavirus disease (COVID-19) lockdown and prior to this period. The changes in daily concentrations of CO, NO, NO_2, O_3 and particulate matter smaller than 10 μm (PM_{10}) were considered for comparison. Bayesian analysis considering serial dependencies and seasonality showed statistically significant decreases of CO, NO, NO_2, and PM_{10} (between −28 and −76%) and O_3 increases (+45%) during lockdown. However, the lockdown concentration decreases of PeCB (−90.5%, from 8.5 to 0.8 pg m^{-3}), HCB (−79%, 25.5–5.4 pg m^{-3}) and some PAHs, such as benz[a]anthracene (−87%, 120–17 pg m^{-3}) and pyrene (−81%, 3,500–680 pg m^{-3}), were even stronger. The PAH depletion ranged between −68 and −87% that could be primarily associated with the strong reduction of traffic mobility during this period (−80%). Besides traffic reduction, the observed air quality improvements could be related to lower generation of solid urban residues (−25%) and the subsequent decrease of urban waste incineration (between −25 and −28%). Tributyl phosphate also showed a reduction in concentration during lockdown but the other OPFRs were seemingly not affected by this restriction, possibly as a result of the uniform release from the emission sources, e.g., construction material, industrial applications, and household products.

Keywords: COVID-19, semi-volatile air pollutants, organic contaminants, passive air sampling, lockdown, air quality

OPEN ACCESS

Edited by:
Dimitris G. Kaskaoutis, National Observatory of Athens, Greece

Reviewed by:
Umesh Dumka, Aryabhatta Research Institute of Observational Sciences, India
Suvarna Sanjeev Fadnavis, Indian Institute of Tropical Meteorology, India

****Correspondence:***
Raimon M. Prats
raimon.martinez@idaea.csic.es

Specialty section:
This article was submitted to Atmosphere and Climate, a section of the journal Frontiers in Environmental Science

Received: *07 January 2021*
Accepted: *23 March 2021*
Published: *13 April 2021*

Citation:
Prats RM, van Drooge BL, Fernández P, Marco E and Grimalt JO (2021) Changes in Urban Gas-Phase Persistent Organic Pollutants During the COVID-19 Lockdown in Barcelona. Front. Environ. Sci. 9:650539. doi: 10.3389/fenvs.2021.650539

INTRODUCTION

The outbreak of a novel respiratory disease in China, caused by the SARS-CoV-2 virus and named coronavirus disease (COVID-19) by the World Health Organization (WHO), was quickly extended to many other countries generating a global pandemic (Sohrabi et al., 2020). On March 14, a lockdown was set in all Spain which mandated individuals to remain home except for needs such as purchasing food and medicines. These measures also included the temporary closure of schools, universities, some businesses and shops.

In general, lockdown measures have led to unprecedented reductions of air pollutant concentrations in many regions of the world, including several of the most polluted areas

(Berman and Ebisu, 2020; Cameletti, 2020; Le Quéré et al., 2020; Li et al., 2020; Venter et al., 2020; Zhang R. et al., 2020; Zhang Z. et al., 2020). Most reports in urban and industrial areas have only focused on air quality gas pollutants such as nitrogen oxides (NO and NO_2), carbon monoxide (CO), and carbon dioxide (CO_2), and particulate matter (PM_{10} and $PM_{2.5}$). The same is the case for satellite imaging methods that can estimate the concentrations of these gases over large geographical areas (Kaufman et al., 1997; Krotkov et al., 2016). However, pollution assessment also requires the measurement of other contaminants that are deleterious for human health, such as organochlorine compounds (OCs) and polycyclic aromatic hydrocarbons (PAHs), among others.

Most OCs and PAHs are persistent organic pollutants (POPs), a group of compounds that are notorious for their resistance to degradation, potential for long-range atmospheric transport, and toxicity. They are recognized as a threat to human and wildlife health (De Voogt et al., 1990; Grimalt et al., 1994; Boström et al., 2002; Lauby-Secretan et al., 2013). PAHs are of great environmental concern, since several parent (non-methylated) compounds of these hydrocarbons are human carcinogens and priority pollutants (Baek et al., 1991; Armstrong et al., 2004). Hexachlorobenzene (HCB) has been related with obesity (Smink et al., 2008; Valvi et al., 2014), low fetal growth (Lopez-Espinosa et al., 2016), disruption of thyroid metabolism (Sala et al., 2001; Llop et al., 2017), and higher incidence of thyroid cancer (Grimalt et al., 1994). Polychlorobiphenyls (PCBs) have also been related with low fetal growth (Casas et al., 2015; Lopez-Espinosa et al., 2016), obesity (Valvi et al., 2012) or alterations of the thyroid function (Chevrier et al., 2008). In addition, they have been associated with metabolic disturbances of 25-hydroxy-vitamin D3 (Morales et al., 2013) and neurotoxicity (Grandjean and Landrigan, 2014). The production and use of these compounds have been restricted in many industrialized countries, resulting in significant endeavors to gradually reduce and prevent their release and diffusion in the environment. A culminating protocol for the elimination and monitoring of POPs was elaborated in 2001 during the Stockholm Convention[1] and has since been amended to include more compounds.

In addition, organophosphate flame retardants (OPFRs) are emerging pollutants that are currently used and produced in increasing amounts to meet the demand for flame retardants and plasticizers in construction material, industrial applications, and household products, including electronic devices (Van der Veen and de Boer, 2012; Du et al., 2019). OPFRs are neurotoxic, may cause haemolysis, and some of them are carcinogenic (Dishaw et al., 2011; Van der Veen and de Boer, 2012). Compared to historical POPs, OPFRs tend to show relatively high concentrations in outdoor air from urban and industrial areas (Salamova et al., 2014; Liu et al., 2016; van Drooge et al., 2018b).

Barcelona is one of the most densely populated cities of Europe, 16,000 inhabitants/km^2. Its metropolitan area lacks significant atmospheric emissions from industries and domestic heating is generally powered by natural gas. The high traffic intensity, 13,000–85,000 vehicles/day downtown in 2018, is the main pollution source (van Drooge and Grimalt, 2015; van Drooge et al., 2018a). Other reports (UNEP, 2010) also point at transport, housing, and related activities as important sources of emissions of pollutants and products of environmental concern in Spain (e.g., around 60% of CO_2 and greenhouse gasses are emitted from transport and housing-related activities). Air pollution is therefore closely related to the activities of its inhabitants. Comparison of the air pollution levels during regular days and the lockdown period may provide guidelines for the ultimate achievable air quality standards, namely POPs, upon ideal management of urban pollution sources. Air samples were collected in the atmosphere of the city of Barcelona by means of passive air sampling (PAS) during regular conditions and lockdown. The results were used to determine possible changes in gas-phase POP concentrations during both periods. These pollutants were also analyzed in a remote continental background location in the Pyrenees for PAS calibration and comparison with the lockdown atmospheric conditions.

MATERIALS AND METHODS

Air Sampling

Two passive gas-phase air samplers for POP analysis were deployed during two periods: B1 (15 October 2019–9 January 2020, 86 days) and B2 (9 January 2020–15 July 2020, 188 days). B1 provided a reference time interval of typical air pollution conditions in the city. B2 was deployed during lockdown, although this period was larger than the specific lockdown time (March 15–June 22, 2020, 100 days). The samples were obtained using GAPS-style polyurethane foam passive air samplers (PUF-PASs) as employed in other studies (e.g., Pozo et al., 2009). The PUF disks (14 cm diameter, 1.35 cm thickness, 369.5 cm^2 surface area, and 0.021 g cm^{-3} density) were previously cleaned with acetone, Soxhlet-extracted with hexane for 6 h, dried under vacuum, and stored in a sealed PET/LLDPE bag at −20°C. Upon deployment, they were spiked with a Performance Reference Compound (PRC) mixture of PCBs 3, 9, 15, 32 (all ^{13}C-labeled), 107, and 198 (unlabeled) (Cambridge Isotope Laboratories, Tewksbury, United States). One field blank was performed for each sample. These blanks were also doped with the PRCs, sealed, and stored at −20°C for the entire duration of the sampling period. The PUFs were immediately extracted after retrieval at the end of the sampling period. The recovery of PRCs from each sample was used for the assessment of the specific sampling rates as explained in the "Theory and Calculations" section below.

Polyurethane foam passive air samplers were also deployed in duplicate, in four 4–10-month periods, at six remote locations in the Pyrenees (September 2017–September 2019). Because of the minimal local contaminant sources, these sites constitute continental background reference regions for air pollution levels. The results obtained with the PUF-PASs were evaluated by comparison with those from active air sampling (AAS) with a high-volume pump (MCV, Collbató; van Drooge et al., 2004) which was used in one of these Pyrenean sites between July and September 2017. The PUF-AAS plugs (6 cm diameter, 5 cm thickness, 0.028 g cm^{-3} density) used for this purpose were

[1] www.pops.int

located behind glass fiber filters that collected the atmospheric particle phase. One field blank was performed for every two duplicate samplers, both for PAS and AAS. All PUFs were cleaned and stored until extraction as described above.

Meteorological and air quality data were obtained for the whole B1 and B2 periods, including the pre- and lockdown intervals within them. Data corresponding to analogous periods in the previous 2 years were also collected for reference and description of seasonal variations. **Table 1** summarizes temperature, accumulated precipitation, and wind speed average values recorded on-site in all locations with Tinytag Plus 2 data loggers (Gemini Data Loggers, Chichester, United Kingdom) and from the automatic meteorological network (XEMA stations VS, Z2, X8, and X4) of the Catalan Meteorological Service. The concentrations of CO, NO, NO_2, PM_{10}, and O_3 in Barcelona were obtained for the same periods from the stations of the Air Quality Network (XVPCA 08019043 and 08019057) of the Catalan Government.

Extraction and Clean-Up

Both the PUF-PAS disks and the PUF-AAS plugs were subjected to Soxhlet extraction with hexane (Merck, Darmstadt, Germany) for 6 h after being spiked with a mixture of recovery standards containing: tetrabromobenzene, PCB209, fluorene-d_{10}, phenanthrene-d_{10}, fluoranthene-d_{10}, pyrene-d_{10}, benz[a]anthracene-d_{12}, and chrysene-d_{12} (Dr. Ehrenstorfer) as well as an alkyl/aryl phosphate mixture containing tributyl phosphate-d_{12}, tris(2-chloroethyl) phosphate-d_{12}, tris(1-chloro-2-propyl) phosphate-d_{18}, tris(1,3-dichloro-2-propyl) phosphate-d_{15} and triphenyl phosphate-d_{15} (Cambridge Isotope Laboratories). The extracts were concentrated down to 2 mL with a rotary evaporator (Büchi, Flawil, Switzerland), quantitatively transferred into gas chromatography vials, and further evaporated to 0.5 mL under a gentle stream of nitrogen.

Fifty μL of each extract were cleaned-up and fractionated using an Agilent 1200 Series Gradient HPLC system (Agilent Technologies, Santa Clara, United States) equipped with a quaternary pump, a vacuum degasser, an autosampler, a thermostated column compartment (set at 30°C), and a preparative fraction collector. A Tracer Excel 120 SI HPLC silica column (25 cm × 3 μm × 0.46 cm i.d.; Teknokroma, Sant Cugat del Vallès) was used for the chromatographic separation. The elution program was as follows: 100% hexane at 0.5 mL min^{-1} flow rate for 8 min, then a linear gradient to 100% dichloromethane at 0.5 mL min^{-1} in 7 min, held until min 20. It was additionally changed to (80:20%) dichloromethane:methanol in order to elute more polar compounds remaining in the column before performing the next fractionation, with a linear flow rate increase from 0.5 to 1 mL min^{-1} in 10 min, and a final holding time of 15 min. The fractions containing the target compounds were collected between minutes 8–15 (PCBs and other OCs) and 15–20 (PAHs). These fractions were evaporated under a gentle nitrogen gas stream, transferred into gas chromatography vials, and further evaporated to 0.5 mL. The OPFRs were analyzed from another extract aliquot, not requiring HPLC fractionation, but dried by elution through 0.5 g of anhydrous sodium sulfate previously activated overnight at 450°C.

Instrumental Analysis

The OC and PAH HPLC fractions were run separately by gas chromatography coupled to mass spectrometry (GC-MS) with a Thermo Trace GC Ultra–DSQ II (Thermo Fisher Scientific, Waltham, United States) equipped with a 60 m × 0.25 mm i.d. × 25 μm film thickness HP-5MS fused capillary column (Agilent Technologies). The MS was operated in electron impact mode (70 eV). The injector, ion source, quadrupole, and transfer line temperatures were 280, 250, 150, and 270°C, respectively. The oven program started at 90°C with a hold time of 1 min, then heated to 150°C at 10°C min^{-1} and to 320°C at 6°C min^{-1}, where it was held for 20 min. Helium was used as a carrier gas at 1 mL min^{-1}. The targeted compounds were the following: polychlorobiphenyls (PCB28, PCB52, PCB101, PCB118, PCB138, PCB153, and PCB180), HCB, pentachlorobenzene (PeCB), α- and γ-hexachlorocyclohexanes (α- and γ-HCH), fluorene (fle), phenanthrene (phe), fluoranthene (flu), pyrene (pyr), benz[a]anthracene (b[a]ant), and chrysene+triphenylene (chr+triph). They were identified by their m/z values and retention times recorded in selected ion monitoring (SIM) mode (**Supplementary Table 1**).

The PUF extract aliquots were run for OPFR analysis by gas chromatography coupled to tandem mass spectrometry (GC-MS/MS) into an Agilent 7000 Series Triple Quad GC/MS (Agilent Technologies) equipped with a 30 m × 0.25 mm i.d. × 0.25 μm film thickness Zebron ZB-PAH capillary column (Phenomenex, Torrance, CA, United States). The MS/MS was operated in electron impact ionization mode. The injector, ion source, quadrupoles, and transfer line temperatures were 280, 230, 150, and 280°C, respectively. The oven temperature program started at 80°C with a hold time of 1.5 min, then heated to 220°C at 10°C min^{-1} and to 315°C at 15°C min^{-1}, where it was held for 5 min. Helium was used as a carrier gas at 1.1 mL min^{-1}. The targeted compounds were the following: tributylphosphate (TBP), tris(2-chloroethyl) phosphate (TCEP), tris(1-chloro-2-propyl) phosphate (TCPP), tris(1,3-dichloro-2-propyl) phosphate (TDCP) and triphenyl phosphate (TPhP). They were identified by their m/z transitions and retention times recorded in multiple reaction monitoring mode (**Supplementary Table 2**).

Quantification was performed with internal standard calibration curves, accounting for extraction and analysis recoveries. The field blank values were subtracted. LOQ values ranged between 0.5 and 2.5 pg in column, or 125–625 pg/sampler for PAHs, OCs, and PCBs, and 250–1,250 pg/sampler for OPFRs. For average effective sampled air volumes, these correspond to 0.3–1.6 pg m^{-3} of air for PAHs, 0.4–2.1 pg m^{-3} for OCs, 0.2–1.2 pg m^{-3} for PCBs, and 0.5–2.4 pg m^{-3} for OPFRs.

Theory and Calculations

As shown in Equation 1 (Harner et al., 2013), the calculation of gas-phase concentrations (C_A, pg m^{-3}) from the pollutant amounts obtained with PAS (N_A) requires the determination of effective sampled volumes (V_A, m^3) that are compound- and location-specific for each sampling period:

TABLE 1 | Sampling locations, periods of study, and average meteorological conditions (± standard deviation).

Location		Altitude (m.a.s.l.)	Period		Temperature (°C)	Precipitation (mm)	Wind speed (m s^{-1})
Barcelona (urban site)	41.388° N, 2.115° E	108	Mean 2018–2019	B1	14.3 ± 0.2	197 ±114	1.21 ±0.21
				B2	16.5 ± 0.1	257 ± 155	1.23 ± 0.02
				Pre-lockdown	11.8 ± 0.2	90 ± 91	1.30 ± 0.19
				Lockdown	17.4 ± 0.6	166 ± 73	1.25 ± 0.03
			2020	B1	14.7 ± 3.6	225	1.99 ± 1.46
				B2	17.3 ± 5.0	513	2.15 ± 1.39
				Pre-lockdown	13.1 ± 2.6	124	2.12 ± 1.62
				Lockdown	18.0 ± 4.0	373	2.15 ± 1.26
Aigüestortes (continental background)	42.572° N, 0.932° E	1,619–2,453	2017–2019	Range of averages[a]	4.7 ± 0.2–8.3 ± 0.7	484 ± 330–1,832 ± 389	3.70 ± 1.00–4.27 ± 0.05

[a] *Values for temperature, accumulated precipitation, and wind speed for the sampling site of Aigüestortes are shown as a range spanning the lowest and highest average values (± standard deviation) registered over four consecutive 4–10-month sampling periods from six studied mountain locations.*

$$C_A = \frac{N_A}{V_A} = \frac{N_A}{V_{PUF}\, K'_{PUF-A}\left[1 - exp\left(\frac{-k_A\, t}{K'_{PUF-A}\, D_{film}}\right)\right]} \quad (1)$$

where N_A is the amount of compound accumulated in the PUF disk during the sampling time (pg sampler^{-1}), V_{PUF} is the volume of the PUF disk (0.00021 m^3), K'_{PUF-A} is the dimensionless PUF density-corrected PUF-Air partition coefficient K_{PUF-A} (K_{PUF-A} multiplied by the PUF density, δ_{PUF} = 21,000 g m^{-3}), k_A is the air-side mass transfer coefficient (m d^{-1}), t is the sampling time (d), and D_{film} is the PUF's effective film thickness (0.00567 m).

The sample-specific k_A values needed for V_A estimation can be derived from the PRC calibration of sampling rates (R_S, m^3 d^{-1}):

$$k_A = \frac{R_S}{A_{PUF}} = \frac{\ln(C/C_0)\; K'_{PUF-A}\, D_{film}}{t} \quad (2)$$

where A_{PUF} is the PUF's surface area (0.0365 m^2) and C/C_0 is the PCR ratio of amounts (g sampler^{-1}) between exposed and non-exposed (field blanks) PUFs.

Compound-specific K_{PUF-A} values for this type of PUFs are correlated to octanol-air partition coefficients (K_{OA}) through the following relationship (Shoeib and Harner, 2002):

$$\log K_{PUF-A} = 0.6366 \log K_{OA} - 3.1774 \quad (3)$$

The $\log K_{OA}$ values were corrected for the average temperature of each sampling site over the sampling period using temperature-dependent relationships reported elsewhere (Odabasi et al., 2006; Chen et al., 2016; Harner, 2016; Wang et al., 2017).

RESULTS AND DISCUSSION

Passive Gas-Phase Air Sampling for POP Analysis

The performance of the PUF-PAS samplers and reliability of the pollutant concentrations obtained with this system were assessed by comparison of the results from simultaneous deployment of these PAS and AAS between September 2017 and September 2019 in Aigüestortes, a continental background location in remote high mountains. The quantitative results obtained with both methods were in good agreement (**Table 2**). Thus, the AAS/PAS ratio differences were 0.7–2.1 for PCBs, 1.1 for HCB, 0.3–0.8 for PAHs and 0.3–1.5 for OPFRs. These ratios have to be compared considering that AAS involves much more variability than PAS, as the former is only collected over a few hours and the latter represents average values of several months of deployment. Therefore, variations in day-to-day meteorological and atmospheric conditions greatly affect the resulting AAS levels, especially for compounds like PAHs that could be influenced by local sources from nearby rural areas that are much more season dependent. Thus, the differences between sampling methods were deemed to be within acceptable ranges, especially at the low observed concentrations, for all compounds < 50 pg m^{-3} except for Fle and Phe. These results concur with other studies that established a strong agreement or no statistical difference between AAS- and PAS-obtained concentrations, even in urban sites with generally higher POP concentrations (He and Balasubramanian, 2012; Kalina et al., 2019). Furthermore, PAS duplicates showed low average relative standard deviations (RSD), between 9.4 and 23.3% for most compounds, with values above 30% only observed for the less volatile compounds such as PCB180, TCPP, TCEP, and TDCP, 34.2, 30.8, 36.3, and 60.1%, respectively (**Supplementary Table 3**).

Urban Concentrations of Organochlorine Compounds, PAHs, and Organophosphate Flame Retardants

The concentrations of HCB found in the B1 and B2 periods in Barcelona, 25.5 and 5.4 pg m^{-3}, respectively (**Table 2**), were generally lower than those found in other urban areas from India: average values of 120–260 pg m^{-3} (Chakraborty et al., 2010), Bangladesh: 70–685 pg m^{-3} (Nost et al., 2015), Bosnia Herzegovina: 34 pg m^{-3} (Lammel et al., 2011), Nepal: 6.3–1,500 pg m^{-3} (Pokhrel et al., 2018), or China: 261 pg m^{-3} (Zhang et al., 2010). The concentrations of PeCB, 8.5 and 0.8 pg m^{-3} in B1 and B2, respectively, were

TABLE 2 | Average compound concentrations in air (gas phase, pg m^{-3} ± standard deviation) in the mountain background (Aigüestortes) and in the urban (Barcelona) locations, obtained using passive air sampling (PAS), and active air sampling (AAS) methods.

Compounds		Aigüestortes (background)				Barcelona PAS (urban)		
		PAS (*n* = 20)		AAS (*n* = 3)		B1	B2	Variation %
PCBs	PCB28	2.9	±1.0	2.4	±1.5	6.8	2.8	−59
	PCB52	2.1	±0.7	1.4	±0.3	11	3.4	−68
	PCB101	2.7	±1.0	5.7	±1.9	15	6.1	−59
	PCB118	2.5	±0.3	4.8	±1.6	13	3.9	−69.5
	PCB138	1.6	±0.7	3.0	±0.9	6.7	4.4	−34
	PCB153	2.3	±0.2	3.2	±0.9	5.8	2.6	−56
	PCB180	0.5	±0.2	0.5	±0.1	b.d.l.[a]	b.d.l.	
	ΣPCBs	14.6		21.0		58.3	23.2	−60
OCs	HCB	45	±8.4	49	±4.9	25.5	5.4	−79
	PeCB	25	±3.2	b.d.l.		8.5	0.8	−90.5
	α-HCH	1.6	±0.3	b.d.l.		3.5	0.5	−86
	γ-HCH	1.0	±0.4	b.d.l.		12.9	3.9	−70
	ΣOCs	72.6		49.0		50.4	10.6	−79
PAHs	Fle	250	±38	72	±3.6	10,000	2,600	−75
	Phe	300	±88	230	±170	18,000	5,800	−68
	Flu	39	±16	28	±14	4,000	1,000	−75
	Pyr	18	±7.6	15	±6.7	3,500	680	−81
	B[a]ant	0.7	±0.5	0.3	±0.1	120	17	−87
	Chr+TriPh	5.3	±2.8	1.4	±0.1	240	63.5	−74
	ΣPAHs	613		347		35,860	10,160	−72
OPFRs	TBP	1.5	±0.3	0.8	±0.4	260	94	−64
	TCEP	6.1	±1.9	2.1	±1.4	230	270	19
	TCPP	14	±16	20.5	±15	4,800	4,700	−3.3
	TDCP	1.5	±0.5	b.d.l.		129	187	45
	TPhP	7.2	±3.5	b.d.l.		284	268	−5.6
	ΣOPFRs	30.3		23.4		5,703	5,519	−3.2

[a]*b.d.l. Below detection limit.*

similar to those described in Bosnia Herzegovina, 9.9 pg m^{-3} (Lammel et al., 2011). The respective α- and γ-HCH concentrations, 3.5 and 12.9 pg m^{-3} during B1 and 0.5 and 3.9 pg m^{-3} during B2, were lower than those reported in other urban areas of Spain: 37 pg m^{-3} for their sum (de la Torre et al., 2016).

The concentrations of total PCBs in B1 and B2, 58 and 23 pg m^{-3}, respectively (sum of congeners reported in **Table 2**), were again generally lower than those found in other urban areas from Italy: 117 pg m^{-3} (Estellano et al., 2012), Spain: 122 pg m^{-3} (Pozo et al., 2009), France: 3,100 pg m^{-3} (Pozo et al., 2009), Turkey: 153–376 pg m^{-3} (Kuzu, 2016), Argentina: 146–200 pg m^{-3} (Tombesi et al., 2014; Astoviza et al., 2016), Chile: 160 pg m^{-3} (Pozo et al., 2012), Canada: 481 pg m^{-3} (Motelay-Massei et al., 2005), Pakistan: 37–293 pg m^{-3} (Nasir et al., 2014), India: 278 pg m^{-3} (Pozo et al., 2011), China: 600–7,600 pg m^{-3} (Cui et al., 2017), and Bangladesh: 7–1,800 pg m^{-3} (Nost et al., 2015). They were similar to those reported in Nepal: 1.2–47 pg m^{-3} (Pokhrel et al., 2018).

Total PAHs in B1 and B2, approximately 36,000 and 10,000 pg m^{-3}, respectively (sum of the compounds reported in **Table 2**), were found in lower concentrations than those found in Strasbourg: 51,000 pg m^{-3} (Morville et al., 2011) and Istanbul, 21,000–290,000 pg m^{-3} (Kuzu, 2016) and higher than those found in the United States: 4,100–12,000 pg m^{-3} (Pratt et al., 2018).

The concentrations of TBP in B1 and B2, 260 and 94 pg m^{-3}, were lower than those found in urban areas of Germany, 1,550 pg m^{-3} (Zhou et al., 2017) and those of TCPP, 4,800 and 4,700 pg m^{-3}, respectively, were higher than those found in these urban areas, 2,700 pg m^{-3} (Zhou et al., 2017). The concentrations of TDCP, 129 pg m^{-3} in B1 and 187 pg m^{-3} in B2, and of TPhP, 284 pg m^{-3} in B1 and 268 pg m^{-3} in B2, were higher than those reported in urban air in Sweden, 7.6 and 47 pg m^{-3}, respectively (Wong et al., 2018).

The concentrations of PCBs in Barcelona in the B1 period, 58 pg m^{-3}, were about four times higher than in the continental background station 14.6 pg m^{-3} (**Table 2**), whereas those of PAHs, 36,000 pg m^{-3}, were about 60 times higher than in Aigüestortes, 613 pg m^{-3}, and those of the OPFRs were between 38 and 340 times higher (**Table 2**). The concentrations of HCHs were two to twelve times higher in Barcelona during the B1 period compared to the background location (**Table 2**). In contrast, HCB and PeCB in the continental background station were nearly two and three times higher than in the B1 period in Barcelona. The differences in PCB, HCB and PeCB air concentrations between

urban and remote sites compared to PAHs and OPFRs could be explained by fundamental differences in emission sources. The production and use of PCBs and most OCs have been restricted for several decades, but they are present in urban waste at low amounts (Wegiel et al., 2011; Neuwahl et al., 2019) which constitute a potential source in cities such as Barcelona. However, these legacy POPs may still be released to the atmosphere from diffusive secondary sources, including other environmental compartments (Grimalt et al., 2009), especially so in cold and remote areas that now might act as repositories for persistent contaminants such as HCB (Meijer et al., 2003). Contrarily, PAHs are still emitted from many primary combustion sources, such as traffic and domestic emissions in urban areas, while OPFRs are widely applied as flame retardants in construction material, household products and electronic equipment.

Assessment of the Lockdown Changes on Airborne POPs and OPFRs

One of the main features of **Table 2** is the strong decrease of HCB and PeCB between B1 and B2 periods, −79 and −90.5%, respectively (**Table 2**). At present, the occurrence of these compounds in the atmosphere of urban areas without industrial activity is mainly related to waste treatment, including incineration (EPA, 1986; Martens et al., 1998; Bailey, 2001; Wegiel et al., 2011). The lockdown period in Barcelona involved a −24.6% reduction of urban waste generation (a reduction of almost 20,000 tons of solid waste) which, in turn, represented incineration decreases between −25 and −28% when quantified as CO_2 emission (Montlleo et al., 2020; State of the City, 2020). These reductions may have contributed to the decrease in the concentrations of these compounds. Other processes, e.g., less transport of materials, may also have been relevant for the observed decrease.

Polycyclic aromatic hydrocarbons also showed high reduction of atmospheric concentrations, between −68 and −87% (**Table 2**). Atmospheric PAHs in urban areas are primarily generated as by-products of motorized transport. Therefore, the observed differences are in agreement with the strong reduction of traffic in Barcelona, −80%, during the lockdown period (Montlleo et al., 2020; State of the City, 2020).

The atmospheric concentrations of PCBs and other OCs like the HCHs were also strongly depleted, between −34 and −69.5%, and between −70 and −86%, respectively. These decreases were probably related with the −24.6% reduction in waste generation during lockdown (Montlleo et al., 2020; State of the City, 2020) as incineration of urban waste is one main PCB source in the air of urban areas (Neuwahl et al., 2019; Arp et al., 2020) due to the presence of such compounds in urban waste and their high resistance to combustion (Neuwahl et al., 2019).

The OPFRs showed different trends (**Table 2**). TBP was the only compound following the concentration differences of OCs and PAHs, which were reflected in a large reduction in concentration, −64%, between the B1 and B2 periods. In contrast, the other OPFRs showed small decreases or even increases in atmospheric concentrations. This is probably related with the fundamentally different sources of OPFRs, e.g., being related with construction material, household products and electronic equipment over time, thus being less susceptible to variations in urban and industrial activities.

Changes in Atmospheric Gases and Particles

The average concentrations of CO, PM_{10}, NO, and NO_2 in Barcelona in the B2 period of 2020 show lower values than those of the 2018–2019 average, whereas these differences are not observed for B1 (**Supplementary Figure 1**). Similarly, the concentrations of these gases and PM_{10} in the lockdown period of 2020 are much lower than those in the equivalent time interval of the 2018–2019 average. This difference is the opposite in the case of O_3, which is consistent with the lack of NO during lockdown and higher insolation during spring months. An initial study encompassing the first lockdown weeks (March 14–March 30) showed consistent changes (Tobias et al., 2020). In the present study, comparison of the data encompassing

TABLE 3 | Results of the Bayesian model for the air pollutant concentrations in the pre-lockdown/lockdown and B1/B2 periods.

Compound	Period	Average concentration			Effect of lockdown		Causality	
		Measured	Predicted ± SD	95% CI	Effect ± SD	95% CI	*p*-value	Probability (%)
CO (mg m^{-3})	Pre/lock	0.22	0.30 ±0.02	[0.26, 0.34]	−28% ± 6.4%	[−40%, −16%]	0.0011	99.89
	B1/B2	0.25	0.37 ± 0.02	[0.33, 0.41]	−32% ± 5.4%	[−43%, −22%]	0.0011	99.89
PM_{10} (μg m^{-3})	Pre/lock	19	31 ± 2.2	[26, 35]	−37% ± 7%	[−50%, −23%]	0.0011	99.89
	B1/B2	24	30 ± 1.8	[27, 34]	−20% ± 5.9%	[−32%, −8.8%]	0.0010	99.90
NO (μg m^{-3})	Pre/lock	7.4	31 ± 4.3	[23, 40]	−76% ± 14%	[−103%, −51%]	0.0011	99.89
	B1/B2	18	31 ± 4.1	[23, 39]	−41% ± 13%	[−66%, −14%]	0.0033	99.67
NO_2 (μg m^{-3})	Pre/lock	22	47 ± 2.0	[43, 51]	−52% ± 4.2%	[−61%, −44%]	0.0011	99.89
	B1/B2	33	52 ± 1.8	[49, 56]	−38% ± 3.4%	[−44%, −31%]	0.0012	99.88
O_3 (μg m^{-3})	Pre/lock	56	38 ± 2.9	[33, 44]	45% ± 7.4%	[31%, 59%]	0.0010	99.90
	B1/B2	45	45 ± 3.0	[39, 51]	−0.12% ±6.7%	[−13%, 12%]	0.4985	50.00

The average concentrations measured during the periods after lockdown restrictions (i.e., lockdown and B2) are compared to the concentrations (± standard deviation, SD) predicted by the model from data including the two previous years. Confidence intervals (95%), p-values, and probability of the observed concentration changes caused by lockdown measures are provided.

the whole lockdown period using a Bayesian structured time-series model (CausalImpact 1.2.4 R package, Brodersen et al., 2015) also allowed to account for the influence of seasonal effects on the concentration changes. Accordingly, the pollutant concentrations of 2020 were used as the response series and the average pollutant data of 2018–2019 as the control series, which was assumed not affected by the lockdown measures, consistently with the absence of restrictions in 2018–2019. The applicability of this model to these data was supported by comparison of the time series and dummy causal impact analyses performed with imaginary intervention periods which provided reasonable predictions and low causality probabilities.

The Bayesian analysis of the whole lockdown period showed noticeable concentration reductions of CO, NO, and NO_2 coinciding with the lockdown measures of March 2020, which picked up slightly after lockdown easing at the end of May 2020 and finally returned to ordinary levels at the end of lockdown (**Figure 1**). The same representations showing the predictions calculated for the B1/B2 sampling periods can be found in **Supplementary Figure 2**. The causal impact analysis of CO, NO, and NO_2 concentrations for the pre-lockdown/lockdown periods yielded statistically significant average variations of −28, −76, and −52%, respectively (p = 0.0011; **Table 3**). Despite the B2 sampling period included some weeks before and after lockdown, similar (−32% CO) or slightly lower (−41% NO, −38% NO_2) but still significant reductions were observed for the same compounds, p = 0.0011, 0.0033, and 0.0012, respectively (**Table 3**). These differences indicated a direct influence of lockdown restrictions as consequence of the steep decline in motor vehicle traffic, the main contributing source of CO and NO through direct emissions (EEA, 2019) as well as NO_2 formation by reaction of NO with atmospheric O_3.

The decrease between the usual polluting conditions and the lockdown period is more intense in areas with a lot of traffic such as downtown Barcelona, although it is also noticeable in the north and west forested areas, as shown in **Figure 2** where the atmospheric NO_2 concentrations are displayed for the B1, B2, and specific lockdown periods. Comparison of the average NO_2 concentrations in the B2 and specific lockdown periods from this figure shows very similar distributions which support the representativeness of the sampled B2 interval concerning lockdown conditions.

Reductions in NO concentrations usually lead to increasing O_3 concentrations (Leighton, 1961), which are also observed in **Figure 1**. However, O_3 levels usually increase in the months leading up to the summer (with higher temperatures and increased solar radiation), which can lead to misidentification of an effect of lockdown on O_3 concentrations. The Bayesian time-series prediction model used here corrects for seasonal effects by taking into account data from the previous 2 years and shows a statistically significant increase of O_3 concentrations in the lockdown period (+45%; p = 0.001) which overcomes these effects. The increases in O_3 during the B2 and lockdown periods are also documented in **Figure 2**. In this case, the increases in O_3 are greater in the forested areas because downtown the NO from traffic still decreases the concentrations of this oxidant. Again, the differences between the B2 and lockdown periods are small.

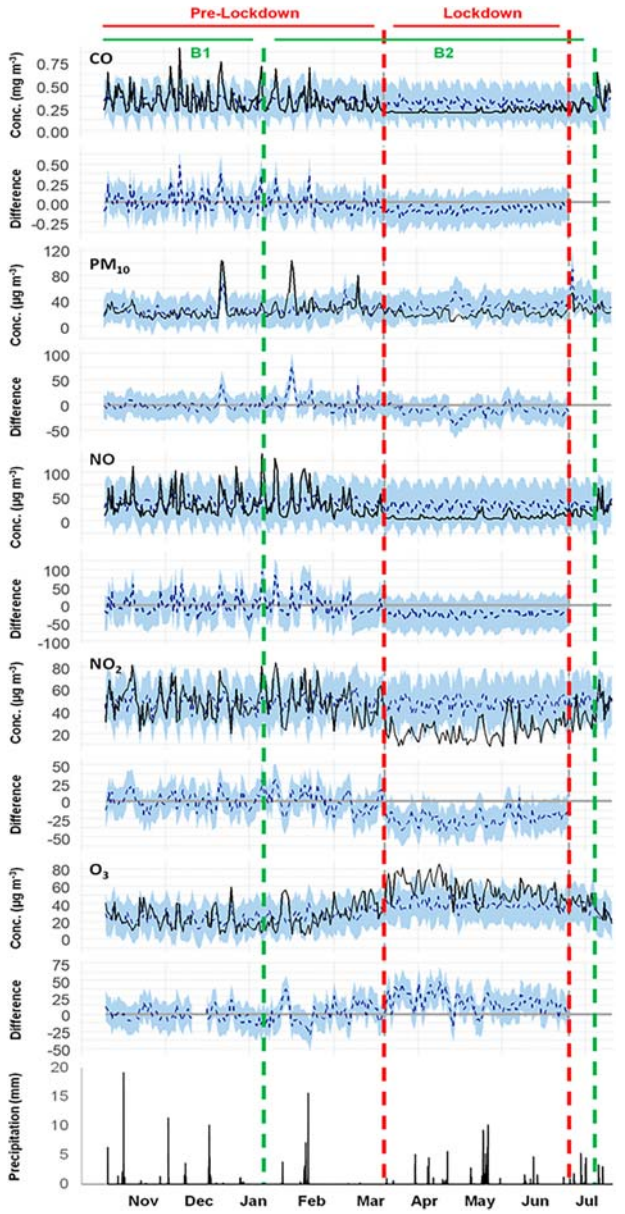

FIGURE 1 | Representation of the concentrations of atmospheric pollutants in Barcelona during the lockdown of 2020 and the corresponding Bayesian model predictions. The pre-lockdown/lockdown and the PAS-sampled B1/B2 periods are delimited by dashed, vertical, red and green lines, respectively. For each compound, the top graphs show daily average concentrations recorded in 2020 (black continuous line) against a counterfactual prediction based on 2018–2019 average values (blue dashed line). The bottom graphs show the difference between the observed data and the counterfactual predictions if lockdown had not occurred. From data of the air monitoring stations of the Catalan Government.

Concerning PM_{10}, the concentration decrease was noticed both for the lockdown (−37%; p = 0.0011) and the B2 periods (−20%; p = 0.001). This change is small in comparison with those observed for the gases except in the case of CO, which suggest that besides traffic other

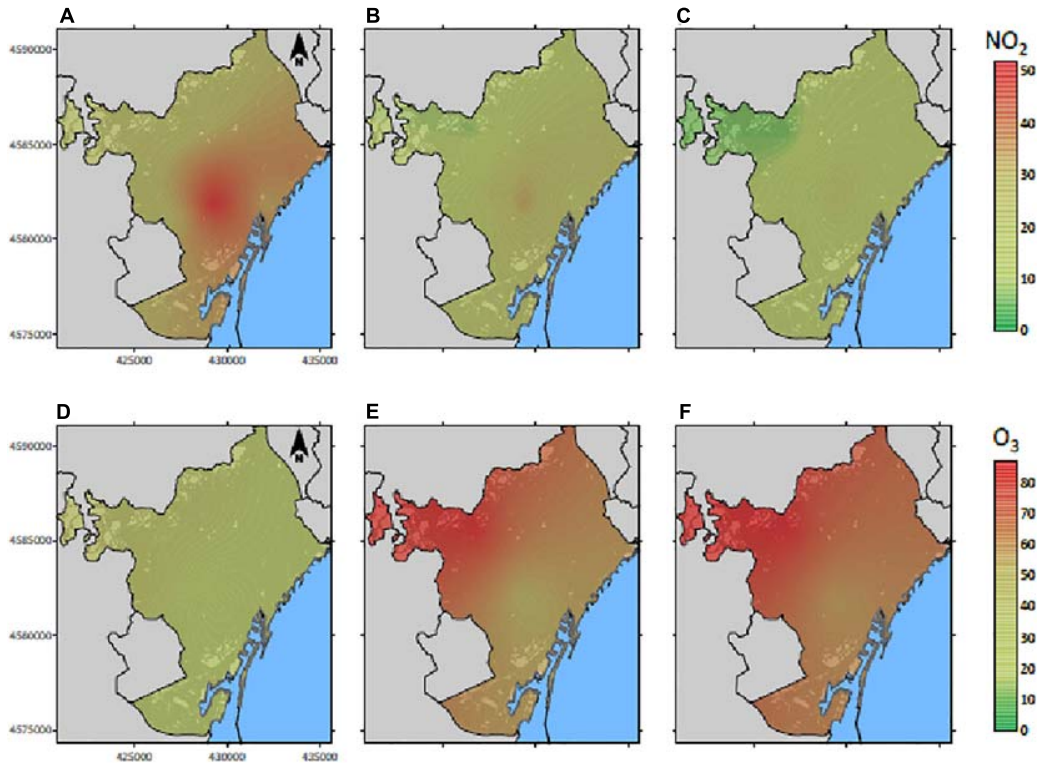

FIGURE 2 | Spatial distributions of airborne NO_2 **(A–C)** and O_3 **(D–F)** Barcelona, averaging in the B1 [15 October 2019–9 January 2020; **(A,D)**], B2 [9 January 2020–15 July 2020; **(B,E)]** and specific lockdown [15 March 2020–22 June 2020; **(C,F)**] periods. The plotted values ($\mu g\ m^{-3}$) are the averages of the daily measurements between 7 and 20 h. Note that the north and west zones are forested. From data of the air monitoring stations of the Catalan Government.

sources contributed to the atmospheric concentrations of PM_{10} in the city.

These results are in the range of those reported in other studies from several European and Mediterranean urban areas that also experienced lockdown conditions during the first half of 2020. Other studies in the city of Barcelona reported NO_2 reductions in concentration of −50% (Baldasano, 2020), −47 to −61% (Petetin et al., 2020), and −51% (Tobias et al., 2020). These values are similar to those reported in Madrid, −39 to −59% (Petetin et al., 2020), −62% (Baldasano, 2020), and −35 to −50% (Shi et al., 2021), and also to the average meteorology-normalized Spanish average of −50% (Petetin et al., 2020). Other European cities also presented comparable NO_2 reductions like −61% in Milan (Collivignarelli et al., 2020), −39% in Lucca and −39% in Florence (Donzelli et al., 2020), −32% in Athens (Grivas et al., 2020), and somewhat larger than −16, −27, −8, −26, and −11% in Milan, Rome, London, Paris, and Berlin, respectively (Shi et al., 2021). Our results for other pollutants are also similar to those reported for PM_{10}: −31% in Barcelona (Tobias et al., 2020), −48% in Milan (Collivignarelli et al., 2020), and −31% in Florence (Donzelli et al., 2020); for CO: −58% in Milan (Collivignarelli et al., 2020) and −35% in Athens (Grivas et al., 2020); and for NO: −42% in Pisa (Donzelli et al., 2020). Finally, compared to our results, other reports show similar O_3 variations in Barcelona: +33% increase during the first lockdown weeks (Tobias et al., 2020); slightly lower variations of −2% to +30% in several European cities (Shi et al., 2021); and much higher variations of +252% in Milan (Collivignarelli et al., 2020).

Moreover, air pollutant concentration reductions over the first weeks of lockdown have also been reported in a broader scale through satellite imaging techniques. The European Space Agency reported central and southern European reductions of NO_2 concentrations in Madrid (−48%), Rome (−49%), Milan (−47%), and Paris (−54%) (ESA, 2020a,b). These values are well in agreement with the values summarized in the paragraph above, as well as in the range of those reported here for the city of Barcelona (**Table 3**).

Finally, daily precipitation episodes are also represented in **Figure 1**. Comparison with the daily concentrations of all gases (i.e., CO, NO, NO_2, and O_3) and PM_{10} evidences that rain events generally do not coincide with noticeable drops in their atmospheric concentrations. This is consistent with results presented by other studies assessing changes in air pollution during lockdown in several cities in Spain, which found no correlation between precipitation values and air pollutant concentrations (Briz-Redón et al., 2021). Contrarily, the overall trend in concentration differences was consistent with the lockdown period, leaving wet precipitation as a minor driving factor in reducing air pollutant concentrations. This observation can be extrapolated to the atmospheric POP distributions. Rainfall rates averaged by sampled time can be derived from **Table 1** and are sufficiently similar for both PAS-sampled periods

(2.6 and 2.7 mm day^{-1} for B1 and B2, respectively) as to not expect considerable differences in washout, leaving the lockdown as the main cause for pollutant reductions.

CONCLUSION

All examined airborne pollutants showed lower concentrations during lockdown than in the regular period. PeCB was the compound displaying the highest lockdown decrease, −90.5%, followed by HCB and some PAHs such as b[a]ant and pyr, −79, −87, and −81%, respectively. In general, PAHs were the pollutants with higher reduction, −68 to −87%. Other compounds such as PCBs decreased by −37 to −69.5%.

The drops in atmospheric PAH concentrations can be associated with the strong traffic decrease during lockdown, −80% on average, and the significant reduction of harbor activities in this time interval, in the order of −65%. The present results regarding atmospheric PAHs indicate that the observed improvement of urban atmospheric quality related with lockdown restrictions was even better than recorded in the changes of nitrogen oxides and CO, providing a more holistic approach.

The study of other pollutants such as HCB, PeCB, and PCBs also evidences other atmospheric improvements related with the lockdown period such as the beneficial effects of reduction in the generation of solid residues and the subsequent reduction of urban waste incineration. The concentrations of PCBs during the B2 period in Barcelona were very close to those of remote sites such as the Pyrenees, with HCB and PeCB showing lower levels than those in these remote areas even during the pre-lockdown period.

Concerning the OPFRs, TBP also showed a decrease during lockdown but the other compounds of this group were seemingly not affected by the restrictions, possibly as a result of distinct and uniform release from their emission sources, e.g., construction material, industrial applications, household products, and others.

All in all, a significant decrease on the gas phase concentrations of atmospheric pollutants with current sources linked with anthropogenic urban activity was observed as consequence of the lockdown restrictions. O_3 is an exception related to processes other than traffic. The present work evidences the effectiveness of reducing overall anthropogenic emissions on a relatively short time span, not only in air quality indicator pollutants but also in many POPs. This highlights the potential of much needed policies that tackle air quality in a more stringent and broader way, which should stem from reports like the one we present. A sustained improvement on air quality, especially in densely populated areas, would contribute to reduce the over four million deaths attributed every year to ambient air pollution (WHO, 2018), as well as improve the health of many more.

DATA AVAILABILITY STATEMENT

The raw data supporting the conclusions of this article will be made available by the authors, without undue reservation.

AUTHOR CONTRIBUTIONS

RP: sampling, analysis, formal analysis, visualization, and writing – original draft. BD: sampling, analysis, supervision, and writing – review and editing. PF: supervision, writing – review and editing. EM: Formal analysis and visualization. JG: conceptualization, writing – review and editing, and funding acquisition. All authors contributed to the article and approved the submitted version.

FUNDING

This work was supported by the Spanish Ministry of Science and Innovation (Projects: CUANTOX CTM2015-71832-P and INTEMPOL PGC2018-10228-B-I00). RP also acknowledges financial support from the Spanish Ministry of Science and Innovation (BES-2016-076339).

ACKNOWLEDGMENTS

Sampling support from Alejandro G. Inarra and Anna Canals-Angerri, and technical assistance from Roser Chaler are acknowledged. Part of this work was performed in the Parc Nacional d'Aigüestortes i Estany de Sant Maurici, in Catalonia, with collaboration from the Department of Territory and Sustainability of the Catalan Government.

SUPPLEMENTARY MATERIAL

The Supplementary Material for this article can be found online at: https://www.frontiersin.org/articles/10.3389/fenvs.2021.650539/full#supplementary-material

REFERENCES

Armstrong, B., Hutchinson, E., Unwin, J., and Fletcher, T. (2004). Lung cancer risk after exposure to polycyclic aromatic hydrocarbons: a review and meta-analysis. *Environ. Health Perspect.* 112, 970–978. doi: 10.1289/ehp.6895

Arp, H. P. H., Morin, N. A. O., Andersson, P. L., Hale, S. E., Wania, F., Breivik, K., et al. (2020). The presence, emission and partitioning behavior of polychlorinated biphenyls in waste, leachate and aerosols from Norwegian waste-handling facilities. *Sci. Total Environ.* 715:136824. doi: 10.1016/j.scitotenv.2020.136824

Astoviza, M. J., Cappelletti, N., Bilos, C., Migoya, M. C., and Colombo, J. C. (2016). Airborne PCB patterns and urban scale in the Southern Río de la Plata Basin, Argentina. *Sci. Total Environ.* 572, 16–22. doi: 10.1016/j.scitotenv.2016.07.101

Baek, S. O., Field, R. A., Goldstone, M. E., Kirk, P. W., Lester, J. N., and Perry, R. (1991). A review of atmospheric polycyclic hydrocarbons: sources, fate and behavior. *Water Air Soil Pollut.* 60, 279–300. doi: 10.1007/BF00282628

Bailey, R. E. (2001). Global hexachlorobenzene emissions. *Chemosphere* 43, 167–182. doi: 10.1016/S0045-6535(00)00186-7

Baldasano, J. M. (2020). COVID-19 lockdown effects on air quality by NO2 in the cities of Barcelona and Madrid (Spain). *Sci. Total Environ.* 741:140353. doi: 10.1016/j.scitotenv.2020.140353

Berman, J. D., and Ebisu, K. (2020). Changes in U.S. air pollution during the COVID-19 pandemic. *Sci. Total Environ.* 739:139864. doi: 10.1016/j.scitotenv.2020.139864

Boström, C. E., Gerde, P., Hanberg, A., Jernström, B., Johansson, C., Kyrklund, T., et al. (2002). Cancer risk assessment, indicators, and guidelines for polycyclic aromatic hydrocarbons in the ambient air. *Environ. Health Perspect.* 110, 451–488. doi: 10.1289/ehp.110-1241197

Brodersen, K. H., Galluser, F., Koehler, J., Remy, N., and Scott, S. L. (2015). *CausalImpact 1.2.4. Ann. Appl. Stat*. Available online at: http://google.github.io/CausalImpact/ (accessed October 15, 2020).

Briz-Redón, Á, Belenguer-Sapiña, C., and Serrano-Aroca, Á (2021). Changes in air pollution during COVID-19 lockdown in Spain: a multi-city study. *J. Environ. Sci.* 101, 16–26. doi: 10.1016/j.jes.2020.07.029

Cameletti, M. (2020). The effect of corona virus lockdown on air pollution: evidence from the city of Brescia in Lombardia Region (Italy). *Atmos. Environ.* 239:117794. doi: 10.1016/j.atmosenv.2020.117794

Casas, M., Nieuwenhuijsen, M., Martinez, D., Ballester, F., Basagaña, X., Barterrechea, M., et al. (2015). Prenatal exposure to PCB-153, p,p'-DDE and birth outcomes in 9000 mother-child pairs: Exposure-response relationship and effect modifiers. *Environ. Int.* 74, 23–31. doi: 10.1016/j.envint.2014.09.013

Chakraborty, P., Zhang, G., Li, J., Xu, Y., Liu, X., Tanabe, S., et al. (2010). Selected organochlorine pesticides in the atmosphere of major Indian cities: levels, regional versus local variations, and sources. *Environ. Sci. Technol.* 44, 8038–8043. doi: 10.1021/es102029t

Chen, Y., Cai, X., Jiang, L., and Li, Y. (2016). Prediction of octanol-air partition coefficients for polychlorinated biphenyls (PCBs) using 3D-QSAR models. *Ecotoxicol. Environ. Saf.* 124, 202–212. doi: 10.1016/j.ecoenv.2015.10.024

Chevrier, J., Eskenazi, B., Holland, N., Bradman, A., and Barr, D. B. (2008). Effects of exposure to polychlorinated biphenyls and organochlorine pesticides on thyroid function during pregnancy. *Am. J. Epidemiol.* 168, 298–310. doi: 10.1093/aje/kwn136

Collivignarelli, M. C., Abbà, A., Bertanza, G., Pedrazzani, R., Ricciardi, P., and Miino, M. C. (2020). Lockdown for CoViD-2019 in Milan: what are the effects on air quality? *Sci. Total Environ.* 732:139280. doi: 10.1016/j.scitotenv.2020.139280

Cui, S., Fu, Q., Li, Y.-F., Li, T.-X., Liu, D., Dong, W.-C., et al. (2017). Spatial–temporal variations, possible sources and soil–air exchange of polychlorinated biphenyls in urban environments in China. *RSC Adv.* 7:14797. doi: 10.1039/C6RA26864A

de la Torre, A., Sanz, P., Navarro, I., and Martínez, M. A. (2016). Time trends of persistent organic pollutants in Spanish air. *Environ. Pollut.* 217, 26–32. doi: 10.1016/j.envpol.2016.01.040

De Voogt, P., Wells, D. E., Reutergardh, L., and Brinkman, U. A. T. (1990). Biological activity, determination and occurrence of planar, mono- and di-ortho PCBs. *Int. J. Environ. Anal. Chem.* 40, 1–46. doi: 10.1080/03067319008030516

Dishaw, L. V., Powers, C. M., Ryde, I. T., Roberts, S. C., Seidler, F. J., Slotkin, T. A., et al. (2011). Is the PentaBDE replacement, tris (1,3-dichloro-2-propyl) phosphate (TDCPP), a developmental neurotoxicant? Studies in PC12 cells. *Toxicol. Appl. Pharmacol.* 256, 281–289. doi: 10.1016/j.taap.2011.01.005

Donzelli, G., Cioni, L., Cancellieri, M., Morales, A. L., and Suárez-Varela, M. M. M. (2020). The Effect of the Covid-19 lockdown on air quality in three Italian medium-sized cities. *Atmosphere* 11:1118. doi: 10.3390/atmos11101118

Du, J., Li, H., Xu, S., Zhou, Q., Jin, M., and Tang, J. (2019). A review of organophosphorus flame retardants (OPFRs): occurrence, bioaccumulation, toxicity, and organism exposure. *Environ. Sci. Pollut. Res.* 26, 22126–22136. doi: 10.1007/s11356-019-05669-y

EEA (2019). *Air Quality in Europe – EEA Report No 10/2019*. Available online at: https://www.eea.europa.eu/publications/air-quality-in-europe-2019 (accessed November 15, 2020).

EPA (1986). *Exposure Assessment for Hexachlorobenzene*. Washington, DC: U.S. Environmental Protection Agency, Office of Pesticides and Toxic Substances.

ESA (2020a). *Nitrogen Dioxide Concentrations Over Spain*. Available online at: http://www.esa.int/ESA_Multimedia/Images/2020/03/Nitrogen_dioxide_concentrations_over_Spain (accessed November 15, 2020).

ESA (2020b). *Air Pollution Remains Low as Europeans Stay at Home*. Available online at: http://www.esa.int/Applications/Observing_the_Earth/Copernicus/Sentinel-5P/Air_pollution_remains_low_as_Europeans_stay_at_home (accessed November 15, 2020).

Estellano, V. H., Pozo, K., Harner, T., Carsolini, S., and Focardi, S. (2012). Using PUF disk passive samplers to simultaneously measure air concentrations of persistent organic pollutants (POPs) across the Tuscany Region, Italy. Atmos. *Pollut. Res.* 3, 88–94. doi: 10.5094/APR.2012.008

Grandjean, P., and Landrigan, P. J. (2014). Neurobehavioural effects of developmental toxicity. *Lancet Neurol.* 13, 330–338. doi: 10.1016/S1474-4422(13)70278-3

Grimalt, J. O., Sunyer, J., Moreno, V., Amaral, O. C., Sala, M., Rosell, A., et al. (1994). Risk excess of soft−tissue sarcoma and thyroid cancer in a community exposed to airborne organochlorinated compound mixtures with a high hexachlorobenzene content. *Int. J. Cancer.* 56, 200–203. doi: 10.1002/ijc.2910560209

Grimalt, J. O., Fernandez, P., and Quiroz, R. (2009). Input of organochlorine compounds by snow to European high mountain lakes. *Freshwater Biol.* 54, 2533–2542. doi: 10.1111/j.1365-2427.2009.02302.x

Grivas, G., Athanasopoulou, E., Kakouri, A., Bailey, J., Liakakou, E., Stavroulas, I., et al. (2020). Integrating in situ measurements and city scale modelling to assess the COVID-19 lockdown effects on emissions and air quality in Athens, Greece. *Atmosphere* 11:1174. doi: 10.3390/atmos11111174

Harner, T., Su, K., Genualdi, S., Karpowicz, J., Ahrens, L., Mihele, C., et al. (2013). Calibration and application of PUF disk passive air samplers for tracking polycyclic aromatic compounds (PACs). *Atmos. Environ.* 75, 123–128. doi: 10.1016/j.atmosenv.2013.04.012

Harner, T. (2016). 2016 v1 3 Template for Calculating PUF and SIP Disk Sample Air Volumes. doi: 10.13140/RG.2.1.3998.8884

He, J., and Balasubramanian, R. (2012). Passive sampling of gaseous persistent organic pollutants in the atmosphere. *Energy Proc.* 16, 494–500. doi: 10.1016/j.egypro.2012.01.080

Kalina, J., White, K. B., Scheringer, M., Pøibylová, P., Kukuèka, P., Audy, O., et al. (2019). Comparability of long-term temporal trends of POPs from co-located active and passive air monitoring networks in Europe. *Environ. Sci. Processes Impacts* 21, 1132–1142. doi: 10.1039/C9EM00136K

Kaufman, Y. J., Tanré, D., Remer, L. A., Vermote, E. F., Chu, A., and Holben, B. N. (1997). Operational remote sensing of tropospheric aerosol over land from EOS moderate resolution imaging spectroradiometer. *J. Geophys. Res. Atmos.* 102, 17051–17067. doi: 10.1029/96jd03988

Krotkov, N. A., McLinden, C. A., Li, C., Lamsal, L. N., Celarier, E. A., Marchenko, S. V., et al. (2016). Aura OMI observations of regional SO2 and NO2 pollution changes from 2005 to 2015. *Atmos. Chem. Phys.* 16, 4605–4629. doi: 10.5194/acp-16-4605-2016

Kuzu, S. L. (2016). Compositional variation of PCBs, PAHs, and OCPs at Gas phase and size segregated particle phase during dust incursion from the Saharan desert in the Northwestern Anatolian peninsula. *Adv. Meteorol.* 2016:7153286. doi: 10.1155/2016/7153286

Lammel, G., Klanova, J., Eric, L., Ilic, P., Kohoutek, J., and Kovacik, I. (2011). Sources of organochlorine pesticides in air in an urban Mediterranean environment: volatilization from soil. *J. Environ. Monit.* 13, 3358–3364. doi: 10.1039/C1EM10479A

Lauby-Secretan, B., Loomis, D., Grosse, Y., El Ghissassi, F., Bouvard, V., Benbrahim-Tallaa, L., et al. (2013). Carcinogenicity of polychlorinated biphenyls and polybrominated biphenyls. *Lancet Oncol.* 14, 287–288. doi: 10.1016/S1470-2045(13)70104-9

Le Quéré, C., Jackson, R. B., Jones, M. W., Smith, A. J. P., Abernethy, S., Andrew, R. M., et al. (2020). Temporary reduction in daily global CO2 emissions during the COVID-19 forced confinement. *Nat. Clim. Chang.* 10, 647–653. doi: 10.1038/s41558-020-0797-x

Leighton, P. A. (1961). *Photochemistry of Air Pollution*. New York, NY: Academic Press.

Li, L., Li, Q., Huang, L., Wang, Q., Zhu, A., Xu, J., et al. (2020). Air quality changes during the COVID-19 lockdown over the Yangtze River Delta Region: an insight into the impact of human activity pattern changes on air pollution variation. *Sci. Total Environ.* 732:139282. doi: 10.1016/j.scitotenv.2020.139282

Liu, D., Lin, T., Shen, K., Li, J., Yu, Z., and Zhang, G. (2016). Occurrence and concentrations of halogenated flame retardants in the atmospheric fine particles in Chinese cities. *Environ. Sci. Technol.* 50, 9846–9854. doi: 10.1021/acs.est.6b01685

Llop, S., Murcia, M., Alvarez-Pedrerol, M., Grimalt, J. O., Santa Marina, L., Julvez, J., et al. (2017). Association between exposure to organochlorine compounds

and maternal thyroid status: Role of the iodothyronine deiodinase 1 gene. *Environ. Int.* 104, 83–90. doi: 10.1016/j.envint.2016.12.013

Lopez-Espinosa, M. J., Murcia, M., Iniguez, C., Vizcaíno, E., Costa, O., Fernández-Somoano, A., et al. (2016). Organochlorine compounds and ultrasound measurements of fetal growth in the INMA Cohort (Spain). *Environ. Health Perspect.* 124, 157–163. doi: 10.1289/ehp.1408907

Martens, D., Balta-Brouma, K., Brotsack, R., Michalke, B., Schramel, P., Klimm, C., et al. (1998). Chemical impact of uncontrolled solid waste combustion to the vicinity of the Kouroupitos Ravine, Crete, Greece. *Chemosphere* 36, 2855–2866. doi: 10.1016/S0045-6535(97)10242-9

Meijer, S. N., Ockenden, W. A., Sweetman, A., Breivik, K., Grimalt, J. O., and Jones, K. C. (2003). Global distribution and budget of PCBs and HCB in Background surface soils: implications for sources and environmental processes. *Environ. Sci. Technol.* 37, 667–672. doi: 10.1021/es010322i

Montlleo, M., Rodriguez, G., Tavares, N., Masvidal, M., Lao, J., Coral, A., et al. (2020). *Observatori COVID-19. Metabolisme de la Ciutat. City Hall of Barcelona*. Available online at: https://www.barcelona.cat/barcelona-pel-clima/sites/default/files/documents/20200729-observatori_covid-19-metabolisme_de_la_ciutat.pdf (accessed November 15, 2020).

Morales, E., Gascon, M., Martinez, D., Casas, M., Ballester, F., Rodriguez-Bernal, C. L., et al. (2013). Associations between blood persistent organic pollutants and 25-hydroxyvitamin D3 in pregnancy. *Environ. Int.* 57–58, 34–41. doi: 10.1016/j.envint.2013.03.011

Morville, S., Delhomme, O., and Millet, M. (2011). Seasonal and diurnal variations of atmospheric PAH concentrations between rural, suburban and urban areas. *Atmos. Pollut. Res.* 2, 366–373. doi: 10.5094/APR.2011.041

Motelay-Massei, A., Harner, T., Shoeib, M., Diamond, M., Stern, G., and Rosenbreg, B. (2005). Using passive air samplers to assess urban-rural trends for persistent organic pollutants and polycyclic aromatic hydrocarbons. 2. Seasonal trends for PAHs, PCBs, and organochlorine pesticides. *Environ. Sci. Technol.* 39, 5763–5773. doi: 10.1021/es0504183

Nasir, J., Wang, X., Xu, B., Wang, C., Joswiak, D. R., Rehman, S., et al. (2014). Selected organochlorine pesticides and polychlorinated biphenyls in urban atmosphere of Pakistan: concentration, spatial variation and sources. *Environ. Sci. Technol.* 48, 2610–2618. doi: 10.1021/es404711n

Neuwahl, F., Cusano, G., Gomez-Benavides, J., Holbrook, S., and Roudier, S. (2019). *Best Available Techniques (BAT). Reference Document for waste incineration. Industrial Emission Directive 2010/75/EU. Integrated Pollution Prevention and Control*. Luxembourg: Publications Office of the European Union.

Nost, T. H., Halse, A. K., Randall, S., Borgen, A. R., Schlabach, M., Paul, A., et al. (2015). High concentrations of organic contaminants in air from ship breaking activities in Chittagong, Bangladesh. *Environ. Sci. Technol.* 49, 11372–11380. doi: 10.1021/acs.est.5b03073

Odabasi, M., Cetin, E., and Sofuoglu, A. (2006). Determination of octanol-air partition coefficients and supercooled liquid vapor pressures of PAHs as a function of temperature: Application to gas-particle partitioning in an urban atmosphere. *Atmos. Environ.* 40, 6615–6625. doi: 10.1016/j.atmosenv.2006.05.051

Petetin, H., Bowdalo, D., Soret, A., Guevara, M., Jorba, O., Serradell, K., et al. (2020). Meteorology-normalized impact of the COVID-19 lockdown upon NO2 pollution in Spain. *Atmos. Chem. Phys.* 20, 11119–11141. doi: 10.5194/acp-20-11119-2020

Pokhrel, B., Gong, P., Wang, X., Khanal, S. N., Ren, J., Wang, C., et al. (2018). Atmospheric organochlorine pesticides and polychlorinated biphenyls in urban areas of Nepal: spatial variation, sources, temporal trends, and long-range transport potential. *Atmos. Chem. Phys.* 18, 1325–1336. doi: 10.5194/acp-18-1325-2018

Pozo, K., Harner, T., Lee, S. C., Wania, F., Muir, D. C. G., and Jones, K. C. (2009). Seasonally resolved concentrations of persistent organic pollutants in the global atmosphere from the first year of the GAPS Study. *Environ. Sci. Technol.* 43, 796–803. doi: 10.1021/es802106a

Pozo, K., Harner, T., Lee, S. C., Sinha, R. K., Sengupta, B., Loewen, M., et al. (2011). Assessing seasonal and spatial trends of persistent organic pollutants (POPs) in Indian agricultural regions using PUF disk passive air samplers. *Environ. Pollut.* 159, 646–653. doi: 10.1016/j.envpol.2010.09.025

Pozo, K., Harner, T., Rudolph, A., Oyola, G., Estellano, V. H., Ahumada-Rudolph, R., et al. (2012). Survey of persistent organic pollutants (POPs) and polycyclic aromatic hydrocarbons (PAHs) in the atmosphere of rural, urban and industrial areas of Concepciün, Chile, using passive air samplers. *Atmos. Poll. Res.* 3, 426–434. doi: 10.5094/APR.2012.049

Pratt, G. C., Herbrandson, C., Krause, M. J., Schmitt, C., Lippert, C. J., McMahon, C. R., et al. (2018). Measurements of gas and particle polycyclic aromatic hydrocarbons (PAHs) in air at urban, rural and near-roadway sites. *Atmos. Environ.* 179, 268–278. doi: 10.1016/j.atmosenv.2018.02.035

Sala, M., Sunyer, J., Herrero, C., To-Figueras, J., and Grimalt, J. O. (2001). Association between serum concentration of hexachlorobenzene and polychlorobiphenyls with thyroid hormone and liver enzymes in a sample of the general population. *Occup. Environ. Med.* 58, 172–177. doi: 10.1136/oem.58.3.172

Salamova, A., Hermanson, M. H., and Hites, R. A. (2014). Organophosphate and halogenated flame retardants in atmospheric particles from a European Arctic site. *Environ. Sci. Technol.* 48, 6133–6140. doi: 10.1021/es500911d

Shi, Z., Song, C., Liu, B., Lu, G., Xu, J., Vu, T. V., et al. (2021). Abrupt but smaller than expected changes in surface air quality attributable to COVID-19 lockdowns. *Sci. Adv.* 7:eabd6696. doi: 10.1126/sciadv.abd6696

Shoeib, M., and Harner, T. (2002). Characterization and comparison of three passive air samplers for persistent organic pollutants. *Environ. Sci. Technol.* 36, 4142–4151. doi: 10.1021/es020635t

Smink, A., Ribas-Fito, N., Garcia, R., Torrent, M., Mendez, M. A., Grimalt, J. O., et al. (2008). Exposure to hexachlorobenzene during pregnancy increases the risk of overweight in children aged 6 years. *Acta Paediatr.* 97, 1465–1469. doi: 10.1111/j.1651-2227.2008.00937.x

Sohrabi, C., Alsafi, Z., O'Neill, N., Khan, M., Kerwan, A., Al-Jabir, A., et al. (2020). World Health Organization declares global emergency: A review of the 2019 novel coronavirus (COVID-19). *Int. J. Surg.* 76, 71–76. doi: 10.1016/j.ijsu.2020.02.034

State of the City (2020). *State of the City. Barcelona City Hall Report. 2020*. Available online at: https://ajuntament.barcelona.cat/premsa/wp-content/uploads/2020/06/200626-Informe-Estat-de-la-ciutat-2019-Document-complementari.pdf (accessed November 15, 2020).

Tobias, A., Carnerero, C., Reche, C., Massagué, J., Via, M., Minguillón, M. C., et al. (2020). Changes in air quality during the lockdown in Barcelona (Spain) one month into the SARS-CoV-2 epidemic. *Sci. Total Environ.* 726:138540. doi: 10.1016/j.scitotenv.2020.138540

Tombesi, N., Pozo, K., and Harner, T. (2014). Persistent organic pollutants (POPs) in the atmosphere of agricultural and urban areas in the Province of Buenos Aires in Argentina using PUF disk passive air samplers. *Atmos. Pollut. Res.* 5, 170–178. doi: 10.5094/APR.2014.021

UNEP (2010). *United Nations Environment Programme. Assessing the Environmental Impacts of Consumption and Production. Priority Products and Materials*. Nairobi: UNEP.

Valvi, D., Mendez, M. A., Martinez, D., Grimalt, J. O., Torrent, M., Sunyer, J., et al. (2012). Prenatal concentrations of polychlorinated biphenyls, DDE, and DDT and overweight in children. A prospective birth cohort study. *Environ. Health Persp.* 120, 451–457. doi: 10.1289/ehp.1103862

Valvi, D., Mendez, M. A., Garcia-Esteban, R., Ballester, F., Ibarluzea, J., Goñi, F., et al. (2014). Prenatal exposure to persistent organic pollutants and rapid weight gain and overweight in infancy. *Obesity* 22, 488–496. doi: 10.1002/oby.20603

Van der Veen, I., and de Boer, J. (2012). Phosphorus flame retardants: Properties, production, environmental occurrence, toxicity and analysis. *Chemosphere* 88, 1119–1153. doi: 10.1016/j.chemosphere.2012.03.067

van Drooge, B. L., Grimalt, J. O., Camarero, L., Catalan, J., Stuchlík, E., and Torres García, C. J. (2004). Atmospheric semivolatile organochlorine compounds in European high-mountain areas (Central Pyrenees and High Tatras). *Environ. Sci. Technol.* 38, 3525–3532. doi: 10.1021/es030108p

van Drooge, B. L., and Grimalt, J. O. (2015). Particle size-resolved source apportionment of primary and secondary organic tracer compounds at urban and rural locations in Spain. *Atmos. Chem. Phys.* 15, 7735–7752. doi: 10.5194/acp-15-7735-2015

van Drooge, B. L., Fontal, M., Fernández, P., Fernández, M. A., Muñoz-Arnanz, J., Jiménez, B., et al. (2018a). Organic molecular tracers in atmospheric PM1 at urban intensive traffic and background sites in two high-insolation European cities. *Atmos. Environ.* 188, 71–81. doi: 10.1016/j.atmosenv.2018.06.024

van Drooge, B. L., Ramos García, D., and Lacorte, S. (2018b). Analysis of organophosphorus flame retardants in submicron atmospheric particulate matter (PM1). *AIMS Environ. Sci.* 5, 294–304. doi: 10.3934/environsci.2018.4.294

Venter, Z. S., Aunan, K., Chowdhury, S., and Lelieveld, J. (2020). COVID-19 lockdowns cause global air pollution declines. *Proc. Natl. Acad. Sci. U.S.A.* 117, 18984–18990. doi: 10.1073/pnas.2006853117

Wang, Q., Zhao, H., Wang, Y., Xie, Q., Chen, J., and Quan, X. (2017). Determination and prediction of octanol-air partition coefficients for organophosphate flame retardants. *Ecotoxicol. Environ. Saf.* 145, 283–288. doi: 10.1016/j.ecoenv.2017.07.040

Wegiel, M., Chrzaszcz, R., Maslanka, A., and Grochowalski, A. (2011). Study on the determination of PCDDs/Fs and HCB in exhaust gas. *Chemosphere* 85, 481–486. doi: 10.1016/j.chemosphere.2011.07.079

WHO (2018). *Ambient (outdoor) Air Pollution*. Geneva: WHO.

Wong, F., de Wit, C. A., and Newton, S. R. (2018). Concentrations and variability of organophosphate esters, halogenated flame retardants, and polybrominated diphenyl ethers in indoor and outdoor air in Stockholm, Sweden. *Environ. Pollut.* 240, 514–522. doi: 10.1016/j.envpol.2018.04.086

Zhang, R., Zhang, Y., Lin, H., Feng, X., Fu, T. M., and Wang, Y. (2020). NOx emission reduction and recovery during COVID-19 in East China. *Atmosphere* 11:433. doi: 10.3390/ATMOS11040433

Zhang, W., Ye, Y., Hu, D., Qu, L., and Wang, X. (2010). Characteristics and transport of organochlorine pesticides in urban environment: air, dust, rain, canopy, throughfall, and runoff. *J. Environ. Monit* 12, 2153–2160. doi: 10.1039/C0EM00110D

Zhang, Z., Arshad, A., Zhang, C., Hussain, S., and Li, W. (2020). Unprecedented temporary reduction in global air pollution associated with COVID-19 forced confinement: A continental and city scale analysis. *Remote Sens.* 12:2420. doi: 10.3390/RS12152420

Zhou, L., Hiltscher, M., Gruber, D., and Püttmann, W. (2017). Organophosphate flame retardants (OPFRs) in indoor and outdoor air in the Rhine/Main area, Germany: comparison of concentrations and distribution profiles in different microenvironments. *Environ. Sci. Pollut. Res.* 24, 10992–11005. doi: 10.1007/s11356-016-6902-z

Conflict of Interest: The authors declare that the research was conducted in the absence of any commercial or financial relationships that could be construed as a potential conflict of interest.

frontiers in Environmental Science

ORIGINAL RESEARCH
published: 20 September 2021
doi: 10.3389/fenvs.2021.746090

Radiative Impacts of Aerosols During COVID-19 Lockdown Period Over the Indian Region

Rohini L. Bhawar[1], Suvarna Fadnavis[2], Vinay Kumar[3], P. R. C. Rahul[2], Tushar Sinha[3] and Simone Lolli[4]*

[1]Department of Atmospheric and Space Sciences, Savitribai Phule Pune University, Pune, India, [2]Indian Institute of Tropical Meteorology, Pune, India, [3]Department of Environmental Engineering, Texas A&M University, Kingsville, TX, United States, [4]CNR-IMAA, Potenza, Italy

The COVID-19 lockdown restrictions influenced global atmospheric aerosols. We report aerosol variations over India using multiple remote sensing datasets [Moderate Resolution Imaging Spectroradiometer (MODIS), Ozone Monitoring Instrument (OMI), Cloud-Aerosol Lidar, and Infrared Pathfinder (CALIPSO)], and model reanalysis [Copernicus Atmosphere Monitoring Service (CAMS)] during the lockdown implemented during the COVID-19 pandemic outbreak period from March 25 to April 14, 2020. Our analysis shows that, during this period, MODIS and CALIPSO showed a 30–40% reduction in aerosol optical depth (AOD) over the Indo-Gangetic Plain (IGP) with respect to decadal climatology (2010–2019). The absorbing aerosol index and dust optical depth measurements also showed a notable reduction over the Indian region, highlighting less emission of anthropogenic dust and also a reduced dust transport from West Asia during the lockdown period. On the contrary, central India showed an ~12% AOD enhancement. CALIPSO measurements revealed that this increase was due to transported biomass burning aerosols. Analysis of MODIS fire data product and CAMS fire fluxes (black carbon, SO_2, organic carbon, and nitrates) showed intense fire activity all over India but densely clustered over central India. Thus, we show that the lockdown restrictions implemented at the government level have significantly improved the air quality over northern India but fires offset its effects over central India. The biomass-burning aerosols formed a layer near 2–4 km (AOD 0.08–0.1) that produced heating at 3–4 K/day and a consequent negative radiative forcing at the surface of ~–65 W/m^2 (±40 W/m^2) over the central Indian region.

Keywords: COVID-19 lockdown, aerosol pollution over India, radiative forcing and heating, aerosol layer in the lower troposphere, fires over central India

OPEN ACCESS

Edited by:
Bin Zhao,
Tsinghua University, China

Reviewed by:
Qianqian Zhang,
National Satellite Meteorological Center (NSMC), China
Hongrong Shi,
Institute of Atmospheric Physics (CAS), China
Dan Chen,
China Meteorological Administration, China

****Correspondence:***
Rohini L. Bhawar
rohinibhawar@gmail.com

Specialty section:
This article was submitted to Atmosphere and Climate, a section of the journal Frontiers in Environmental Science

Received: *23 July 2021*
Accepted: *06 September 2021*
Published: *20 September 2021*

Citation:
Bhawar RL, Fadnavis S, Kumar V, Rahul PRC, Sinha T and Lolli S (2021) Radiative Impacts of Aerosols During COVID-19 Lockdown Period Over the Indian Region. Front. Environ. Sci. 9:746090. doi: 10.3389/fenvs.2021.746090

1 INTRODUCTION

There are growing concerns about aerosol pollution over the Indian region due to the negative effects they produce on health and the hydrological cycle (Meehl et al., 2013; Vinoj et al., 2014; D'Errico et al., 2015; Fadnavis et al., 2017a; Fadnavis et al., 2019a). During the past decade, India recorded the highest levels of air pollution (World Bank and International report 2020). In India, ~51% of the 1.4 billion people population are persistently exposed to air pollution. Aerosol pollution over India has increased hazy days at a rate of 2.6 days per year (Thomas et al., 2019). This aerosol pollution has

caused 8.8% of the total deaths (Report by Indian Council of Medical Research, 2017; IHME Report, 2019). Other than anthropogenic sources, smog events have proven fatal during the last decade (Spears et al., 2019; Pandey and Vinoj, 2021).

Aerosol pollution over the Indian region is attributed to economic development, traffic emissions, and land-use changes (Fadnavis et al., 2013; Guttikunda et al., 2014; Hama et al., 2020). Aerosol Radiative Forcing over India (ARFI) net observations show the rate of increase at 2.3% per year in aerosol loading over India (Krishna Moorthy et al., 2013). Pollution levels over urban and rural regions are equally high (Dey et al., 2012; Hammer et al., 2020). According to the Intergovernmental Panel on Climate Change (IPCC, 2014), India contributes ~38–78% to the anthropogenic aerosol global mean and 3–9% to biomass-burning aerosol (David et al., 2019; IPCC, 2014). Agricultural fires and crop residue activity during winter/spring cause a substantial increase (43%) in aerosol loading over North India (Jethva et al., 2019; Fadnavis et al., 2021).

The novel coronavirus (COVID-19) made its first appearance in December 2019 and quickly spread all over the world (Fadnavis et al., 2021). Transmission during the COVID-19 pandemic outbreak was facilitated by certain atmospheric conditions and pollutants (Lolli et al., 2020; Lolli and Vivone, 2020; Jiang et al., 2021). To restrict the spread of COVID-19, lockdown measures were imposed in January in China, and later in other countries all over the world (Chauhan and Singh, 2020; Paital, 2020; Yunus et al., 2020). India confirmed its first case on January 30, 2020, and later COVID-19 spread started rising exponentially. To strengthen the health infrastructure and restrict the spread of COVID-19, the Indian government imposed a Janata curfew on March 22, 2020 and, after that, a complete lockdown between March 25–April 14, 2020 (Chauhan and Singh, 2020).

The lockdown measures implemented at government level, e.g., restrictions on public transport, freights flights, shutting down industries, etc. reduced the aerosol optical depth (AOD) in different parts of the globe (Le Quéré et al., 2020; Kaskaoutis et al., 2021). The MODIS observations showed an ~40% reduction in aerosols over North India (Gautam, 2020; Jain and Sharma, 2020; Fadnavis et al., 2021). The *in-situ* observations over Kanpur, a station in North India, showed a reduction of 20–30% of AOD compared to 2017–2019 (Shukla et al., 2020). A drop in AOD by 0.16 over the entire Indian landmass was reported by Mishra and Rathore (2021). There was a substantial decrease of ~35% in the PM2.5 concentrations across the cities in the Indo-Gangetic belt (Das et al., 2021). However, there was an increase in AOD over south India (Le Quéré et al., 2020; Pandey and Vinoj 2021). The aerosol enhancement over South India is linked to local biomass burning activity (Singh et al., 2020; Sanap, 2021).

In this paper, we report how the aerosol vertical distribution impacted the heating rates and radiative forcing over India during the lockdown period of March 25–April 14, 2020. Our analysis shows a decrease in AOD over North India and enhancement over Central India (78°E–85°E, 18°N–25°N). The aerosol enhancement over central India is due to large amounts of fires associated with agricultural activities. Further, we show that the smoke aerosols formed a layer of nearly 3–4 km that caused atmospheric heating and affected the radiative forcing over India. The results are derived from satellite observations (MODIS, OMI, CALIPSO) and CAMS reanalysis during March–April 2020. The paper is organized as follows: data and methodology are described in **Section 2**, results and discussions are given in **Section 3**, and conclusion are made in **Section 4**.

2 DATA AND METHODOLOGY

2.1 Satellite Retrievals

High-resolution vertical profiles of clouds and aerosols were obtained from the Cloud-Aerosol Lidar and Infrared Pathfinder Satellite (CALIPSO) (Winker et al.,2010; Winker et al., 2007). The CALIPSO payload, polarization-sensitive backscatter lidar, known as the Cloud-Aerosol Lidar with Orthogonal Polarization (CALIOP), operates at 532 and 1,064 nm wavelengths. The CALIPSO satellite has been observing the vertical distribution of aerosols since June 2006. The primary instrument on CALIPSO is CALIOP, a nadir-viewing dual-wavelength (532 and 1,064 nm) dual polarization at 532 nm, elastic back-scatter lidar (Hunt et al., 2009). Level 2 algorithms detect features, assign type classification for aerosols, and retrieve extinction coefficients from the attenuated backscattered signals. The extinction algorithm retrieves vertical profiles of extinction, reported separately for aerosols and clouds. Aerosol extinction is not reported within clouds because the lidar signals are dominated by cloud scattering and so atmospheric features are classified as either aerosols or clouds and the retrieved extinction is reported for only one or the other. The aerosol profile product combines the profiles retrieved within aerosol layers to report vertical profiles of extinction coefficients at 5 km horizontal resolution. The vertical resolution is 60 m from 0.5 to 20.2 km and 180 m above 20.2 km. For the 5 km along CALIPSO track horizontal averaging, 15 consecutive level 1 B profiles are used (Tackett et al., 2018). The lidar ratios and their uncertainties for several of the aerosol subtypes have been revised in version 4 (Kim et al., 2018). It is said that the reductions in the relative uncertainties associated with the improved lidar ratios will reduce the relative uncertainties in the retrieved extinction coefficients and optical depths. These improved lidar ratios in V4 are a better representative of actual conditions than in previous data releases (Young et al., 2018). Here, in the present study, we used the level 2 version 4.10/4.20 CALIPSO aerosol profile (APro) data for the period 2010–2020 (https://asdc.larc.nasa.gov/project/CALIPSO). The details of the lidar ratio selection algorithm are well documented by Kim et al. (2018). We used the extinction profiles of aerosol and the optical depth for dust and elevated smoke aerosols at 532 nm. These extinction profiles were used to calculate the aerosol optical depth profiles at pre-defined altitudes including higher numbers in the altitude-range 1–10 km. We gridded these profiles at a 1× 1 degree resolution.

The aerosol optical depth data obtained from the Moderate Resolution Imaging Spectroradiometer (MODIS) were also analyzed to understand aerosol variations over India. The

MODIS sensor measures radiances at 36 bands, ranging from visible to infrared and varying spatial resolutions. Here, we used daily AOD at 550 nm from the MODIS (MOD08_D3) collection 6.1 level 3, combined dark target and deep blue, from 2010 to 2020 (Hsu et al., 2013; Levy et al., 2013; Wei et al., 2019a; Wei et al., 2019b) (https://giovanni.gsfc.nasa.gov/giovanni). The past studies show that CALIPSO AOD is biased towards lower values as compared to MODIS (Kim et al., 2013). Kittaka et al. (2011) found that the biases between them vary with season and are higher over land than ocean. The observed biases may due to various reasons, e.g., MODIS has a higher frequency than CALIPSO (Ma et al., 2013).

We also analyzed Absorbing Aerosol Index (AAI) from the Ozone Monitoring Instrument (OMI) launched in 2004 (Torres et al., 2007). The level 3 data for the period 2010–2020 were obtained from http://giovanni.gsfc.nasa.gov/giovanni/. MODIS fire data (https://firms.modaps.eosdis.nasa.gov/active_fire/) were used to plot the location of fires during March–April 2020. The fire data with a confidence level above 80 were used to locate the fires.

2.2 Reanalysis Data Sets

We also used the Copernicus Atmosphere Monitoring Service (CAMS) near-real-time observations of the location and intensity of active fires to estimate the emissions of pollutants. The Copernicus Atmosphere Monitoring Services (CAMS) uses wildfire as a general term to describe active vegetation fires detectable by the satellite. This also includes forest, grassland and peat fires, and open burning of agricultural waste (https://atmosphere.copernicus.eu/fire-monitoring). We referred to it as fires since during the lockdown period fires were mostly from agricultural burning. CAMS estimates are based on the Global Fire Assimilation System (GFAS). We also used the CAMS-derived fluxes of black carbon, organic carbon, total carbon, sulphate, ammonia, and particulate matter that have a diameter of less than 2.5 μm (PM2.5) for the period 2010–2020 (https://apps.ecmwf.int/datasets/data/cams-gfas/).

It should be noted that the horizontal resolution of all data sets used in this study (CALIPSO, MODIS, OMI, CAMS) is 1× 1 degree and for the period 2010–2020. We show changes in AOD, dust optical depth, and elevated smoke optical depth during the lockdown period in comparison to climatology (2010–2019). To check whether these changes are significantly different than climatology, we apply two-sided Student's t-test (Zimmerman, 1987; Walpole and Raymond, 2006). If the *p*-value is less than 0.05 (95% significance level), then we reject the null hypothesis and conclude that the differences are significant.

2.3 Radiative Transfer Model

The direct aerosol radiative forcing and heating rate are assessed through the one-dimensional parallel plane Fu-Liou-Gu (FLG) Radiative Transfer (RT) model (Fu and Liou, 1992; Fu and Liou, 1993; Gu et al., 2003; Gu et al., 2011; Lolli et al., 2019). The FLG RT code is initialized with the lidar vertically resolved CALIPSO optical depth profiles corresponding to the different aerosol species, which were matched to the Optical Properties of Aerosol and Clouds (OPAC) (D'Almeida et al., 1991; Tegen and Lacis, 1996; Hess et al., 1998). Catalog-based physical and optical models are embedded in the code (Gu et al., 2011). The number of levels of the RT model is adjusted to match CALIOP lidar resolution, i.e., the RT model and the vertically resolved lidar optical depth observation will have the same spatial resolution. The total aerosol radiative forcing is computed adding all contributions (in terms of optical depth) from the different aerosol species identified by the CALIPSO classification algorithm in the considered region and matched with the corresponding FLG aerosol species (Tosca et al., 2017).

From CALIOP data, among the 18 aerosol types parameterized within the FLG RT model from the OPAC catalog, we considered only the main two types of interest that match the CALIPSO classification: transported dust (CALIPSO: "dust") and black carbon (CALIPSO: "smoke"). To compute the radiative forcing at the top of the atmosphere and at the surface, the FLG RT model, which also accounts for aerosol hygroscopicity, solves the radiative fluxes at each level for 18 spectral bands (12 short-wave, 6 long-wave, Fu and Liou, 1992; Fu and Liou, 1993). Nevertheless, an important source of error (potential) is represented by Version 4 CALIOP aerosol types parameterization into FLG RT. The CALIPSO classification algorithm is not able to distinguish between local urban pollution and an advected smoke aerosol layer from distant sources that descend below 2.5 km. However, it is reasonable to suppose that those episodes are infrequent, but they can still occasionally introduce a bias in the analysis. For each annually averaged lidar extinction profile used as input in the FLG code, the aerosol direct radiative forcing (DRF) at the bottom of the atmosphere (surface) and top of the atmosphere (TOA) and the vertically resolved heating rate (HR) are computed. These estimates are obtained by subtracting the net radiative flux when the aerosols are present in the atmosphere from the net radiative flux obtained during pristine conditions, as shown in the following equation:

$$\mathrm{DRF, HR} = \mathrm{FLG}^{\mathrm{TotalSky}} - \mathrm{FLG}^{\mathrm{Pristine}}$$

The other data that are needed as input to the FLG model (i.e., the temperature, the atmospheric thermodynamic variable profiles, the ozone concentration, and the mixing ratio) are obtained from the tropical standard atmosphere (USS976). The FLG radiative transfer model also needs the Solar Zenith Angle (SZA) for the computation. We use SZA for each box at noon local time of the 15th day of that month. Following the approach used in Landi et al. (2021), we applied a constant (wavelength-independent) albedo value of 0.12 for urban environments, 0.15 for vegetated areas, and 0.37 for desertic regions (obtained integrating the hemispherical directional reflectance, Strahler et al., 1999) while the infrared surface emissivity is set to a constant value of 0.98.

3 RESULTS AND DISCUSSIONS

3.1 Impact on Aerosol Optical Depth

A significant reduction in AOD (~40%) over Western and Northern India during the lockdown period is evident from MODIS observations (**Figure 1A**). A similar reduction (a drop of ~45% in AOD with respect to climatology 2010–2019) is also

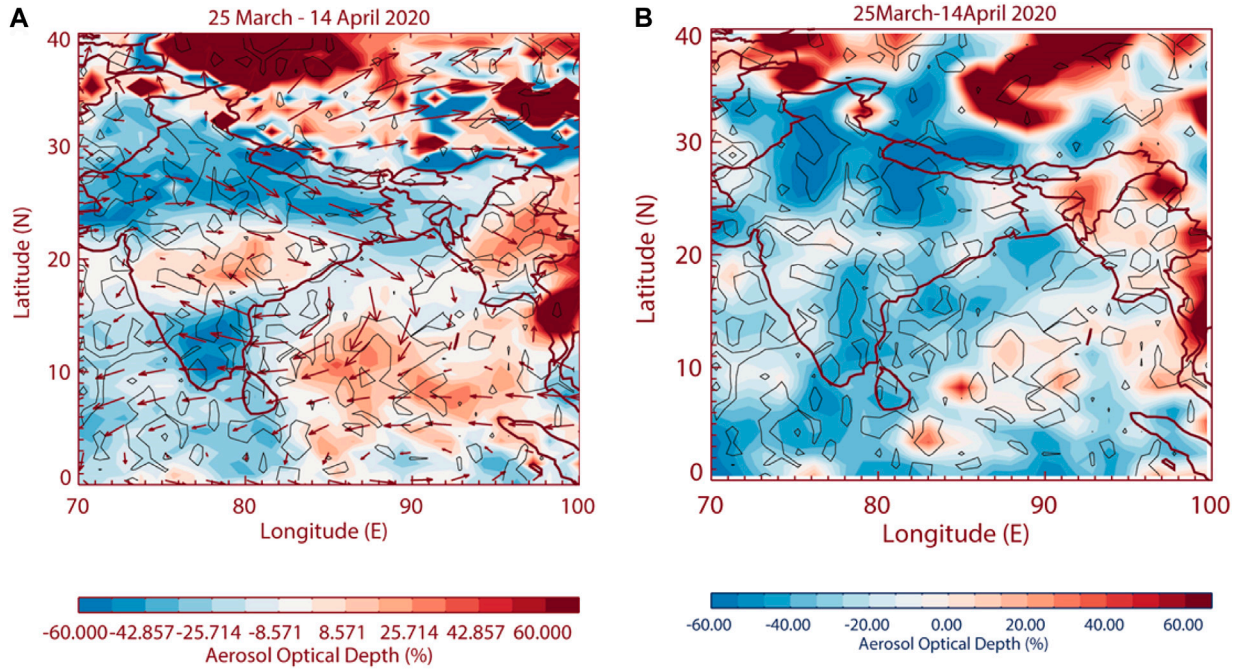

FIGURE 1 | (A) Spatial distribution of changes in AOD (2020-climatology) from MODIS at 550 nm (%) and wind vectors at 850 hPa averaged for the lockdown period (March 25–April 14, 2020) are also shown in **(A)**, **(B)** same as **(A)** but changes in AOD (2020-climatology) from CALIPSO at 532 nm. Contours in Panels **(A,B)** indicate 90% significance level.

showed by CALIPSO measurements over this region during the same period (**Figure 1B**). Recently, other studies also reported aerosol reduction over the parts of the Indian region during the lockdown period, e.g., Pathakoti et al. (2021) showed a decrease in AOD over the Indo-Gangetic plain by ~24% (climatology 2015–2019) using MODIS data. While a study by Sanap (2021) showed a reduction of aerosols (~16–27%) over north India (climatology 2000–2020). Mishra and Rathore (2021) also reported an overall decrease in AOD by 60% (in comparison to 2019) over the Indian landmass.

MODIS AOD (**Figure 1A**) shows enhancement (5–30%) over central India but it is faintly seen in CALIPSO (**Figure 1B**). It may be due to limited CALIPSO data (every 16 days overpass at the same location) during the lockdown period (Winker et al., 2007). The AOD enhancement over central India may be associated with aerosols emitted from fires (see discussions in **Section 3.2**). Interestingly, enhancement in AOD is also seen over the Bay of Bengal (12%) and parts of the North Arabian Sea (~22°N) (5%) in MODIS data (**Figure 1A**). The atmospheric circulation (wind at 850 hPa) indicates that aerosol loading over the Bay of Bengal is associated with transport from India and Myanmar regions. During spring, anthropogenic and dust aerosols are transported from the Indo-Gangetic Plain and Myanmar region to the Bay of Bengal (Nair et al., 2016). In agreement with our results, past studies show evidence of anthropogenic (Satheesh et al., 2001; Kumar et al., 2014; Nair et al., 2016) and dust (Lakshmi et al., 2017) aerosol loading over the Bay of Bengal during the spring season. Trajectory analysis-based studies also show that anthropogenic aerosols over the Bay of Bengal are associated with transport from the Indian region (Nair et al., 2016). The aerosol enhancement over the Arabian Sea is due to transport from West Asia (Lau and Kim 2006). During spring, westerly winds transport dust from West Asia to the Arabian Sea (Vinoj et al., 2014; Fadnavis et al., 2017b). However, in spring 2020 dust transport from West Asia was suppressed (Fadnavis et al., 2021). A small enhancement (5%) in AOD over the Arabian Sea may be due to the transport of small amounts of dust and biomass-burning aerosols from Saudi Arabia (**Figure 1A**) (Discussed in **Section 3.2**). The enhancement in AOD over the Bay of Bengal (85°E–95°E, 0°N–10°N) is smaller in CALIPSO measurements than MODIS (**Figure 1B**) and no enhancement is seen over the Arabian Sea. It may be due to limited CALIPSO data as mentioned above.

3.2 Distribution of Dust and Smoke Aerosols During Lockdown Period

We understand the influence of dust transport from West Asia on the Indian region which occurs in spring (Lau and Kim 2006), here we show the changes in dust during the lockdown period using CALIPSO measurements of dust optical depth and the OMI aerosol index (OMI-AAI). The OMI-AAI over the deep inland area indicates dust aerosols (Brooks et al., 2019). The CALIPSO dust optical depth and OMI-AAI shows a reduction of ~30% over the Indian region (**Figures 2A,B**). The Arabian Sea and Bay of Bengal regions show a widespread decrease (~20%) with pockets of a small enhancement in dust optical depth (~14%) and OMI-AAI (~20%) (**Figures 2A,B**). It shows that during the lockdown

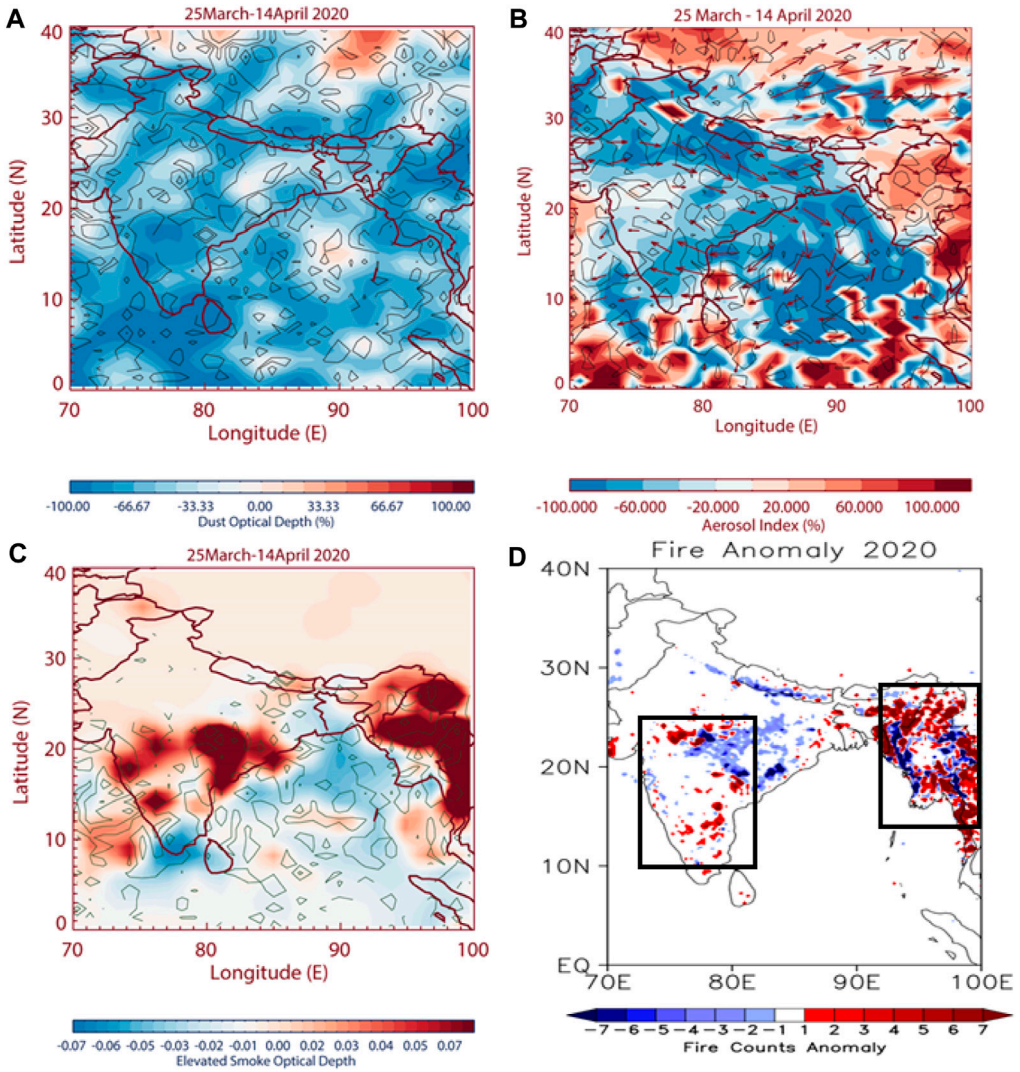

FIGURE 2 | (A) Spatial distribution of changes in dust optical depth (%) from CALIPSO at 532 nm, **(B)** spatial distribution of changes in OMI aerosol index (%), **(C)** same as **(A)** but for CALIPSO elevated smoke optical depth at 532 nm, **(D)** changes in fire counts distribution (2020-climatology) from MODIS. All the datasets are from the lockdown period March 25 to April 14. Contours in Panels **(A–C)** indicate a 95% significance level. Boxes (10°N–25°N; 72°E–81°E) in Panel **(D)** indicate the location of large numbers of fire anomalies.

period, in spring 2020, transport of dust from West Asia was lower than the climatology. The model simulations for COVID-19 anthropogenic emission changes also showed a reduction of dust aerosols over the Arabian Sea in the spring of 2020. These simulations showed that the anthropogenic emission reductions had induced changes in atmospheric circulation that inhibited the transport of dust from West Asia to the Tibetan Plateau during spring 2020 (Fadnavis et al., 2021).

Further, we show anomalies in the vertical distribution of elevated smoke aerosols from the CALIPSO measurements during the lockdown period in **Figure 2C**. The elevated smoke is a name of a CALIPSO product for smoke layers with tops higher than the 2.5 km above the planetary boundary layer (McGrath-Spangler and Denning 2013; Kim et al., 2018). It shows positive anomalies over different parts of India that may be due to the presence of local fires as well as the long-range transport of biomass-burning aerosols. A striking feature seen in **Figure 2C** is a large enhancement (an increase of 0.08–0.1 with respect to climatology) in elevated smoke optical depth over 1) the central peninsular (72°E–81°E, 10°N–25°N), 2) North-East-India-Myanmar region (93°E–100°E, 15°N–25°N), and a part of IGP (81°E–88°E, 26°N–31°N. Also, a high amount of smoke AOD is seen over eastern parts of central India (15°N–24°N; 77°E–82°E). Other parts of India also show a small enhancement in smoke optical depth that is substantially less than over the central peninsula, eastern-central India, and the North-East-India-Myanmar region (positive anomalies 0.02–0.03) above two regions. Smoke aerosols may be associated with the fire events hence we show anomalies of MODIS fire during the lockdown period (**Figure 2D**). **Figure 2D** shows negative anomalies over

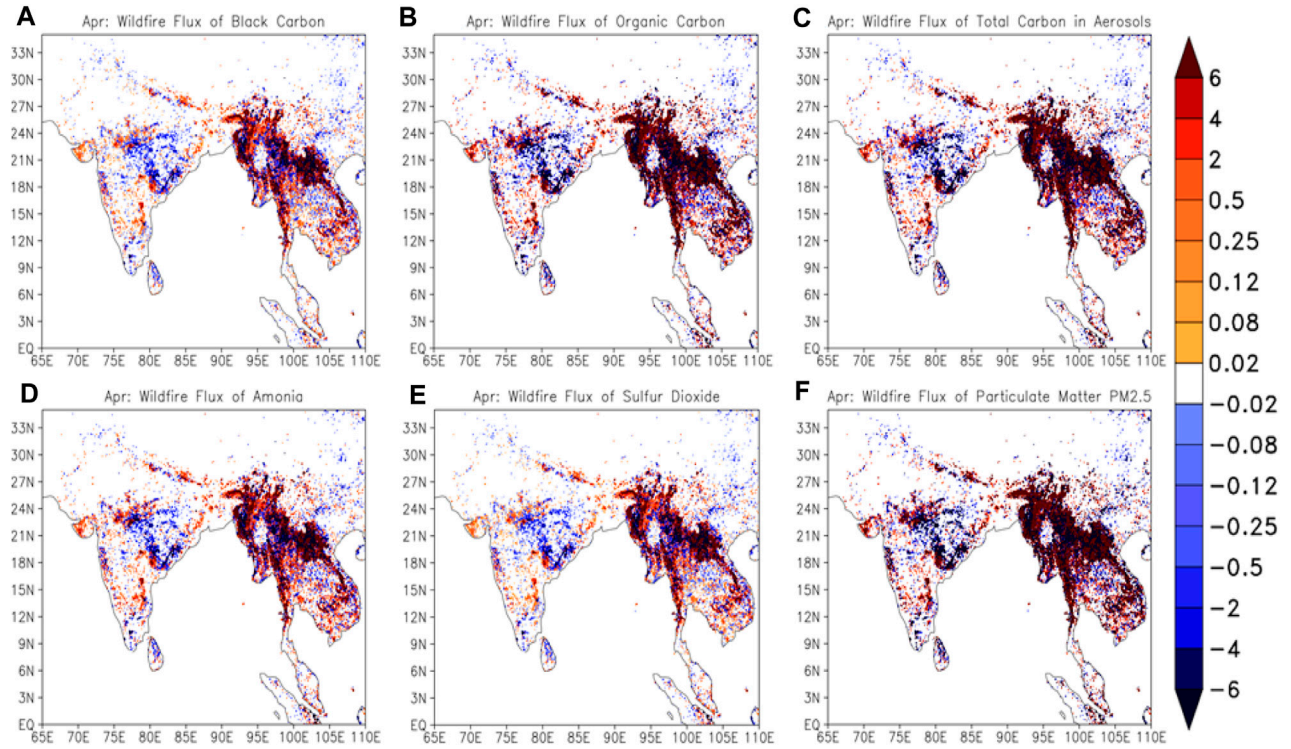

FIGURE 3 | (A–F): Fire flux (kg m^{-2} s^{-1}) data for black carbon, organic carbon, total carbon, ammonia, sulfur dioxide, and particulate matter (PM2.5) for the lockdown period.

North India (blue color) and positive anomalies over southern India, the Northeast-India-Myanmar region, and over central India (indicated by boxes in **Figure 2D**). The regions of dense fire are collocated with higher amounts of smoke optical depth (**Figure 2C**). The contribution to elevated smoke aerosol optical depth over central India is due to these local fires as well as the transport of smoke aerosols emitted from the surrounding regions. High amounts of smoke anomalies over the eastern parts of central India are due to transport (see circulation in **Figure 2B**) and not directly emitted by the fires, since the fire anomalies are negative over eastern parts of central India. Higher amounts of smoke aerosols (positive anomalies 0.04–0.06) are seen over the Arabian Sea. The wind vectors indicate this enhancement is due to transport from central India (**Figure 2C**).

3.3 Distribution of Fire Fluxes During Lockdown Period

In this section, we show anomalies in the fire fluxes of black carbon, organic carbon, ammonia, sulfur dioxide, particulate matter (PM2.5), and total carbon aerosols during the lockdown period (**Figures 3A–F**). Regions of positive anomalies (>1.5) are referred to as emission hotspots. The emission hotspots for organic carbon, black carbon, ammonia, sulphur dioxide fluxes (leads to the formation of sulfate aerosols), and particulate matter (PM 2.5) are collocated with the regions of dense fires during the lockdown (central peninsular and the North-East-India-Myanmar region). The positive anomalies of fire fluxes over southern India (**Figure 3**) are collocated with MODIS fire location (**Figure 2D**). This confirms that the increase in anomalous aerosol loading over 1) the central peninsular and 2) North-East-India-Myanmar region is due to fire emissions. **Figures 1–3** show that, although the contribution of anthropogenic aerosols had reduced, the smoke aerosols over the central peninsular and North-East-India-Myanmar region caused an enhancement in AOD over these regions (**Figures 1A,B**, **2C,D**).

3.4 Heating Rate and Radiative Forcing

Carbonaceous aerosols are key components of smoke that absorb solar radiation producing local atmospheric heating (Galanter et al., 2000; Zhang et al., 2020), while they produce a cooling effect on the climate *via* inhibiting solar radiation from reaching the surface (Shawki et al., 2018; Fadnavis et al., 2019b). During the lockdown period, enhanced smoke aerosols may have affected atmospheric heating. Here, we deliberate on heating rates and radiative forcing estimated from elevated smoke optical depth/profiles averaged for the lockdown period.

Figure 4A shows the spatial distribution of elevated smoke optical depth from CALIPSO at 532 nm during the lockdown period. It shows a high amount of elevated smoke optical depth (**Figure 2C**), over 1) the central-peninsular region and 2) Northeast-India-Myanmar region, and low smoke optical

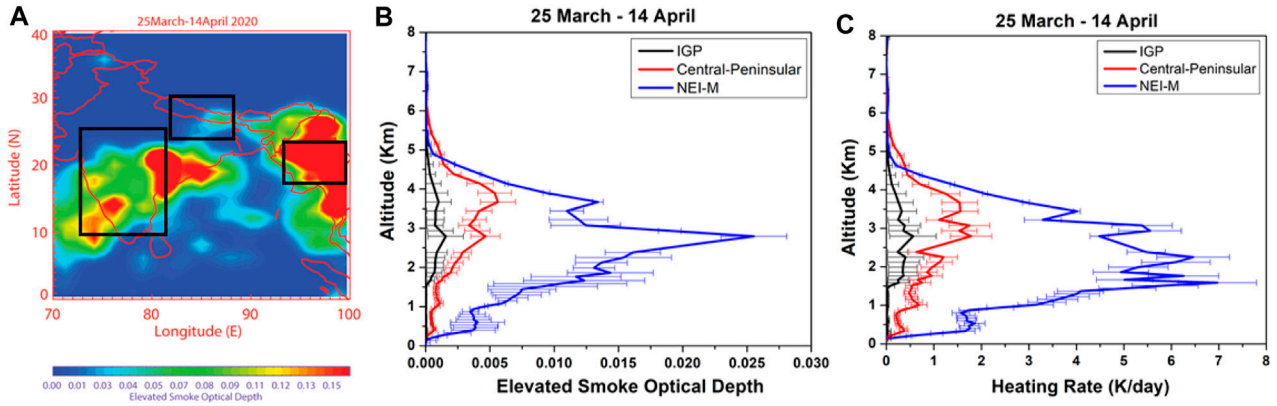

FIGURE 4 | (A) Spatial distribution of elevated smoke optical depth from CALIPSO, **(B)** profiles of elevated smoke optical depth averaged over the central peninsular, Northeast-India-Myanmar region, and IGP, **(C)** same as **(B)** but for heating rate (K/day). The horizontal lines in Panels **(B,C)** indicate standard deviation.

depth in 3) the IGP (depicted in **Figure 4A** by boxes). The high values of elevated smoke optical depth are also seen over eastern parts of central India due to transport (discussed in **Section 3.2**). Further we show vertical distribution of elevated smoke optical depth at the above three regions. There is a significant enhancement in elevated smoke aerosol optical depth (0.002 ± 0.001 to 0.0065 ± 0.002) in the lower troposphere (2–5 km) over the central-peninsular region and (0.008 ± 0.001 to 0.025 ± 0.003) over the Northeast-India-Myanmar region. The enhancement over the IGP is significantly less than the above-mentioned two regions due to comparatively fewer fires over the IGP. Interestingly, all three regions show an elevated layer of smoke aerosols between altitudes 2–5 km. The elevated layers of smoke aerosols corroborate well with the regions of high aerosol optical depths observed over the central-peninsular and Northeast-India-Myanmar regions (**Figure 3**). Our analysis shows that the mean contribution due to elevated smoke aerosols to altitudes ranging from 2 to 5 km is ~57% of the total columnar optical depth over the central peninsular and ~68% over the Northeast-India-Myanmar region. While elevated smoke aerosols over the IGP contributed ~18% to columnar optical depth the during lockdown period. Sarangi et al. (2016) reported the mean contribution of the aerosol layer from a 1.5–5.5 km altitude as ~51–60% to the total columnar aerosol optical depth for the years 2009–2011 during May–June over Kanpur.

Figure 4C shows profiles of heating rate estimated from CALIPSO observations of elevated smoke aerosols over 1) the central peninsular, 2) Northeast-India-Myanmar region, and 3) IGP. Heating rate profiles over the Northeast-India-Myanmar region show a higher amount of heating than over the central-peninsular region of India. It is quite evident that high amounts of elevated smoke aerosols during lockdown at altitudes between 2 and 5 km over the central peninsular have produced significant heating at 1.6 K/day ±0.5 K/day at those altitudes and ~6.5 K/day ±0.5 K/day heating over the Northeast-India-Myanmar region. The IGP region shows comparatively less heating at ~0.5 K/day ±0.3 K/day at those altitudes due to smaller amounts of smoke aerosols. Strong warming is seen locally in the altitudes corresponding to higher amounts of elevated smoke optical depth. Also, a large increase in the heating rates is noticed below the peak in the smoke aerosol profile. For example, a peak in heating rates over the central peninsular is seen at 3 km while smoke aerosols show a peak at 3.8 km. Similarly, over the Northeast-India-Myanmar region, heating rates are maximum at 2.2 km while the aerosol profile has a peak at 2.8 km. This indicates that the peak in smoke aerosols and heating rates occurs at different altitudes. This may be due to aerosol heating occurring within a layer of atmosphere that retains and changes pressure values (Tripathi et al., 2007). Past studies showed enhancement in carbonaceous aerosols and increases in the heating rates by 0.08 K/day in the lower troposphere over India (Fadnavis et al., 2017a). The annual mean atmospheric heating rate due to the BC aerosols was 0.86 K/day over the Guwahati region during 2014. Pani et al. (2018) estimated atmospheric heating of ~1.4–3.6 K/day due to biomass-burning aerosols in the dry season over a station in southeast Asia.

Aerosol radiative forcing is defined as the net radiative change by aerosols present in the Earth system. Aerosols significantly impact the regional climate and this phenomenon has been largely studied (IPCC, 2014; Vinoj et al., 2014; Fadnavis et al., 2019a). Decoupling the elevated smoke aerosol optical depth from the atmospheric column, we estimate the biomass burning radiative forcing at the surface and top of the atmosphere (TOA) over 1) the central peninsular, 2) Northeast-India-Myanmar region, and 3) Indo-Gangetic Plain averaged for the lockdown period (**Figure 5**). The estimated radiative forcing at the TOA shows warming of ~4.8 W/m^2 over the central-peninsular region, ~15 W/m^2 over the Northeast-India-Myanmar region, and ~1 W/m^2 over the IGP. The lower-tropospheric warming caused by elevated smoke aerosols has an implication on atmospheric circulation and cloud cover (Fadnavis et al., 2017b; Fadnavis et al., 2019b).

The estimated surface radiative forcing due to smoke aerosols over the central-peninsular region is ~−38 W/m^2 (±15 W/m^2), ~−152 W/m^2 (±50 W/m^2) over the North-India-Myanmar

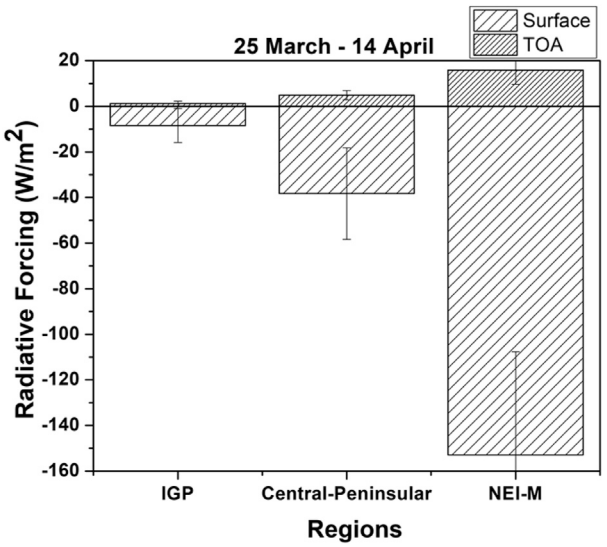

FIGURE 5 | Radiative forcing at the top of the atmosphere (TOA) and at the surface over central India, the Northeast-India-Myanmar region (NEI-M), and IGP. Vertical bars indicate standard deviation.

region, and ~−8 W/m^2 (±9 W/m^2) over the IGP. The amount of radiative forcing at the TOA (positive) and surface (negative) over the three regions is proportional to the amount of smoke aerosol, e.g., a large amount of smoke aerosols in the North-India-Myanmar region has imposed higher radiative impacts there than in the central peninsula and IGP (higher amount of surface cooling and warming at the TOA). All the three regions show warming in the atmosphere (in-atmospheric radiative forcing, TOA-surface), central India: ~73 W/m^2 (±40 W/m^2), North-India-Myanmar region: ~167 W/m^2 (±50 W/m^2), and IGP: ~9 W/m^2 (±9 W/m^2).

A previous study also showed positive radiative forcing due to black carbon aerosols at the top of the atmosphere (~5 W/m^2 over Bangalore, ~9.5 W/m^2 over Guwahati), negative radiative forcing at the surface (~−23 W/m^2 over Bangalore and ~−21.1 W/m^2 over Guwahati), and in-atmospheric warming (~27 W/m^2 ± 9 W/m^2 over the Indian region) (Babu et al., 2002; Tiwari et al., 2016; Nair et al., 2017).

Importantly, these studies show that smoke/carbonaceous aerosols produce positive radiative forcing at the top of the atmosphere, negative radiative forcing at the surface, and in-atmospheric warming is agreement with our results. The atmospheric heating generated by smoke aerosols has implications on atmospheric circulation and cloud cover while the surface cooling might have effects on the precipitation changes (Lohmann and Feichter, 2005; Ward et al., 2012).

4 CONCLUSION

Diagnostic analysis of multiple data sets from Moderate Resolution Imaging Spectroradiometer (MODIS), Ozone Monitoring Instrument (OMI), Cloud-Aerosol Lidar, and Infrared Pathfinder (CALIPSO), and Copernicus Atmosphere Monitoring Service (CAMS) during the lockdown period, March 25–April 14, 2020, showed that aerosols, in general, had reduced over north India, but there was an aerosol enhancement over central India and the Northeast-India-Myanmar region. This aerosol enhancement was due to fires. The fire-emitted smoke aerosols formed a layer at altitudes ranging from 2 to 5 km with subsequent enhancement in the aerosol optical depth of 0.002–0.005 over the central peninsular and 0.008–0.025 over the Northeast-India-Myanmar region. The fires and smoke aerosols, both, were comparatively less over the IGP.

Elevated smoke aerosols have produced heating locally in the altitudes corresponding to the higher amount of elevated smoke optical depth. Also, a large increase in the heating rates is noticed below the peak in the smoke aerosol profile. For example, a peak in heating rates over central India is seen at 3 km while smoke aerosols show a peak at 3.5 km. Similarly, over the Northeast-India-Myanmar region, heating rates were maximum at 2.2 km while aerosol profiles peaked at 2.8 km. In general, heating of ~1.6 K/day is seen over the central peninsula, ~6 K/day over the Northeast-India-Myanmar region, and ~0.3 K/day over the IGP. The smoke aerosols produced significant radiative impacts, warming effects at the top of the atmosphere, radiative forcing of ~4.8 W/m^2 in the central peninsula and ~15 W/m^2 in the Northeast-India-Myanmar region. The radiative forcing over the IGP was comparatively less (1 W/m^2) than the other two regions. A layer of smoke aerosol had produced a cooling effect at the surface over the Indian region (surface radiative forcing of ~−38 W/m^2 over the central peninsula, ~ −152 W/m^2 over the Northeast-India-Myanmar region, and −8 W/m^2 over the IGP) and warming in the atmosphere (central peninsula: ~42.8 W/m^2 (±15W/m^2), North-India-Myanmar region: ~167 W/m^2 (±50 W/m^2), and IGP: ~9 W/m^2 (±9 W/m^2). Thus, our study shows that significant atmospheric warming was produced by the smoke produced from fires, although anthropogenic aerosols were reduced during the lockdown period. Atmospheric warming has implications on circulation and precipitation (Fadnavis et al., 2021) and heats the lower atmosphere which causes in-cloud heating and changes in cloud albedos.

DATA AVAILABILITY STATEMENT

The original contributions presented in the study are included in the article/Supplementary Material, further inquiries can be directed to the corresponding author.

AUTHOR CONTRIBUTIONS

This article is the combined effort of all the authors. RB and SF formulated and wrote the article, with contributions from all co-authors. VK, PR, TS, and SL contributed to the analysis. SL carried computation of heating rates and radiative forcing using a radiative transfer model.

ACKNOWLEDGMENTS

The authors thank all the reviewers for useful comments which helped improve the paper drastically. The author RB acknowledges with gratitude the Department of Science and Technology (DST), GoI, and Indo-US Science and Technology Forum (IUSSTF) for providing a WISTEMM Fellowship when the work was initiated. She also acknowledges the Ministry of Earth Sciences (MoES) as the data used and analyzed to prepare the paper were funded from this project. The UGC-FRP. CALIPSO, MODIS, OMI, and CAMS database teams and NASA websites from where data were downloaded are also acknowledged.

REFERENCES

Babu, S. S., Satheesh, S. K., and Moorthy, K. K. (2002). Aerosol Radiative Forcing Due to Enhanced Black Carbon at an Urban Site in India. *Geophys. Res. Lett.* 29), 1880. doi:10.1029/2002GL015826

Brooks, J., Allan, J. D., Williams, P. I., Liu, D., Fox, C., Haywood, J., et al. (2019). Vertical and Horizontal Distribution of Submicron Aerosol Chemical Composition and Physical Characteristics across Northern India during Pre-monsoon and Monsoon Seasons. *Atmos. Chem. Phys.* 19, 5615–5634. doi:10.5194/acp-19-5615-2019

Chauhan, A., and Singh, R. P. (2020). Decline in PM2.5 Concentrations Over Major Cities Around the World Associated with COVID-19. *Environ. Res.* 187, 109634. doi:10.1016/j.envres.2020.109634

D'Errico, M., Cagnazzo, C., Fogli, P. G., Lau, W. K. M., Hardenberg, J., Fierli, F., et al. (2015). Indian Monsoon and the Elevated-heat-pump Mechanism in a Coupled Aerosol-Climate Model. *J. Geophys. Res. Atmos.* 120, 8712–8723. doi:10.1002/2015JD023346

D'Almeida, G. A., Koepke, P., and Shettle, E. P. (1991). *Atmospheric Aerosol: Global Climatology and Radiative Characteristics*. Hampton, Va: A. Deepak.

Das, M., Das, A., Sarkar, R., Saha, S., and Mandal, A. (2021). Examining the Impact of Lockdown (Due to COVID-19) on Ambient Aerosols (PM2.5): A Study on Indo-Gangetic Plain (IGP) Cities, India. *Stoch Environ. Res. Risk Assess.* 35, 1301–1317. doi:10.1007/s00477-020-01905-x

David, L. M., Ravishankara, A. R., Kodros, J. K., Pierce, J. R., Venkataraman, C., and Sadavarte, P. (2019). Premature Mortality Due to PM2.5Over India: Effect of Atmospheric Transport and Anthropogenic Emissions. *GeoHealth* 3, 2–10. doi:10.1029/2018gh000169

Dey, S., Di Girolamo, L., van Donkelaar, A., Tripathi, S. N., Gupta, T., and Mohan, M. (2012). Variability of Outdoor fine Particulate (PM2.5) Concentration in the Indian Subcontinent: A Remote Sensing Approach. *Remote sensing Environ.* 127, 153–161. doi:10.1016/j.rse.2012.08.021

Fadnavis, S., Sabin, T. P., Rap, A., Müller, R., Kubin, A., and Heinold, B. (2021). The Impact of COVID-19 Lockdown Measures on the Indian Summer Monsoon. *Environ. Res. Lett.* 16, 074054. doi:10.1088/1748-9326/ac109c

Fadnavis, S., Kalita, G., Kumar, K. R., Gasparini, B., and Li, J.-L. F. (2017b). Potential Impact of Carbonaceous Aerosol on the Upper Troposphere and Lower Stratosphere (UTLS) and Precipitation during Asian Summer Monsoon in a Global Model Simulation. *Atmos. Chem. Phys.* 17, 11637–11654. doi:10.5194/acp-17-11637-2017

Fadnavis, S., Müller, R., Kalita, G., Rowlinson, M., Rap, A., Li, J.-L. F., et al. (2019a). The Impact of Recent Changes in Asian Anthropogenic Emissions of SO_2 on Sulfate Loading in the Upper Troposphere and Lower Stratosphere and the Associated Radiative Changes. *Atmos. Chem. Phys.* 19, 9989–10008. doi:10.5194/acp-19-9989-2019

Fadnavis, S., Roy, C., Sabin, T. P., Ayantika, D. C., and Ashok, K. (2017a). Potential Modulations of Pre-Monsoon Aerosols during El Niño: Impact on Indian Summer Monsoon. *Clim. Dyn.* 49, 2279–2290. doi:10.1007/s00382-016-3451-6

Fadnavis, S., Sabin, T. P., Roy, C., Rowlinson, M., Rap, A., Vernier, J.-P., et al. (2019b). Elevated Aerosol Layer over South Asia Worsens the Indian Droughts. *Sci. Rep.* 9, 10268. doi:10.1038/s41598-019-46704-9

Fadnavis, S., Semeniuk, K., Pozzoli, L., Schultz, M. G., Ghude, S. D., Das, S., et al. (2013). Transport of Aerosols into the UTLS and Their Impact on the Asian Monsoon Region as Seen in a Global Model Simulation. *Atmos. Chem. Phys.* 13, 8771–8786. doi:10.5194/acp-13-8771-2013

Fu, Q., and Liou, K. N. (1992). On the Correlatedk-Distribution Method for Radiative Transfer in Nonhomogeneous Atmospheres. *J. Atmos. Sci.* 49, 2139–2156. doi:10.1175/1520-0469(1992)049<2139:otcdmf>2.0.co;2

Fu, Q., and Liou, K. N. (1993). Parameterization of the Radiative Properties of Cirrus Clouds. *J. Atmos. Sci.* 50, 2008–2025. doi:10.1175/1520-0469(1993)050<2008:potrpo>2.0.co;2

Galanter, M., Levy, H., and Carmichael, G. R. (2000). Impacts of Biomass Burning on Tropospheric CO, NOx, and O3. *J. Geophys. Res.* 105, 6633–6653. doi:10.1029/1999jd901113

Gautam, S. (2020). COVID-19: Air Pollution Remains Low as People Stay at home. *Air Qual. Atmos. Health* 13, 853–857. doi:10.1007/s11869-020-00842-6

Gu, Y., Farrara, J., Liou, K. N., and Mechoso, C. R. (2003). Parameterization of Cloud-Radiation Processes in the UCLA General Circulation Model. *J. Clim.* 16, 3357–3370. doi:10.1175/1520-0442(2003)016<3357:pocpit>2.0.co;2

Gu, Y., Liou, K. N., Ou, S. C., and Fovell, R. (2011). Cirrus Cloud Simulations Using WRF with Improved Radiation Parameterization and Increased Vertical Resolution. *J. Geophys. Res.* 116, D06119. doi:10.1029/2010JD014574

Guttikunda, S. K., Goel, R., and Pant, P. (2014). Nature of Air Pollution, Emission Sources, and Management in the Indian Cities. *Atmos. Environ.* 95, 501–510. doi:10.1016/j.atmosenv.2014.07.006

Hama, S. M. L., Kumar, P., Harrison, R. M., Bloss, W. J., Khare, M., Mishra, S., et al. (2020). Four-year Assessment of Ambient Particulate Matter and Trace Gases in theDelhi-NCR Region of India. *Sustain. Cities Soc.* 54, 102003. doi:10.1016/j.scs.2019.102003

Hammer, M. S., van Donkelaar, A., Li, C., Lyapustin, A., Sayer, A. M., Hsu, N. C., et al. (2020). Global Estimates and Long-Term Trends of Fine Particulate Matter Concentrations (1998-2018). *Environ. Sci. Technol.* 54 (13), 7879–7890. doi:10.1021/acs.est.0c01764

Hess, M., Koepke, P., and Schult, I. (1998). Optical Properties of Aerosols and Clouds: The Software Package OPAC. *Bull. Amer. Meteorol. Soc.* 79, 831–844. doi:10.1175/1520-0477(1998)079<0831:opoaac>2.0.co;2

Hsu, N. C., Jeong, M.-J., Bettenhausen, C., Sayer, A. M., Hansell, R., Seftor, C. S., et al. (2013). Enhanced Deep Blue Aerosol Retrieval Algorithm: the Second Generation. *J. Geophys. Res. Atmos.* 118 (16), 9296–9315. doi:10.1002/jgrd.50712

Hunt, W. H., Winker, D. M., Vaughan, M. A., Powell, K. A., Lucker, P. L., and Weimer, C. (2009). CALIPSO Lidar Description and Performance Assessment. *J. Atmos. Oceanic Technol.* 26, 1214–1228. doi:10.1175/2009JTECHA1223.1

IHME Report (2019). Health and Economic Impact of Air Pollution in the States of India: The Global Burden of Disease Study 2019. *Lancet Planet. Health* 5, e25–38. doi:10.1016/S2542-5196(20)30298-9

IPCC (2014). *Climate Change 2014: Synthesis Report. Contribution of Working Groups I, II and III to the Fifth Assessment Report of the Intergovernmental Panel on Climate Change. Lancet Planet. Health*. Editors R. K. Pachauri and L. A. Meyer (Geneva, Switzerland: IPCC), 151.

Jain, S., and Sharma, T. (2020). Social and Travel Lockdown Impact Considering Coronavirus Disease (COVID-19) on Air Quality in Megacities of India: Present Benefits, Future Challenges and Way Forward. *Aerosol Air Qual. Res.* 20, 1222–1236. doi:10.4209/aaqr.2020.04.0171

Jethva, H., Torres, O., Field, R. D., Lyapustin, A., Gautam, R., and Kayetha, V. (2019). Connecting Crop Productivity, Residue Fires, and Air Quality over Northern India. *Sci. Rep.* 9 (1), 16594. doi:10.1038/s41598-019-52799-x

Jiang, Z., Shi, H., Zhao, B., Gu, Y., Zhu, Y., Miyazaki, K., et al. (2021). Modeling the Impact of COVID-19 on Air Quality in Southern California: Implications for Future Control Policies. *Atmos. Chem. Phys.* 21, 8693–8708. doi:10.5194/acp-21-8693-2021

Kaskaoutis, D. G., Grivas, G., Liakakou, E., Kalivitis, N., Kouvarakis, G., Stavroulas, I., et al. (2021). Assessment of the COVID-19 Lockdown Effects on Spectral Aerosol Scattering and Absorption Properties in Athens, Greece. *Atmosphere* 12, 231. doi:10.3390/atmos12020231

Kim, M.-H., Kim, S.-W., Yoon, S.-C., and Omar, A. H. (2013). Comparison of Aerosol Optical Depth between CALIOP and MODIS-AQUA for CALIOP

Aerosol Subtypes over the Ocean. *J. Geophys. Res. Atmos.* 118, 13241–13252. doi:10.1002/2013JD019527

Kim, M.-H., Omar, A. H., Tackett, J. L., Vaughan, M. A., Winker, D. M., Trepte, C. R., et al. (2018). The CALIPSO Version 4 Automated Aerosol Classification and Lidar Ratio Selection Algorithm. *Atmos. Meas. Tech.* 11, 6107–6135. doi:10.5194/amt-11-6107-2018

Kittaka, C., Winker, D. M., Vaughan, M. A., Omar, A., and Remer, L. A. (2011). Intercomparison of Column Aerosol Optical Depths from CALIPSO and MODIS-Aqua. *Atmos. Meas. Tech.* 4, 131–141. doi:10.5194/amt-4-131-2011

Krishna Moorthy, K., Suresh Babu, S., Manoj, M. R., and Satheesh, S. K. (2013). Buildup of Aerosols over the Indian Region. *Geophys. Res. Lett.* 40, 1011–1014. doi:10.1002/grl.50165

Kumar, R., Barth, M. C., Madronich, S., Naja, M., Carmichael, G. R., Pfister, G. G., et al. (2014). Effects of Dust Aerosols on Tropospheric Chemistry during a Typical Pre-monsoon Season Dust Storm in Northern India. *Atmos. Chem. Phys.* 14 (13), 6813–6834. doi:10.5194/acp-14-6813-2014

Lakshmi, N. B., Nair, V. S., and Suresh Babu, S. (2017). Vertical Structure of Aerosols and mineral Dust over the Bay of Bengal from Multisatellite Observations. *J. Geophys. Res. Atmos.* 122, 12,845–12,861. doi:10.1002/2017JD027643

Landi, T., Bonasoni, P., Brunetti, M., Campbell, J., Marquis, J., Di Girolamo, P., et al. (2021). Aerosol Direct Radiative Effects under Cloud-Free Conditions over Highly-Polluted Areas in Europe and Mediterranean: A Ten-Years Analysis (2007-2016). *Remote Sensing* 13 (15), 2933. doi:10.3390/rs13152933

Lau, K.-M., and Kim, K.-M. (2006). Observational Relationships between Aerosol and Asian Monsoon Rainfall, and Circulation. *Geophys. Res. Lett.* 33, L21810. doi:10.1029/2006GL027546

Le Quéré, C., Jackson, R. B., Jones, M. W., Smith, A. J. P., Abernethy, S., Andrew, R. M., et al. (2020). Temporary Reduction in Daily Global CO2 Emissions during the COVID-19 Forced Confinement. *Nat. Clim. Chang.* 10 (7), 647–653. doi:10.1038/s41558-020-0797-x

Levy, R. C., Mattoo, S., Munchak, L. A., Remer, L. A., Sayer, A. M., Patadia, F., et al. (2013). The Collection 6 MODIS Aerosol Products over Land and Ocean. *Atmos. Meas. Tech.* 6, 2989–3034. doi:10.5194/amt-6-2989-2013

Lohmann, U., and Feichter, J. (2005). Global Indirect Aerosol Effects: A Review. *Atmos. Chem. Phys.* 5, 715–737. doi:10.5194/acp-5-715-2005

Lolli, S., Chen, Y.-C., Wang, S.-H., and Vivone, G. (2020). Impact of Meteorological Conditions and Air Pollution on COVID-19 Pandemic Transmission in Italy. *Sci. Rep.* 10, 16213. doi:10.1038/s41598-020-73197-8

Lolli, S., Khor, W. Y., Matjafri, M. Z., and Lim, H. S. (2019). Monsoon Season Quantitative Assessment of Biomass Burning Clear-Sky Aerosol Radiative Effect at Surface by Ground-Based Lidar Observations in Pulau Pinang, Malaysia in 2014. *Remote Sensing* 11, 2660. doi:10.3390/rs11222660

Lolli, S., and Vivone, G. (2020). The Role of Tropospheric Ozone in Flagging COVID-19 Pandemic Transmission. *Bull. Atmos. Sci. Technol.* 1, 551–555. doi:10.1007/s42865-020-00026-1

Ma, X., Bartlett, K., Harmon, K., and Yu, F. (2013). Comparison of AOD between CALIPSO and MODIS: Significant Differences Over Major Dust and Biomass Burning Regions. *Atmos. Meas. Tech.* 6, 2391–2401. doi:10.5194/amt-6-2391-2013

McGrath-Spangler, E. L., and Denning, A. S. (2013). Global Seasonal Variations of Midday Planetary Boundary Layer Depth from CALIPSO Space-Borne LIDAR. *J. Geophys. Res. Atmos.* 118, 1226–1233. doi:10.1002/jgrd.50198

Meehl, G. A., Washington, W. M., Arblaster, J. M., Hu, A., Teng, H., Kay, J. E., et al. (2013). Climate Change Projections in CESM1(CAM5) Compared to CCSM4. *J. Clim.* 26, 6287–6308. doi:10.1175/JCLI-D-12-00572.1

Mishra, M. K., and Rathore, P. S. (2021). Impact of Nationwide COVID-19 Lockdown on Indian Air Quality in Terms of Aerosols as Observed from the Space. *Aerosol Air Qual. Res.* 21, 200461. doi:10.4209/aaqr.2020.07.0461

Nair, V. S., Babu, S. S., Gogoi, M. M., and Moorthy, K. K. (2016). Large-scale Enhancement in Aerosol Absorption in the Lower Free Troposphere over continental India during spring. *Geophys. Res. Lett.* 43, 11453–11461. doi:10.1002/2016GL070669

Nair, V. S., Babu, S. S., Manoj, M. R., Moorthy, K. K., and Chin, M. (2017). Direct Radiative Effects of Aerosols over South Asia from Observations and Modeling. *Clim. Dyn.* 49, 1411–1428. doi:10.1007/s00382-016-3384-0

Paital, B. (2020). Nurture to Nature via COVID-19, a Self-Regenerating Environmental Strategy of Environment in Global Context. *Sci. Total Environ.* 729, 139088. doi:10.1016/j.scitotenv.2020.139088

Pandey, S. K., and Vinoj, V. (2021). Surprising Changes in Aerosol Loading over India amid COVID-19 Lockdown. *Aerosol Air Qual. Res.* 21, 200466. doi:10.4209/aaqr.2020.07.0466

Pani, S. K., Lin, N.-H., Chantara, S., Wang, S.-H., Khamkaew, C., Prapamontol, T., et al. (2018). Radiative Response of Biomass-Burning Aerosols over an Urban Atmosphere in Northern Peninsular Southeast Asia. *Sci. Total Environ.* 633, 892–911. doi:10.1016/j.scitotenv.2018.03.204

Pathakoti, M., Muppalla, A., Hazra, S., Mahalakshmi, D. V., Sagar, K. K. V., Shekhar, R., et al. (2021). Measurement Report: An Assessment of the Impact of a Nationwide Lockdown on Air Pollution – a Remote Sensing Perspective over India. *Atmos. chem. Phys.* doi:10.5194/acp-21-9047-2021

Report by Indian Council of Medical Research (2017). ISBN: 978-81-910091-94.

Sanap, S. D. (2021). Global and Regional Variations in Aerosol Loading during COVID-19 Imposed Lockdown. *Atmos. Environ.* 246, 118132. doi:10.1016/j.atmosenv.2020.118132

Sarangi, C., Tripathi, S. N., Mishra, A. K., Goel, A., and Welton, E. J. (2016). Elevated Aerosol Layers and Their Radiative Impact over Kanpur during Monsoon Onset Period. *J. Geophys. Res. Atmos.* 121, 7936–7957. doi:10.1002/2015JD024711

Satheesh, S. K., Moorthy, K. K., and Das, I. (2001). Aerosol Optical Depths Over Bay of Bengal, Indian Ocean and Arabian Sea. *Curr. Sci.* 81, 1617–1625.

Shawki, D., Voulgarakis, A., Chakraborty, A., Kasoar, M., and Srinivasan, J. (2018). The South Asian Monsoon Response to Remote Aerosols: Global and Regional Mechanisms. *J. Geophys. Res. Atmos.* 123, 11585–11601. doi:10.1029/2018JD028623

Shukla, N., Sharma, G. K., Baruah, P., Shukla, V. K., and Gargava, P. (2020). Impact of Shutdown Due to COVID-19 Pandemic on Aerosol Characteristics in Kanpur, India. *J. Health Pollut.* 10 (28), 201201. doi:10.5696/2156-9614-10.28.201201

Singh, T., Ravindra, K., Sreekanth, V., Gupta, P., Sembhi, H., Tripathi, S. N., et al. (2020). Climatological Trends in Satellite-Derived Aerosol Optical Depth over North India and its Relationship with Crop Residue Burning: Rural-Urban Contrast. *Sci. Total Environ.* 748, 140963. doi:10.1016/j.scitotenv.2020.140963

Spears, D., Dey, S., Chowdhury, S., Scovronick, N., Vyas, S., and Apte, J. (2019). The Association of Early-Life Exposure to Ambient PM2.5 and Later-Childhood Height-For-Age in India: an Observational Study. *Environ. Health* 18, 62. doi:10.1186/s12940-019-0501-7

Strahler, A. H., Muller, J., Lucht, W., Schaaf, C., Tsang, T., Gao, F., et al. (1999). MODIS BRDF/albedo Product: Algorithm Theoretical Basis Document Version 5.0. *MODIS documentation* 23 (4), 42–47.

Tackett, J. L., Winker, D. M., Getzewich, B. J., Vaughan, M. A., Young, S. A., and Kar, J. (2018). CALIPSO Lidar Level 3 Aerosol Profile Product: Version 3 Algorithm Design. *Atmos. Meas. Tech.* 11, 4129–4152. doi:10.5194/amt-11-4129-2018

Tegen, I., and Lacis, A. A. (1996). Modeling of Particle Size Distribution and its Influence on the Radiative Properties of mineral Dust Aerosol. *J. Geophys. Res.* 101, 19237–19244. doi:10.1029/95jd03610

Thomas, A., Sarangi, C., and Kanawade, V. P. (2019). Recent Increase in Winter Hazy Days over Central India and the Arabian Sea. *Sci. Rep.* 9, 17406. doi:10.1038/s41598-019-53630-3

Tiwari, S., Hopke, P. K., Attri, S. D., Soni, V. K., and Singh, A. K. (2016). Variability in Optical Properties of Atmospheric Aerosols and Their Frequency Distribution over a Mega City "New Delhi," India. *Environ. Sci. Pollut. Res.* 23 (9), 8781–8793. doi:10.1007/s11356-016-6060-3

Torres, O., Tanskanen, A., Veihelmann, B., Ahn, C., Braak, R., Bhartia, P. K., et al. (2007). Aerosols and Surface UV Products from Ozone Monitoring Instrument Observations: An Overview. *J. Geophys. Res.* 112, D24S47. doi:10.1029/2007JD008809

Tosca, M., Campbell, J., Garay, M., Lolli, S., Seidel, F., Marquis, J., et al. (2017). Attributing Accelerated Summertime Warming in the Southeast United States to Recent Reductions in Aerosol Burden: Indications from Vertically-Resolved Observations. *Remote Sensing* 9, 674. doi:10.3390/rs9070674

Tripathi, S. N., Srivastava, A. K., Dey, S., Satheesh, S. K., and Krishnamoorthy, K. (2007). The Vertical Profile of Atmospheric Heating Rate of Black Carbon Aerosols at Kanpur in Northern India. *Atmos. Environ.* 41, 6909–6915. doi:10.1016/j.atmosenv.2007.06.032

Vinoj, V., Rasch, P. J., Yoon, H. J.-H., Landu, P.-L. K., and Singh, B. (2014). Short-term Modulation of Indian Summer Monsoon Rainfall by West Asian Dust. *Nat. Geosci.* 7, 308–313. doi:10.1038/ngeo2107

Walpole, R. E., and Raymond, M. H. (2006). *Probability & Statistics for Engineers & Scientists*. 7th ed. New Delhi: Pearson. ISBN 81-7758-404-9. OCLC 818811849.

Ward, D. S., Kloster, S., Mahowald, N. M., Rogers, B. M., Randerson, J. T., and Hess, P. G. (2012). The Changing Radiative Forcing of Fires: Global Model Estimates for Past, Present and Future. *Atmos. Chem. Phys.* 12, 10857–10886. doi:10.5194/acp-12-10857-2012

Wei, J., Li, Z., Peng, Y., and Sun, L. (2019a). MODIS Collection 6.1 Aerosol Optical Depth Products over Land and Ocean: Validation and Comparison. *Atmos. Environ.* 201, 428–440. doi:10.1016/j.atmosenv.2018.12.004

Wei, J., Li, Z., Sun, L., Peng, Y., and Wang, L. (2019b). Improved Merge Schemes for MODIS Collection 6.1 Dark Target and Deep Blue Combined Aerosol Products. *Atmos. Environ.* 202, 315–327. doi:10.1016/j.atmosenv.2019.01.016

Winker, D. M., Hunt, W. H., and McGill, M. J. (2007). Initial Performance Assessment of CALIOP. *Geophys. Res. Lett.* 34, L19803. doi:10.1029/2007GL030135

Winker, D. M., Pelon, J., Coakley, J. A., Jr., Ackerman, S. A., Charlson, R. J., Colarco, P. R., et al. (2010). The CALIPSO Mission. *Bull. Amer. Meteorol. Soc.* 91, 1211–1230. doi:10.1175/2010BAMS3009.1

Young, S. A., Vaughan, M. A., Garnier, A., Tackett, J. L., Lambeth, J. D., and Powell, K. A. (2018). Extinction and Optical Depth Retrievals for CALIPSO's Version 4 Data Release. *Atmos. Meas. Tech.* 11, 5701–5727. doi:10.5194/amt-11-5701-2018

Yunus, A. P., Masago, Y., and Hijioka, Y. (2020). COVID-19 and Surface Water Quality: Improved lake Water Quality during the Lockdown. *Sci. Total Environ.* 731, 139012. doi:10.1016/j.scitotenv.2020.139012

Zhang, Y., Li, Z., Chen, Y., de Leeuw, G., Zhang, C., Xie, Y., et al. (2020). Improved Inversion of Aerosol Components in the Atmospheric Column from Remote Sensing Data. *Atmos. Chem. Phys.* 20, 12795–12811. doi:10.5194/acp-20-12795-2020

Zimmerman, D. W. (1987). Comparative Power of StudentTTest and Mann-WhitneyUTest for Unequal Sample Sizes and Variances. *J. Exp. Educ.* 55 (3), 171–174. doi:10.1080/00220973.1987.10806451

Conflict of Interest: The authors declare that the research was conducted in the absence of any commercial or financial relationships that could be construed as a potential conflict of interest.

Publisher's Note: All claims expressed in this article are solely those of the authors and do not necessarily represent those of their affiliated organizations, or those of the publisher, the editors and the reviewers. Any product that may be evaluated in this article, or claim that may be made by its manufacturer, is not guaranteed or endorsed by the publisher.

frontiers in Environmental Science

ORIGINAL RESEARCH
published: 13 October 2021
doi: 10.3389/fenvs.2021.743894

Effect of Lockdown on Pollutant Levels in the Delhi Megacity: Role of Local Emission Sources and Chemical Lifetimes

Chinmay Mallik[1], Harish Gadhavi[2], Shyam Lal[2], Rahul Kant Yadav[1], R. Boopathy[3] and Trupti Das[3]*

[1]Department of Atmospheric Science, Central University of Rajasthan, Ajmer, India, [2]Physical Research Laboratory, Ahmedabad, India, [3]Environment and Sustainability Department, CSIR-Institute of Minerals and Materials Technology, Bhubaneswar, India

The COVID-19 pandemic resulted in changed emission regimes all over the world. India also imposed complete lockdown on all modes of travel and industrial activities for about 2 months from 25-March-2020 and later unlocked these activities in a phased manner. Here, we study signatures of emissions changes on levels of atmospheric trace gases and aerosols contributing to air pollution over multiple sites in India's capital Delhi covering various lockdown and unlock phases using satellite data and *in-situ* observations. The resulting changes in the levels of these species were compared with respect to their average of 2015–2019 to attribute for year to year and seasonal changes. A clear impact of lockdown was observed for AOD, PM, NO_2, CO, and SO_2 as a result of emission changes, while changed precursor levels led to a change in O_3 chemical regimes impacting its concentrations. A detailed analysis of FLEXPART trajectories revealed increased PM levels over Delhi in north-westerly air masses sourced to Punjab region all the way up to Pakistan. Changes in aerosols and NO_2 were not only restricted to the surface but transcended the total tropospheric column. The maximum decrease in PM, NO_2, CO, and SO_2 was observed during the month of total lockdown in April. The lockdown impact varied with species e.g., PM_{10} and $PM_{2.5}$ as well as locations even within the periphery of Delhi. While surface level aerosols and NO_2 showed significant and almost similar changes, AOD showed much lower decrease than tropospheric column NO_2.

Keywords: trace gases, aerosols, lockdown, ozone chemistry, tropospheric NO_2, FLEXPART trajectories

OPEN ACCESS

Edited by:
Suvarna Sanjeev Fadnavis, Indian Institute of Tropical Meteorology (IITM), India

Reviewed by:
Rohini Bhawar, Savitribai Phule Pune University, India
Sabine Griessbach, Julich-Forschungszentrum, Helmholtz-Verband Deutscher Forschungszentren (HZ), Germany

****Correspondence:***
Chinmay Mallik
chinmay.mallik@curaj.ac.in

Specialty section:
This article was submitted to Atmosphere and Climate, a section of the journal Frontiers in Environmental Science

Received: *19 July 2021*
Accepted: *10 September 2021*
Published: *13 October 2021*

Citation:
Mallik C, Gadhavi H, Lal S, Yadav RK, Boopathy R and Das T (2021) Effect of Lockdown on Pollutant Levels in the Delhi Megacity: Role of Local Emission Sources and Chemical Lifetimes. Front. Environ. Sci. 9:743894. doi: 10.3389/fenvs.2021.743894

INTRODUCTION

Delhi is known for its high levels of air pollution with increasing emissions from various anthropogenic sources. Apart from local, anthropogenic emissions, Delhi's air quality is also impacted by transport of pollutants from the nearby industrial and agricultural sources. Transport of pollutants from the agriculture residue burning both toward the end of autumn and spring in the nearby states of Punjab and Haryana is a regular feature every year. Planning effective strategies for controlling the levels of pollutants needs accurate emission inventories of various sources. The COVID-19 pandemic in India is part of the worldwide pandemic of coronavirus disease 2019 (COVID-19) caused by severe acute respiratory syndrome coronavirus 2 (SARS-CoV-2). The COVID-19 containment effort such as countrywide lockdown provided a unique opportunity to study how pollutant levels change in an

TABLE 1 | Various phases of lockdown in India to arrest the spread of the infection due to COVID-19.

Type	Duration	Details
Janata Curfew	22 March, 2020 (Sunday)	All activities totally closed
Phase 1	25 March–14 April, 2020 (21 days)	All activities totally closed except emergency services
Phase 2	15 April–3 May, 2020 (19 days)	All activities totally closed except emergency services, essential items
Phase 3	4 May–17 May, 2020 (14 days)	All activities totally closed with some relaxation for limited transport services, interstate trucks for essential items etc.
Phase 4	18 May–31 May, 2020 (14 days)	All activities totally closed except emergency, limited domestic air travel started on 25th May
Phase 5	Unlock phase 1: 1–30 June, 2020 (30 days)	Most of the activities allowed except in highly affected areas. Shopping malls, religious places, hotels, and restaurants allowed to reopen from 8 June. Educational institutions and cinema halls remained closed. No metro train service
Phase 6	Unlock phase 2: 1–31 July, 2020 (31 days)	Lockdown measures were only imposed in containment zones. In all other areas, most activities were permitted. Night curfews were effective only from 10 p.m. to 5 a.m. Intra- and inter-state travel was allowed. International travel remained closed except for limited travel as part of the Vande Bharat Mission. Educational institutions and cinema halls remained closed. No metro train service

otherwise highly polluted urban atmosphere following a curb in various anthropogenic emission sources. While this pandemic started in November 2019 in China, India saw the first case of COVID-19 on January 30, 2020 and the first reported death on March 12 (Andrews et al., 2020; [1]). Henceforth, the infection rate continued to increase. A single-day trial lockdown was announced in India on March 22, followed by the first phase from March 25 and later various other phases for lockdown followed by phasewise unlock as detailed in **Table 1** [2,3]. There are various studies related to the impact of lockdown on pollutant levels in different parts of the world (Le et al., 2020; Sicard et al., 2020; Xu et al., 2020) as well as in India (Dhaka et al., 2020; Jain and Sharma 2020; Mahato et al., 2020; Singh et al., 2020; Nath et al., 2021; Panda et al., 2021). Although this was a nationwide lockdown but we chose to study the impact over Delhi as it is the most polluted major urban region in India. This article provides a detailed account of the changes until almost the end of the government-enforced planned lockdown/unlock periods in 2020 and with respect to emission sources and lifetimes using surface-based *in situ* measurements as well as satellite-based measurements.

MATERIALS AND METHODS

The Study Locations

For the present analysis, we have focused on the Delhi metropolitan region (28.20–28.71°N, 77.17–77.38°E). The reasons are that Delhi is a megacity and home to a population of 29 million estimated in 2018 and projected to be the world's most populous in a decade[4,5]. With an area of approximately 1,500 square kilometers, a population density of approximately 19,400 per square km, and being the capital city of India, Delhi is also a hub of connection with close to 11 million vehicles daily plying the roads of Delhi with a growth rate of 5% in 2018[6,7]. Apart from that, Delhi also witnesses a significant flux of industrial emissions including the power plants. The Delhi-Mumbai industrial corridor is one of the biggest in the world. Additionally, a significant amount of pollution in Delhi is attributed to adjoining agriculture waste burning emissions (Perrino et al., 2011; Rajput et al., 2014). Emissions and air pollution were also found to impact the vertical temperature structure over Delhi, leading to accelerated warming (Mallik and Lal, 2011). So, when the COVID-19 was announced and the entire functioning transport system came to a halt suddenly, the impacts were expected to be significant. To understand the impact of lockdown on the emissions and the subsequent impact of these changed emissions as a result of enforcement of various lockdown/unlock phases on atmospheric concentrations of particulate matter (PM: 10 and 2.5), nitrogen dioxide (NO_2), ozone (O_3), cabon monoxide (CO), and sulphur dioxide (SO_2), we have analyzed the respective data from six different locations in Delhi. These locations are given in **Table 2** and are also shown in **Figure 1**. The study sites are: Anand Vihar (AnVh), Punjabi Bagh (PnBg), Shadipur (SdPr), Central Road Research Institute (CRRI), NSIT Dwarka (NstD), and EPA/US Embassy Delhi (EPA-D).

Anand Vihar is a posh locality in the Eastern part of Delhi with many residential colonies and shopping complexes. It harbors a major railway station and is situated in the east of the River Yamuna. The major emission sources in this region are likely to be the residential and traffic sectors. However, in the western part, there are a few industries manufacturing paper, glass, and chemicals. While paper industries can be a secondary source

[1]https://archive.pib.gov.in/archive2/erelease.aspx (Release IDs: 200168 & 200237)
[2]https://www.mha.gov.in/notifications/circulars-covid-19
[3]https://www.mha.gov.in/sites/default/files/MHAorder%20copy_0.pdf
[4]https://www.populationu.com/in/delhi-population
[5]http://delhiplanning.nic.in/sites/default/files/2%29%20Demographic%20Profile.pdf
[6]http://delhiplanning.nic.in/sites/default/files/12%29%20Transport.pdf
[7]https://transport.delhi.gov.in/sites/default/files/All-PDF/Total%2BVehicles%2BRegistered%2Bupto%2B31.03.2018.pdf

TABLE 2 | Location and characteristics of sites chosen for this study.

Station	Latitude (°N)	Longitude (°E)	Emission characteristic
Anand Vihar (AnVh)	28.65	77.30	Residential, major interstate bus terminal
Punjabi Bagh (PnBg)	28.67	77.13	Residential cum commercial
Shadipur (SdPr)	28.65	77.16	Residential cum commercial
Central Road Research Institute (CRRI)	28.55	77.27	Waste disposal, major highway with heavy traffic
NSIT-Dwarka (NstD)	28.61	77.04	Waste disposal, residential
EPA/US Embassy Delhi (EPA-D)	28.60	77.19	Office area, gardens around

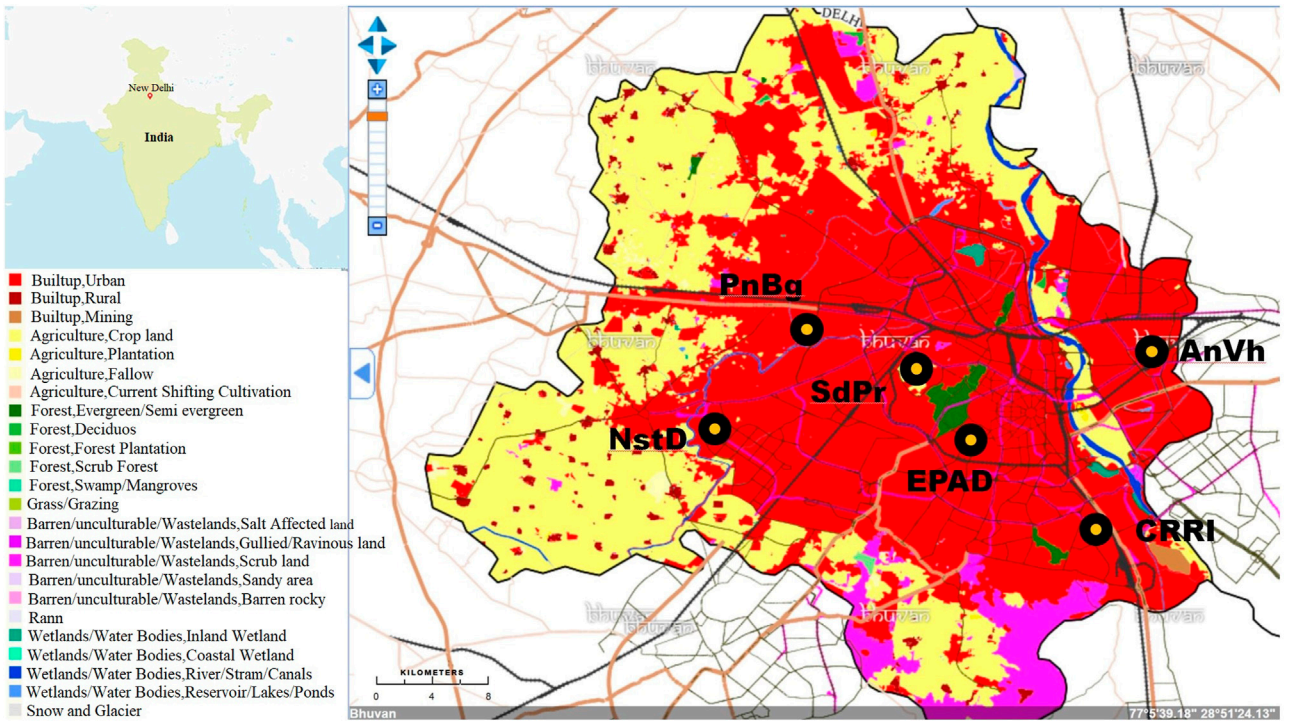

FIGURE 1 | Map of Delhi showing the study locations. The Land Use Land Cover (LULC) map is downloaded from Bhuvan(https://bhuvan-app1.nrsc.gov.in/thematic/thematic/index.php). The study sites are: Anand Vihar (AnVh), Punjabi Bagh (PnBg), Shadipur (SdPr), Central Road Research Institute (CRRI), NSIT-Dwarka (NstD), and EPA/US Embassy Delhi (EPA-D).

of SO_2, petrol pumps (and vehicles plying) in the region can be a significant source of hydrocarbons and NO_x impacting local O_3 chemistry.

The Central Road Research Institute is housed in a green campus in south east Delhi, just 1 km west of the Okhla Bird sanctuary on Mathura Road. Despite being in a green area, the measurements here would be significantly affected by sulfur and hydrocarbon emissions from landfill, with the Okhla Disposable Area of Delhi being in the immediate eastern neighborhood. The area also has several industries related to waste and garbage management. The area is surrounded by large educational hubs with IIT Delhi in the south-west and Jamia Millia Islamia in the north-east. There are a few hospitals toward the north, while industrial parks are located to the south.

The US Embassy is located in the very green and planned Chanakyapuri area of New Delhi surrounded by parks and other tourist attractions. The Rashtrapati Bhavan is less than 1 km to the north, Central Ridge Reserve Forest to the west, office/market/religious areas to the south, and Safdarjung Airport to the east. The major local emissions in this area are likely to be from the transport sector, mostly light motor vehicles. Shadipur and Punjabi Bagh are located less than 2 km apart in Central West Delhi and can be characterized as residential cum commercial area. Additionally, the Naraina Industrial Area lies 1 km south of Shadipur, while the Mangolpuri Industrial Area and Ordinance Depot (Shakurbasti) lie north of Punjabi Bagh, so both these areas are likely to be impacted by mixed emission regimes. Netaji Subhas University of Technology, Dwarka (NstD, henceforth NSIT-Dwarka) is located in the western part of Delhi in the vicinity of Indira Gandhi International Airport, the later lying to the east of the monitoring station in the educational institute.

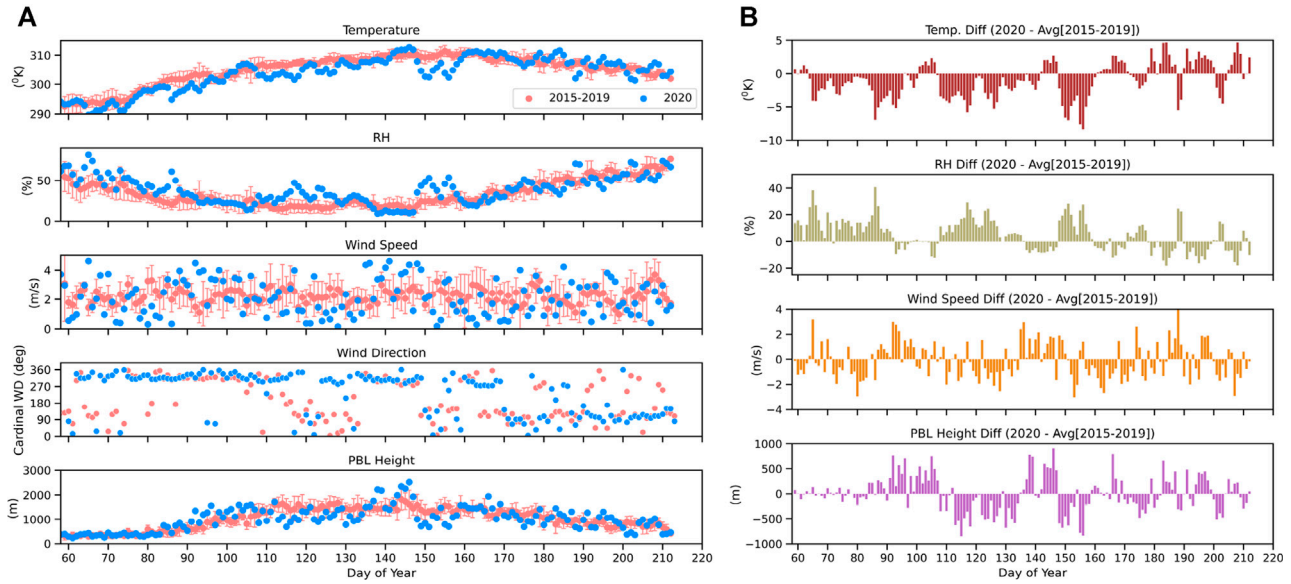

FIGURE 2 | (A) Variations in daily average meteorological parameters during COVID-19 lockdown and unlock phases and comparison with daily 5-year average for the years 2015–2019. **(B)** Difference plot for meteorological parameters.

About 6 km to the north is situated the Scion Waste Water treatment plant. The Keshopur Sewage Treatment Plant is also in close vicinity.

Meteorological Parameters

The National Centres for Environmental Prediction (NCEP) Final (NCEP FNL) operational global analysis data are produced at $1^{\circ} \times 1^{\circ}$ grid horizontally and 26 pressure levels vertically every 6 h using Global Data Assimilation System (GDAS). The GDAS assimilates all the observations such that the model produced gridded values are consistent with observations. For all practical purposes the reanalysis data are proxy for observations. The same data-set was also used to run the FLEXPART model described later. **Figure 2** shows the 24 h average values of meteorology over New Delhi using NCEP FNL reanalysis data (National Centers for Environmental Prediction (NCEP)/National Weather Service/NOAA/U.S. Department of Commerce, 2000). The red dots show the daily 5 year (2015–2019) average of the value on a given day along with standard deviation whereas blue dots show the daily average of 2020. Five year mean values of temperatures steadily rose from March to mid-May and then started decreasing. The temperature in 2020 followed nearly the same trend as 5 year mean but in about three instances that were around day numbers 85, 110, and 150, a sudden decrease in temperature for a few days was observed. Corresponding to each of these three events, an increase in Relative Humidity (RH) and wind speed was observed. Overall, RH follows an inverse pattern of temperature variation and there is no systematic seasonal variation in wind speed. The planetary boundary layer height is low in March. It rises steadily in April and then remains high till the middle of June. Subsequently, it decreases but rather slowly.

Source of Data

Trace Gases and Particulate Matter

The Central Pollution Control Board (CPCB) monitors ambient air quality across stations spanning the entire Indian region with the help of the State Pollution Control Boards and other agencies under the National Air Quality Monitoring Programme (NAMP). Under NAMP, four air pollutants, viz. SO_2, oxides of nitrogen as NO_2, suspended particulate matter, and respirable suspended particulate matter, were identified for regular monitoring[8]. Along with it, measurements of O_3 and CO are also available for many stations. PM measurements include $PM_{2.5}$ and PM_{10}. The suite of instruments constitutes a Continuous Ambient Air Quality Monitoring (CAAQM) station. Currently, monitoring is carried out over 233 CAAQM stations, mostly representing urban and industrial locations. In most cases, the monitoring data is available on an hourly basis. The data can be downloaded from the CPCB portal[9]. A major objective of CBCB for making these measurements is to present the Air Quality Indices (AQI)[10]. The AQI are used for resource allocation, enforcement of standards, to determine evolution (improvement/degradation) of air quality, to raise public awareness using simple infographics, and of course to help in scientific research. For this study, CAAQM station data were downloaded for 6 sites in Delhi as described in *The Study Locations*. The parameters considered for this study are PM_{10}, $PM_{2.5}$, NO_2, O_3, CO, and SO_2.

[8]http://cpcb.nic.in/air.php

[9]https://app.cpcbccr.com/ccr/#/caaqm-dashboard/caaqm-landing/caaqm-comparison-data

[10]https://app.cpcbccr.com/ccr_docs/FINAL-REPORT_AQI_.pdf

The ultraviolet photometric O_3 gas analyzers work on the standard principle of absorption of radiation at 254.7 nm by atmospheric O_3. The lower detection limit of the instrument is 1 ppb with a response time of 30 s or less. The CO instruments are based on gas filter correlation technology and operate on the principle of infrared absorption at 4.67 μm vibration-rotation band of CO (Nedelec et al., 2003). It has a lower detection limit of 100 ppbv at a 60 s response time. The zero noise of the instrument is 20 ppbv root-mean-square (RMS) at 30 s averaging time. The NO_x instruments are based on the detection of chemiluminescence produced by the oxidation of nitric oxide (NO) by O_3 molecules, which peak at 630 nm radiation (Navas et al., 1997). The method is specific to NO only. NO_2 is measured by converting it into NO using a molybdenum convertor and then measuring total NO_x as NO. Unfortunately, the reduction of NO_2 to NO is not specific for NO_2, and other nitrogen species are also reduced to NO and act as interferences in the NO_2 measurements. The lower detection limits of these instruments are approximately 1 ppb at a response time of 120 s or less. The SO_2 measurements are based on UV fluorescence wherein SO_2 is excited using 214 nm and a band pass filter centered approximately 350 nm is used to collect the fluorescence (Mallik et al., 2016). The PM_{10} measurements are based on the principle of β-ray attenuation. The particulate matter in ambient air is sampled through the instrument at a flow rate of 16 liters per minute and collected on fiberglass filter tape. Comparison of measurements of β-ray radiation by scintillation/G.M. counter before and after sampling gives a measure of the amount of PM_{10}. The $PM_{2.5}$ measurements are similar to PM_{10} but the particle size cutoff is in the range of 0–2.5 μm. The instrument specifications for obtaining these measurements can be found in the CPCB website[8].

We have used daily average data for 5 selected sites from January, 2015 to July, 2020. However, there are data gaps for various species e.g. data for Central Road Research Institute are only available from the last quarter of 2017 (except availability of intermittent data in 2015: Jan–Apr, Sep–Nov), while data from Anand Vihar are missing during Jun–Oct 2017. Similarly data from Punjabi Bagh are missing from Nov 2016 to Oct 2017, while data from Shadipur is missing during Apr–Sep 2017. PM data of NSIT-Dwarka is missing during Dec 2015–Sep 2017.

Satellite Data

Ozone Monitoring Instrument (OMI) is a spectrometer on board NASA EOS Aura satellite in sun-synchronous orbit with local equator crossing time 13:45 ± 0:15 h (Levelt et al., 2006). The spectrometer has a field of view 13 km × 24 km near nadir and 24 km × 160 km at the edges of swath. It has three channels—two in UV wavelength range and one in visible wavelength range with subnanometer spectral resolution. Columnar NO_2 concentrations are estimated using visible channel radiance values in wavelength range 405–465 using the algorithm described in Lamsal et al. (2020). The NO_2 spatial maps (0.25° × 0.25°) are made using cloud screened L3 data (Version 3) from OMI obtained through Giovanni iterface11. For the rest of the calculations and plots in this work, Version 4 OMI NO_2 standard product (Krotkov et al., 2019) is used. The version 4 update includes use of field of view specific geometry dependent Lambertian surface reflectivity in NO_2 retrieval and more accurate terrain pressure among several other improvements and has uncertainty less than 30%.

Visible Infrared Imager-Radiometer Suite (VIIRS) is a whiskbroom radiometer with 22 channels ranging from 0.41 to 12.01 μm on board Suomi National Polar-orbiting Partnership (NPP) satellite platform that was launched in October 2011. The VIIRS sensor is designed to extend and improve upon its predecessor namely MODIS and AVHRR. There are two different algorithms to estimate aerosol optical depth (AOD) (Levy et al., 2015; Sawyer et al., 2020). In this work, AOD estimated using the dark target algorithm is used (Levy et al., 2020)[12].

FLEXPART Model

FLEXPART (FLEXible PARTicle dispersion model) is an open-source Lagrangian particle dispersion model. The FLEXPART model can be run in forward or backward mode using user-supplied meteorological fields and allows for physical processes such as dry deposition, wet deposition, diffusion, convective transport, etc. to estimate dispersion or source-receptor relationships (Seibert and Frank, 2004; Pisso et al., 2019). The latest version 10.4 was run in backward mode to calculate source-receptor relationship for Delhi for each day starting from 15 January to 31 July in the current work. The source-receptor relationship is the sensitivity to the emissions located at a given grid-box for the receptor location. It represents the normalized total time spent by the back-trajectories in a given grid-box. We used 50000 trajectories spread over 24 h to estimate source receptor relationship for each day. A few source-receptor relationships for the grid-boxes close to the earth's surface are shown in **Figure 7**.

Emission Sources and Lifetimes of Species

Emission Sources of Various Species

The National Capital Region (NCR) covering Delhi and adjoining regions is changing with time and so are the emissions of various species. The major factors are increasing population, vehicular activities, industries, demand for power, domestic emissions, etc. There were various attempts to estimate the emissions from these sources. Guttikunda and Calori (2013) made emission inventory for particulate matter and various trace species at a resolution of 1 km × 1 km (**Table 3**). The major pollution sources are transportation, power generation, and construction activities. Sindhwani et al. (2015) developed emission inventory for the criteria pollutants such as PM_{10}, NOx, SO_2, and CO at 2 km × 2 km resolution for the NCR for 2010. Major emission sources of the region include vehicular exhaust, road-dust, domestic, industrial, power plants, brick kiln etc. Sahu et al. (2015) developed a high-resolution emission inventory for two major atmospheric pollutants, NO_x and CO. The inventory was developed with a grid resolution of 1.67 km × 1.67 km for the

[8]http://cpcb.nic.in/air.php

[11]https://giovanni.gsfc.nasa.gov/giovanni/

[12]https://ladsweb.modaps.eosdis.nasa.gov/

TABLE 3 | Sector-wise source contributions (%) to particulate matter and various trace gases.

Source	$PM_{2.5}$	PM_{10}		NO_x			CO			SO_2		VOCs
	GC	GC	Setal	GC	Setal	SB	GC	Setal	SB	GC	Setal	GC
Transport	17	13	19	53	47	63	18	46	60	2	14	51
Power plant	16	15	13	7	7	3	31	-	-	55	67	13
Industries	14	11	10	11	13	31	15	16	2	23	9	5
Domestic	12	8	7	1	1	3	14	15	38	6	2	7
Brick Kiln	15	11	11	2	2	-	12	12	-	11	4	9
Construction	5	9	1	-	-	-	-	-	-	-	-	-
Waste burning	8	7	6	1	2	-	2	3	-	2	1	-
Diesel Gen sets	6	4	5	25	27	-	7	8	4	2	14	-
Road dust	6	22	20	-	-	-	-	-		-	-	-
Total kTons/yr	63.0	114.0	107.6	376.0	342.3	255.4	1,425.0	1,290.1	703.2	37.0	83.2	261.0

NCR using Geographical Information System (GIS) technique for base year 2010. The emission estimates from these inventories are presented in **Table 3**.

Lifetimes of Species

The chemical lifetime for a species, which has photochemical loss, is defined as the inverse of its total loss rate (Seinfeld and Pandis, 2006). More reactive species will have shorter lifetimes. Particles do not have fast chemical loss like gases but they settle down to various surfaces. Coarse (bigger) particles (such as PM_{10} and bigger) have shorter lifetime, while the finer (smaller) ones ($PM_{2.5}$) have longer lifetime (Textor et al., 2006; Croft et al., 2014; Kristiansen et al., 2016). Many species such as SO_2 and O_3 also have significant loss due to dry deposition. Furthermore, loss rates are higher leading to shorter lifetimes in a polluted atmosphere compared to cleaner regions. Also, chemical lifetimes are shorter in summer than in winter for species having photochemical losses. Williams et al. (2012) have estimated aerosol lifetime as a function of particle size and as a function of altitude using data gathered during Indian Ocean Experiment. They found a lifetime of approximately 1.5 days for aerosols in the boundary layer for particle sizes between 0.08 and 0.1 μm. Larger size particles known as super micron size particles (1.1–10 μm) have shorter residence time. Grythe et al. (2017) found a lifetime of particles greater than 1 μm radius to be less than a day.

O_3 has a short lifetime, typically hours, in polluted urban regions where concentrations of its precursors are high (Stevenson et al., 2006; Conley et al., 2012; Young et al., 2013; Monks et al., 2015). Based on the estimated values of hydroxyl radical (OH) over the northern Indian Ocean, which were several times higher than the global average OH concentration of approximately 1×10^6 molecules cm^{-3}, Lawrence and Lelieveld (2010) found lifetime of CO of only ~15 days near the surface, and a NO_x lifetime of less than a day.

The atmospheric lifetime of NO_x depends on various processes occurring in the atmosphere including the photolysis of NO_2 and the hydroxyl-mediated oxidation of NO_2; thus, its lifetime depends on the concentration of other constituents (Levy et al., 1999; Shah et al., 2020). Liu et al. (2016) estimated the NO_x lifetime using OMI satellite data and ECMWF wind fields over polluted cities and power plants in polluted background and have found it to be 3.8 ± 1.0 h. The lifetime of SO_2 is approximately 1.8 days within the boundary layer depending upon the meteorological conditions and the removal by OH-induced gas-phase conversion into gaseous sulphuric acid (Inomata et al., 2006; Lee et al., 2008).

RESULTS AND DISCUSSIONS

Satellite Observations

Figure 3 shows a pictorial representation of COVID-19 effect on anthropogenic air pollution represented by tropospheric column NO_2 (Tropo col NO_2) changes during COVID-19 months (2020) over the Indian region w.r.t. similar period in the previous year (2019). Most of the boundary layer NO_2 can be specifically attributed to its anthropogenic sources, which were the most impacted as a result of lockdown. The effect is clearly visible in much reduced tropospheric column NO_2 concentrations during COVID-19 months.

Figure 4 shows monthly average columnar concentration of tropospheric col NO_2 over a latitude longitude range of 28.465°N–28.715°N and 77.065°E–77.315°E that covers the NCR around New Delhi. The vertical bars are ±1 sigma standard deviations. A clear decrease of tropospheric column NO_2 amount can be seen in the months of April (−45%), May (−42%), and June (−26%). March 2020 does not show a clear decrease because the lockdown was implemented only in the last week of March (**Table 1**). The decrease in NO_2 ceases to be significant in July (−6%) as lockdown measures were restricted to few containment zones (**Table 1**).

Figure 5 shows monthly average of aerosol optical depth (AOD) over New Delhi. Despite a large year to year and monthly variability, a significant decrease in AOD is observed. Usually an increase in AOD values is observed over Delhi from March to June (Pandithurai et al., 2008) but in 2020, AOD values were low during the lockdown period starting from April to June compared to the same month in previous years. We believe this was because of reduced anthropogenic emissions during the lockdown. A major source of aerosols in Delhi during summer has been found to be fugitive dust particles from roads, and the construction sector accentuated by windblown dust. A receptor-based modeling approach by ARAI and TERI estimated influence of nearly 42% to PM_{10} and 34% to $PM_{2.5}$ from this sector for the summer months (ARAI and TERI, 2018). The road transport and the construction works were severely limited during the

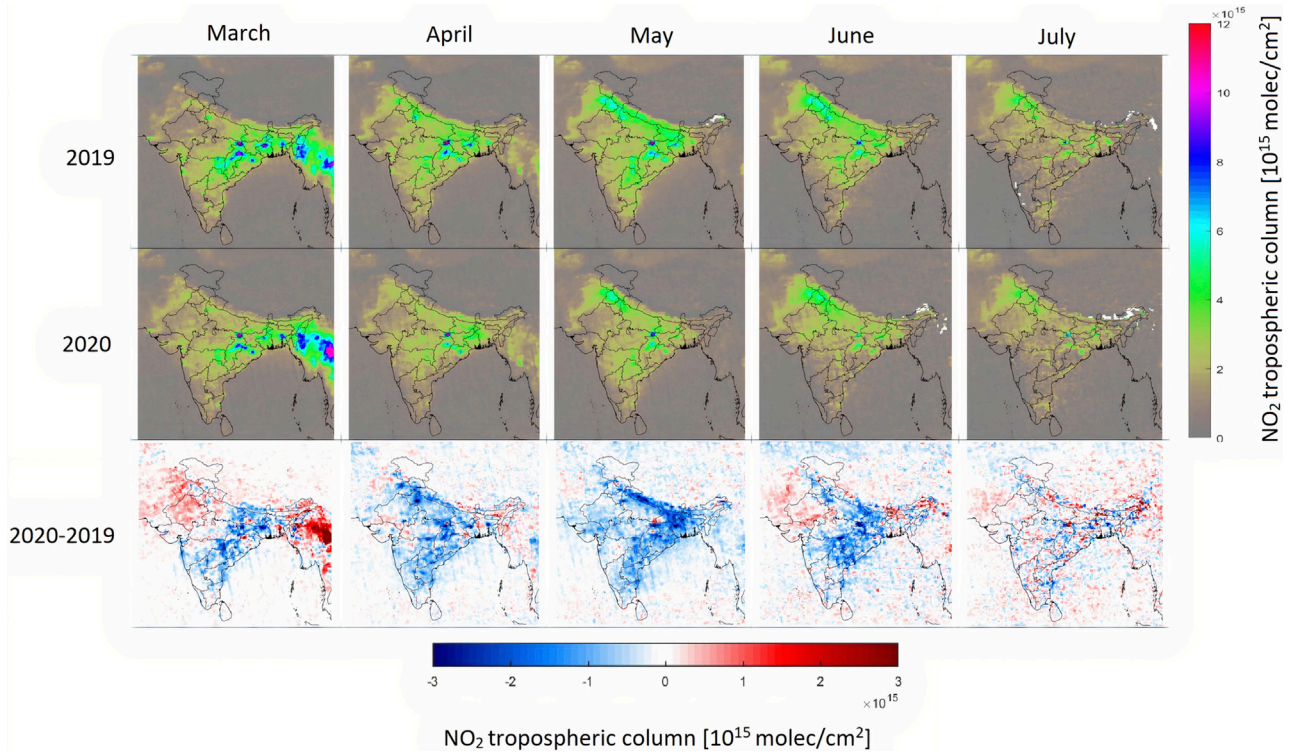

FIGURE 3 | Satellite observations of tropospheric column NO_2 over the Indian region during the months corresponding to COVID-19 lockdown and unlock phases (March, April, May, June, July) during 2020 **(B)** and comparison to 2019 **(A)**. **(C)** shows the monthly difference between 2020 and 2019.

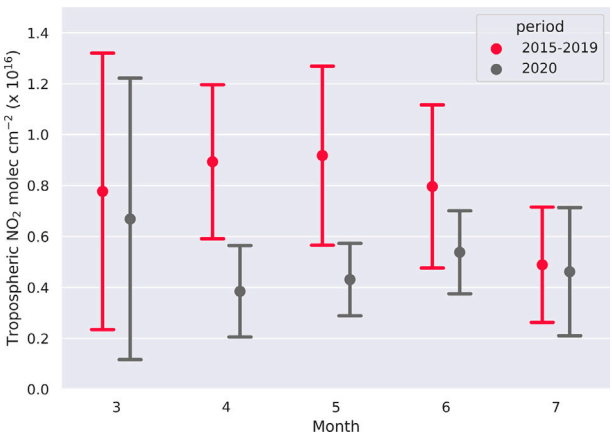

FIGURE 4 | OMI retrievals of tropospheric NO_2 column over Delhi during months corresponding to COVID-19 lockdown and unlock phases during 2020 and comparison with previous years.

lockdown period, due to both Government mandate and exodus of migrant workers from Delhi. As a result, the natural increase in AOD was balanced by a decrease from the anthropogenic sector, cumulating into a scenario where AOD remained peculiarly flat during the summer months with lower values during 2020 year compared to previous years (2015–2019) and a decrease in monthly values until June is observed. A recent study revealed that AOD decrease over India during lockdown was of the order of 45%, while the AOD anomaly over Delhi NCR was −24.6% during the 2nd half of April and −44.2% during the first half of May (Ranjan et al., 2020). Furthermore, we observe an enhancement of AOD during March (10.4%) but reductions of 25.3 and 22.5% in April and May respectively when calculating the anomaly against 2015–2019. In June, the AOD values were only 7% lower than the 5 year mean and in July, the AOD values for 2020 were 2.4% higher than 5 year mean. The difference between our estimates and Ranjan et al.'s (2020) estimates is because of the fact that Ranjan et al. have used average from 2000 to 2019 whereas we have used average of 2015–2019 for the comparison (**Figure 5B**). Another reason could be the resolution of the data used; we have used 0.5 × 0.5 degree area while Ranjan et al. have used very high spatial resolution (1 km) data.

Ground-Based Observations

The above explanations for AOD and NO_2 represent an integrated atmospheric change as a result of COVID-19 lockdown. However, most of the emission changes occur close to the surface. Therefore, we present a detailed analysis of surface observations.

To understand the changes in atmospheric concentrations of trace gases and particulate matter as a result of changed emission scenarios, the daily variation of these parameters during March–July, 2020 is compared with the average of 2015–2019 of the same period and for the same parameters. An example plot

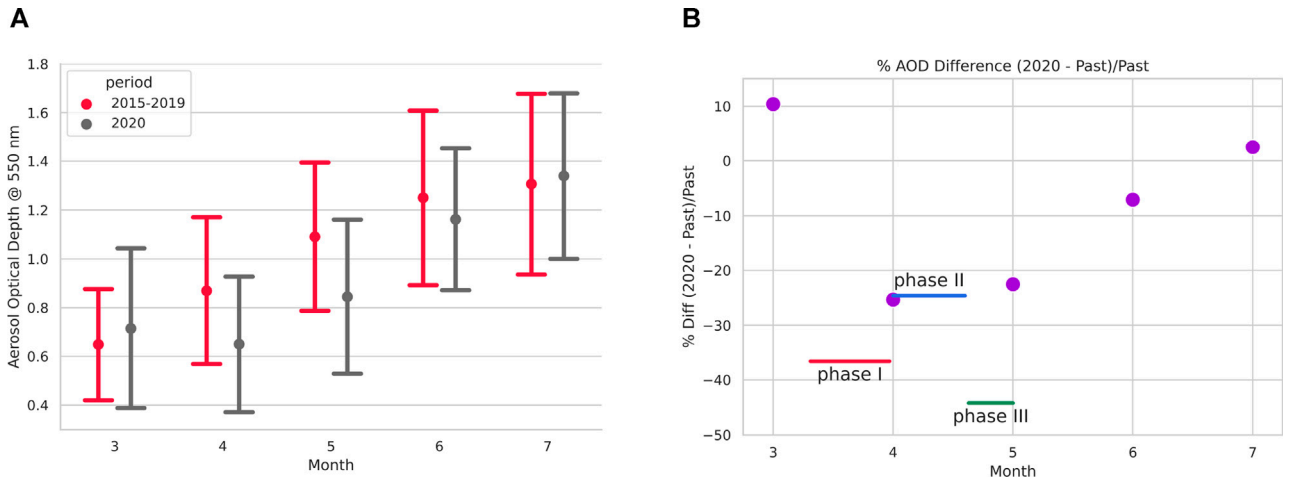

FIGURE 5 | (A) VIIRS observations of AOD over Delhi during months corresponding to COVID-19 lockdown and unlock phases during 2020 and comparison with the average of 2015–2019. **(B)** Percentage changes in AOD; the points show monthly % changes from the present study while the lines show data from Ranjan et al. (2020), with x-span of the line representing the period for which the change is calculated.

for Anand Vihar is shown in **Figure 6**. It is observed that the two datasets start to diverge around day of year (DOY) -85, representing 25 March, the day of initiation of nationwide lockdown (**Table 1**). The divergence around this period is maximum for NO_2 followed by PM_{10} and $PM_{2.5}$. The divergence is also significant in O_3. This indicates that the sources impacted by lockdown play a crucial role in the budgets of NO_2 and PM (2.5 and 10). The patterns for PM and NO_2 are more or less similar for different stations but this does not hold so for O_3. This is on expected lines as the major sources of PM e.g., transport sector and road dust account for 30–40% of PM_{10} over Delhi. Similarly, transport sector makes a major contribution in the anthropogenic NO_2 sources. As a result, the departure in NO_2 is drastic both in satellite-based columnar data and at surface level (**Figures 4**, **6**). However, not much change is observed for CO, as major sources of CO are related to combustion i.e., biofuels and biomass burning which were not directly affected by lockdown processes. However, O_3 presents a different picture as its concentration is a complex interplay of atmospheric transport processes, changes in primary emissions, meteorology and photochemistry in addition to chemical and depositional losses. These changes in surface level pollutants are further discussed below.

Aerosols

High amounts of atmospheric aerosols negatively affect health and air quality, and hence constitute criteria pollutant for the measure of air quality. Indian cities in general suffer from poor air quality mostly due to aerosols (SOGA, 2020). India's capital city, Delhi, is particularly badly affected by air pollution. In a particularly grave event, $PM_{2.5}$ concentrations (peak 24 h average 650 $\mu g\ m^{-3}$) exceeded the Indian air quality standards by 11 times and the World Health Organisation (WHO) guidelines by 25 times in early November 2017. Beig et al. (2019) studied this event and found that combined effect of a dust storm in the middle-east, agricultural waste burning in upwind states, and stagnation of local air pollution led to this event. The mortality rate due to pollution in Delhi is estimated to be very high and the city is projected to be among the top 5 cities in the world to have high fatality rates (Apte et al., 2015; Lelieveld et al., 2015). Air pollution caused between 10000 and 30000 premature deaths in Delhi in 2015 (Bithal, 2018). While air pollution is particularly bad in winter over Delhi, the $PM_{2.5}$ levels are often higher than the WHO limit of 25 $\mu g\ m^{-3}$ and the Indian Air Quality Standard of 60 $\mu g\ m^{-3}$ for most part of year except during the rainy months of July and August (Bali et al., 2019; Hama et al., 2020). Main sources of $PM_{2.5}$ particles are anthropogenic emissions except when there is a dust storm like event. In a past study, chemical make-up of PM_{10} aerosol over Delhi was found to be 20% organic, 6% combustion, 31% secondary inorganic, and 43% soil particles during the spring season. While for the most part of India, the residential sector is a major emitter of $PM_{2.5}$ particles, over Delhi it is the transport sector with nearly 64% contribution (Conibear et al., 2018; Reddington et al., 2019). Beig et al. (2019) attributed 65% of observed $PM_{2.5}$ concentration to dust and smoke transport from upwind regions for a high pollution event during November 2017. However, this fractionation may not be applicable for all seasons and local emissions may have far more dominating influence on the total concentration. This is because overall wind direction and boundary layer characteristics are different in summer and winter as one can see from the FLEXPART output (**Figure 7**), as well as the meteorological plots shown in **Figure 2**. While winter time air pollution over Delhi is studied more frequently because of very high aerosol concentration making them visible and perceptible as a health threat in public mind, concentrations in summer, even though lower than the winter months, are still high enough to pose serious health hazards when exposed for a long time but they are less frequently studied. A campaign-based study during January–March, 2018 over multiple sites in Delhi region using three aerosol mass spectrometers (AMS) for non-refractory fraction, two aethalometers, and one single particle soot

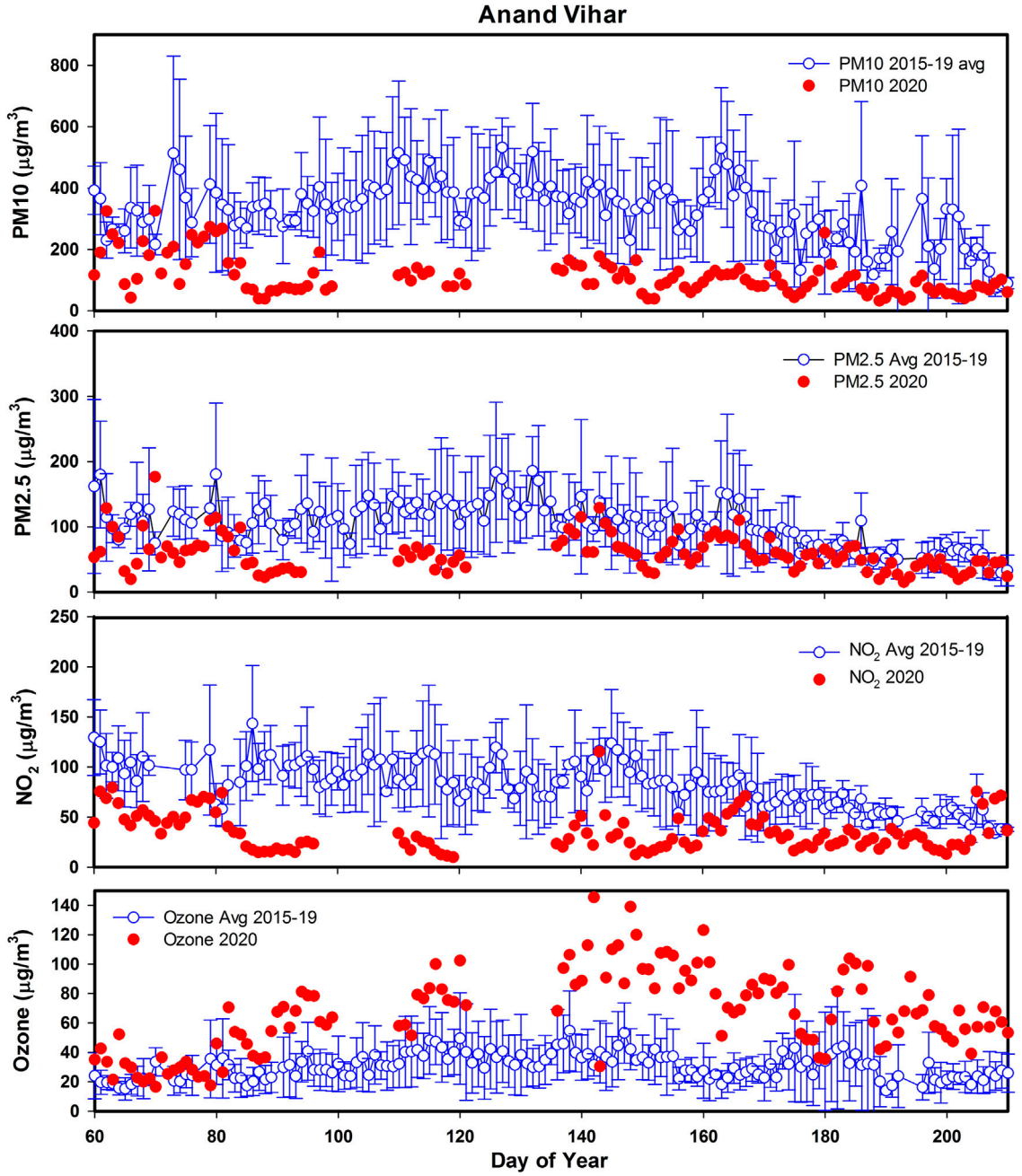

FIGURE 6 | Particulate matter and trace gases variations over a representative study location (Anand Vihar), Delhi during months corresponding to COVID-19 lockdown and unlock phases during 2020 and comparison with the average variation during 2015–2019.

photometer concluded that local pollution was dominating over regional pollution during this period (Lalchandani et al., 2021). This was based on the observation of similar chemical composition both within Delhi-NCR and downwind region with mean $PM_{2.5}$ reaching 153.8 ± 109.4 µg m^{-3} with major contribution from organics (43–47%) followed by chloride (11–17%), ammonium (9–13%), sulfate (8–13%), nitrate (9–11%), and (5–16%) black carbon. However, significant fraction of highly oxidized, low volatile organic aerosols to the oxygenated organic aerosol (OOA) fraction indicated influence of regional transport, which was attributed to the north-west direction of the study sites. A detailed chemical characterization of $PM_{2.5}$ over Delhi for heavy and trace elements using the Energy Dispersive X-ray Fluorescence technique during post-monsoon of 2019 concluded large influence from agriculture-residue burning emissions in north-west Indo-Gangetic Plains (IGP) (Bangar et al., 2021). In contrast to winter pattern, during warm season, Jain et al. (2020) observed

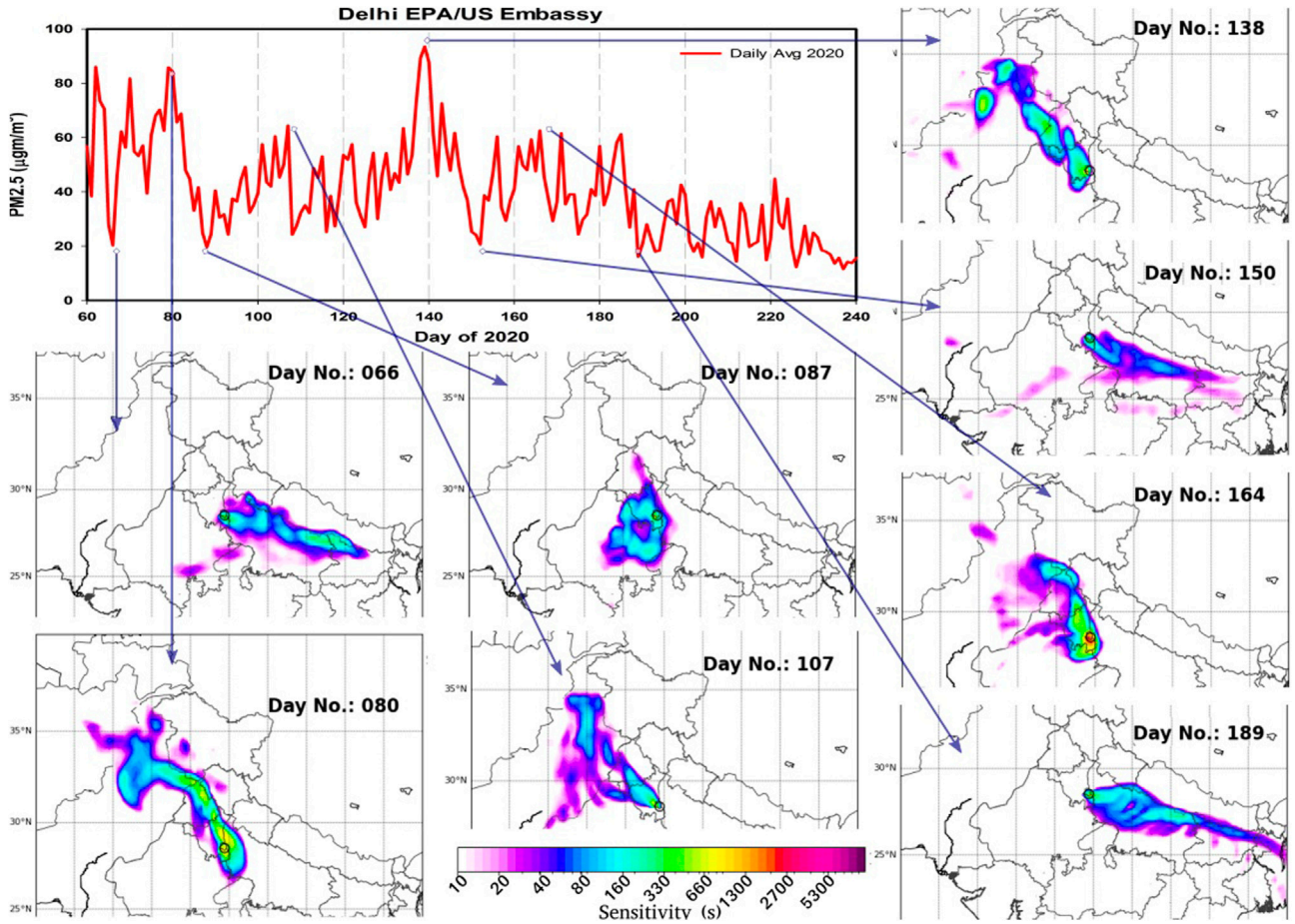

FIGURE 7 | FLEXPART-based source region estimations for Delhi during months corresponding to COVID-19 lockdown and unlock phases during 2020 and comparison with previous years. The sensitivity (s) is given in seconds.

higher amount of secondary sulphate over secondary nitrate indicating higher contribution from point sources. A higher contribution of secondary organic carbon during pre-monsoon compared to post-monsoon was found over Delhi during a study employing stable carbon isotope analysis (Singh et al., 2021). The study confirmed the dominance of C3 plant-derived aerosols over Delhi, which could be sourced from agriculture residue burning transported from outside the city. Air mass trajectory cluster analysis using HYSPLIT over Delhi during January 2013–June 2014 indicates that the air mass approaches from 4 sides [north-western IGP, Pakistan (10%); north-western IGP, north-west Asia (45%); eastern IGP (38%); Pakistan and Arabian Sea (6%)] (Sharma et al., 2016). The authors concluded that PM_{10} over Delhi is dominated by soil dust (22.7%) followed by secondary aerosols (20.5%), vehicle emissions (17.0%), fossil fuel burning (15.5%), biomass burning (12.2%), industrial emissions (7.3%), and sea salts (4.8%). The lockdown provided a unique opportunity to study causes of air pollution and evaluate sectoral contributions during the summer months.

Figure 7 shows the source-receptor matrix calculated using FLEXPART for select days when $PM_{2.5}$ concentrations were observed high or low. The air masses were from the north-west direction during initial phases of lockdown (March), but during later phases after the onset of monsoon over Delhi in June, the air masses became easterly over Delhi, bringing in pollutants from the eastern IGP. Interestingly, in **Figure 7**, higher peaks in $PM_{2.5}$ coincide with north-westerly air-masses sourced to industrial regions in Haryana and Punjab of India all the way back to Lahore in Pakistan and further back to the north-west. Lalchandani et al. (2021) have shown through high-precision AMS measurements that air mass transport from north-west air over different sites in Delhi is associated with conspicuous amount of highly volatile and semi-volatile OOA. Higher levels of tropospheric NO_2 column values can be seen in the month of May (**Figure 3**) toward the north-west of Delhi and up to Pakistan in the IGP which suggests heavy pollution due to industrialization in this area. The high patch of NO_2 column gets diluted in June as the influence of monsoon winds starts. Lower values of $PM_{2.5}$ are related to the atmospheric transport either circulating around NCR or coming from the eastern part of IGP, where NO_2 columns already evince relatively lower values. Hence, major changes in $PM_{2.5}$ are likely associated with the transport from the corresponding NO_2 column regions.

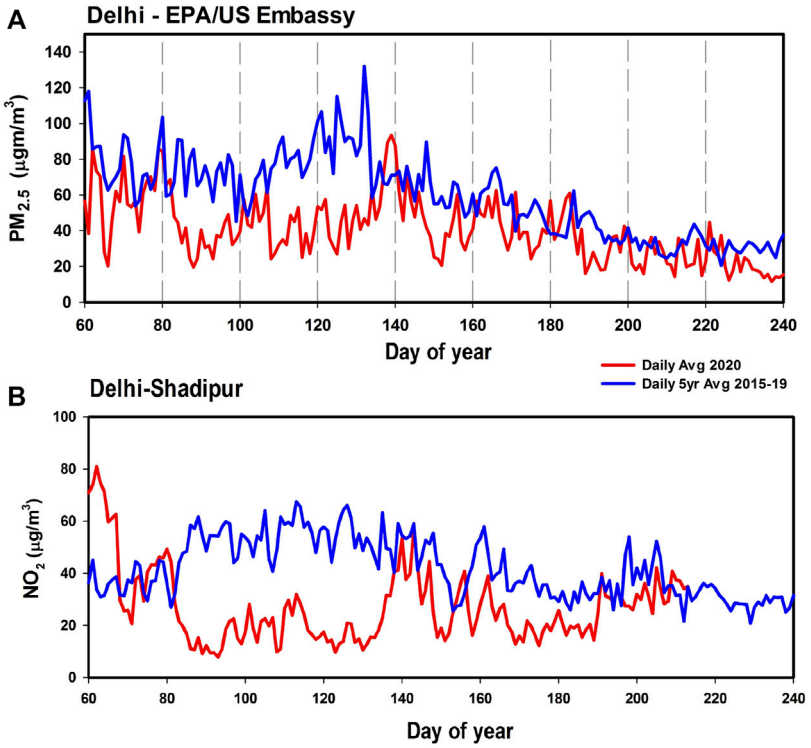

FIGURE 8 | (A) $PM_{2.5}$ variation observed at US Embassy New Delhi during the COVID period from 1 March to 31 July (red curve). It is compared with 5 year period (2015–2019) (blue line). **(B)** Similar to $PM_{2.5}$ but for NO_2 observed at Shadipur, a location near the US Embassy site.

The PM_{10} concentration, which is found to be in the range of 80–270 µg m^{-3} in IGP in the previous years, was reduced to ~70 µg m^{-3} during the lockdown. Daily average variations of $PM_{2.5}$ and surface level NO_2 over two nearby study sites in Delhi during the lockdown period are shown in **Figures 8A,B** against the daily 5 year average of 2015–2019. As mentioned earlier, there is large variability in the 5 year average as well as during the 2020 due to transport of pollutants from the surrounding regions. While there is a general decreasing pattern from May to August because of the change in wind direction, a significant decrease in $PM_{2.5}$ is seen for the lock-down period despite that. Since lifetime of $PM_{2.5}$ is only 1–2 days (**Table 4**), sharp decrease in the levels of $PM_{2.5}$ was observed from the inception of the lockdown on 25th March (day #85) till at least May end (day #152). The rapid decrease also suggests that anthropogenic emissions are the significant sources of $PM_{2.5}$ particles over Delhi. Of course, there are two events of high $PM_{2.5}$, the first from day #90 to day #105 and the second peak around day #140. Similar changes are observed even in NO_2 at a nearby location for example at Shadipur as shown in **Figure 8B**. This shows that these major changes are not local but in a large area covering the NCR and are due to transport from different regions as discussed above using the FLEXPART trajectories. The region in north-west of Delhi seems to contain very large sources of particulate pollution, as whenever the source region is north-west of Delhi, $PM_{2.5}$ concentrations are high. Aethelometer black carbon measurements over Delhi showed increased local contributions (fossil fuel fraction) with the progress from lockdown to unlock phase, but the fossil fuel contribution specifically dipped during 4–17 May due to intensive crop residue burning in neighboring states (Goel et al., 2021). Gadhavi et al. (2015) who analyzed black carbon concentration over a rural location in South India, also found high concentrations of black carbon particles for the days when the source region extended to north-west of Delhi compared to other days. While looking at the $PM_{2.5}$ concentration maps available in the literature (Bali et al., 2019; Reddington et al., 2019), one can see whole of IGP region filled with high amount of particles. The temporal variation of PM concentration when looked in connotation with FLEXPART trajectories, east of Delhi region seems to contribute much smaller amount of air pollution compared to when wind is blowing from west.

TABLE 4 | Lifetimes of particulate matter (PM) and various gaseous species.

Species	Lifetime	References
PM_{10}	Minutes to days	Seinfeld and Pandis (2006) Grythe et al. (2017)
$PM_{2.5}$	1–2 days	Williams et al. (2012)
NO_2	~1 day to ~ few hrs	Lawrence and Lelieveld (2010) Liu et al. (2016)
Ozone	Hours	Monks et al. (2015)
CO	15 days	Lawrence and Lelieveld (2010)
SO_2	~1.8 days	Lee et al. (2008)

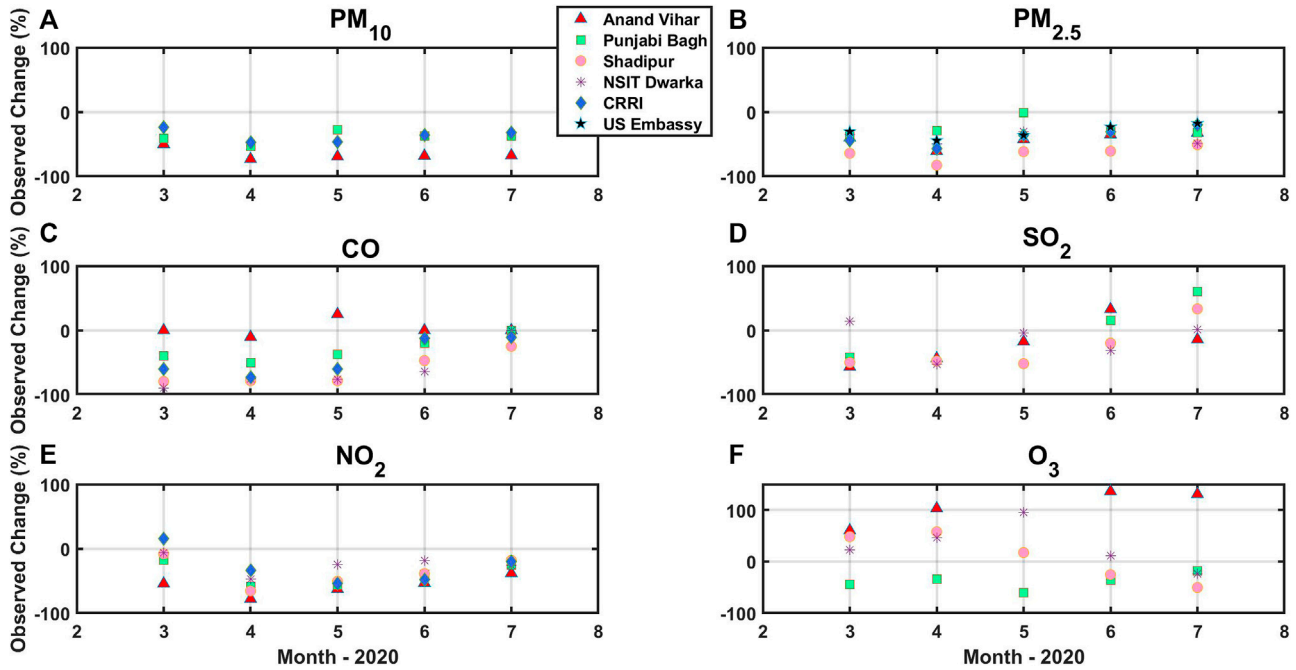

FIGURE 9 | Percentage change in monthly mean concentrations at various locations with respect to the average of 2015–2019 for **(A)** PM_{10}, **(B)** $PM_{2.5}$, **(C)** CO, **(D)** SO_2, **(E)** NO_2, **(F)** O_3.

Figures 9A,B show monthly average percentage changes in 2020 with respect to the 5 year average of 2015–2019, $[(X_{2020}–X_{2015–2019})/X_{2015–2019}] \times 100$, in PM_{10} and $PM_{2.5}$ respectively. Unfortunately, PM_{10} data are available only for the 3 stations from the selected locations for this work (**Figure 9A**). Anand Vihar shows the largest decrease in PM_{10} as compared with the other two locations, while the other two locations show almost similar changes. Highest decrease of about 73% is observed in April, which was the month of very strict lockdown with almost all transport and industries closed. As the lockdown starts easing during each month, levels of PM_{10} continue to increase. However, even in July the decrease is significant, smallest approximately 33% for Central Road Research Institute. This could be due to continuation of lockdown for certain activities such as educational institutes, metro services, cinema halls, restricted attendance at offices, limited domestic air travel etc., as listed in **Table 1**. The major sources of PM_{10} are transport, industries, brick kiln, and dust from roads and construction activities (**Table 4**). All these remained closed during the lockdown and slowly and progressively allowed to return to normal. Since the lifetime of PM_{10} is very short, only a few hours (**Table 3**), it shows almost an instant effect of the changes. The ratio of decreases between Punjabi Bagh and Central Road Research Institute during different months shows an average value of 1.1, which indicates a uniform impact of lockdown on PM_{10} from north-west to south-east of urban Delhi (**Figure 1**). If these ratios are computed with respect to Anand Vihar to the other sites, the value is much higher, revealing that the magnitude of lockdown effect has been larger over this site with respect to PM_{10}. As mentioned in *The Study Locations*, Anand Vihar is located to the East of River Yamuna, comparatively more congested and impacted by mixed emissions from industries and transport sector. Furthermore, the magnitude of decreases evinces an overwhelming anthropogenic control of PM_{10} over Delhi.

Changes in the monthly average levels of $PM_{2.5}$ are shown for all the five locations selected for this work (**Figure 9B**) and additionally include the EPA data for the US Embassy in Delhi. In general and as for PM_{10} and also for other species, maximum decrease is observed in April. There is large variability from location to location. Shadipur shows the highest decrease of approximately 83% with respect to the 5 year average followed by Anand Vihar (approximately 61%) and other locations. Again, even in July the levels of $PM_{2.5}$ have not become normal, with the smallest decrease approximately 18% for the US Embassy. The emission sources of $PM_{2.5}$ are almost similar to that of PM_{10} but there is a significant contribution of secondary aerosols to $PM_{2.5}$. Some studies show almost 50% contribution from secondary aerosols to $PM_{2.5}$ mass of which nearly 30% is from secondary organic aerosol (Perrino et al., 2011; Rastogi et al., 2014). The formation of secondary aerosols is initiated by various gaseous pollutants such as NO_x, SO_2 as well as hydrocarbon oxidation. Hence, changes in these precursors also get reflected in the levels of $PM_{2.5}$. Another source apportionment study estimated daily $PM_{2.5}$ emissions over Delhi to be 58.7 ton/day, contributed by road dust (38%), vehicles (20%), domestic fuel burning (12%), industrial point sources (11%), concrete batching plant (6%), hotels/restaurants (3%), and municipal solid waste (MSW) burning (3%) (Nagar et al., 2017). Furthermore, the contribution from coal/fly-ash to $PM_{2.5}$ increased from 4.8%

in winter to 26% in summer, while the contribution from secondary inorganic aerosol decreased from 30% in winter to 15% in summer (Nagar et al., 2017). While PM_{10} decrease was highest for the Anand Vihar site (east Delhi), the $PM_{2.5}$ decrease was highest over Central Delhi for Shadipur. The ratios of Shadipur to Anand Vihar are 1.6, 1.4, 1.5, 1.7, and 1.6, respectively, for March–July months, with an average of 1.5. This near constant ratio evinces a 50% higher impact to $PM_{2.5}$ in Central Delhi compared to Eastern Delhi due to lockdown. Possibly, the chances of SOA formation locally can be accentuated by local emissions of precursor gases such as SO_2, NO_2 and hydrocarbons at Shadipur from industry, transport, and tourism sectors, as new construction activities as well as road dust are very limited over this region. Chemical characterization studies during summer over Delhi have found a higher contribution of SO_4^{2-}, NO_3^-, and NH_4^+ to $PM_{2.5}$ compared to PM_{10} (ARAI and TERI, 2018). Source apportionment studies point to potential chloride sources northwest of the Indian Institute of Technology (IIT) Delhi, such as industries of salt and metal processing and thermal power plants to fine PM (Jaiprakash et al., 2017).

Carbon Monoxide and Sulfur Dioxide

Both these species are considered primary pollutants. SO_2 contributes to respiratory symptoms. High levels of CO can reduce the amount of oxygen that can be transported in the bloodstream to critical organs such as the heart and the brain resulting in dizziness, confusion, unconsciousness, and even death. Both these species are not very reactive. SO_2 is formed during the burning of sulphur containing fuels, such as coal and oil, while CO is formed during the incomplete combustions e.g., fuels such as petrol, coal, or wood. In an urban environment, major sources of CO are transport, domestic cooking, brick kiln, industries, and power plants; while those of SO_2 are coal burning in power plants and industries, transport sector, and diesel-generating sets (**Table 3**). Lifetime of CO is approximately 15 days in a polluted region, while the main sink of SO_2 is deposition and has a lifetime of approximately 2 days (**Table 4**). Data for these two species are available for all the considered locations except for Central Road Research Institute, where SO_2 is not available. However, there seem to be large variations.

Figure 9C shows the observed monthly CO changes during 2020 with respect to the 5 year average of 2015–2019. CO shows large decrease in March for Punjabi Bagh, Shadipur, Central Road Research Institute, and NSIT-Dwarka. However, the change is negligible over Anand Vihar in East Delhi. While the decrease continues over Punjabi Bagh and Central Road Research Institute in April, over NSIT-Dwarka there is a negligible increase. The May values show a decrease in Punjabi Bagh, Shadipur, and Central Road Research Institute, while an increase is observed over Anand Vihar and NSIT-Dwarka. The maximum decrease in CO is observed for Central Road Research Institute (approximately 57, 71, 63% in March, April, and May) followed by Punjabi Bagh. Although biogenic emissions constitute a major source of CO, large changes in CO similar to other anthropogenic markers e.g., SO_2 indicate overwhelming anthropogenic components in Delhi. In a comprehensive study of air quality in 15 major cities of India using remotely sensed data, surface concentration measurements of CPCB, and Air Quality Zonal Modelling, more than 40% decrease was observed for CO in north Indian cities but for Delhi, an increase of 36% was observed (Rahaman et al., 2021). The study used data covering 43 days before and after lockdown; however, MEERA-2 observations by the same study showed a negligible decrease of 2.52%. The data for Rahaman et al. (2021) are taken from the ITO site at Delhi, which is approximately 7 km from Anand Vihar site, which shows a negligible decrease in CO unlike other sites in our study. On an average, CO decreases by over 50% during March-May, but there is large variability between individual sites e.g., negligible decrease in Anand Vihar to over 90% decrease in NSIT-Dwarka. Based on the data from the 134 observation sites of CPCB, Singh et al. (2020) concluded a decrease of CO over most parts of India. However, for the north-west region, the interquartile range for CO varied from +10% to −40% (Singh et al., 2020).

Large changes in SO_2 are observed in the lockdown months of March–May in the order of 35–50% in line with NO_2 and PM (**Figure 9D**). As the major sources of SO_2 are large point sources such as power plants, under influence of a given air mass, they are likely to have a similar impact over a larger region. This is evinced by very close values of percent changes during the lockdown months. However, unlike other sites, NSIT-Dwarka did not show a decrease in SO_2 during March 2020 (**Figure 9D**). A closer look at the site data revealed that the overall SO_2 levels had been higher in the first quarter of 2020 compared to similar periods in other years. This can be attributed to increasing construction activities in this western edge of urban Delhi including sewage treatment plants. Painting activities at construction sites are also a source of SO_2. A good marker of SO_2 source types is the SO_2 to NO_2 ratios. Renuka et al. (2020) have used it to show seasonal variation of sources at a rural site in South India. High SO_2 to NO_2 ratio indicates predominant impact of point sources such as power plants, while lower values indicate vehicular emissions that are rich in NO_x compared to SO_2 (Mallik et al., 2015). An increase in this ratio during the initial lockdown phases indicates that the impact of vehicular emissions decreased (reduced denominator in the form of NO_2) in comparison with point sources. The increase is particularly very clear over Anand Vihar (figure not shown). The impact of air mass change is also very evident in these ratios e.g., the values were higher over NSIT-Dwarka before onset of pre-monsoon winds indicating larger influence of point sources, while there is a sudden decrease in this ratio since mid of March. After this, as an effect of lockdown, the ratio starts to increase like other sites. Rahaman et al. (2021) have observed approximately 25% decrease in SO_2 based on ITO CPCB data while an increase of 23% was observed in a nearby site (Ghaziabad, 30 km east of ITO). Satellite observations over Delhi also showed approximately 40% decrease in the Rahman et al. study. In Singh et al. (2020) study, the variation of SO_2 is similar to CO with interquartile range for north-west India between +8% and −38%. Various estimates for SO_2 are calculated for Delhi e.g., 9% decrease (Chhikara and Kumar, 2020), 19% decrease (Kumari

and Toshniwal, 2020), 23% decrease (Singh et al., 2020), the differences may be attributed to the different periods of estimations, but overall all studies show a decrease.

NO_2

Oxides of nitrogen such as NO and NO_2, together called NO_x, are important pollutants emitted from combustion at high temperature. While emissions of NO_x are mostly in the form of NO, it is later converted into NO_2 by the reaction of NO with O_3, HO_2, RO_2, and other oxidants. During daytime conditions of sufficient O_3 and radiation, NO and NO_2 are in a fast photochemical equilibrium, or "photo-stationary state." The photolysis of NO_2 during the day is a direct source of tropospheric O_3. The NO_x concentration determines both the HO_x and O_3 cycles. At very high concentrations, NO_2 can be titrated by OH, eventually leading to HNO_3 formation. At very low concentrations, HO_2 loss through self-reactions and cross reactions with RO_2 lead to net HO_x loss. But as NO_x increases, the HO_2-NO reaction becomes competitive and HO_2 is recycled into OH increasing the chain length. Despite a short lifetime, NO_x can also be transported from one place to another either in its original gaseous state or in the form of nitrates, PAN etc., and nighttime chemistry becomes important (Levy et al., 1999). In high NO_x regimes like urban regions, including Delhi, the production of O_3 is generally limited by volatile organic compounds (VOCs). Both NO and NO_2 are measured at several locations in Delhi but we discuss results of NO_2, here as it is observed at all the locations selected and column NO_2 is also measured by satellites. The change in the monthly average levels of NO_2 during 2020 compared to the average of 2015–2019 is shown in **Figure 9E**. While average surface NO_2 levels decreased by only 43% for the study sites over Delhi, the average decrease was 57, 50, 40, and 26%, respectively, for April, May, June, and July. On a different perspective, tropospheric NO_2 decreased by 57, 53, 32, and −6% for April, May, June, and July i.e., for the same months. The numbers are self-explanatory as April was a complete lockdown and May was a partial lockdown, while in March (average decrease of 14% only), lockdown was implemented in the last week only. The April NO_2 levels came down from 30 $\mu g\, m^{-}3$ in the previous years (2015–2019 average) to approximately 11 $\mu g\, m^{-3}$ in the lockdown. Because the major influence on NO_2 concentrations is from anthropogenic emissions, the impact of lockdown is nicely traced in surface NO_2 measurements. The lowest levels of NO_2 among the study sites are observed for NSIT-Dwarka, while the highest levels are observed for Anand Vihar in the east of Delhi. This is because NSIT-Dwarka is a more planned area with open spaces and airport, while Anand Vihar is congested with multiple emission sources. Furthermore, it is to be noted that Anand Vihar has a major inter-state bus terminal and the bus service as well as local travel is still not to full scale. Punjabi Bagh and Shadipur show almost similar patterns from 2015 to 2020, including the sudden decrease during the lockdown. The maximum change by approximately 76% is observed in April at Anand Vihar. As the lockdown is relaxed gradually, the 2020 levels start coming toward the normal. The decrease at Anand Vihar became approximately 38% in July. Levels of NO_2 at other locations also have not come to normal levels. An early study of lockdown effect on NO_2 for different states of India using Aura/OMI data revealed that among the other states of India, the maximum decrease was observed over Delhi (62% over 2019 values and 54% over 2015–2019 average values) with higher decrease in phase I (25 March–14 April, 2020) compared to phase 2 (15 April–3 May, 2020) (Pathakoti et al., 2020). Similar decreases over Delhi were concluded by various studies: 63.9% (Bedi et al., 2020), 42.27% (Chhikara and Kumar, 2020), 60% (Kumari and Toshniwal, 2020), 56% (Singh et al., 2020); the differences being the varied periods for averaging as well as varying reference periods. Even in our study, in contrast to SO_2, the variability of NO_2 among different stations exhibited an overall decrease from March to April to May to June. This indicates that as lockdown measures strengthened from March to April, people settled in their homes leading to minimum vehicular and industrial emissions, decrease in both NO_2 levels as well as the variability between different sites in Delhi was evident. The homogeneity between sites strengthened until May as people settled into similar patterns of life with similar patterns of emissions. This continued even in June when values started to increase with relaxations in activities, but the pattern remained similar leading to lower variability in terms of decrease in different sites in Delhi (**Figure 9E**; **Table 1**).

O_3

The daytime chemical production and loss of surface O_3 in the troposphere is controlled by competing reactions involving many of its precursors such as NO_2, NO, CO and hydrocarbons in the presence of sunlight (Seinfeld and Pandis, 2006). It is produced by the reaction of atomic oxygen with molecular oxygen as in the stratosphere. However, this atomic oxygen does not come from the dissociation of molecular oxygen as in the stratosphere but from the dissociation of NO_2 as shown in the following simple reactions scheme.

$$CH_4 + OH \rightarrow CH_3 + H_2O \quad \text{(R1)}$$

$$CH_3 + O_2 \rightarrow CH_3O_2 \quad \text{(R2)}$$

$$CH_3O_2 + NO \rightarrow CH_3O + NO_2 \quad \text{(R3)}$$

$$NO_2 + h\nu\,(\lambda < 424\ nm) \rightarrow NO + O(^3P) \quad \text{(R4)}$$

$$O(^3P) + O_2 \rightarrow O_3 + M \quad \text{(R5)}$$

OH is produced from the reaction of water with $O(^1D)$, which in turn is produced from the photolysis of O_3 at wavelengths <320 nm.

$$O_3 + h\nu \rightarrow O(^1D) + O_2 \quad \text{(R6)}$$

$$HO + O_3 \rightarrow HO_2 + O_2 \quad \text{(R7)}$$

$$HO_2 + O_3 \rightarrow OH + 2O_2 \quad \text{(R8)}$$

$$NO + O_3 \rightarrow NO_2 + O_2 \quad \text{(R9)}$$

In the absence of competing reactions, the net effect of reactions R4, R5, and R9 is zero. The reaction of OH initiates the breakdown of CO and VOCs, resulting in the formation of RO_x (e.g., R1). The simplest is HO_2, formed from the oxidation of CO to CO_2. While radical-radical self and cross reactions are dominant at low NO, with increasing NO_x, NO

gradually outcompetes the peroxide-forming reactions, leading to rapid recycling between OH and HO_2. At very high concentrations, there is net loss in the form of HNO_3, while at very low concentrations of NO_x, there is HO_x loss in the form of peroxides. Depending on VOC to NO_x ratio, the oxidation capacity increases at intermediate NO_x levels. Mertens et al. (2021) employed a combination of regional chemistry climate model (CCM-COSMO) and global chemistry climate model (CCM_EMAC) with a general circulation base model (ECHAM5) to make a sector-wise attribution of O_3 changes resulting out of emission reductions during the lockdown over Europe. Interestingly, the authors found that despite reduced O_3 production due to reduced anthropogenic emissions, the O_3 production efficiency (OPE) i.e., net O_3 production per molecule of NOx increased. It was also observed that the ratio of H_2O_2 (HO_2 sink) to HNO_3 (OH sink) production rates exhibited an enhancement during the lockdown period indicating a shift from NOx-saturated to NOx-limited regime. Despite increased OPE, there was a net O_3 reduction as anthropogenic emission reduction overcompensated the enhanced OPE and natural emissions. Furthermore, as O_3 has a fairly long lifetime, the impact of atmospheric transport can compensate for immediate chemical changes in a region. In another study, sensitivity of global tropospheric O_3 burden to anthropogenic NOx reductions (COVID-2020 emission anomaly over 2010–2019) was studied employing the state-of-the-art multi-constituent satellite data assimilation system, which was used to ingest multiple satellite observations to simultaneously optimize concentrations and emissions of trace species and simulating their chemical interaction (Miyazaki et al., 2021). Strong O_3 response to NOx reductions in highly polluted areas attributed to NOx titrations and enhanced oxidation capacity led to local O_3 enhancements. The role of atmospheric transport was revealed in Miyazaki et al. study such that O_3 reductions in Central Eastern Eurasia were attributed to emission reductions over North America. In this study, global reductions were also estimated for peroxyacetyl nitrate (NOx reservoir) and OH. Using generalized additive models fed by reanalysis meteorological data, Ordóñez et al. (2020) showed that while NO_2 concentration variations in Europe were attributed to reduced emissions, O_3 concentration changes were mostly explained by meteorology. Over Delhi, O_3 reduction upto 13% was observed by Datta et al. (2021); the authors use statistical analysis to show that O_3 concentration variations were not explained by lockdown effects unlike PM variations, which were largely contributed by lockdown-induced emission changes.

Community Multi-Scale Air Quality (CMAQ) model estimations revealed that during lockdown, there was a 15% decrease in maximum daily 8 h average (MDA8) O_3 (Zhang et al., 2021). However, in some VOC-limited urban regions, O_3 enhancement was observed mainly due to higher reduction of NOx compared to VOCs. If both VOCs and NO_x are low for example in the pristine regions, production of O_3 is very low. If both are high for example in a polluted urban region, high levels of O_3 can be produced (Seinfeld and Pandis, 2006). In the intermediate regime, O_3 production or loss depends upon the levels of NO_x and hydrocarbons. The transition from VOC-limited to NOx-limited regimes can be gauged through various proxies. OPE (i.e., $\Delta O_3/\Delta NOz$) is a simple measure to infer the O_3 formation regimes with values less than 4 indicating VOC limited and greater than 7 indicating NOx limited (Wang et al., 2017). Another popular proxy is the ratio of OH-reactivity of NOx to OH-reactivity of VOC (Sinha et al., 2012). If this ratio exceeds 0.2 (±0.1), the O_3 production regime is VOC limited, whereas if it is below 0.01, the O_3 production regime is considered NOx limited. The intermediate range, $0.01 < 2 < 0.2$, indicates that the peak O_3 production depends strongly on both NOx and VOC levels. Furthermore, as the production of HCHO is proportional to reactions of reactive organics with OH, the HCHO/NOy ratio can also be used to segregate the two regimes with 0.28 marking the transition from VOC limited to NOx limited (Sillman, 1995).

In the VOC-limited regime, decreasing VOC emissions reduces the chemical production of organic radicals (RO_2), leading to decreased cycling with NOx thus reducing O_3 (Wang et al., 2021). In the NOx-limited regime, decreasing NOx emission reduces NO_2 photolysis, directly reducing O_3. In contrast, in the VOC-limited regime, NOx acts to reduce O_3, so decreased NOx emissions promote O_3 production (Kleinman, 1994). Furthermore, in the NOx-limited regime (or VOC-saturated), O_3 production is proportional to square root of HOx (OH + HO_2) production while in the VOC-limited (or NOx-saturated) regime, O_3 production is directly proportional to HOx production. A WRF-Chem modelling study revealed that the IGP region (including Delhi) is in a NOx to VOC transition regime (Chutia et al., 2019). A box model study using the NCAR master mechanism found that O_3 production in Delhi/NCR is limited by the abundance of VOCs even though NOx is higher (Chen et al., 2021). In such VOCs-limited regimes, a decrease in NO_x would lead to enhancement in O_3. During the lockdown most of the vehicular emissions came to total halt except emergency vehicles. Various industries were closed as well as many other anthropogenic sources of emissions of these pollutants. However, power generation did not stop but got reduced. Major sources of NO_x in Delhi are transport, industries, and diesel generator sets (**Table 3**). All these three sources were almost closed during the lockdown. Similarly, major sources of VOCs include transportation (~50%), brick kiln, and power plants (Guttikunda and Calori, 2013). The first two were totally closed during the lockdown. So the lockdown would lead to a much larger reduction in NO_x. However, in the absence of VOC measurements over Delhi, it will be difficult to quantify the transition regions from VOC limited to NOx limited.

Surface O_3 shows different features at different study sites in Delhi (**Figure 9F**). The O_3 results for the Central Road Research Institute are not used here as there are often breaks in the data. One explanation for this variation is related to the ratio of VOCs to NO_x. A clear increase in O_3 values is observed over Anand Vihar and NSIT-Dwarka, while the unlock phase brings back the O_3 values down. In a normal scenario, spring peak in O_3 is observed over Delhi as a result of biomass burning in the adjoining areas. Over Shadipur and NSIT-Dwarka, the levels had been similar before lockdown and all were showing a gradual increase from February to March. However, over

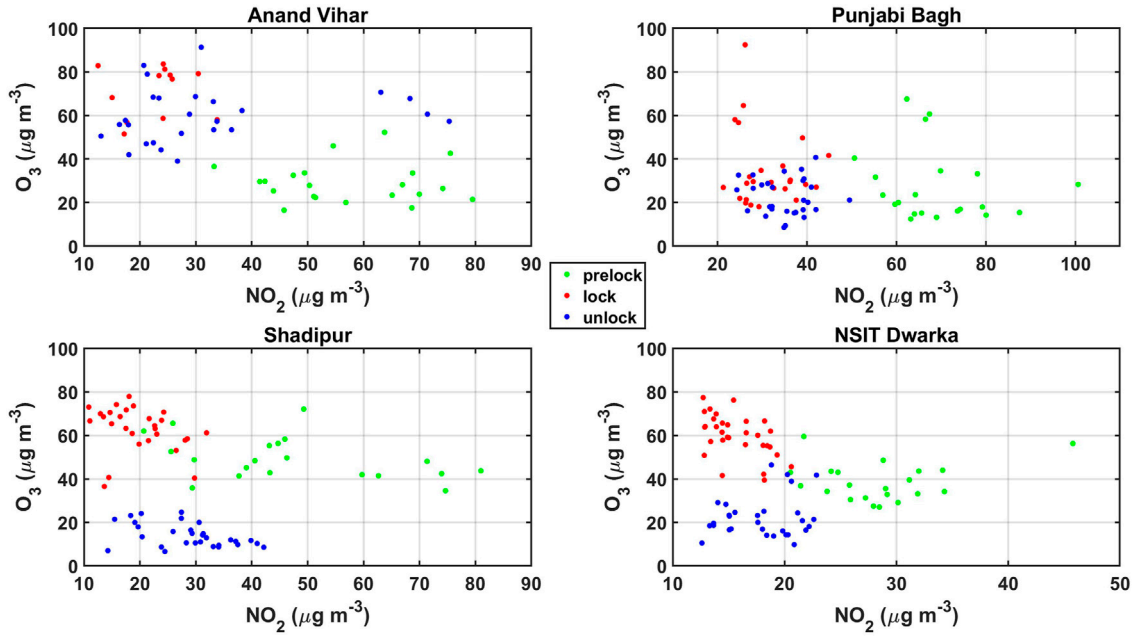

FIGURE 10 | O_3-NO_2 relationships for different lockdown phases and for different study sites.

Anand Vihar and Punjabi Bagh, the increase was not gradual but there had been a decrease in the 1st week of March followed by an increase just before lockdown. However, since the onset of lockdown, O_3 over Anand Vihar continued to increase and daily average remained over 60 μg m^{-3} until air masses changed in late June when O_3 levels started coming down. NSIT-Dwarka, located on the western part of Delhi, also showed concurrent features like Anand Vihar (east Delhi) increasing till Phase 3. However, in Phase 3, as relaxations start in transport services, the plummet in O_3 levels coincided exactly with an increase in NO_2. This shows that during lockdown, as anthropogenic emissions decreased, O_3 over Delhi which is normally in a VOC-limited regime is now controlled by titration effects with NO_x. The feature is specifically visible over NSIT-Dwarka, where overall NO_x levels are lower among the studied sites and decreased further during lockdown (**Figure 10**). The O_3-NOx relationships show different patterns between pre-lockdown, lockdown, and unlock periods at different sites. For instance, over Punjabi Bagh and Anand Vihar, lockdown and unlock data are indiscernible while over Shadipur and NSIT Dwarka, there is a distinct reduction in O_3 levels between lockdown and unlock periods. It must be mentioned here that for these O_3-NOx relationships, we have not considered the variation of VOCs. However, since these are natural atmospheric data, VOCs in **Figure 10**, although not shown (due to nonavailability of data), would also be different for each individual point. As mentioned before from the Zhang et al. (2021) analysis, NOx reductions are likely to be much larger than VOC reductions. This is because the major sources of NOx are few and were severely impacted by the lockdown e.g., vehicular emissions but VOC sources are much more varied and all were not impacted by lockdown e.g., residential emissions.

CONCLUSION

India started taking precaution in the initial phase of the spread of the corona virus by imposing strict lockdown from 25th March, 2020 itself. This led to closing down of all the industrial activities, all kinds of travel, educational institutes and people were asked to remain in their houses. We studied the impact of these closed anthropogenic sources of emissions during the lockdown from 25th March to almost May end and later unlocking of these till the end of July 2020 at 5 selected locations covering Delhi using *in-situ* measurements and satellite-based measurements of important pollutants. Daily and monthly average values of these pollutants for 2020 were compared with the 5-year average values from 2015 to 2019. Satellite-based measurements of monthly average AOD and tropospheric column of NO_2 for the entire Delhi showed changes from the 5 year average and are listed in **Table 5**. Comparing the average decrease of different species, it was observed that the species most affected by the lockdown as observed for April data are PM (includes both fine and coarse modes), NO_2 (includes both surface level and tropospheric column), and CO. In terms of percentage changes, the different species (except AOD and O_3) were clumped together in April when lockdown was in full force. Overall O_3 showed an increase over Delhi while AOD showed a much lower decrease compared to PM. The large decrease for CO during lockdown indicates predominant contributions of anthropogenic sources in Delhi for this species. Similar decreases in both surface and columnar NO_2 during March-June indicate dominant contribution of surface sources to NO_2 columns over Delhi. While tropospheric col NO_2 concentrations during COVID-19 months decreased by −56.9%, −53%, and −32.4% in April, May, and June, the AOD values decreased

TABLE 5 | Average combined percentage change for all the stations considered here as representative for changes in Delhi in monthly mean concentrations of various species during COVID-19 months with respect to average of 2015–19.

	March	April	May	June	July
AOD	10.4	−25.3	−22.5	−7.1	2.5
Tropo Col NO_2	−13.4	−56.9	−53.0	−32.4	−5.5
PM_{10}	−38.4 ± 13.2	−58.0 ± 13.6	−47.8 ± 20.8	−47.2 ± 18.2	−45.8 ± 19.1
$PM_{2.5}$	−42.1 ± 11.8	−54.0 ± 17.9	−34.7 ± 19.6	35.0 ± 13.2	−33.7 ± 14.0
NO_2	−14.4 ± 25.4	−56.7 ± 17.1	−49.6 ± 14.8	−39.8 ± 13.1	−25.6 ± 7.7
CO	−53.8 ± 35.6	−57.4 ± 28.5	−45.3 ± 42.6	−28.8 ± 26.3	−7.2 ± 11.0
O_3	21.6 ± 46.7	43.4 ± 57.0	17.3 ± 78.3	21.4 ± 79.4	9.5 ± 82.2
SO_2	−33.7 ± 32.5	−48.1 ± 4.5	−24.6 ± 24.5	−0.7 ± 30.0	20.9 ± 32.7

only by −25.3% in April, 2020 with respect to the 5 years average. These slow changes in AOD continued with −22.5% and −7.1% in May and June respectively. By July 2020, the AOD values have almost become normal. It is to be noted that AOD showed much lower decrease than tropospheric column NO_2. A similar difference is also observed by Pope et al. (2018). This could be due to the fact that loss of aerosols through deposition occurs near the Earth's surface. The smaller aerosols in the boundary layer as well as in the free troposphere coagulate to form bigger particles, which also contribute to AOD. The lifetimes of aerosols near the surface are very short as mentioned in **Table 4** but much longer in the free troposphere. So when emission of aerosols reduces at the surface, column values (AOD) do not change that much. However, NO_2 is photochemically dissociated to form NO, which is highly reactive and reacts with various gases forming nitrates as well as reforming NO_2. This happens even more at the higher heights due to intense solar radiation. Hence, when the supply from the emission sources at the surface reduces, column NO_2 also reduces.

The *in-situ* measurements of surface level PM_{10} and $PM_{2.5}$ also showed maximum decrease of −58% and −54% respectively for April, 2020. However, there was a significant decrease in March itself for both the species by −38.4% and −42.1% respectively for PM_{10} and $PM_{2.5}$. This was due to 8 days of lockdown in March coupled to seasonal change in wind direction resulting in different source regions. A decrease of −45.8% and −33.7% was observed in July also for both these species even during the second unlock phase. Also, PM_{10} showed slightly more decrease than $PM_{2.5}$ in the same period. This could be because of the lifetime of PM_{10} being shorter than $PM_{2.5}$ (**Table 4**). Decrease in NO_2 was almost similar to that of PM_{10} and $PM_{2.5}$. Major sources of aerosols and NO_2 are transport and industries (**Table 3**), which were totally closed during the first two phases of the lockdown. Although biogenic emissions constitute a major source of CO, large changes in CO similar to other anthropogenic markers e.g., SO_2 indicate overwhelming anthropogenic components in Delhi. It is to be noted that the lifetime of CO is much higher than that of SO_2 and other species. Singh et al. (2020) have analyzed data for the Indian region and have shown an average decrease in PM_{10}, $PM_{2.5}$, NO_2, and CO by about −58%, −45%, −50%, and −38% respectively.

O_3, as discussed in **Section 4.6**, has complex chemistry depending not only on the levels of its precursors but also on the balance of NOx and hydrocarbons. Model estimates for Delhi show that it is hydrocarbon controlled (Chen et al., 2021). We observed mixed signals (increase as well as decrease) in the levels of O_3 at different locations. This could be possible due to different combinations of NOx and hydrocarbons, as these locations have different emission sources, some are heavily transport (NOx) impacted, while others have higher hydrocarbon emissions. During lockdown, as anthropogenic emissions decreased, O_3 over Delhi which is normally in a VOC-limited regime is now controlled by NOx. The feature is specifically visible over NSIT-Dwarka, where overall NOx levels were lower among the studied sites and decreased further during lockdown. A clear increase in O_3 values was observed over Anand Vihar and NSIT-Dwarka, while the unlock phase evinced a fall in the O_3 values. Singh et al. (2020) have found mixed variations in O_3 due to lockdown in different parts of India. Similar studies from China and Europe found slight increases in O_3 levels during the lockdown (Shi and Brasseur, 2020; Xu et al., 2020; Sicard et al., 2020).

Overall, the effect on the levels of pollutants was mainly due to the reduced vehicular emissions and atmospheric transport from the surrounding regions as well as due to power generation and other point sources. The higher peaks in $PM_{2.5}$ coincide with north-westerly air-masses sourced to industrial regions in Haryana and Punjab of India all the way back to Lahore in Pakistan and further back to the north-west. Simultaneously, higher levels of tropospheric NO_2 column values were observed in the month of May toward the north-west of Delhi and up to Pakistan in the IGP which suggests heavy pollution due to industrialization in this area acting as a source for Delhi. The ratio of decreased PM_{10} between Punjabi Bagh and Central Road Research Institute during different months showed an average value of 1.1, which indicates a uniform impact of lockdown on PM_{10} from north-west to south-east of urban Delhi. However for $PM_{2.5}$, the ratios of Shadipur to Anand Vihar are 1.6, 1.4, 1.5, 1.7, and 1.6, respectively, for March to July months, with an average of 1.5. This near constant ratio evinces a 50% higher impact on $PM_{2.5}$ in Central Delhi compared to Eastern Delhi due to lockdown. It is to be noted that the lockdown was all over India. We have seen that Delhi gets affected from the surrounding regions, states, as well as even from the nearby countries such as Pakistan and Afghanistan (**Figure 7**). Hence, these effects are cumulative. In this context, it is worth mentioning that the control of pollution by the local government through restriction of odd-even vehicular movement (only 4 wheelers and in Delhi city only) did not yield the desired results (Chandra et al., 2018).

Hence, changes in the levels of various pollutants during the lockdown-2020 were variable depending upon the emission sources, lifetimes, and chemistry. These results are very useful

for testing and updating the emission inventories as well as for models.

DATA AVAILABILITY STATEMENT

Publicly available datasets were analyzed in this study. This data can be found here: https://app.cpcbccr.com/ccr/#/caaqm-dashboard/caaqm-landing/caaqm-comparison-data.

AUTHOR CONTRIBUTIONS

CM: conceptualization, overall data analysis, review and write-up. HG: FlexPart and AOD data analysis, review and write-up. SL: conceptualization, overall data analysis, review and write-up. RKY: NO2 columnar data analysis, review and editing. RB: data analysis, review and editing. TD: data analysis, review and editing.

ACKNOWLEDGMENTS

We acknowledge that OMI NO_2 column data were downloaded from https://disc.gsfc.nasa.gov/. VIIRS AOD data were downloaded from https://ladsweb.modaps.eosdis.nasa.gov/. The reanalysis data of meteorology were downloaded from https://rda.ucar.edu/datasets/ds083.2/. Authors thank science teams and personnel associated with generating these data. The FLEXPART model was downloaded from https://www.flexpart.eu/. Authors thank developers and scientists associated with FLEXPART model development. SL is grateful to the Director PRL, Ahmedabad and to CSIR, New Delhi for their support for his position. TD and RB are grateful to Director CSIR-IMMT, Bhubaneswar for support and ISRO-GBP (ATCTM) for funding. Authors sincerely thank the two reviewers for their constructive comments that has improved the MS to its present form. We also thank the editor for quick and timely processing of the MS.

REFERENCES

Andrews, M., Areekal, B., Rajesh, K., Krishnan, J., Suryakala, R., Krishnan, B., et al. (2020). First Confirmed Case of COVID-19 Infection in India: A Case Report. *Indian J. Med. Res.* 151 (5), 490–492. doi:10.4103/ijmr.IJMR_2131_20

Apte, J. S., Marshall, J. D., Cohen, A. J., and Brauer, M. (2015). Addressing Global Mortality from Ambient PM2.5. *Environ. Sci. Technol.* 49 (13), 8057–8066. doi:10.1021/acs.est.5b01236

ARAI and TERI (2018). Executive SUmmary: Source Apportionment of PM2.5 & PM10 of Delhi NCR for Identification of Major Sources. Report No. ARAI/16-17/DHI-SA-NCR/Exec_Summ. Available at: https://www.teriin.org/sites/default/files/2018-08/Exec-summary.pdf

Bali, K., Dey, S., Ganguly, D., and Smith, K. R. (2019). Space-time Variability of Ambient PM2.5 Diurnal Pattern over India from 18-years (2000-2017) of MERRA-2 Reanalysis Data. *Atmos. Chem. Phys. Discuss.*, 1–23. doi:10.5194/acp-2019-731

Bangar, V., Mishra, A. K., Jangid, M., and Rajput, P. (2021). Elemental Characteristics and Source-Apportionment of PM2.5 during the Post-monsoon Season in Delhi, India. *Front. Sustain. Cities* 3, 648551. doi:10.3389/frsc.2021.648551

Bedi, J. S., Dhaka, P., Vijay, D., Aulakh, R. S., and Gill, J. P. S. (2020). Assessment of Air Quality Changes in the Four Metropolitan Cities of India during COVID-19 Pandemic Lockdown. *Aerosol Air Qual. Res.* 20, 2062–2070. doi:10.4209/aaqr.2020.05.0209

Beig, G., Srinivas, R., Parkhi, N. S., Carmichael, G. R., Singh, S., Sahu, S. K., et al. (2019). Anatomy of the winter 2017 Air Quality Emergency in Delhi. *Sci. Total Environ.* 681, 305–311. doi:10.1016/j.scitotenv.2019.04.347

Bithal, S. (2018). Delhi Loses 80 Lives to Air Pollution Every Day, Says Study: Outdoor Air Pollution Is the Fifth Largest Killer in India, Down to Earth published on, , https://www.downtoearth.org.in/news/delhi-loses-80-lives-to-air-pollution-every-day-says-study-50222 (Accessed 10 Dec 2018).

Chandra, B. P., Sinha, V., Hakkim, H., Kumar, A., Pawar, H., Mishra, A. K., et al. (2018). Odd-even Traffic Rule Implementation during winter 2016 in Delhi Did Not Reduce Traffic Emissions of VOCs, Carbon Dioxide, Methane and Carbon Monoxide. *Curr. Sci.* 114 (6), 1318–1325. doi:10.18520/cs/v114/i06/1318-1325

Chen, Y., Beig, G., Archer-Nicholls, S., Drysdale, W., Acton, W. J. F., Lowe, D., et al. (2021). Avoiding High Ozone Pollution in Delhi, India. *Faraday Discuss.* 226, 502–514. doi:10.1039/D0FD00079E

Chhikara, A., and Kumar, N. (2020). COVID-19 Lockdown: Impact on Air Quality of Three Metro Cities in India. *ajae* 14 (4), 378–393. doi:10.5572/ajae.2020.14.4.378

Chutia, L., Ojha, N., Girach, I. A., Sahu, L. K., Alvarado, L. M. A., Burrows, J. P., et al. (2019). Distribution of Volatile Organic Compounds over Indian Subcontinent during winter: WRF-Chem Simulation versus Observations. *Environ. Pollut.* 252, 256–269. doi:10.1016/j.envpol.2019.05.097

Conibear, L., Butt, E. W., Knote, C., Arnold, S. R., and Spracklen, D. V. (2018). Residential Energy Use Emissions Dominate Health Impacts from Exposure to Ambient Particulate Matter in India. *Nat. Commun.* 9, 617. doi:10.1038/s41467-018-02986-7

Conley, S. A., Faloona, I. C., Lenschow, D. H., Campos, T., Heizer, C., Weinheimer, A., et al. (2011). A Complete Dynamical Ozone Budget Measured in the Tropical marine Boundary Layer during PASE. *J. Atmos. Chem.* 68, 55–70. doi:10.1007/s10874-011-9195-0

Croft, B., Pierce, J. R., and Martin, R. V. (2014). Interpreting Aerosol Lifetimes Using the GEOS-Chem Model and Constraints from Radionuclide Measurements. *Atmos. Chem. Phys.* 14, 4313–4325. doi:10.5194/acp-14-4313-2014

Datta, A., Rahman, M. H., and Suresh, R. (2021). Did the COVID-19 Lockdown in Delhi and Kolkata Improve the Ambient Air Quality of the Two Cities? *J. Environ. Qual.* 50 (2), 485–493. doi:10.1002/jeq2.20192Epub 2021 Jan 25

Dhaka, S. K., Chetna, V. K., Dimri, A. P., Singh, N., et al. (2020). PM2.5 Diminution and Haze Events over Delhi during the COVID-19 Lockdown Period: an Interplay between the Baseline Pollution and Meteorology. *Sci. Rep.* 10, 13442. doi:10.1038/s41598-020-70179-8

Gadhavi, H. S., Renuka, K., Kiran, V. R., Jayaraman, A., Stohl, A., Klimont, Z., et al. (2015). Evaluation of black carbon emission inventories using a Lagrangian dispersion model a case study over southern India. *Atmos. Chem. Phys.* 15, 1447–1461. doi:10.5194/acp-15-1447-2015

Goel, V., Hazarika, N., Kumar, M., Singh, V., Thamban, N. M., and Tripathi, S. N. (2021). Variations in Black Carbon Concentration and Sources during COVID-19 Lockdown in Delhi. *Chemosphere* 270, 129435. doi:10.1016/j.chemosphere.2020.129435

Grythe, H., Kristiansen, N. I., Groot Zwaaftink, C. D., Eckhardt, S., Ström, J., Tunved, P., et al. (2017). A New Aerosol Wet Removal Scheme for the Lagrangian Particle Model FLEXPART V10. *Geosci. Model. Dev.* 10, 1447–1466. doi:10.5194/gmd-10-1447-2017

Guttikunda, S. K., and Calori, G. (2013). A GIS Based Emissions Inventory at 1 Km × 1 Km Spatial Resolution for Air Pollution Analysis in Delhi, India. *Atmos. Environ.* 67, 101–111. doi:10.1016/j.atmosenv.2012.10.040

Hama, S. M. L., Kumar, P., Harrison, R. M., Bloss, W. J., Khare, M., Mishra, S., et al. (2020). Four-year Assessment of Ambient Particulate Matter and Trace Gases in the Delhi-NCR Region of India. *Sust. Cities Soc.* 54, 102003. doi:10.1016/j.scs.2019.102003

Inomata, Y., Iwasaka, Y., Osada, K., Hayashi, M., Mori, I., Kido, M., et al. (2006). Vertical Distributions of Particles and Sulfur Gases (Volatile Sulfur Compounds and SO2) over East Asia: Comparison with Two Aircraft-Borne Measurements under the Asian Continental Outflow in Spring and Winter. *Atmos. Environ.* 40, 430–444. doi:10.1016/j.atmosenv.2005.09.055

Jain, S., Sharma, S. K., Vijayan, N., and Mandal, T. K. (2020). Seasonal Characteristics of Aerosols (PM2.5 and PM10) and Their Source

Apportionment Using PMF: A Four Year Study over Delhi, India. *Environ. Pollut.* 262, 114337. doi:10.1016/j.envpol.2020.114337

Jain, S., and Sharma, T. (2020). Social and Travel Lockdown Impact Considering Coronavirus Disease (COVID-19) on Air Quality in Megacities of India: Present Benefits, Future Challenges and Way Forward. *Aerosol Air Qual. Res.* 20 (6), 1222–1236. doi:10.4209/aaqr.2020.04.0171

Jaiprakash, S. A., Habib, G., Raman, R., and Gupta, T. (2017). Chemical characterization of PM1 aerosol in Delhi and source apportionment using positive matrix factorization. *Environ. Sci. Pollut. Res.* 24, 445–462. doi:10.1007/s11356-016-7708-8

Kleinman, L. I. (1994). Low and High NOxtropospheric Photochemistry. *J. Geophys. Res.* 99, 16831–16838. doi:10.1029/94jd01028

Kristiansen, N. I., Stohl, A., Olivié, D. J. L., Croft, B., Søvde, O. A., Klein, H., et al. (2016). Evaluation of Observed and Modelled Aerosol Lifetimes Using Radioactive Tracers of Opportunity and an Ensemble of 19 Global Models. *Atmos. Chem. Phys.* 16, 3525–3561. doi:10.5194/acp-16-3525-2016

Krotkov, N. A., Lamsal, L. N., Marchenko, S. V., Bucsela, E. J., and Swartz, W. H. (2019). *OMI/Aura Nitrogen Dioxide (NO2) Total and Tropospheric Column 1-orbit L2 Swath 13x24 Km V003*. Greenbelt, MD, USA: Goddard Earth Sciences Data and Information Services Center (GES DISC). Joiner, J. and the OMI core team. doi:10.5067/Aura/OMI/DATA2017

Kumari, P., and Toshniwal, D. (2020). Impact of Lockdown Measures during COVID-19 on Air Quality- A Case Study of India. *Int. J. Environ. Health Res.* 00 (00), 1–8. doi:10.1080/09603123.2020.1778646

Lalchandani, V., Kumar, V., Tobler, A., M. Thamban, N., Mishra, S., Slowik, J. G., et al. (2021). Real-time Characterization and Source Apportionment of fine Particulate Matter in the Delhi Megacity Area during Late winter. *Sci. Total Environ.* 770, 145324. doi:10.1016/j.scitotenv.2021.145324

Lamsal, L. N., Krotkov, N. A., Vasilkov, A., Marchenko, S., Qin, W., Yang, E.-S., et al. (2020). OMI/Aura Nitrogen Dioxide Standard Product with Improved Surface and Cloud Treatments. *Atmos. Meas. Tech.* 14 (1), 455–479. doi:10.5194/amt-2020-200

Lawrence, M. G., and Lelieveld, J. (2010). Atmospheric pollutant outflow from southern Asia: a review. *Atmos. Chem. Phys.* 10, 11017–11096. doi:10.5194/acp-10-11017-2010

Le, T., Wang, Y., Liu, L., Yang, J., Yung, Y. L., Li, G., et al. (2020). Unexpected Air Pollution with Marked Emission Reductions during the COVID-19 Outbreak in China. *Science* 369 (6504), 702–706. doi:10.1126/science.abb7431

Lee, C., Richter, A., Lee, H., Kim, Y. J., Burrows, J. P., Lee, Y. G., et al. (2008). Impact of Transport of Sulfur Dioxide from the Asian Continent on the Air Quality over Korea during May 2005. *Atmos. Environ.* 42, 1461–1475. doi:10.1016/j.atmosenv.2007.11.006

Lelieveld, J., Evans, J. S., Fnais, M., Giannadaki, D., and Pozzer, A. (2015). The contribution of outdoor air pollution sources to premature mortality on a global scale. *Nature* 525, 367–371. doi:10.1038/nature15371

Levelt, P. F., Van Den Oord, G. H. J., Dobber, M. R., Malkki, A., Visser, H., Vries, J., et al. (2006). The Ozone Monitoring Instrument. *IEEE Trans. Geosci. Remote Sensing* 44, 1093–1101. doi:10.1109/tgrs.2006.872333

Levy, H., II, Moxim, W. J., Klonecki, A. A., and Kasibhatla, P. S. (1999). Simulated Tropospheric NOx: Its Evaluation, Global Distribution and Individual Source Contributions. *J. Geophys. Res.* 104, 26279–26306. doi:10.1029/1999JD900442

Levy, R. C., Mattoo, S., Sawyer, V., and Munchak, L. A. (2020). *AERDT_L2_VIIRS_SNPP - VIIRS/SNPP Dark Target Aerosol L2 6-Min Swath 6 Km*. accessed on: 2020-09-01. doi:10.5067/VIIRS/AERDT_L2_VIIRS_SNPP.001

Levy, R. C., Munchak, L. A., Mattoo, S., Patadia, F., Remer, L. A., and Holz, R. E. (2015). Towards a Long-Term Global Aerosol Optical Depth Record: Applying a Consistent Aerosol Retrieval Algorithm to MODIS and VIIRS-Observed Reflectance. *Atmos. Meas. Tech.* 8, 4083–4110. doi:10.5194/amt-8-4083-2015

Liu, F., Beirle, S., Zhang, Q., Dörner, S., He, K., and Wagner, T. (2016). NOx Lifetimes and Emissions of Cities and Power Plants in Polluted Background Estimated by Satellite Observations. *Atmos. Chem. Phys.* 16, 5283–5298. doi:10.5194/acp-16-5283-2016

Mahato, S., Pal, S., and Ghosh, K. G. (2020). Effect of Lockdown amid COVID-19 Pandemic on Air Quality of the Megacity Delhi, India. *Sci. Total Environ.* 730, 139086. doi:10.1016/j.scitotenv.2020.139086

Mallik, C., and Lal, S. (2011). Changing Long-Term Trends in Tropospheric Temperature over Two Megacities in the Indo-Gangetic Plain. *Curr. Sci.* 101 (5), 637–644.

Mallik, C., Venkataramani, S., and Lal, S. (2015). Trace gases over a semi-arid urban site in western India: variability and inter-correlations. *J. Atmos. Chem.* 72, 143–164. doi:10.1007/s10874-015-9311-7

Mallik, C., Chandra, N., Venkataramani, S., and Lal, S. (2016). Variability of Atmospheric Carbonyl Sulfide at a Semi-arid Urban Site in Western India. *Sci. Total Environ.* 551-552, 725–737. doi:10.1016/j.scitotenv.2016.02.014

Mertens, M., Jöckel, P., Matthes, S., Nützel, M., Grewe, V., and Sausen, R. (2021). COVID-19 Induced Lower-Tropospheric Ozone Changes. *Environ. Res. Lett.* 16 (6), 064005. doi:10.1088/1748-9326/abf191

Miyazaki, K., Bowman, K., Sekiya, T., Takigawa, M., Neu, J. L., Sudo, K., et al. (2021). Global Tropospheric Ozone Responses to Reduced NOx Emissions Linked to the COVID-19 Worldwide Lockdowns. *Sci. Adv.* 7, eabf7460, 2021 . 09 Jun 2021. doi:10.1126/sciadv.abf7460

Monks, P. S., Archibald, A. T., Colette, A., Cooper, O., Coyle, M., Derwent, R., et al. (2015). Tropospheric Ozone and its Precursors From the Urban to the Global Scale From Air Quality to Short-Lived Climate Forcer. *Atmos. Chem. Phys.* 15, 8889–8973. doi:10.5194/acp-15-8889-2015

Nagar, P. K., Singh, D., Sharma, M., Kumar, A., Aneja, V. P., George, M. P., et al. (2015). Characterization of PM2.5 in Delhi: role and impact of secondary aerosol, burning of biomass, and municipal solid waste and crustal matter. *Environ. Sci. Pollut. Res.* 24, 25179–25189. doi:10.1007/s11356-017-0171-3

Nath, J., Panda, S., Patra, S. S., Ramasamy, B., and Das, T. (2021). Variation of Black Carbon and Particulate Matter in Bhubaneswar during the Pre-monsoon: Possible Impact of Meteorology and COVID-19 Lockdown. *Curr. Sci.* 120 (2), 313–321. doi:10.18520/cs/v120/i2/313-321

National Centers for Environmental Prediction (NCEP)/National Weather Service/NOAA/U.S. Department of Commerce (2000). *Research Data Archive at the National Center for Atmospheric Research*. Boulder, CO: Computational and Information Systems Laboratory. updated daily. NCEP FNL Operational Model Global Tropospheric Analyses, continuing from July 1999. doi:10.5065/D6M043C6(Accessed Sep 01, 2020)

Navas, M. J., Jiménez, A. M., and Galán, G. (1997). Air Analysis: Determination of Nitrogen Compounds by Chemiluminescence. *Atmos. Environ.* 31 (3), 603–3608. doi:10.1016/s1352-2310(97)00153-2

Nedelec, P., Cammas, J.-P., Thouret, V., Athier, G., Cousin, J.-M., Legrand, C., et al. (2003). An Improved Infrared Carbon Monoxide Analyser for Routine Measurements Aboard Commercial Airbus Aircraft: Technical Validation and First Scientific Results of the MOZAIC III Programme. *Atmos. Chem. Phys.* 3, 1551–1564. doi:10.5194/acp-3-1551-2003

Ordóñez, C., Garrido-Perez, J. M., and García-Herrera, R. (2020). Early spring Near-Surface Ozone in Europe during the COVID-19 Shutdown: Meteorological Effects Outweigh Emission Changes. *Sci. Total Environ.* 747, 141322. doi:10.1016/j.scitotenv.2020.141322

Panda, S., Mallik, C., Nath, J., Das, T., and Ramasamy, B. (2021). A Study on Variation of Atmospheric Pollutants over Bhubaneswar during Imposition of Nationwide Lockdown in India for the COVID-19 Pandemic. *Air Qual. Atmos. Health* 14, 97–108. doi:10.1007/s11869-020-00916-5

Pandithurai, G., Dipu, S., Dani, K. K., Tiwari, S., Bisht, D. S., Devara, P. C. S., et al. (2008). Aerosol Radiative Forcing during Dust Events over New Delhi, India. *J. Geophys. Res.* 113, 26279–26306. doi:10.1029/2008JD009804

Pathakoti, M., Muppalla, A., Hazra, S., Dangeti, M., Shekhar, R., Jella, S., et al. (2020). An Assessment of the Impact of a Nation-wide Lockdown on Air Pollution - a Remote Sensing Perspective over India. *Atmos. Chem. Phys.* 2020, 1–16. doi:10.5194/acp-2020-621

Perrino, C., Tiwari, S., Catrambone, M., Torre, S. D., Rantica, E., and Canepari, S. (2011). Chemical Characterization of Atmospheric PM in Delhi, India, during Different Periods of the Year Including Diwali Festival. *Atmos. Pollut. Res.* 2 (4), 418–427. doi:10.5094/APR.2011.048

Pisso, I., Sollum, E., Grythe, H., Kristiansen, N. I., Cassiani, M., Eckhardt, S., et al. (2019). The Lagrangian Particle Dispersion Model FLEXPART Version 10.4. *Geosci. Model. Dev.* 12, 4955–4997. doi:10.5194/gmd-12-4955-2019

Pope, R. J., Arnold, S. R., Chipperfield, M. P., Latter, B. G., Siddans, R., and Kerridge, B. J. (2018). Widespread Changes in UK Air Quality Observed from Space. *Atmos. Sci. Lett.* 19, e817. doi:10.1002/asl.817

Rahaman, S., Jahangir, S., Chen, R., Kumar, P., and Thakur, S. (2021). COVID-19's Lockdown Effect on Air Quality in Indian Cities Using Air Quality Zonal Modeling. *Urban Clim.* 36, 100802. doi:10.1016/j.uclim.2021.100802

Ranjan, A. K., Patra, A. K., and Gorai, A. K. (2020). Effect of lockdown due to SARS COVID-19 on aerosol optical depth (AOD) over urban and mining regions in India. *Sci. Total Environ.* 745, 141024. doi:10.1016/j.scitotenv.2020.141024

Rajput, P., Sarin, M., Sharma, D., and Singh, D. (2014). Characteristics and Emission Budget of Carbonaceous Species from post-harvest Agricultural-Waste Burning in Source Region of the Indo-Gangetic Plain. *Tellus B: Chem. Phys. Meteorology* 66 (1), 21026. doi:10.3402/tellusb.v66.21026

Rastogi, N., Singh, A., Singh, D., and Sarin, M. M. (2014). Chemical characteristics of PM2.5 at a source region of biomass burning emissions: Evidence for secondary aerosol formation. *Environ. Pollut.* 184, 563–569. doi:10.1016/j.envpol.2013.09.037

Reddington, C. L., Conibear, L., Knote, C., Silver, B. J., Li, Y. J., Chan, C. K., et al. (2019). Exploring the Impacts of Anthropogenic Emission Sectors on PM2.5 and Human Health in South and East Asia. *Atmos. Chem. Phys.* 19 (18), 11887–11910. doi:10.5194/acp-19-11887-2019

Renuka, K., Gadhavi, H., Jayaraman, A., Rao, S., and Lal, S. (2020). Study of mixing ratios of SO2 in a tropical rural environment in south India. *J. Earth Sys. Sci.* 129 (104). doi:10.1007/s12040-020-1366-4

Sahu, S. K., Beig, G., and Parkhi, N. (2015). High Resolution Emission Inventory of NOx and CO for Mega City Delhi, India. *Aerosol Air Qual. Res.* 15, 1137–1144. doi:10.4209/aaqr.2014.07.0132

Sawyer, V., Levy, R. C., Mattoo, S., Cureton, G., Shi, Y., and Remer, L. A. (2020). Continuing the MODIS Dark Target Aerosol Time Series with VIIRS. *Remote Sensing* 12, 308. doi:10.3390/rs12020308

Seibert, P., and Frank, A. (2004). Source-receptor Matrix Calculation with a Lagrangian Particle Dispersion Model in Backward Mode. *Atmos. Chem. Phys.* 4, 51–63. doi:10.5194/acp-4-51-2004

Seinfeld, J. H., and Pandis, S. N. (2006). *Atmospheric Chemistry and Physics: From Air Pollution to Climate Change*. John Wiley & Sons.

Shah, V., Jacob, D. J., Li, K., Silvern, R. F., Zhai, S., Liu, M., et al. (2020). Effect of Changing NOx Lifetime on the Seasonality and Long-Term Trends of Satellite-Observed Tropospheric NO2 Columns over China. *Atmos. Chem. Phys.* 20, 1483–1495. doi:10.5194/acp-20-1483-2020

Sharma, S. K., Sharma, A., Saxena, M., Choudhary, N., Masiwal, R., Mandal, T. K., et al. (2016). Chemical Characterization and Source Apportionment of Aerosol at an Urban Area of Central Delhi, India. *Atmos. Pollut. Res.* 7 (1), 110–121. doi:10.1016/j.apr.2015.08.002

Shi, X., and Brasseur, G. P. (2020). The response in air quality to the reduction of Chinese economic activities during the COVID-19 outbreak. *Geophys. Res. Lett.* 47, e2020GL088070. doi:10.1029/2020GL088070

Sicard, P., De Marco, A., Agathokleous, E., Feng, Z., Xu, X., Paoletti, E., et al. (2020). Amplified Ozone Pollution in Cities during the COVID-19 Lockdown. *Sci. Total Environ.* 735, 139542. doi:10.1016/j.scitotenv.2020.139542

Sillman, S. (1995). The Use of NOy, H2O2, and HNO3as Indicators for Ozone-NOx-Hydrocarbon Sensitivity in Urban Locations. *J. Geophys. Res.* 100, 14175–14188. doi:10.1029/94jd02953

Sindhwani, R., Goyal, P., Kumar, S., and Kumar, A. (2015). Anthropogenic Emission Inventory of Criteria Air Pollutants of an Urban Agglomeration - National Capital Region (NCR), Delhi. *Aerosol Air Qual. Res.* 15, 1681–1697. doi:10.4209/aaqr.2014.11.0271

Singh, G. K., Choudhary, V., Rajeev, P., Paul, D., and Gupta, T. (2021). Understanding the Origin of Carbonaceous Aerosols during Periods of Extensive Biomass Burning in Northern India. *Environ. Pollut.* 270, 116082. doi:10.1016/j.envpol.2020.116082

Singh, V., Singh, S., Biswal, A., Kesarkar, A. P., Mor, S., and Ravindra, K. (2020). Diurnal and Temporal Changes in Air Pollution during COVID-19 Strict Lockdown over Different Regions of India. *Environ. Pollut.* 266, 115368. doi:10.1016/j.envpol.2020.115368

Sinha, V., Williams, J., Diesch, J. M., Drewnick, F., Martinez, M., Harder, H., et al. (2012). Constraints on Instantaneous Ozone Production Rates and Regimes during DOMINO Derived Using *In-Situ* OH Reactivity Measurements. *Atmos. Chem. Phys.* 12, 7269–7283. doi:10.5194/acp-12-7269-2012

Stevenson, D. S., Dentener, F. J., Schultz, M. G., Ellingsen, K., van Noije, T. P. C., Wild, O., et al. (2006). Multimodel Ensemble Simulations of Present-Day and Near-Future Tropospheric Ozone. *J. Geophys. Res.* 111, D08301. doi:10.1029/2005JD006338

Textor, C., Schulz, M., Guibert, S., Kinne, S., Balkanski, Y., Bauer, S., et al. (2006). Analysis and Quantification of the Diversities of Aerosol Life Cycles within AeroCom. *Atmos. Chem. Phys.* 6, 1777–1813. doi:10.5194/acp-6-1777-2006

Wang, T., Xue, L., Brimblecombe, P., Lam, Y. F., Li, L., and Zhang, L. (2017). Ozone Pollution in China: A Review of Concentrations, Meteorological Influences, Chemical Precursors, and Effects. *Sci. Total Environ.* 575, 1582–1596. doi:10.1016/j.scitotenv.2016.10.081

Wang, W., van der A, R., Ding, J., van Weele, M., and Cheng, T. (2021). Spatial and Temporal Changes of the Ozone Sensitivity in China Based on Satellite and Ground-Based Observations. *Atmos. Chem. Phys.* 21, 7253–7269. doi:10.5194/acp-21-7253-2021

Williams, J. E., Weele, M. V., Velthoven, P. F. J. v., Scheele, M. P., Liousse, C., and Werf, G. R. v. d. (2012). The Impact of Uncertainties in African Biomass Burning Emission Estimates on Modeling Global Air Quality, Long Range Transport and Tropospheric Chemical Lifetimes. *Atmosphere* 3 (1), 132–163. doi:10.3390/atmos3010132

Xu, K., Cui, K., Young, L.-H., Hsieh, Y.-K., Wang, Y.-F., Zhang, J., et al. (2020). Impact of the COVID-19 Event on Air Quality in Central China. *Aerosol Air Qual. Res.* 20, 915–929. doi:10.4209/aaqr.2020.04.0150

Young, P. J., Archibald, A. T., Bowman, K. W., Lamarque, J.-F., Naik, V., Stevenson, D. S., et al. (2013). Pre-industrial to End 21st century Projections of Tropospheric Ozone from the Atmospheric Chemistry and Climate Model Intercomparison Project (ACCMIP). *Atmos. Chem. Phys.* 13, 2063–2090. doi:10.5194/acp-13-2063-2013

Zhang, M., Katiyar, A., Zhu, S., Shen, J., Xia, M., Ma, J., et al. (2021). Impact of Reduced Anthropogenic Emissions during COVID-19 on Air Quality in India. *Atmos. Chem. Phys.* 21, 4025–4037. doi:10.5194/acp-21-4025-2021

Conflict of Interest: The authors declare that the research was conducted in the absence of any commercial or financial relationships that could be construed as a potential conflict of interest.

frontiers in Environmental Science

BRIEF RESEARCH REPORT
published: 14 January 2022
doi: 10.3389/fenvs.2021.784959

A Comparative Study of Particulate Matter Between New Delhi, India and Riyadh, Saudi Arabia During the COVID-19 Lockdown Period

Bhupendra Pratap Singh[1]*, *Gaber E. Eldesoky*[2], *Pramod Kumar*[3], *Prakash Chandra*[4], *Md Ataul Islam*[5] and *Shakilur Rahman*[6]

[1]Department of Environmental Studies, Deshbandhu College, University of Delhi, New Delhi, India, [2]Chemistry Department, College of Science, King Saud University, Riyadh, Saudi Arabia, [3]Department of Chemistry, Sri Aurobindo College, University of Delhi, New Delhi, India, [4]Department of Biotechnology, Delhi Technological University, New Delhi, India, [5]Division of Pharmacy and Optometry, School of Health Sciences, Faculty of Biology, Medicine, and Health, University of Manchester, Manchester, United Kingdom, [6]Department of Medical Elementology and Toxicology, School of Chemical and Life Sciences, Jamia Hamdard, New Delhi

OPEN ACCESS

Edited by:
Suvarna Sanjeev Fadnavis, Indian Institute of Tropical Meteorology (IITM), India

Reviewed by:
J. Abbas, Shanghai Jiao Tong University, China
Rohini Bhawar, Savitribai Phule Pune University, India

***Correspondence:**
Bhupendra Pratap Singh
bpsingh0783@gmail.com
0000-0002-0513-9082

Specialty section:
This article was submitted to Atmosphere and Climate, a section of the journal Frontiers in Environmental Science

Received: 28 September 2021
Accepted: 27 December 2021
Published: 14 January 2022

Citation:
Singh BP, Eldesoky GE, Kumar P, Chandra P, Islam MA and Rahman S (2022) A Comparative Study of Particulate Matter Between New Delhi, India and Riyadh, Saudi Arabia During the COVID-19 Lockdown Period. Front. Environ. Sci. 9:784959. doi: 10.3389/fenvs.2021.784959

Novel Coronavirus disease (COVID-19), after being identified in late December 2019 in Wuhan city of China, spread very fast and has affected all the countries in the world. The impact of lockdowns on particulate matter during the lockdown period needs attention to explore the correlation between anthropogenic and natural emissions. The current study has demonstrated the changes in fine particulate matter $PM_{2.5}$, PM_{10} and their effect on air quality during the lockdown. The air quality before the lockdown was low in New Delhi (India) and Riyadh (Saudi Arabia), among major cities worldwide. The air quality of India is influenced by dust and sand from the desert and surrounding areas. Thus, the current study becomes important to analyse changes in the air quality of the Indian sub-continent as impacted by dust storms from long distances. The result indicated a significant reduction of $PM_{2.5}$ and PM_{10} from 93.24 to 37.89 $\mu g/m^3$ and from 176.55 to 98.87 $\mu g/m^3$ during the lockdown period as compared to pre lockdown period, respectively. The study shows that average concentrations of PM_{10} and $PM_{2.5}$ have declined by -44% and -59% during the lockdown period in Delhi. The average value of median PM_{10} was calculated at 33.71 $\mu g/m^3$ for Riyadh, which was lower than that value for New Delhi during the same period. The values of PM_{10} were different for pre and during the lockdown periods in Riyadh, indicating the considerable influence on air quality, especially the concentration of PM_{10}, from both the natural (sand and dust storms) and the anthropogenic sources during the lockdown periods. However, relatively smaller gains in the improvement of air quality in Riyadh were correlated to the imposition of milder lockdown and the predominance of natural factors over the anthropogenic factors there. The Air Quality Index (AQI) data for Delhi showed the air quality to be 'satisfactory' and in the green category during the lockdown period. This study attempts to better understand the impact of particulate matter on the short- and long-term air quality in Delhi during the lockdown. This study has the scope of being scaled

up nationwide, and this might be helpful in formulation air pollution reduction and sustainable management policies in the future.

Keywords: COVID-19, air quality, particulate matter, New Delhi, Riyadh

INTRODUCTION

The COVID-19 originated from the city of Wuhan in China, supposedly in December 2019after the detection of the first COVID-19 positive case (Bashir et al., 2020; Chen et al., 2020). COVID-19 has become a pandemic impacting the entire population. Corona Virus causes respiratory infection in people and is known as SARS-CoV-2 (Zheng, 2020). The World Health Organisation (WHO) declared the Corona Virus outbreak a pandemic on March 11, 2020 (World Health Organisation, 2020).

Several studies have confirmed high transmissivity of the Corona Virus, which affects many people within a short period (Gautam and Trivedi, 2020; Sharma et al., 2020). As of October 04, 2021, more than 248 million people have been affected, and more than five million people have died across countries (including India) because of the COVID-19 virus (World metros, 2021; Ritchie et al., 2020). The effects of the COVID-19 pandemic went far beyond just health to economic, social, psychological, and occupational (Abbas et al., 2019; Mubeen et al., 2020; Liu et al., 2021a; Abbasi et al., 2021; Paulson et al., 2021; Wang et al., 2021). The pandemic has impacted the mental well-being of a huge proportion of the population in the form of distress, stress, and depression, as revealed by several studies (Abbas et al., 2019; Aqeel et al., 2021; Lebni et al., 2021; Local Burden of Disease, 2021). Su et al. (2021b) reported that COVID-19 induced unprecedented illness perception has caused mental disorders, including anxiety and depression, which have severely impacted individuals' mental health. Furthermore, a study reported the relationship between the COVID-19 infection and vaccine non-adopters in terms of detection of the number of new corona cases (Su et al., 2020). Several research scholars claimed that reduced stress and depression lead to better mental health (Li et al., 2021). Better social and educational support to vulnerable individuals might help explain differences in the scale of observed mental health problems across countries. (Azadi et al., 2021; Abbas., 2021; Su et al., 2021a; Azizi et al., 2021; Abbas et al., 2019).

India ranked third after the USA and Brazil among the top countries with more than 12 million cases and more than 0.16 million deaths (Ritchie et al., 2020; world metros, 2021). In India, the Ministry of Health and Family Welfare reported the first COVID-19 case in Kerala on 30th January, 2020 (Gutam and Hens, 2020), and the first death was reported on 12th March, 2020 (World Health Organisation, 2020b). On 22nd March, 2020, the Central Government imposed an emergency "Janata Curfew" in the whole country, which was intensified by a city-scale quarantine and nationwide lockdown starting from March 24, 2020 (Khetan et al., 2020).

Since then, more restrictive measures have been introduced except for essential services, such as fire, police, and health. Then industrial activities, hospital services, and educational institutions were also suspended until further notice. The government took these steps to flatten the infection curve. Since the lockdown meant the least movement and transportation and a considerable reduction in construction activities, the air quality improved quite significantly. Similar socio-economic activity restrictions were also seen in other countries in response to the pandemic (Kerimray et al., 2020). A drop in air pollutants has been recorded because of these initiatives (Dutheil et al., 2020).

India is considered one of the most severely polluted countries globally, especially for particulate matter and dust particles. The air quality in India is impacted by meteorological parameters such as winds which bring a huge quantity of dust and sand from the desert and surrounding areas (Knippertz et al., 2007; Pye, 2015; Albugami et al., 2019). Many studies have reported variations in aerosol loading (dust particle in the atmosphere), surface cooling, and their possible relationships with meteorological factors such as rainfall, wind speed in India and East Asia (Krishnan and Ramanathan, 2002; Devara et al., 2003; Cheng et al., 2005; Prasad et al., 2006; Nakajima, 2007; George et al., 2008). The air quality of the Indian subcontinent, including the north-western part of India, is possibly influenced by the dust storms which may originate from Arabian Peninsula.

This study tried to correlate the possible changes in the air quality of Delhi with the dust storms from Arabian Peninsula (Saudi Arabia). Dust storms are common in the north-western part of the Indian subcontinent, the Arabian Peninsula, China, and the Sahara Desert (Wang, 2015). The transport of dust particles originated from the Arabian Peninsula and enter India through Afghanistan, Pakistan via land routes and through the Arabian Sea via sea routes (Middleton, 1986; Kedia et al., 2018). In addition, dust storms can severely affect air quality and particulate matter concentrations ($PM_{2.5}$ and PM_{10}). A study suggested a significant positive correlation between precipitation and the increase of dust emissions, especially in Saudi Arabia, Oman, and the Thar Desert, India (Kaskaoutis et al., 2012; Namdari et al., 2018).

Several literatures reported that the frequency and the intensity of dust storms have been increasing, which is positively associated with land-use and land-cover changes and meteorological factors in some regions of the world like the Arabian Peninsula (Yu et al., 2015; Alobaidi et al., 2017; Gherboudj et al., 2017; Almazroui et al., 2018), and the Middle-East (Rashki et al., 2012; Türkeş, 2017; Namdari et al., 2018) as well as Central Asia (Indoitu et al., 2015; Xi and Sokolik 2015). Furthermore, a positive correlation between dust and meteorological factors is attributed to dust emission over Arabian Peninsula and its transportation to the Indian subcontinent (Jin et al., 2021). In addition, the Indian

subcontinent, especially northern parts of India, is a potential source of pollution originating from the Thar desert located in northwestern India (Sarkar et al., 2019; Jin et al., 2021).

A sudden halt of all anthropogenic activities (mainly transportation and industrial activities) during the lockdown measures in India improved the air quality. Several studies conducted throughout the world reported an association between short term exposure to particulate matter and COVID-19 confirmed cases such as an outbreak in over major cities of Saudi Arabia (Farahat et al., 2021) Northern Italy (Bashir et al., 2020; Report et al., 2020), China (Mehmood et al., 2020; Wang et al., 2020a; Zhu et al., 2020), in Malaysia (Suhaimi et al., 2020) and a similar result for the United States (Wu et al., 2020).

Several studies have reported a significant improvement in air quality during the lockdown period (Gautam, 2020; Zhu et al., 2020) especially, Particulate Matter $PM_{2.5}$ (size <2.5 μm^3) and PM_{10} (size <10 μm^3), which are considered significant air pollutants directly associated with adverse health effects on human beings (Kumar et al., 2014a; Singh et al., 2014; Singh et al., 2021a). A study in China reported a positive association between short-term exposure to air pollution and coronavirus disease (Muhammad et al., 2020; Zhu et al., 2020). Another study in China also suggested a positive correlation between particulate matter ($PM_{2.5}$ and PM_{10}) and mortality rates of COVID-19 (Bashir et al., 2020). Another study from China has also shown that ambient temperature might play a crucial role in COVID-19 infection (Xie and Zhu, 2020). Several recent studies have highlighted a significant improvement in air quality with respect to reduction of $PM_{2.5}$ by 34–73.85%, of PM_{10} by 40–58%, (), of NO_2 by 3–79%, of CO by 2–60%, of NH_3 by 30–75%, (), and of SO_2 by 15–58% () in different cities across India during the lockdown period (Dutta & Jinsart, 2020; Kumari and Toshniwal, 2020; Navinya et al., 2020; Pant et al., 2020; Resmi et al., 2020; Vadrevu et al., 2020; Kumar et al., 2020; Kumar & Tyagi, 2021; Khan et al., 2021; Maji et al., 2021; Sathe et al., 2021).

Several studies have been conducted in different parts of cities to assess the impact of COVID-19 lockdown on air quality but for a short period of time (Kotnala et al., 2020 (January–March 2020); Kumar, 2020 (March–May 2020); Kumar et al., 2020 (March–April 2015–2020); Mahato et al., 2002 (3 March–14 April 2020); Navinya et al., 2020 (1 February–3 May 2019–2020); Srivastava et al., 2020 (1^{st}–20^{th} February and 24 March–14 April 2020). The present investigation was an attempt to evaluate the changes in the level of the particulate matter before and during the complete lockdown period (1 January–31^{th} May 2020)

Northwest Indian sub-continent faces the adverse impacts of dulust particles, including particulate matter from distant places like Saudi Arabia and meteorological parameters such as wind and precipitation. Both of these factors played a crucial role in the deterioration of the air quality in India. Therefore, the present investigation attempted to evaluate the changes in the level of the particulate matter before (January 1, 2020 to 23^{rd} March, 2020) and during the entire lockdown period (24^{th} March, 2020 to May 31, 2020) in Delhi India. Hence, the present study also aims to evaluate the levels of particulate matter in two different cities (New Delhi and Riyadh) during the lockdown period (1st January to May 31, 2020). Further, the study compared the concentration of particulate matter for pre-lockdown and during the lockdown periods and explored the potential natural and anthropogenic emission sources.

Further, the study aims to increase the scientific rigor of research in this area. However, some of the limitations of the current manuscript required access to meteorological parameters, including rainfall, relative humidity, solar radiation, and wind speed. These limitations can be tackled in future studies with larger sample sizes and the inclusion of more factors in the analysis to draw exciting results.

MATERIALS AND METHODS

To investigate the effect of restricted mobility on the concentration levels of particulate matter in the ambient atmosphere of Delhi (India) and Riyadh (Saudi Arabia), we utilized the air quality index (AQI) data from the respective Air Quality Monitoring Stations. The pandemic situation was classified into two periods, before lockdown and during lockdown for both the cities (Delhi and Riyadh). The time for Delhi, India before lockdown (between 1^{st} January, 2020, and 24^{th} March, 2020) was termed as 'pre-lockdown' period, and the time between 25^{th} March and May 31, 2020 was termed as 'during-lockdown' period. The time for Riyadh, Saudi Arabia before lockdown (between January 2020, and March 2020) was termed as "pre-lockdown" period, and the time between March and May 2020 was termed as 'during-lockdown' period. So, in the current study authors have studied and compared the air quality in both these cities in a comparable time frame.

Data and Sources

The hourly and daily data on air pollutants were obtained from the online portal of the Central Pollution Control Board (CPCB), particularly the data for PM_{10} (size of particulate matter <10 microns), $PM_{2.5}$ (size of particulate matter <2.5 microns), and meteorological parameters. In this paper, we focused and collected secondary data for only PM_{10} and $PM_{2.5}$ from 1^{st} January, to 31^{st} May, 2020 to determine the relative changes (in %) in air quality from the CPCB monitoring site (https://app.cpcbccr.com/ccr/#/caaqm-dashboard-all/caaqm-landing). In addition, the data on PM_{10} for Riyadh, Saudi Arabiawere procured from the World Air Quality Index from 1^{st} January to April 10, 2020 (https://aqicn.org/data-platform/covid19/). CPCB in India provides high-quality data through rigorous quality assurance or quality control (QA/QC) programs via scientific sampling, analysis, and calibration (Mahato et al., 2002).

Air Quality Index (AQI) is a tool for identifying the pollutant criteria and is also used to report the severity of air pollution to the public. In addition, AQI plays an important role in deliberating an individual pollutant into a whole index using the aggregation method (Ott, 1978).

AQI India provides air pollution data with a real-time Air Quality Index for various air pollutants. The National Ambient Air Quality Standard (NAAQS) revised AQI by considering eight parameters, namely, PM_{10}, $PM_{2.5}$, NO_2, SO_2, CO, O_3, NH_3, and

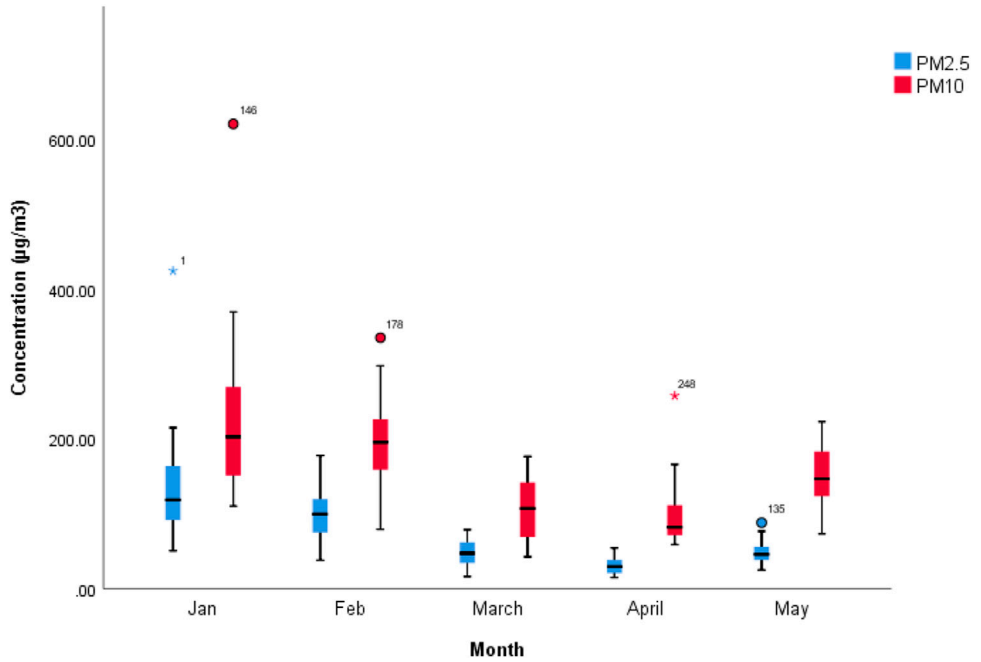

FIGURE 1 | The box plot for concentration of $PM_{2.5}$ and PM_{10} during the pandemic, North Campus Delhi University.

Pb for a short term (up to 24 hourly average) period (Kumar et al., 2014b; CPCB, 2016). An AQI is used to provide information about the quality of air in terms of pollution level. It is directly associated with public health. The public health risk increases with an increase in the AQI level. Six AQI categories have been defined for health risk, namely, "Good", "Satisfactory", "Moderately polluted", "Poor", "Very Poor", and "Severe".

Further, this index provides information to the public who are sensitive to air pollution (Beig et al., 2010). To identify the overall improvement in air quality over Delhi, AQI was calculated, and details of AQI are available elsewhere (Sharma et al., 2020). The AQI is divided into five categories: good (0–50), satisfactory (51–100), moderate (101–200), poor (201–300), very poor (301–400), and severe (401–500) respectively. AQI method that provides sub-index approach using six criteria pollutants (i.e. PM_{10}, $PM_{2.5}$, SO_2, NO_2 CO and O_3) were converted into AQI standard value. The AQI for each pollutant was calculated by the following formula given by Sahu & Kota (2017).

$$AQIi = \frac{\text{IHI} - \text{ILO}}{\text{BreakHI} - \text{BreakLO}} x\ (\text{Ci} - \text{BreakLO}) + \text{ILO}$$

where C_i is the observed concentration of the pollutant "i"; $Break_{HI}$ and $Break_{LO}$ are breakpoint concentrations, greater and smaller to C_i; and I_{HI} and I_{LO} are corresponding AQI ranges.

For the final calculation of AQI for individual pollutants, at least a minimum of three pollutants for the AQI value is required. In this study, we have also considered the daily average values of other pollutants (NO_X and O_3) to calculate AQI values. The formula for calculating the AQI value was presented in the **Supplementary File**. The AQI values for particulate matter ($PM_{2.5}$ and PM_{10}) before and during lockdown were calculated corresponding to the other pollutants.

Data Analysis and Procedure

The present study analyzed the total data ($n = 152$ and $n = 90$) for a monitoring station, North Campus, Delhi University, New Delhi, and Riyadh, Saudi Arabia, to evaluate the variable changes in particulate matter in the comparative time frame. Time series plotting techniques were used to investigate variable changes over time during the pre and lockdown period. Statistical Package for the Social Sciences (SPSS) software was used to perform the statistical analysis (version 26.0 SPSS Inc., Chicago, IL, United States). The wind rose plot was drawn using Lake Environment software with wind speed input parameters.

RESULTS AND DISCUSSION

$PM_{2.5}$ and PM_{10} Levels in New Delhi, India

In the present paper, particulate matter ($PM_{2.5}$ and PM_{10}) levels have shown a significant decline from January to May 2020 during the pandemic situation (**Figure 1**). According to Singh & Kumar (2021) the continuous reduction in the levels of particulate matter ($PM_{2.5}$ and PM_{10}) was observed in subsequent months during the complete lockdown caused by the restriction of non-essential services such as transport and complete closure of markets and industrial activities. Average concentrations of $PM_{2.5}$ and PM_{10} were 123.24 μgm^{-3} and 151.24 $\mu gm^{-3,}$ respectively, in North Campus, Delhi University. The maximum concentrations of $PM_{2.5}$ and PM_{10} were

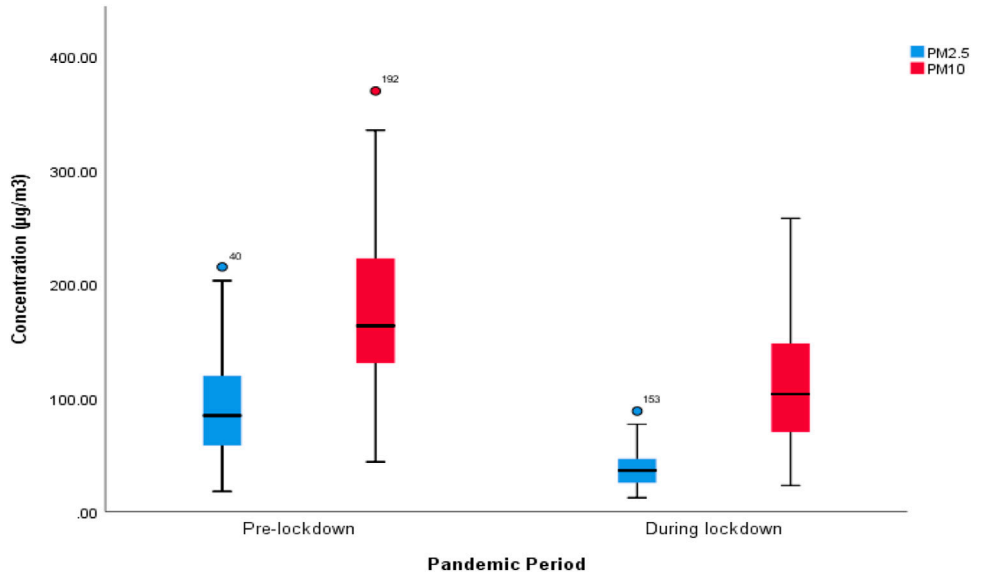

FIGURE 2 | The box plot for concentration of $PM_{2.5}$ and PM_{10} during pre- and during the lockdown period, North Campus Delhi University.

178.2 μgm^{-3} and 335.43 μgm^{-3} respectively during the month of February, whereas the minimum were 12.36 μgm^{-3} and 23.06 μgm^{-3} during the month of May. In addition, the lowest mean concentrations were 31.42 μgm^{-3} and 100.16 $\mu gm^{-3,}$ respectively, during the month of April (**Supplementary Figure S1**). Thus, the concentration of $PM_{2.5}$ was observed far below the prescribed standard value of CPCB (40 μgm^{-3}) in the month of April. The significant reduction in $PM_{2.5/10}$ was caused by restrictions on the use of private vehicles and other non-essential transportation, halt on construction and industrial activities. This led to a general reduction of anthropogenic PM pollution (Klimont et al., 2017). The linear decline in the average concentration of $PM_{2.5}$ was reported even in New York (μgm^{-3}) from December 2019 to March 2020 (Chauhan and Singh 2020). Singh et al. (2021b) claimed that the mean concentrations of $PM_{2.5}$ and PM_{10} were slightly higher during the month of May owing to the start of use of necessary transportation and controlled industrial activities in non-containment zones in Delhi. (**Supplementary figure S2**).

The present study focused on determining drastic changes in the concentrations of air pollutants, especially particulate matter $PM_{2.5}$ and PM_{10} concentrations, during the pandemic situation in India, including Delhi. The $PM_{2.5}$ and PM_{10} concentrations significantly declined from January 2020 to May 2020 during the pandemic situation in Delhi. A constant decline in the $PM_{2.5}$ and PM_{10} concentrations was observed in subsequent months due to complete lockdown, during which international and trains, traffic activities, markets, and industrial activities were suspended. The average concentrations of $PM_{2.5}$ and PM_{10} in the pre-lockdown period were observed to be 93.24 μgm^{-3} and 176.55 $\mu gm^{-3,}$ whereas, during the lockdown period, they were 36.09 μgm^{-3} and 98.87 μgm^{-3}, respectively (**Figure 2**). Several recent studies on Delhi reported similar results for PM2.5 concentration values; Singh et al., 2021 (41.41 µgm-3), Dutta and Jinsart, 2020 (42.15 µgm-3), Chaudhary et al., (33.09–122.2 µgm-3), Roy and Balling (46.5–39.1 µgm-3). This significant reduction was mainly attributable to government's orders on non-use of private vehicles and other non-essential transportation since transport sector is the primary source of particulate matter in the atmosphere.

The maximum value of $PM_{2.5}$ and PM_{10} in the pre-lockdown period was calculated to be 215.5 μgm^{-3} and 369.94 μgm^{-3} whereas, during the lockdown period, it was estimated to be 88.5 μgm^{-3} and 93.24 μgm^{-3} respectively during the month of April. In terms of minimum concentrations of $PM_{2.5}$ and PM_{10}, pre-lockdown values were recorded to be 17.84 μgm^{-3} and 43.82 μgm^{-3} respectively during the month of March; whereas, during the lockdown period, these respective values were 12.36 μgm^{-3} and 23.03 μgm^{-3} during the month of April (**Supplementary Figure S3**). The present study shows that average concentrations of $PM_{2.5}$ and PM_{10} declined by -59% and -44%, respectively, during the lockdown period in Delhi.

According to Kerimra, spatial reduction in the value of $PM_{2.5}$ varied between 6 and 34% during the lockdown period in Almaty, Kazakhstan (Kerimray et al., 2020). A study conducted in Zaragoza, Spain, also reported a decline in the concentration of $PM_{2.5}$ by -58% during March 2020 compared with February 2020. Similar changes were also observed in Beijing and other cities of China during the lockdown period (Sharma et al., 2020). Another study found a reduction in the concentration of PM_{10} in urban areas and traffic areas by -27.8% and -31%, respectively, in Barcelona (Spain) during their lockdown periods (Tobias et al., 2020). Thus, the significant reduction in the concentration of $PM_{2.5}$ and PM_{10} during the lockdown period could also be attributed to a lower frequency of temperature inversion, atmospheric temperature, increasing wind speeds, and changes in wind direction.

TABLE 1 | Several recent studies across the world during the lockdown period.

The study area (city, country)	Key findings for $PM_{2.5}$ and PM_{10}	Author (year)
Present Study (Delhi, India)	Average concentrations for $PM_{2.5}$ and PM_{10} during the lockdown period were observed to be 36.09 μg/m^3 and 98.87 μg/m^3, respectively	Present Study
Delhi (India)	Average concentrations for $PM_{2.5}$ and PM_{10} were varied from 41.14 to 60.56 μg/m^3 and 86.81–169.32 μg/m^3 for different lockdowns in Delhi, India, respectively.	Singh & Kumar (2021)
Delhi (India)	Reductions in $PM_{2.5}$ (39%) and PM_{10} (60%) as compared to 2019.	Mahato et al. (2002)
Delhi (India)	A similar study conducted in Delhi, the result showed that $PM_{2.5}$ and PM_{10} levels declined up to 55–65% during the lockdown period	Garg et al. (2021)
Delhi (India)	The average concentrations of atmospheric air pollutants $PM_{2.5}$ and PM_{10} were reduced to 42.15 μg/m^3, and 128.68 μg/m^3 and where 73.85%, and 46.48% lower than pre-COVID-19 levels.	Dutta & Jinsart (2020)
Chennai (India)	overall $PM_{2.5}$ values decreased for the lockdown (ranging from ~32–187%), weekly analysis shows the variation in reduction/increase.	Singh and Tyagi (2020)
Uttar Pradesh (India)	A significant reduction in the ground-level pollution load of $PM_{2.5}$ and PM_{10} has been observed during the lockdown period in Uttar Pradesh.	Kumar (2021)
Uttar Pradesh and the Delhi-National Capital Region (India)	The $PM_{2.5}$ concentrations during lockdown Phase 1 were approximately 44.6% lower for cities in Uttar Pradesh and about 58.5% lower for the Delhi-NCR	Goel et al. (2020)
Delhi, Mumbai, Kolkata, Chennai, and Hyderabad (India)	The average concentration levels of $PM_{2.5}$ and PM_{10} have decreased nationwide by 33%, and 34% respectively during the nationwide lockdown compared to their concentration levels before the lockdown.	Verma and Kamyotra (2021)
Delhi, Mumbai, Kolkata, and Bangalore (India)	Concentration declined in $PM_{2.5}$ (~41%) and PM10 (52%).	Jain & Sharma, (2020)
Delhi, Mumbai, Kolkata, and Chennai (India)	The findings conclude a significant improvement in air quality with respect to a reduction of 49–73%, 17–63%, in the mean concentration of $PM_{2.5}$ and PM_{10}, respectively.	Pant et al. (2020)
India (22 different cites)	Reduction in concentration for $PM_{2.5}$ (43%) and PM_{10} (31%)	Sharma et al. (2020)
Dwarka river basin within Jharkhand and West Bengal (India)	PM_{10} concentration was reduced from 189-278 μg/m^{3}in the pre-lockdown period to 50–60 μg/m^3.	Mandal & Pal (2020)
Lucknow, and New Delhi, (India)	$PM_{2.5}$ concentration for Lucknow and New Delhi declined from 54–222 and 47–204 μg/m^3 during the lockdown period (25th March to 14 April, respectively.	Srivastava et al. (2020)
Gujarat (India)	The concentrations of $PM_{2.5}$ and PM_{10} were reduced by 38–78%, and 32–80%, in Gujarat respectively.	Selvam et al. (2020)
Mecca, Madinah, and Jeddah (Saudi Arabia)	No major changes in PM_{10} were observed, whereas other findings were 44% reduction in NO_2 and 16% reduction in CO concentrations during COVID-19 restrictions.	Farahat et al. (2020)
Makkha city (Saudi Arabia)	Findings indicate the presence of a significant decrease of concentration rates during the lockdown period, compared with the pre-pandemic period, by 26.34% for SO_2, 28.99% for NO_2, 26.24% for CO, 11.62% for O_3, and 30.03% for PM_{10}.	Morsy et al. (2020)
Riyadh, Makkha, and Jeddah (Saudi Arabia)	The percentage changes in concentrations of CO (33.60%) and SO_2 (44.16%) were higher in Jeddah; PM_{10} (91.12%) in Riyadh, while NO_2 (44.35%) and O_3 (18.98%) were highest in Makkah	Aljahdali et al. (2021)
Eastern Province (Saudi Arabia)	The Eastern Province, Saudi Arabia experienced significant concentration reductions at varying rates for PM_{10} (21–70%), CO (5.8–55%), and SO_2 (8.7–30%), while O_3 concentrations showed increasing rates ranging between 6.3 and 45%.	Anil & Alagha (2020)
Riyadh (Saudi Arabia)	After sandstorm, the air pollutants, CO level increased by 84.25%; $PM_{2.5}$: 76. 71%; O_3: 40.41%; NO_2: 12.03%; and SARS-CoV-2 cases increased by 33. 87%. However, the number of deaths decreased by 22.39%.	(Meo, 2021)
Global countries (34 countries including Saudi Arabia)	On a global average basis, a 34.0% reduction in NO_2 concentration and a 15.0% reduction in $PM_{2.5}$ were estimated during the strict lockdown period (until April 30, 2020). Global average O_3 concentration increased by 86.0% during this same period.	Torkmahalleh et al. (2020)
Cairo, Egypt and Riyadh (Saudi Arabia)	The results demonstrated that the lockdown was associated with a reduction in NO_2 by 40.3 and 23% in Riyadh and Cairo, respectively.	Abdelsattar et al. (2021)
China and Europe (France, Germany, Spain, and Italy)	Decreased $PM_{2.5}$ in 367 cities (18.9 μg/m3), and Wuhan (-1.4 μg/m3)	Zambrano-Monserrate et al. (2020)
New York, Los Angeles, Zaragoza, Rome, Dubai, Delhi, Mumbai, Beijing, and Shanghai	Declined $PM_{2.5}$ concentration in Delhi (35%), Mumbai (14%), Beijing (50%), Shanghai (50%), Dubai (11%), New York (32%), Los Angeles (4%), and Zaragoza and Rome (no changes).	Chauhan & Singh (2020)

(Continued on following page)

TABLE 1 | (*Continued*) Several recent studies across the world during the lockdown period.

The study area (city, country)	Key findings for $PM_{2.5}$ and PM_{10}	Author (year)
Spain (Barcelona)	Decline PM_{10} concentration in Spain from -28% to -31%.	Tobias et al. (2020)
Malaysia and Southeast Asia	Reduced concentration in PM_{10} for (industrial: 28–39%, urban: 26–31%), and $PM_{2.5}$ (industrial: 20–42%, urban: 23–32%) respectively.	Kanniah et al. (2020)
Southern European cities (Nice, Rome, Valencia and Turin) and Wuhan (China)	Declined in $PM_{2.5}$ and PM_{10} (~8% in Europe and ~42% in Wuhan) at urban stations, respectively.	Sicard et al. (2020)
Yangtze River Delta Region (China)	Reductions in $PM_{2.5}$ (27–46%) in China.	Li et al. (2020)
44 cities in northern China	The AQI for $PM_{2.5}$, and PM_{10}, decreased by 6.76%, and 5.93%, respectively.	Bao & Zhang, (2020)
Almaty (Kazakhstan)	Reduction in $PM_{2.5}$ (21%, spatial variations: 6–34%).	Kerimray et al. (2020)
Northern China	Reduction in $PM_{2.5}$ (29 ± 22%), and (31 ± 6%) in Northern China and Wuhan respectively.	Shi & Brasseur (2020)
Sale City (Morocco)	PM_{10} was reduced by 75% in Sale City.	Otmani et al. (2020)
China (Beijing, Shanghai, Guangzhou, and Wuhan)	Decreased $PM_{2.5}$ in Beijing, Shanghai, Guangzhou, and Wuhan by 9.23, 6.37, 5.35, and 30.79 $\mu g/m^3$, respectively.	Wang et al. (2020b)

Role of Meteorological Parameters

The meteorological parameters such as temperature, mixing height, wind speed, and rainfall played a significant role in changing $PM_{2.5}$ and PM_{10} levels during the lockdown period. $PM_{2.5}$ and PM_{10} levels were observed to rise in the second week of phase-I of lockdown, primarily attributed to changes in meteorological conditions over Delhi and NCR.

Due to the onset of summers, the temperature started to increase with an average temperature of 20.9 °C on March 16, 2020 to 30.4 oC on 1st May 2020, leading to dry and dusty conditions. Moreover, it was reported that a mild dust storm from the western part of the country and even from the gulf regions hit Delhi on 14th–15th April 2020, thus rapidly increasing the PM_{10} levels in Delhi and NCR. It is important to mention here that meteorological factors with average mixing height and wind speed improved the level of $PM_{2.5}$ and PM_{10} for pre-lockdown and lockdown phases against the same periods in the previous year. Wind speed and mixing height were also higher in the first lockdown phase than pre-lockdown levels. Spells of light to moderate rains were also recorded in Delhi NCR on 5th March, 14th March, 27th March, 28th—29th March, 17th, and 18th April, 25th and 26th April, and 3rd May during 2020, assisting in air quality improvement (CPCB, 2020).

The salient findings from several recent studies worldwide, including India and Saudi Arabia, during the lockdown period are presented in **Table 1**. A negative correlation between concentrations of $PM_{2.5}$, $PM_{10,}$ and ambient temperature was reported during the lockdown period, which indicated vertical dispersion of PM pollutants caused by high temperature (Singh et al., 2016; Singh et al., 2021c). The present study revealed a significant negative correlation between wind speed and particulate matter pollutants which possibly indicated the predominance of local sources as well as transportation of dust particles from longer distances over Delhi during the pre-lockdown period (**Supplementary Table S1**). The wind rose for Delhi during the lockdown period was depicted in the **Figure 3**. The wind rose blow from north-east much of the time during the lockdown period. This westerly wind and rainfall along the Mediterranean Sea could play a possible role in washing out the particulate matter during March, which led to further decline of the PM pollutant from the ambient atmosphere (Singh & Kumar, 2021).

PM_{10} Levels in Riyad, Saudi Arabia

The maximum and minimum median values in Riyadh were 245 $\mu gm^{-3,}$ and 6.0 $\mu gm^{-3,}$ respectively, during the same period. The average median of PM_{10} during the lockdown period was 33.71 μgm^{-3}. A similar result for Riyadh was reported (24.10 ± 4.78 μgm^{-3}) during the lockdown period by Aljahdali et al., 2021. The value of PM_{10} was observed much lower than the standard value (80 μgm^{-3} annual means) by prescribed Presidency of Meteorology and Environment (PME) (Munir et al., 2016).

The present study finds no major changes in particulate matter pre- and post-lockdown periods in Riyad, Saudi Arabia, which could be due to frequent dust events during the same period. Farahat also suggested similar findings over major cities (Mecca, Jeddah, Madinah) of Saudi Arabia during the Hajj Period of 2019–2020, where the winds played a crucial role in the transportation of dust (Farahat et al., 2021). Another study conducted in the Eastern Province of Saudi Arabia experienced a significant reduction in the concentration of PM_{10} (21–70%) during the lockdown period (Anil & Alagha, 2020). Morsy indicated a considerable decrease in concentration levels during the lockdown period, compared with the pre-pandemic period, by 30.3% for PM_{10} in Makkah city, Saudi Arabia (Morsy et al., 2021). The flatted peak of PM_{10} during the pandemic lockdown period was interpreted by the commitment of Makkah residents due to precautionary measures of COVID-19.

Furthermore, preventive measures such as curfew enforcement had contributed to lowering the level of particulate matter to a great extent in the capital of Riyadh. The complete lockdown and restricted industrial activities and vehicular movement resulted in a significant reduction in air pollutants, as recorded by some air quality monitoring stations located throughout the city (Saudi Gazette, 2020). A comparative graph between New Delhi (India) and Riyadh (Saudi Arabia) for particulate matter has been presented in **Figure 4** during the pandemic lockdown periods.

Air Quality Index

Delhi is considered as one of the most polluted cities on the Earth, with transport (41%), industry (18.61%), power plants (4.92%),

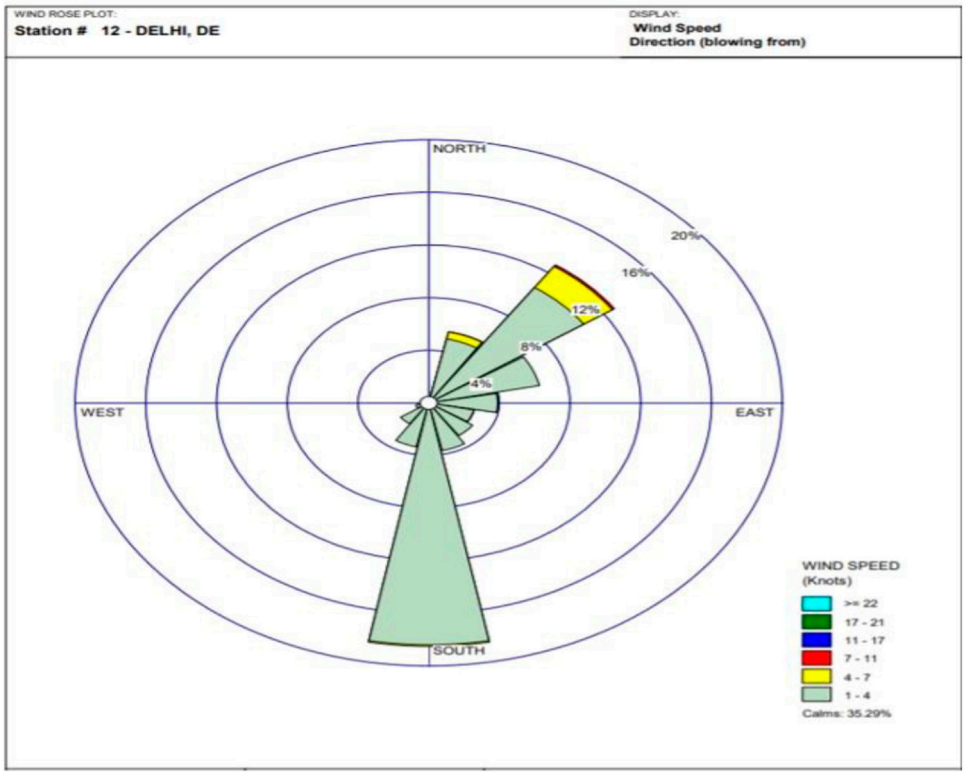

FIGURE 3 | Wind rose diagram for Delhi monitoring station.

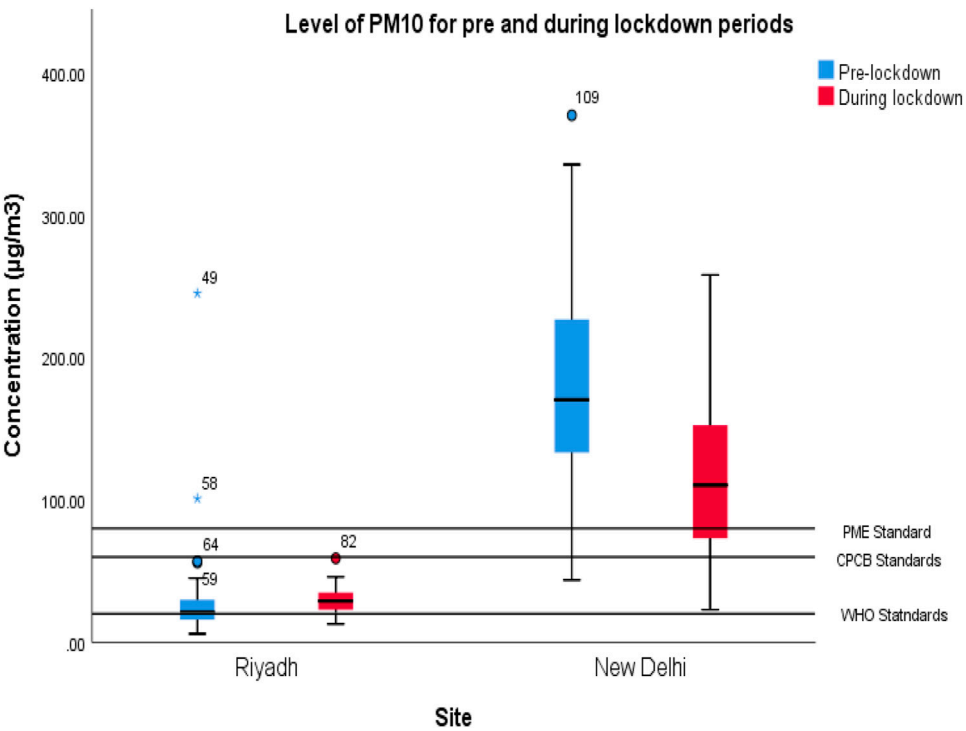

FIGURE 4 | Comparative study of PM_{10} for Riyadh and New Delhi during the pandemic periods.

TABLE 2 | National AQI classes, range, health impacts and health breakpoints for the seven pollutants (Scale: 0–500).

AQI category (range)	Associated Heath Impacts	$PM_{10}PM_{2.5}$ 24-h	24-h	Pre-lockdown		During lockdown	
				$PM_{10}PM_{2.5}$ 24-h	PM_{10}24-h	$PM_{2.5}$ 24-h	24-h
Good (0–50)	Minimal Impact	0–50	0–50				
Satisfactory (51–100)	Minor breathing discomfort to sensitive people	31–60	51–100			58	**99**
Moderately Polluted (101–200)	Breathing discomfort to the people with lung disease	61–90	101–250		151		
Poor (201–300)	Breathing discomfort to the people with prolonged exposure	91–120	251–350				
Very Poor (301–400)	Breathing illness to the people with prolonged exposure	121–250	251–430	211			
Sever (401–500)	Respiratory effects even on healthy people	250+	430+				

and residential emissions (2.96%) being the major contributing factors. The levels of $PM_{2.5}$ and PM_{10} in Delhi drastically declined during the pandemic. The AQI data for the present study shows that the mean concentrations of $PM_{2.5}$ and PM_{10} in the pre-lockdown period were 93.24 μgm-3 (indicating 'poor' air quality) 176.55 μgm^{-3} (indicating "moderately polluted" air quality) respectively. The average values of $PM_{2.5}$ and PM_{10} during the lockdown period were found to be 37.89 μgm^{-3} and 98.87 μgm^{-3} respectively, indicating a "satisfactory" green category of air quality equivalent to a few of the European cities during the lockdown period (**Table 2**). The drastic change in Delhi's air quality could be attributed to a decrease in socio-economic activities in the city. The concentrations of $PM_{2.5}$ and PM_{10} decreased by 59 and 44% during the lockdown period: a marked improvement in air quality. A similar finding was reported with a maximum reduction of 49% in AQI value in Delhi (Sharma et al., 2020). This led to a drastic improvement of the AQI values in Delhi. The air quality levels drastically improved because of the complete absence of major sources of primary air pollutants, such as emissions from vehicles, industry, construction, and brick kilns, during the lockdown period.

Apart from this, another study focused on exploring adverse effects on global public health and social media's indispensable role in providing the correct information in the COVID-19 health crisis (NeJhaddadgar et al., 2020; Liu et al., 2021b). A study claimed that human–pathogen interactions, such as data from Unit 731, can help epidemiologists better understand pandemics of COVID-19's scale (Su et al., 2021a; Su et al., 2021b).

CONCLUSION

The outcome of lockdown on air quality was assessed from 1st January, 2020 to 31st May, 2020 for New Delhi (India) and from 1st January, 2020 to 10th April, 2020 for Riyadh (Saudi Arabia). The significant reduction in the concentration levels of $PM_{2.5}$ and PM_{10} was caused by restrictions on the usage of private vehicles, suspension of non-essential transportation, construction, and industrial activities during the pandemic. The reduction in the concentration value of $PM_{2.5}$ was calculated to be more than the value of PM_{10} during the lockdown period, which indicates that traffic was a significant source for the emission of $PM_{2.5}$. Average concentrations of $PM_{2.5}$ and PM_{10} were calculated to be 123.24 $\mu g/m^3$ and 151.24 $\mu g/m^{3,}$ respectively, in North Campus, Delhi University. Average concentrations of $PM_{2.5}$ and PM_{10} in the pre-lockdown period were observed to be 93.24 $\mu g/m^3$ and 176.55 $\mu g/m^3$, respectively, whereas, during the lockdown period, their respective concentrations were 37.89 $\mu g/m^3$ and 98.87 $\mu g/m^3$. The values of PM_{10} showed different trends in Riyadh compared to New Delhi, indicating significant influence from natural (sand and dust storms) and anthropogenic sources during the lockdown periods. This could be attributed to no major changes for particulate matter for pre- and during the lockdown periods. The COVID-19 provided a rare opportunity to countries, including India, to collect air pollution baseline data during the nationwide lockdown. Air pollutants from transport, industries, and commercial activities were reduced significantly during this period. This baseline data could be very relevant to air pollution reduction policies.

Despite this, there are several challenges in the present study, particularly in selecting only one monitoring station. This is a small-scale study with a limited number of sites, which shows significant results. A detailed analysis with a greater number of monitoring stations is desirable. Identification of the sources of air pollution may be incomplete, and certain temporal aspects need to be further studied. In addition, meteorological parameters play a significant role in the transmission of COVID-19 that need to be examined in detail. The non-enforcement of India's anti-pollution laws is one of the major factors contributing to the high pollution load in India. More research emphasizing these areas is needed. The government should make efforts to maintain positive air quality by instituting advanced emission control technologies because it can significantly improve the environment and thus the health of the people.

The relationship between the air quality and COVID-19 induced lockdowns is significant, subject to the strength of local meteorological and other natural factors. For example, the magnitude of improvement in the air quality in Delhi, shown by a drastic reduction in the concentration of air pollutants, especially $PM_{2.5}$ and PM_{10}, is mainly correlated with the on-ground implementation of the lockdown and prevalence of support local factors, including meteorological

factors like wind speed etc. However, relatively smaller gains in the improvement of air quality in Riyadh are correlated to the imposition of milder lockdown and the predominance of natural factors over the anthropogenic factors there.

The paper conveys the positive impact of lockdowns on air quality in metropolitan cities. The gains are subject to many factors, two of which have been established in the current study in the form of the intensity of lockdown and prevalence and relative strength of local meteorological and natural factors against their anthropogenic counterparts.

DATA AVAILABILITY STATEMENT

The original contributions presented in the study are included in the article/**Supplementary Material**, further inquiries can be directed to the corresponding author.

AUTHOR CONTRIBUTIONS

BS: Conceptualization, introduction analysis, methodology section. GE: Analysis of the result and discussion for particulate matter for Saudi Arabia. PK: Framing the fine particulate matter associated with New Delhi. PC: Conceptualise the Air Quality Index of the current manuscript. MI improves the quality of the current draft, Writing review and editing. SR: Preparing a literature review and table for a comparative study between New Delhi India and Riyadh, Saudi Arabia

ACKNOWLEDGMENTS

The authors are grateful to the Researchers Supporting Project No. (RSP-2021/161). King Saud University, Riyadh, Saudi Arabia. The first author thanks Ms. Sonia Kumari and Dr. Sadaf Nazneen for insightful discussion and valuable suggestions during the preparation of the paper. The authors also appreciate Ms. Pallvi Rana, Ms. Nishtha Mittal, and Ms. Pooja deep proofreading the current manuscript.

SUPPLEMENTARY MATERIAL

The Supplementary Material for this article can be found online at: https://www.frontiersin.org/articles/10.3389/fenvs.2021.784959/full#supplementary-material

REFERENCES

Abbas, J., Aman, J., Nurunnabi, M., and Bano, S. (2019). The Impact of Social media on Learning Behavior for Sustainable Education: Evidence of Students from Selected Universities in Pakistan. *Sustainability* 11 (6), 1683. doi:10.3390/su11061683

Abbas, J. (2021). Crisis Management, Transnational Healthcare Challenges and Opportunities: The Intersection of COVID-19 Pandemic and Global Mental Health. *Res. Globalization* 3, 100037. doi:10.1016/j.resglo.2021.100037

Abbasi, K. R., Abbas, J., and Tufail, M. (2021). Revisiting Electricity Consumption, price, and Real GDP: A Modified Sectoral Level Analysis from Pakistan. *Energy Policy* 149, 112087. doi:10.1016/j.enpol.2020.112087

Abdelsattar, A. S., Dawoud, A., Makky, S., Nafoal, R., Aziz, R. K., and El-Shibiny, A. (2021). Bacteriophages: From Isolation to Application. *Current Pharmaceutical Biotechnology*.

Albugami, S., Palmer, S., Cinnamon, J., and Meersmans, J. (2019). Spatial and Temporal Variations in the Incidence of Dust Storms in Saudi Arabia Revealed from *In Situ* Observations. *Geosciences* 9, 162. doi:10.3390/geosciences9040162

Aljahdali, M. O., Alhassan, A. B., and Zhang, Z. (2021). Environmental Factors Causing Stress in *Avicennia marina* Mangrove in Rabigh Lagoon Along the Red Sea: Based on a Multi-Approach Study. *Frontiers in Marine Science*.

Almazroui, M., Alobaidi, M., Saeed, S., Mashat, A., and Assiri, M. (2018). The Possible Impact of the Circumglobal Wave Train on the Wet Season Dust Storm Activity over the Northern Arabian Peninsula. *Clim. Dyn.* 50, 2257–2268. doi:10.1007/s00382-017-3747-1

Alobaidi, M., Almazroui, M., Mashat, A., and Jones, P. D. (2017). Arabian Peninsula Wet Season Dust Storm Distribution: Regionalization and Trends Analysis (1983-2013). *Int. J. Climatol.* 37, 1356–1373. doi:10.1002/joc.4782

Anil, I, and Alagha, O. (2020). Source Apportionment of Ambient Black Carbon During the COVID-19 Lockdown. *Int. J. Environ. Res. Public Health* 17 (23), 9021.

Aqeel, M., et al. (2021). The Influence of Illness Perception, Anxiety and Depression Disorders on Students Mental Health during COVID-19 Outbreak in Pakistan: A Web-Based Cross- Sectional Survey. *Int. J. Hum. Rights Healthc.* 14. doi:10.1108/ijhrh-10-2020-0095

Azadi, N. A., Ziapour, A., Lebni, J. Y., Irandoost, S. F., Abbas, J., and Chaboksavar, F. (2021). May 5)The Effect of Education Based on Health Belief Model on Promoting Preventive Behaviors of Hypertensive Disease in Staff of the Iran University of Medical Sciences. *Arch. Public Health* 79 (1), 69. doi:10.1186/s13690-021-00594-4

Azizi, M. R., Atlasi, R., Ziapour, A., Abbas, J., and Naemi, R. (2021). Innovative Human Resource Management Strategies during the COVID-19 Pandemic: A Systematic Narrative Review Approach. *Heliyon* 7 (12), e07233. doi:10.1016/j.heliyon.2021.e07233

Bashir, M. F., Ma, B. J., Bilal, B., Komal, B., Bashir, M. A., Farooq, T. H., et al. (2020). Correlation between Environmental Pollution Indicators and COVID-19 Pandemic: A Brief Study in Californian Context. *Environ. Res.* 187, 109652. doi:10.1016/j.envres.2020.109652

Beig, G., Ghude, S. D., and Deshpande, A. (2010). *Scientific Evaluation of Air Quality Standards and Defining Air Quality index for India*. Pune, India: Pune: Indian Institute of Tropical Meteorology, Ministry of Earth Science Government of India.

Chauhan, A., and Singh, R. P. (2020). Decline in PM2.5 Concentrations over Major Cities Around the World Associated with COVID-19. *Environ. Res.* 187, 109634. doi:10.1016/j.envres.2020.109634

Chen, K., Wang, M., Huang, C., Kinney, P. L., and Anastas, P. T. (2020). Air Pollution Reduction and Mortality Benefit during the COVID-19 Outbreak in China. *Lancet Planet. Health* 4 (6), e210–212. doi:10.1016/S2542-5196(20)30107-8

Cheng, Y., Lohmann, U., Zhang, J., Luo, Y., Liu, Z., and Lesins, G. (2005). Contribution of Changes in Sea Surface Temperature and Aerosol Loading to the Decreasing Precipitation Trend in Southern China. *J. Clim.* 18, 1381–1390. doi:10.1175/jcli3341.1

Cpcb (2020). *Central Pollution Control Board (CPCB), Ministry of Environment, Forest and Climate Change*. New Delhi: Government of India. https://app.cpcbccr.com/ccr/#/caaqm-dashboard-all/caaqm-landing.

Cpcb (2016). *NAQI Status of Indian Cities in 2015–16. Central Pollution Control Board (CPCB)*. New Delhi: Ministry of Environment, Forest and Climate Change, Government of India.

Devara, P. C. S., Raj, P. E., Pandithurai, G., Dani, K. K., and Maheskumar, R. S. (2003). Relationship between Lidar-Based Observations of Aerosol Content and Monsoon Precipitation over a Tropical Station, Pune, India. *Meteorol. Appl.* 10, 253–262. doi:10.1017/s1350482703003050

Dutheil, F., Baker, J. S., and Navel, V. (2020). COVID-19 as a Factor Influencing Air Pollution. *Environ. Pollut.* 263 (Pt), 114466. doi:10.1016/j.envpol.2020.114466

Dutta, A., and Jinsart, W. (2021). Air Quality, Atmospheric Variables and Spread of COVID-19 in Delhi (India): An Analysis. *Aerosol Air Qual. Res.* 21, 200417. doi:10.4209/aaqr.2020.07.0417

Farahat, A., Chauhan, A., Al Otaibi, M., and Singh, R. P. (2021). Air Quality Over Major Cities of Saudi Arabia During Hajj Periods of 2019 and 2020. *Earth Systems and Environment* 5 (1), 101–114.

Gautam, S., and Hens, L. (2020). SARS-CoV-2 Pandemic in India: what Might We Expect. *Environ. Dev. Sustain.* 22, 3867–3869. doi:10.1007/s10668-020-00739-5

Gautam, S. (2020). The Influence of COVID-19 on Air Quality in India: A Boon or Inutile. *Bull. Environ. Contam. Toxicol.* 104 (6), 724–726. doi:10.1007/s00128-020-02877-y

Gautam, S., and Trivedi, U. (2020). Global Implications of Bio-Aerosol in Pandemic. *Environ. Dev. Sustain.* 22, 3861–3865. doi:10.1007/s10668-020-00704-2

George, J. P., Harenduprakash, L., and Mohan, M. (2008). Multi Year Changes of Aerosol Optical Depth in the Monsoon Region of the Indian Ocean since 1986 as Seen in the AVHRR and TOMS Data. *Ann. Geophys.* 26, 7–11. doi:10.5194/angeo-26-7-2008

Gherboudj, I., Naseema Beegum, S., and Ghedira, H. (2017). Identifying Natural Dust Source Regions over the Middle-East and North-Africa: Estimation of Dust Emission Potential. *Earth-Science Rev.* 165, 342–355. doi:10.1016/J.EARSCIREV.2016.12.010

Goel, S., Kanazawa, A., and Malik, J. (2020). Shape and Viewpoint Without Keypoints. *European Conference on Computer Vision*. Cham: Springer, 88–104.

Indoitu, R., Kozhoridze, G., Batyrbaeva, M., Vitkovskaya, I., Orlovsky, N., Blumberg, D., et al. (2015). Dust Emission and Environmental Changes in the Dried Bottom of the Aral Sea. *Aeolian Res.* 17, 101–115. doi:10.1016/J.AEOLIA.2015.02.004

Jain, S., and Sharma, T. (2020). Social and Travel Lockdown Impact Considering Coronavirus Disease (Covid-19) on Air Quality in Megacities of india: Present Benefits, Future Challenges and Way Forward. *Aerosol Air Qual. Res.* 20 (6), 1222–1236. doi:10.4209/aaqr.2020.04.0171

Jin, Q., Wei, J., Lau, W. K. M., Pu, B., and Wang, C. (2021). Interactions of Asian mineral Dust with Indian Summer Monsoon: Recent Advances and Challenges. *Earth-Science Rev.* 215, 103562. doi:10.1016/j.earscirev.2021.103562

Kanniah, K. D., Kamarul Zaman, N. A. F., Kaskaoutis, D. G., and Latif, M. T. (2020). COVID-19's Impact on the Atmospheric Environment in the Southeast Asia Region. *Sci. Total Environ.* 736, 139658. doi:10.1016/j.scitotenv.2020.139658

Kaskaoutis, D. G., Kosmopoulos, P. G., Nastos, P. T., Kambezidis, H. D., Sharma, M., and Mehdi, W. (2012). Transport Pathways of Sahara Dust over Athens, Greece as Detected by MODIS and TOMS. *Geomatics, Nat. Hazards Risk* 3 (1), 35–54. doi:10.1080/19475705.2011.574296

Kedia, S., Kumar, R., Islam, S., Sathe, Y., and Kaginalkar, A. (2018). Radiative Impact of a Heavy Dust Storm over India and Surrounding Oceanic Regions. *Atmos. Environ.* 185, 109–120. doi:10.1016/j.atmosenv.2018.05.005

Kerimray, A., Baimatova, N., Ibragimova, O. P., Bukenov, B., Kenessov, B., Plotitsyn, P., et al. (2020). Assessing Air Quality Changes in Large Cities during COVID-19 Lockdowns: The Impacts of Traffic-free Urban Conditions in Almaty, Kazakhstan. *Sci. Total Environ.* 730, 139179. doi:10.1016/j.scitotenv.2020.139179

Khan, A., Khorat, S., Khatun, R., Doan, Q.-V., Nair, U. S. U. S., and Niyogi, D. (2021). Variable Impact of COVID-19 Lockdown on Air Quality across 91 Indian Cities. *Am. Meteorol. Soc.* 25, 57–75. doi:10.1175/EI-D-20-0017.1

Khetan, M. S., Vaishnao, L. S., Kewalramani, M., Kewalramani, M., and Shah, R. J. (2020). Effect of Lockdown Due to COVID-19 Pandemic on Mental Health of Pre-medical Students of Maharashtra. *Int. J. Community Med. Public Health* 7 (9), 3524–3530. doi:10.18203/2394-6040.ijcmph20203917

Klimont, Z., Kupiainen, K., Heyes, C., Purohit, P., Cofala, J., Rafaj, P., et al. (2017). Global Anthropogenic Emissions of Particulate Matter Including Black Carbon. *Atmos. Chem. Phys.* 17, 8681–8723. doi:10.5194/acp-17-8681-2017

Knippertz, P., Deutscher, C., Kandler, K., Müller, T., Schulz, O., and Schütz, L. (2007). Dust Mobilization Due to Density Currents in the Atlas Region: Observations from the Saharan Mineral Dust Experiment 2006 Field Campaign. *J. Geophys. Res.* 112. doi:10.1029/2007jd008774

Kotnala, G., Mandal, T. K., Sharma, S. K., and Kotnala, R. K. (2020). Emergence of Blue Sky over Delhi Due to Coronavirus Disease (COVID-19) Lockdown Implications. *Aerosol Sci. Eng.* 4, 228–238. doi:10.1007/s41810-020-00062-6

Krishnan, R., and Ramanathan, V. (2002). Evidence of Surface Cooling from Absorbing Aerosols. *Geophys. Res. Lett.* 29, 54–61. doi:10.1029/2002GL014687

Kumar, A., Singh, B. P., Punia, M., Singh, D., Kumar, K., and Jain, V. K. (2014a). Assessment of Indoor Air Concentrations of VOCs and Their Associated Health Risks in the Library of Jawaharlal Nehru University, New Delhi. *Environ. Sci. Pollut. Res.* 21 (3), 2240–2248. doi:10.1007/s11356-013-2150-7

Kumar, A., Singh, B. P., Punia, M., Singh, D., Kumar, K., and Jain, V. K. (2014b). Determination of Volatile Organic Compounds and Associated Health Risk Assessment in Residential Homes and Hostels within an Academic institute, New Delhi. *Indoor Air* 24 (5), 474–483. doi:10.1111/ina.12096

Kumar, N., and Tyagi, R. (2021). Various Impacts of COVID-19 on Environmental Pollution. *Int. J. Hum. Capital Urban Manage.* 6 (1), 1–10. doi:10.22034/IJHCUM.2021.01.01

Kumar, P., Hama, S., Omidvarborna, H., Sharma, A., Sahani, J., Abhijith, K. V., et al. (2020). Temporary Reduction in fine Particulate Matter Due to 'anthropogenic Emissions Switch-Off' during COVID-19 Lockdown in Indian Cities. *Sust. Cities Soc.* 62 (May), 102382. doi:10.1016/j.scs.2020.102382

Kumar, S. (2020). Effect of Meteorological Parameters on Spread of COVID-19 in India and Air Quality during Lockdown. *Sci. Total Environ.* 745, 141021. doi:10.1016/j.scitotenv.2020.141021

Kumari, P., and Toshniwal, D. (2020). Impact of Lockdown Measures during COVID-19 on Air Quality- A Case Study of India. *Int. J. Environ. Health Res.* 00 (00), 1–8. doi:10.1080/09603123.2020.1778646

Li, J., Wang, D., Duan, K., and Mubeen, R. (2021). Tourists' Health Risk Threats amid COVID-19 Era: Role of Technology Innovation, Transformation, and Recovery Implications for Sustainable Tourism. *Front. Psychol.* 12, 769175. doi:10.3389/fpsyg.2021.769175

Li, L., Li, Q., Huang, L., Wang, Q., Zhu, A., Xu, J., et al. (2020). Air Quality Changes during the COVID-19 Lockdown over the Yangtze River Delta Region: An Insight into the Impact of Human Activity Pattern Changes on Air Pollution Variation. *Sci. Total Environ.* 732, 139282. doi:10.1016/j.scitotenv.2020.139282

Liu, F., Wang, D., Duan, K., and Mubeen, R. (2021a). 2021-September-03)Social media Efficacy in Crisis Management: Effectiveness of Non-pharmaceutical Interventions to Manage the COVID-19 Challenges [Original Research]. *Front. Psychiatry* 12 (1099), 626134. doi:10.3389/fpsyt.2021.626134

Liu, Q., Qu, X., Wang, D., and Mubeen, R. (2021b). Product Market Competition and Firm Performance: Business Survival through Innovation and Entrepreneurial Orientation amid COVID-19 Financial Crisis. *Front. Psychol.* 12 (4910), 790923. doi:10.3389/fpsyg.2021.79092310.3389/fpsyg.2021.707971

Local Burden of Disease, H. I. V. C. (2021). Mapping Subnational HIV Mortality in Six Latin American Countries with Incomplete Vital Registration Systems. *BMC Med.* 19 (1), 4. doi:10.1186/s12916-020-01876-4

Mahato, S., Pal, S., and Ghosh, K. G. (2002). Effect of Lockdown amid COVID-19 Pandemic on Air Quality of the Megacity Delhi, India. *Sci. Total Environ.* 730, 139086. doi:10.1016/j.scitotenv.2020.139086

Maji, K. J., Namdeo, A., Bell, M., Goodman, P., Nagendra, S. M. S., Barnes, J. H., et al. (2021). Unprecedented Reduction in Air Pollution and Corresponding Short-Term Premature Mortality Associated with COVID-19 Lockdown in Delhi, India. *J. Air Waste Manag. Assoc.* 71, 1085–1101. doi:10.1080/10962247.2021.1905104

Mandal, I., and Pal, S. (2020). COVID-19 Pandemic Persuaded Lockdown Effects on Environment over Stone Quarrying and Crushing Areas. *Sci. Total Environ.* 732, 139281. doi:10.1016/j.scitotenv.2020.139281

Mehmood, K., SaifullahIqbal, M., Iqbal, M., and Abrar, M. M. (2020). Can Exposure to PM2.5 Particles Increase the Incidence of Coronavirus Disease 2019 (COVID-19). *Sci. Total Environ.* 741, 140441. doi:10.1016/j.scitotenv.2020.140441

Meo, S. A., Bukhari, I. A., Akram, J., Meo, A. S., and Klonoff, D. C. (2021). COVID-19 Vaccines: Comparison of Biological, Pharmacological Characteristics and Adverse Effects of Pfizer/BioNTech and Moderna Vaccines. *Eur. Rev. Med. Pharmacol. Sci.*, 1663–1669.

Morsy, M. A., Abdel-Aziz, A. M., Abdel-Hafez, S., Venugopala, K. N., Nair, A. B., and Abdel-Gaber, S. A. (2020). The Possible Contribution of P-Glycoprotein in the Protective Effect of Paeonol Against Methotrexate-Induced Testicular Injury in Rats. *Pharmaceuticals* 13 (9), 223.

Morsy, H., Salami, A., and Mukasa, A. N. (2021). Opportunities Amid COVID-19: Advancing Intra-African Food Integration. *World Development* 139, 105308.

Middleton, N. J. (1986). A Geography of Dust Storms in South-West Asia. *J. Climatol.* 6 (2), 183–196. doi:10.1002/joc.3370060207

Mubeen, R., Han, D., Abbas, J., and Hussain, I. (2020). The Effects of Market Competition, Capital Structure, and CEO Duality on Firm Performance: A Mediation Analysis by Incorporating the GMM Model Technique. *Sustainability* 12 (8), 3480. doi:10.3390/su12083480

Munir, M., Nazeer, W., Rafique, S., and Kang, S. M. (2016). M-Polynomial and Degree-Based Topological Indices of Polyhex Nanotubes. *Symmetry* 8 (12), 149.

Nakajima, T., Yoon, S.-C., Ramanathan, V., Shi, G.-Y., Takemura, T., Higurashi, A., et al. (2007). Overview of the Atmospheric Brown Cloud East Asian Regional Experiment 2005 and a Study of the Aerosol Direct Radiative Forcing in East Asia. *J. Geophys. Res.* 112. doi:10.1029/2007JD009009

Namdari, S., Karimi, N., Sorooshian, A., Mohammadi, G., and Sehatkashani, S. (2018). Impacts of Climate and Synoptic Fluctuations on Dust Storm Activity over the Middle East. *Atmos. Environ.* 173, 265–276. doi:10.1016/J.ATMOSENV.2017.11.016

Navinya, C., Patidar, G., and Phuleria, H. C. (2020). Examining Effects of the COVID-19 National Lockdown on Ambient Air Quality across Urban India. *Aerosol Air Qual. Res.* 20, 1759–1771. doi:10.4209/aaqr.2020.05.0256

NeJhaddadgar, N., Ziapour, A., Zakkipour, G., Abbas, J., Abolfathi, M., and Shabani, M. (2020). Effectiveness of Telephone-Based Screening and Triage during COVID-19 Outbreak in the Promoted Primary Healthcare System: a Case Study in Ardabil Province, Iran. *J. Public Health (Berl.)* 29, 1–6. doi:10.1007/s10389-020-01407-8

Otmani, A., Benchrif, A., Tahri, M., Bounakhla, M., Chakir, E. M., El Bouch, M., et al. (2020). Impact of Covid-19 Lockdown on PM10, SO2 and NO2 Concentrations in Salé City (Morocco). *Sci. Total Environ.* 735 (2), 139541. doi:10.1016/j.scitotenv.2020.139541

Ott, W. R. (1978). Environmental Indices: Theory and Practice.

Pant, G., Alka, D., Garlapati, D., Gaur, A., Hossain, K., Singh, S. V., et al. (2020). Air Quality Assessment Among Populous Sites of Major Metropolitan Cities in India during COVID-19 Pandemic Confinement. *Environ. Sci. Pollut. Res.* 27, 44629–44636. doi:10.1007/s11356-020-11061-y

Paulson, K. R., Kamath, A. M., Alam, T., Bienhoff, K., Abady, G. G., and Kassebaum, N. J. (2021). Global, Regional, and National Progress towards Sustainable Development Goal 3.2 for Neonatal and Child Health: All-Cause and Cause-specific Mortality Findings from the Global Burden of Disease Study 2019. *The Lancet*, 1–36. doi:10.1016/s0140-6736(21)01207-1

Prasad, A. K., Singh, R. P., and Singh, A. (2006). Seasonal Climatology of Aerosol Optical Depth over the Indian Subcontinent: Trend and Departures in Recent Years. *Int. J. Remote Sensing* 27, 2323–2329. doi:10.1080/01431160500043665

Pye, K. (2015). *Aeolian Dust and Dust Deposits*. London, UK: ElsevierAcademic Press, 334.

Rashki, A., Kaskaoutis, D. G., Rautenbach, C. J. d., Eriksson, P. G., Qiang, M., and Gupta, P. (2012). Dust Storms and Their Horizontal Dust Loading in the Sistan Region, Iran. *Aeolian Res.* 5, 51–62. doi:10.1016/J.AEOLIA.2011.12.001

Report, M. W., Yao, Y., Ph, D., Asadi, S., Bouvier, N., Wexler, A. S., et al. (2020). Evaluation of the Potential Relationship between Particulate Matter (PM) Pollution and COVID-19 Infection Spread in Italy. *Atmos. Meas. Tech.* 21 (March), 939–949. doi:10.1080/02786826.2020.1749229

Resmi, C. T., Nishanth, T., Satheesh Kumar, M. K., Manoj, M. G., Balachandramohan, M., and Valsaraj, K. T. (2020). Air Quality Improvement during Triple-Lockdown in the Coastal City of Kannur, Kerala to Combat Covid-19 Transmission. *PeerJ* 8, e9642–20. doi:10.7717/peerj.96422

Ritchie, H., Ortiz-Ospina, E., Hasell, J., Macdonald, B., Giattino, C., and Roser, M. (2020). *Coronavirus Pandemic (COVID-19). Our World in Data – Statistics and Research*. England: Oxford Martin School, The University of Oxford, UK. Global Change Data Lab. Available from: https://ourworldindata.org/coronavirus/ (accessed September 17, 2020).

Selvam, S., Muthukumar, P., Venkatramanan, S., Roy, P. D., Bharath, K. M., and Jesuraja, K. (2020). SARS-CoV-2 Pandemic Lockdown: Effects on Air Quality in the Industrialized Gujarat State of India. *Sci. Total Environ.* 737, 140391.

Sahu, S. K., and Kota, S. H. (2017). Significance of PM2.5 Air Quality at the Indian Capital. *Aerosol Air Qual. Res.* 17, 588–597. doi:10.4209/aaqr.2016.06.0262

Sarkar, S., Chauhan, A., Kumar, R., and Singh, R. P. (2019). Impact of Deadly Dust Storms (May 2018) on Air Quality, Meteorological, and Atmospheric Parameters over the Northern Parts of India. *GeoHealth* 3, 67–80. doi:10.1029/2018GH000170

Sathe, Y., Gupta, P., Bawase, M., Lamsal, L., Patadia, F., and Thipse, S. (2021). Surface and Satellite Observations of Air Pollution in India during COVID-19 Lockdown: Implication to Air Quality. *Sust. Cities Soc.* 66, 102688. doi:10.1016/j.scs.2020.102688

Sharma, S., Zhang, M., Anshika, J., Gao, J., Zhang, H., and Kota, S. H. (2020). Effect of Restricted Emissions during COVID-19 on Air Quality in India. *Sci. Total Environ.* 728, 138878. doi:10.1016/j.scitotenv.2020.138878

Shi, X., and Brasseur, G. P. (2020). The Response in Air Quality to the Reduction of Chinese Economic Activities during the COVID-19 Outbreak. *Geophys. Res. Lett.* 47, 1. doi:10.1029/2020GL088070

Sicard, P., De Marco, A., Agathokleous, E., Feng, Z., Xu, X., Paoletti, E., et al. (2020). Amplified Ozone Pollution in Cities during the COVID-19 Lockdown. *Sci. Total Environ.* 735, 139542. doi:10.1016/j.scitotenv.2020.139542

Singh, B. P., Kumar, A., Singh, D., Punia, M., Kumar, K., and Jain, V. K. (2014). An Assessment of Ozone Levels, UV Radiation and Their Occupational Health hazard Estimation during Photocopying Operation. *J. Hazard. Mater.* 275, 55–62. doi:10.1016/j.jhazmat.2014.04.049

Singh, B. P., Kumar, K., and Jain, V. K. (2021c). Distribution of Ring PAHs in Particulate/gaseous Phase in the Urban City of Delhi, India: Seasonal Variation and Cancer Risk Assessment. *Urban Clim.* 40, 101010. doi:10.1016/j.uclim.2021.101010

Singh, B. P., Kumar, K., and Jain, V. K., (2021a). Source Identification and Health Risk Assessment Associated with Particulate- and Gaseous-phase PAHs at Residential Sites in Delhi, India. *Air Qual. Atmos. Health*, 14, 1505, 1521. doi:10.1007/s11869-021-01035-5

Singh, B. P., and Kumar, P. (2021). Spatio-temporal Variation in fine Particulate Matter and Effect on Air Quality during the COVID-19 in New Delhi, India. *Urban Clim.* 40, 101013. doi:10.1016/j.uclim.2021.101013

Singh, B. P., Singh, K., Kumar, K., and Jain, V. K. (2021b). Study of Seasonal Variation of PM2.5 Concentration Associated with Meteorological Parameters at Residential Sites in Delhi, India. *J. Atmos. Chem*. doi:10.1007/s10874-021-09419

Singh, D., Kumar, A., Kumar, K., Singh, B., Mina, U., Singh, B. B., et al. (2016). Statistical Modeling of O3, NOx, CO, PM2.5, VOCs and Noise Levels in Commercial Complex and Associated Health Risk Assessment in an Academic Institution. *Sci. Total Environ.* 572, 586–594. doi:10.1016/j.scitotenv.2016.08.086

Srivastava, S., Kumar, A., Bauddh, K., Gautam, A. S., and Kumar, S. (2020). 21-Day Lockdown in India Dramatically Reduced Air Pollution Indices in Lucknow and New Delhi, India. *Bull. Environ. Contam. Toxicol.* 105, 9–17. doi:10.1007/s00128-020-02895-w

Su, Z., McDonnell, D., Cheshmehzangi, A., Abbas, J., Li, X., and Cai, Y. (2021a). The Promise and Perils of Unit 731 Data to advance COVID-19 Research. *BMJ Glob. Health* 6 (5), e004772. doi:10.1136/bmjgh-2020-004772

Su, Z., McDonnell, D., Wen, J., Kozak, M., Abbas, J., Šegalo, S., et al. (2021b). Mental Health Consequences of COVID-19 media Coverage: the Need for Effective Crisis Communication Practices. *Glob. Health* 17 (1), 4. doi:10.1186/s12992-020-00654-4

Su, Z., WenMcDonnell, J., Abbas, J., McDonnell, D., Cheshmehzangi, A., Li, X., et al. (2020). A Race for a Better Understanding of COVID-19 Vaccine Non-adopters. *Brain Behav. Immun. - Health* 9, 100159. doi:10.1016/j.bbih.2020.100159

Suhaimi, N. F., Jalaludin, J., and Latif, M. T. (2020). Demystifying a Possible Relationship between COVID-19, Air Quality and Meteorological Factors: Evidence from Kuala Lumpur, Malaysia. *Aerosol Air Qual. Res.* 20, 1520–1529. doi:10.4209/aaqr.2020.05.0218

Tobías, A., Carnerero, C., Reche, C., Massagué, J., Via, M., Minguillón, M. C., et al. (2020). Changes in Air Quality during the Lockdown in Barcelona (Spain) One Month into the SARS-CoV-2 Epidemic. *Sci. Total Environ.* 726, 138540. doi:10.1016/j.scitotenv.2020.138540

Torkmahalleh, M. A., Hopke, P. K., Broomandi, P., Naseri, M., Abdrakhmanov, T., Ishanov, A., et al. (2020). Exposure to Particulate Matter and Gaseous Pollutants During Cab Commuting in Nur-Sultan City of Kazakhstan. *Atmospheric Pollution Research* 11 (5), 880–885.

Türkeş, M. (2017). "Recent Spatiotemporal Variations of Synoptic Meteorological Sand and Dust Storm Events Observed over the Middle East and Surrounding Regions," in Proceedings of the 5th International Workshop on Sand and Dust Storms (SDS): Dust Sources and their Impacts in the Middle East, 23–25 October 2017 (Turkey: Istanbul), 45–59.

Vadrevu, K. P., Eaturu, A., Biswas, S., Lasko, K., Sahu, S., Garg, J. K., et al. (2020). Spatial and Temporal Variations of Air Pollution over 41 Cities of India during the COVID-19 Lockdown Period. *Sci. Rep.* 10, 1–15. doi:10.1038/s41598-020-72271-5

Verma, R. L., and Kamyotra, J. S. (2021). Impacts of COVID-19 on Air Quality in India. *Aerosol and Air Quality Research*, 21.

Wang, C., Wang, D., Abbas, J., Duan, K., and Mubeen, R. (2021). Global Financial Crisis, Smart Lockdown Strategies, and the COVID-19 Spillover Impacts: A Global Perspective Implications from Southeast Asia. *Front. Psychiatry* 12 (1099), 643783. doi:10.3389/fpsyt.2021.643783

Wang, J. X. L. (2015). Mapping the Global Dust Storm Records: Review of Dust Data Sources in Supporting Modeling/Climate Study. *Curr. Pollut. Rep* 1, 82–94. doi:10.1007/s40726-015-0008-y

Wang, P., Chen, K., Zhu, S., Wang, P., and Zhang, H. (2020a). Severe Air Pollution Events Not Avoided by Reduced Anthropogenic Activities during COVID-19 Outbreak. *Resour. Conservation Recycling* 158 (February), 104814. doi:10.1016/j.resconrec.2020.104814

Wang, P., Qiao, X., and Zhang, H. (2020b). Modeling PM2.5 and O3 with Aerosol Feedbacks Using WRF/Chem over the Sichuan Basin, Southwestern China. *Chemosphere* 254, 126735. doi:10.1016/j.chemosphere.12673510.1016/j.chemosphere.2020.126735

Wang, Y., Yuan, Y., Wang, Q., Liu, C., Zhi, Q., and Cao, J. (2020). Changes in Air Quality Related to the Control of Coronavirus in China: Implications for Traffic and Industrial Emissions. *Sci. Total Environ.* 731 (December 2019), 139133. doi:10.1016/j.scitotenv.2020.139133

World Health Organisation (2020). World Health Organization Coronavirus Disease (COVID-19) Pandemic, WHO. Accessed from https://www.who.int/emergencies/diseases/novel-coronavirus-2019 on 31 March 2020.

World Health Organisation (2020). *World Health Organization, Coronavirus Disease*. (COVID-2019) India Situation Report – 1 https://www.who.int/docs/default-source/wrindia/india-situation-report-1.pdf?sfvrsn=5ca2a672_0 (Accessed January 31, 2020).

World metros (2021). (Accessed October 4, 2021)https://www.worldometers.info/coronavirus/.

Wu, F., Zhao, S., Yu, B., Chen, Y.-M., Wang, W., Song, Z.-G., et al. (2020). A New Coronavirus Associated with Human Respiratory Disease in China. *Nature* 579 (7798), 265–269. doi:10.1038/s41586-020-2008-3

Xi, X., and Sokolik, I. N. (2015). Seasonal Dynamics of Threshold Friction Velocity and Dust Emission in Central Asia. *J. Geophys. Res. Atmos.* 120, 1536–1564. doi:10.1002/2014JD022471

Xie, J., and Zhu, Y. (2020). Association between Ambient Temperature and COVID-19 Infection in 122 Cities from China. *Sci. Total Environ.* 724, 138201. doi:10.1016/j.scitotenv.2020.138201

Lebni, J., Abbas, J., Khorami, F., Khosravi, B., Jalali, A., and Ziapour, A. (2020). Challenges Facing Women Survivors of Self-Immolation in the Kurdish Regions of Iran: A Qualitative Study. *Front. Psychiatry* 11, 778. doi:10.3389/fpsyt.2020.00778

Yu, K., D'Odorico, P., Bhattachan, A., Okin, G. S., and Evan, A. T. (2015). Dust-rainfall Feedback in West African Sahel. *Geophys. Res. Lett.* 42, 7563–7571. doi:10.1002/2015GL065533

Zambrano-Monserrate, M. A., Ruano, M. A., and Sanchez-Alcalde, L. (2020). Indirect Effects of COVID-19 on the Environment. *Sci. Total Environ.* 728, 138813. doi:10.1016/j.scitotenv.2020.138813

Zheng, J. (2020). SARS-CoV-2: an Emerging Coronavirus that Causes a Global Threat. *Int. J. Biol. Sci.* 16 (10), 1678–1685. doi:10.7150/ijbs.45053

Zhu, Y., Xie, J., Huang, F., and Cao, L. (2020). Association between Short-Term Exposure to Air Pollution and COVID-19 Infection: Evidence from China. *Sci. Total Environ.* 727, 138704. doi:10.1016/j.scitotenv.2020.138704

Conflict of Interest: The authors declare that the research was conducted in the absence of any commercial or financial relationships that could be construed as a potential conflict of interest.

Publisher's Note: All claims expressed in this article are solely those of the authors and do not necessarily represent those of their affiliated organizations, or those of the publisher, the editors and the reviewers. Any product that may be evaluated in this article, or claim that may be made by its manufacturer, is not guaranteed or endorsed by the publisher.

frontiers in Environmental Science

ORIGINAL RESEARCH
published: 15 March 2022
doi: 10.3389/fenvs.2022.838778

Variability of Aerosols and Clouds Over North Indian and Myanmar During the COVID-19 Lockdown Period

Divyaja Lawand[1], *Sudheer Bhakare*[2], *Suvarna Fadnavis*[2], *Rohini L. Bhawar*[1]*, *P. R. C. Rahul*[2], *Pradeep Kumar Pallath*[1] *and Simone Lolli*[3]

[1]Department of Atmospheric and Space Sciences, Savitribai Phule Pune University, Pune, India, [2]Indian Institute of Tropical Meteorology, Pune, India, [3]CNR-IMAA, Contrada S. Loja, Potenza, Italy

The implementation of a nationwide lockdown to curb the spread of COVID-19 disease has reduced the loading of anthropogenic aerosols. However, AOD distribution over South Asia during the lockdown period shows a dipole pattern: reduction over North Indian and enhancement over the Myanmar region. This dipole pattern is evident in some datasets (MODIS, MERRA, and CALIPSO). MODIS fire counts collocated with CALIPSO smoke aerosols show enhancement over Myanmar indicating the contribution from fires. However, over the North India region number of fires during the lockdown period are less compared to climatology. Thus, the observed reduction in AOD is due to fires and anthropogenic sources. Our analysis shows that aerosols originating from biomass burning forms a layer (900–600 hPa) over the Myanmar region that produces atmospheric heating (0–2.8 K/day) that eventually leads to cloud dissipation/burning (negative in-atmospheric cloud radiative forcing ~ −13 W/m^2) and precipitation reduction (−1 to −4 mm) over Myanmar. In contrast, the aerosol reduction over North India favors cloud formation, that is, increase in cloud cover and reduction in specific cloud liquid water content leading to precipitation enhancement, indicating the anti-Twomey effect.

Keywords: aerosols, clouds, biomass burning, radiative forcing, precipitation

OPEN ACCESS

Edited by:
Yang Gao,
Ocean University of China, China

Reviewed by:
Eduardo Landulfo,
Instituto de Pesquisas Energéticas e Nucleares (IPEN), Brazil
Shweta Yadav,
Central University of Jammu, India

***Correspondence:**
Rohini L. Bhawar
rohinibhawar@gmail.com

Specialty section:
This article was submitted to Atmosphere and Climate, a section of the journal Frontiers in Environmental Science

Received: *18 December 2021*
Accepted: *24 February 2022*
Published: *15 March 2022*

Citation:
Lawand D, Bhakare S, Fadnavis S, Bhawar RL, Rahul PRC, Pallath PK and Lolli S (2022) Variability of Aerosols and Clouds Over North Indian and Myanmar During the COVID-19 Lockdown Period. Front. Environ. Sci. 10:838778. doi: 10.3389/fenvs.2022.838778

1 INTRODUCTION

Clouds are critical in controlling Earth's radiation budget, and aerosols are inherently a major component of the clouds. Aerosols act as nuclei over which water vapor condense and form the cloud droplet. An increase in anthropogenic activity has led to an increase in aerosol emissions at a global scale, which led to an increase in cloud condensation nuclei (CCN) and ice nucleating particles (INP) (Seinfeld et al., 2016). However, the increase in CCN does not lead to enhanced precipitation, indicating complex microphysical processes affecting the precipitation (Koren et al., 2008; Bhawar and Rahul, 2013). Previous studies reported an adverse effect of aerosol increase and thereby giant CCN formation on precipitation (Posselt and Lohmann 2008). These studies elucidate that an increase in aerosol loading (thereby CCN) leads to numerous smaller cloud droplets when these aerosols interact with warm clouds (Twomey, 1977). Furthermore, with the increase in the droplet number, the total droplet surface area also resulted in the higher scattering of sunlight to space (Seinfeld et al., 2016). Aerosols participate in the cloud microphysical processes by acting as nuclei,

leading to the increase in cloud droplet number concentration, changes in the cloud drop sizes, and radiative properties of clouds, well known as the Twomey effect (Twomey, 1977). Thus, smaller cloud droplets reduce warm rain formation by increasing cloud lifetime or dissipation of clouds (Albrecht, 1989). Thus, aerosol-cloud-radiation interaction causes changes in temperature, moisture, and cloud water content, which essentially changes cloud microphysical processes and, in turn, affects the precipitation rates (Albrecht, 1989; Pincus and Baker, 1994; Johnson and Onwuegbuzie, 2004). These complex aerosol-cloud-interaction processes are not fully understood (IPCC, 2013).

The complexity of aerosol-cloud-radiation effects on precipitation is further convoluted by different types of aerosols with varied impacts on the cloud droplet size, cloud lifetime, and cloud radiative effects, especially over large metropolitan regions (Zheng et al., 2020). Both natural and anthropogenic forest fires have been affecting atmospheric aerosol amounts for centuries. Fire aerosols affect local weather by affecting the cloud microphysical properties, serving as CCN or ice nuclei and consequently changing cloud droplet sizes. Jones et al. (2007) reported that the increasing fire aerosol emissions from the preindustrial period to the present day had cooled global near-surface air temperatures by 0.258°C. The fire aerosols decreased precipitation over excessive biomass burning regions in Africa and South America (Tosca et al., 2013). Fire-emitted BC causes stratification in the troposphere that inhibits convection and reduces precipitation (Ackerman et al., 2000; Andreae and Rosenfeld 2008). Fire aerosols also suppress cloud formation and precipitation if black carbon is embedded in the clouds (Feingold et al., 2005; Kaufman et al., 2005).

Over South Asia, open crop burning during spring is a source of enormous carbonaceous aerosols (Reddy et al., 2012; Song et al., 2012; Liu et al., 2014; Zhang et al., 2015). These biomass burring aerosols may suppress or enhance cloud fraction depending on aerosol concentration (Koren et al., 2008; Li et al., 2018). Biomass burning aerosols tend to enhance the formation and lifetime of warm clouds and suppress high-level clouds by reducing updrafts as part of the aerosol-cloud interaction process (Lolli et al., 2019; Liu et al., 2020). Liu et al., 2020 further reported that, in high biomass burning aerosol loading conditions, aerosol-radiation interaction dominates, which can cause a decrease in the occurrence frequency and rate of precipitation. Wagh et al., 2021 found that the ice nuclei concentration during Delhi's 2016–2017 winter fog episodes was significantly correlated with black carbon. Delhi's fog episodes are caused by industrial, vehicular, and biomass burning activities in the surrounding regions. Among Asian countries, Myanmar is the largest hot spot of woodland fires in spring (Biswas et al., 2015; Vadrevu et al., 2015). Emissions from biomass burning in Southeast Asia have been observed up to an altitude of 3 km (Lin et al., 2009).

The novel pandemic COVID-19 originated in China in December 2019 and spread to Italy and Europe at the beginning of 2020 (Lolli et al., 2020). The first reported case in India was in January 2020. The pandemic outbreak spread very quickly (Paital, 2020; Singh and Chauhan, 2020). The Indian government imposed what is called a "Janata curfew" (lockdown-like situation) on 22 March 2020 and, later, a complete lockdown between 25 March and 14 April 2020, which extended up to May 2020 (Singh and Chauhan, 2020; Fadnavis et al., 2021). The implemented restrictions include a complete shutdown of industries, public transport, and so on. These restrictions helped curb the spread of COVID-19 to a large extent (Paital, 2020; Yunus et al., 2020). Different studies over the Indian region showed a drastic reduction of aerosol loading over the North Indian region (Jain and Sharma, 2020; Fadnavis et al., 2021; Mishra and Rathore, 2021). However, biomass burning caused an enhancement in AOD over central India (Bhawar et al., 2021). The biomass burning aerosols formed a layer at altitudes 2–4 km over Myanmar and produced heating of 3–4 K/day near the layer. The biomass burning aerosol-induced heating may affect the clouds and precipitation. Thus, during the COVID-19 lockdown period (spring 2020), although there was a reduction in anthropogenic aerosols, biomass burning fires may still be a source of aerosols within South Asia, especially over central India and Myanmar region that may affect the local clouds, radiative effects, and precipitation. This study assesses the impact of biomass burning aerosols on clouds, radiative effects, and precipitation over two contrasting fire aerosol loading regions (low over North India and high over Myanmar) that formed a dipole structure within South Asia. It is organized as follows: **Section 2** describes the methodology and data used in this study, **Section 3** mentions the results and discussions, and **Section 4** summarizes and concludes the main findings.

2 DATA METHODOLOGY

2.1 Satellite Data

2.1.1 Moderate Resolution Imaging Spectroradiometer

Moderate Resolution Imaging Spectroradiometer (MODIS) is an instrument onboard the polar-orbiting Earth Observation satellites (EOS) Aqua/Terra that provides atmosphere, land, and cryosphere products with equatorial crossing times of 10:30 and 13:30, local time (Remer et al., 2005). MODIS provides the observations of aerosols for more than 20 years during the cloud-free scenarios by measuring radiances at 36 wavelengths from 0.41 to 14 μm with near-global coverage every day. The uncertainties in MODIS aerosol product at 550 nm over land ±(0.05 to ±15%) and ocean ±(0.03 to ±5%) respectively (Remer et al., 2008; Levy et al., 2010) may be due to the assumptions on surface reflectance, location, season, and aerosol retrieval algorithm (Remer et al., 2005; Levy et al., 2010; Breon et al., 2011). Herein, we used the level 3, C6.1, and gridded (1 × 1 degree) aerosol optical depth (AOD) data from MODIS combined Dark Target and Deep blue at 550 nm. The data can be downloaded from https://giovanni.gsfc.nasa.gov/giovanni/.

2.1.2 The Cloud-Aerosol Lidar and Infrared Pathfinder

Cloud-Aerosol Lidar and Infrared Pathfinder Satellite Observations (CALIPSO) has been providing 3D aerosol and

cloud observation globally with a 16-day repeating cycle crossing the equator at 1:30 p.m and 1:30 a.m. (Ma et al., 2012). Cloud-Aerosol Lidar with Orthogonal Polarization (CALIOP) is the primary instrument that profiles the cloud and aerosol layers at two wavelengths of 1064 nm and 532 nm (linear depolarization is derived from 532 nm) (Hunt et al., 2009). The lidar ratios are used to retrieve aerosol extinction above clouds and below optically thin clouds and in the cloud-free columns. In contrast, the optical depth is measured from attenuated backscatter (Young and Vaughan, 2009; King et al., 2018). This study uses CALIPSO lidar level 2 version 4.10/4.20 standard aerosol profile product, which represents near actual conditions. The extinction profiles are used to derive AOD at 532 nm and gridded at 1 × 1 degree resolution for the study period. The data were downloaded from https://asdc.larc.nasa.gov/project/CALIPSO (details available in Bhawar et al., 2021). We analyzed CALIPSO observed elevated smoke product. The smoke aerosols occurring above the boundary layer are termed elevated layers (McGrath-Spangler and Denning 2013; Kim et al., 2018).

2.2 Reanalysis Datasets

2.2.1 The Modern-Era Retrospective Analysis for Research and Applications

We used the Modern-Era Retrospective Analysis for Research and Applications (MERRA) reanalysis dataset based on the Goddard Earth Observing System Data Analysis System, version 5 (GEOS-5 DAS; Rienecker et al., 2011). MERRA uses three-dimensional variational data assimilation (3DVAR) analysis algorithm based on the Gridpoint Statistical Interpolation scheme (Wu et al., 2002; Derber et al., 2003) with a 6 h update cycle. The monthly mean AOD and cloud fraction gridded on ½° latitude × ⅔° longitude, with 72 vertical levels, from the surface to 0.01 hPa were analyzed here. The AOD and cloud fraction data are available at https://giovanni.gsfc.nasa.gov/giovanni/.

2.2.2 European Centre for Medium-Range Weather Forecasting Reanalysis Version 5

We analyzed European Centre for Medium-Range Weather Forecasting Reanalysis version 5 (ERA5) global model (Poli et al., 2016). ERA5 analysis is produced at a 1-hour time step advanced 4D-var assimilation scheme. It has a horizontal resolution of approximately 30 km (0.25° × 0.25°). In the present work, ERA5 Cloud base height and specific cloud water liquid content monthly data are used. Cloud water liquid content data are analyzed for 37 pressure levels from 1,000 to 1 hPa. The above datasets are available at https://cds.climate.copernicus.eu/cdsapp#!/dataset/.

2.3 Global Precipitation Measurement

The Global Precipitation Measurement GPM Level 3 IMERG daily data at 10 × 10 km (GPM_3IMERGDF) derived from the half-hour GPM_3IMERGHH are analyzed. The IMERG products were downloaded from Giovanni—Time Averaged Map (nasa.gov). The level-3 GPM product uses the algorithm Day-1 U.S. multi-satellite precipitation estimation, which relies on three existing algorithms: TMPA, CMORPH, and PERSIANN (Huffman et al., 2015).

All the datasets have been used for 2 months, April and May, during the period from 2010 to 2020. The analysis is performed for two regions: North India (22–30°N and 74–81°E) and Myanmar region (12–25°N and 92–100°E).

2.4 Radiative Transfer Model

To evaluate the radiative effects of clouds over the whole atmospheric column, we computed the heating rate (HR) and the Cloud Radiative Effect both at the surface (SFC) and at the top-of-the-atmosphere (TOA) through the Fu-Liou-Gu (FLG) radiative transfer model (Fu and Liou, 1992; Fu and Liou, 1993; Gu et al., 2003; Gu et al., 2011). The FLG model is a one-dimensional plane-parallel model that needs the vertical profile of the most common meteorological variables such as temperature, pressure, and relative humidity as input, besides the vertically resolved optical properties of the clouds obtained from lidar observations. To correctly compute the radiative effect of clouds concerning a pristine atmosphere (no clouds present, **Eq. 1**), the Solar Zenith Angle (SZA), the vertical profile of ozone concentration, the surface albedo, and emissivity are needed. The FLG model computes the radiative calculations over 18 bands covering both the spectrum of the shortwave (SW) solar radiation and the outgoing longwave (LW) radiation.

$$\mathrm{CRE, HR} = \mathrm{FLG}^{\mathrm{TotalSky}} - \mathrm{FLG}^{\mathrm{Pristine}}. \quad (1)$$

The FLG radiative transfer model has been recently used to assess aerosol and cloud radiative properties over strategic regions very sensitive to climate change (Bhawar et al., 2021) or to retrieve the AOD using photovoltaic solar panels (Lolli, 2021). In those works, it is possible to find a very detailed description of the FLG model and a discussion on the choice of the above-cited variables.

3 RESULTS AND DISCUSSION

3.1 Variability in Fires and Aerosol Loading

Significant reduction in AOD over North India during the COVID-19 lockdown period is quite visible in MODIS (−0.1, ~48%) and MERRA (−0.1, ~50%) data (**Figure 1**). This decrease is associated with a reduction in anthropogenic emissions and suppressed dust transport from the western region during 2020 (Fadnavis et al., 2021). Interestingly, there is a significant reduction in AOD over the Northern Bay of Bengal region (15–22°N) as seen in the MODIS (−0.1, ~50%) and MERRA (−0.05, ~22%) data. The reduction in AOD in MERRA data is lower in magnitude than the MODIS over the Bay of Bengal region. Past studies have shown that, during the spring season, large amounts of aerosols (BC, OC sulfate, and dust) are transported from Indo-Gangetic Plain and Northeast India to the North Bay of Bengal (Hsu et al., 2012; Thomas et al., 2021). The COVID-19 lockdown restrictions have caused a reduction of aerosol amounts over the Indo Gangetic plain and Northeast India. Thus, their transport to the North Bay of Bengal region is

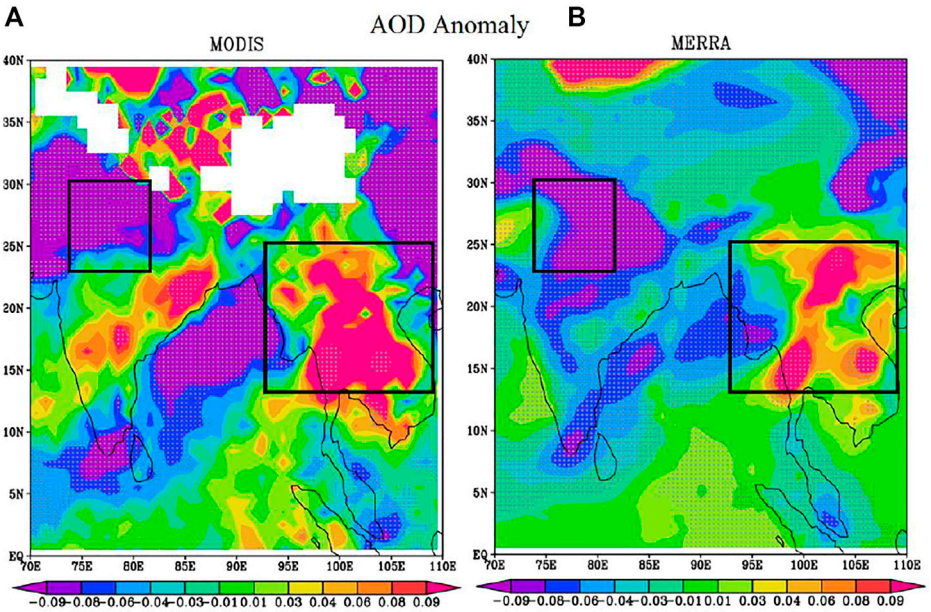

FIGURE 1 | Spatial distribution of anomaly (2020-climatology) in aerosol optical depth (AOD) averaged for the lockdown period from **(A)** MODIS and **(B)** MERRA. The white dots plotted on Figures **(A,B)** indicate a 99% significance level. Boxes in **(A)** and **(B)** indicate North India and Myanmar regions.

also reduced in 2020 compared to climatology. In agreement with our results, some past studies reported ~14%–30% decrease in aerosol amounts (including absorbing aerosols) over the northern Indian region that improved regional air quality (Muhammad et al., 2020; Yunus et al., 2020; Pathakoti et al. (2021); Sanap 2021; Mishra and Rathore, 2021). **Figure 1** also shows an increase in AOD over the eastern and central Indian regions as seen in MODIS (~10%–25%) and MERRA data. Nevertheless, the MERRA AOD increase is less predominant (~2%–5%). A similar increase in AOD over the eastern and central Indian region during the lockdown period is also reported by Bhawar et al. (2021). This AOD enhancement was due to biomass burning emissions (Bhawar et al., 2021). The AOD reduction over Northern India of ~40% and increase in AOD over the central Indian region by 0.1 (12%) seen in **Figure 1** is in agreement with Pandey and Vinoj (2021) and Bhawar et al. (2021). **Figure 1** also shows higher amounts of aerosols over the Myanmar region (positive anomalies) in both the MODIS (~30%) and MERRA (~22%) datasets. Thus, aerosol distribution in **Figure 1** shows a dipole-like structure: 1) reduction in aerosols (negative AOD anomalies) over North India (longitude: 74°E to 84°E; latitude: 22–30°N) and 2) enhancement in AOD (positive AOD anomalies) over the east India-Myanmar region (longitude: 92–110°E latitude: 12–25°N). These changes in aerosols during the lockdown period may affect local clouds, radiative forcing, and precipitation. We provide further insight on aerosols and their effects on clouds, radiative forcing, and precipitation over these two regions.

The enhanced aerosol amounts over Central India and Myanmar regions seen in **Figure 1** may be due to aerosols emitted from fires. Large numbers of fires occur every spring over the Myanmar region (Shi et al., 2014; Kaskaoutis et al., 2011). We show fire anomaly during the lockdown in **Figure 2A**. It shows positive anomalies over Myanmar and eastern and central Indian regions. The spatial distribution of elevated smoke aerosol anomaly from the CALIPSO measurements during April-May is shown in **Figure 2B**. Positive anomalies in the elevated smoke aerosol are observed over the eastern, central, and Myanmar regions, coinciding with the fire anomalies seen in **Figure 2A**. There is a large enhancement in smoke optical depth over the Myanmar region by +0.04, whereas the North Indian region shows a reduction by −0.01. This confirms that the observed increase in AOD Myanmar and central Indian regions has been caused by large amounts of fires. A past study shows that fires emit smoke/carbonaceous aerosols peak in spring over the Myanmar region (Chavan et al., 2021). It will be interesting to observe the vertical structure of fire-emitted smoke. We show the longitudinal vertical distribution of CALIPSO elevated smoke aerosols and their anomalies over North India and Myanmar regions.

3.2 Vertical Variability of Smoke Aerosols and Specific Cloud Liquid Water Content

Further, we show vertical profiles of CALIPSO observed elevated smoke aerosols over the central part of North India (22–30°N and 74–81°E) and Myanmar (12–25°N and 92–100°E) during the lockdown period in **Figure 3A**. It shows that the elevated smoke aerosols over the Myanmar region reach up to the height of 400 mb. In contrast, over the North Indian region, there is a small enhancement of 700–670 hPa. The Myanmar region shows a peak in the elevated smoke aerosol optical depth at 870 hPa, whereas North India shows negative anomalies at this altitude. The aerosol reduction over North India might have resulted in negative

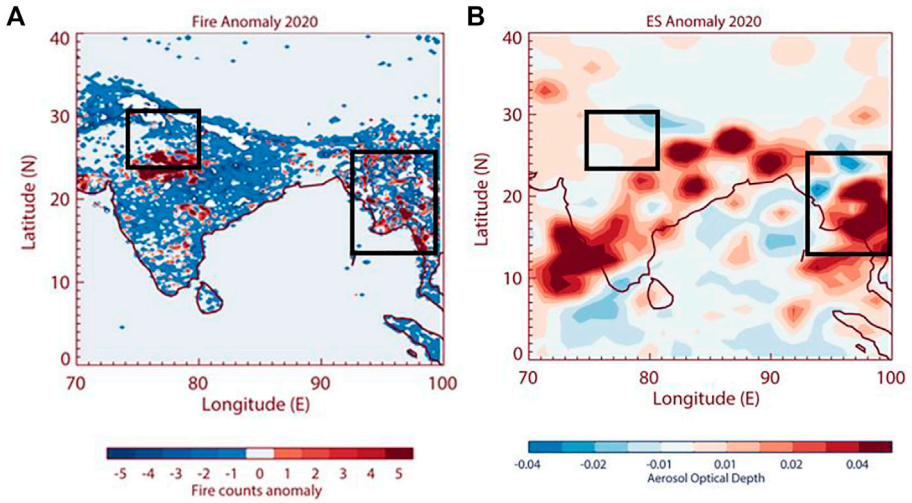

FIGURE 2 | (A) Spatial distribution of changes in fire counts during the lockdown period from **(A)** MODIS (2020-climatology). **(B)** Elevated smoke aerosol optical depth from CALIPSO at 532 nm (2020-climatology) Boxes in **(A,B)** indicate North India and Myanmar regions.

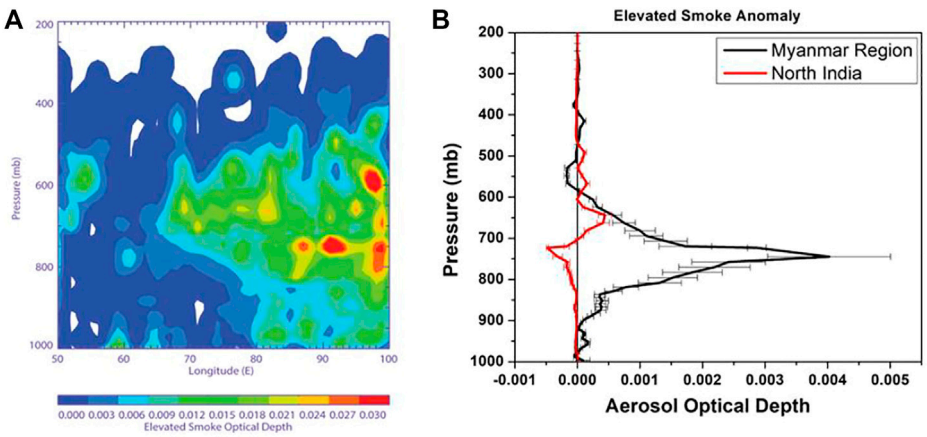

FIGURE 3 | (A) Longitudinal variation of elevated smoke aerosols from CALIPSO at 532 nm during the lockdown period. **(B)** Profile of elevated smoke aerosol anomaly (2020-climatology) averaged for the lockdown period and over for the two regions: Myanmar (12–25°N and 92–100°E) and North India (22–30°N and 74–81°E). Horizontal lines in **Figure 3B** indicate standard deviation.

anomalies near 600 hPa. The small enhancement of elevated smoke aerosols over North India is near 650 hPa. It may be due to the aerosol advection from the nearby regions. The most obvious feature is the enhanced amounts of elevated smoke optical depths by 0.03 at levels 800–500 hPa over the Myanmar region. This enhancement is 2.5 times higher than that in North India.

To understand the association of enhanced/reduced aerosols with clouds, we show the vertical distribution of specific cloud liquid water content over North India and Myanmar regions in **Figure 4**.

Figure 4 shows negative anomalies in specific cloud liquid water content over the Myanmar region. It should be noted that anomalies in elevated smoke aerosols are positive at the same region, although altitude differs (**Figure 3**). Moreover, the vertical distribution of specific cloud liquid water content and elevated smoke aerosols over North India are opposite to the Myanmar region (**Figures 3**, **4**). The minimum altitude in cloud liquid water content of 500 hPa and 900 hPa is at a higher level than the maximum altitude in elevated smoke aerosols (750 hPa) in Myanmar. It indicates that atmospheric heating by aerosol due to aerosol-radiation interaction spread above and below the layer of aerosols (Liu et al., 2020) that may be causing burning of low (900 hPa) and high clouds (500 hPa).

In general, there is a decrease in specific cloud liquid water content over the Myanmar region. It may be due to the increase in the elevated smoke aerosols (**Figure 3B**), which may be causing enhanced warming and suppression of low-level clouds through

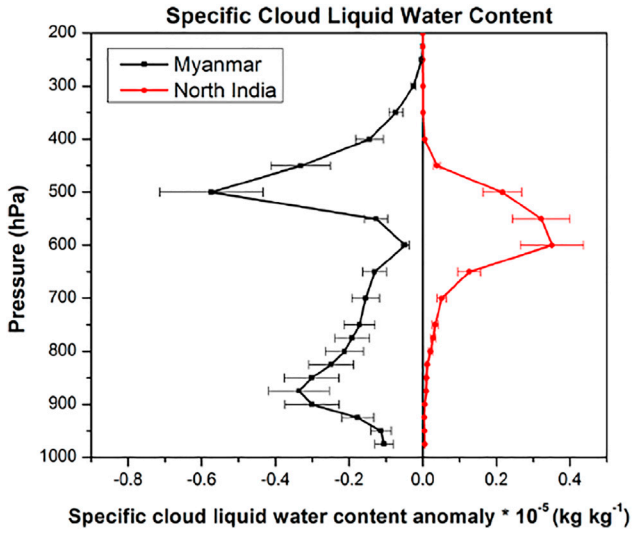

FIGURE 4 | Anomalous specific cloud liquid water content for the two regions Myanmar (12–25°N and 92–100°E) and North India (22–30°N and 74–81°E) from the ERA data for the period of April-May. Horizontal lines in the figure indicate standard deviation.

the radiative impacts (discussed in **Section 3.4**). It indicates the role of aerosols in the cloud formation process. We investigate the role of the Twomey effect; that is, aerosols act as cloud condensation nuclei and lead to a greater number of smaller cloud droplets in the presence of a constant amount of cloud liquid water content (Twomey, 1977.) **Figures 2–4** show that the Myanmar region is associated with a high amount of biomass burning activity paired with high elevated smoke optical depths and negative cloud liquid water content, indicating that aerosols contributed to smaller cloud droplet formation. In contrast, the North Indian region is associated with lower elevated smoke aerosols accompanied with enhancement in specific cloud liquid water content, indicating larger cloud droplets and anti-Twomey effect. The aerosol impact on cloud formation and consequently on precipitation is still a challenge due to the complexity of aerosols (Flossmann and Wobrock, 2019; Morrison et al., 2020). Zhang et al. (2008) and Feingold et al. (2005) also showed that the increase in biomass burning aerosols leads to reduced cloudiness, which further stabilizes the boundary layer *via* surface cooling and elevated heating. Thus, enhanced absorbing aerosols over the Myanmar region have eventually dissipated the clouds (discussed in **Section 3.3**).

3.3 Impact on Cloud Fraction

Figure 5A,B shows the total cloud fraction anomaly from MODIS and MERRA during the lockdown period. It shows a reduction in cloud fraction over Myanmar −10% (−0.1) and enhancement over North India +10% (+0.1) in MODIS and MERRA. The high aerosol loading region over Myanmar is collocated with a negative cloud fraction anomaly. Huang et al., 2019 showed that biomass burning aerosols reaching ~ 2 km altitudes absorb solar radiation and evaporate cloud droplets, reducing LWC, IWC, and cloud cover (decrease by 7%). In contrast, over the North Indian region, positive anomalies of cloud fraction are collocated with negative AOD anomalies.

Figures 1–5 indicate that the carbonaceous aerosols, emitted from biomass burning, might have suppressed local cloud fraction. Changes in aerosols affect the radiative forcing and therefore the atmosphere dynamics that, in turn, cause aerosol redistribution. Thus, aerosols produce feedback on dynamics and

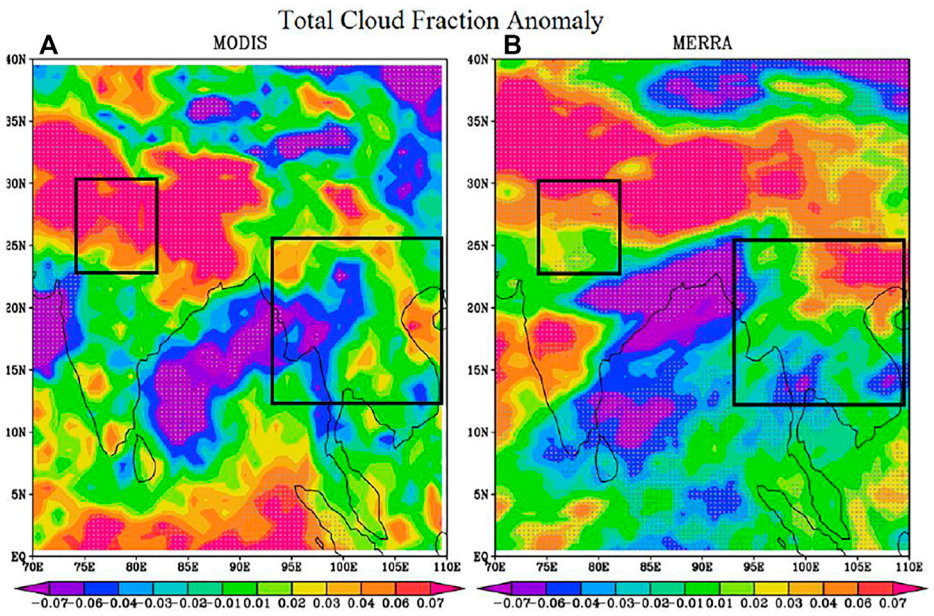

FIGURE 5 | Total cloud fraction anomaly (2020-climatology) from MODIS and MERRA for the lockdown period of April-May. White dots in **(A,B)** indicate a 99% significance level. Boxes in **(A,B)** indicate North India and Myanmar regions.

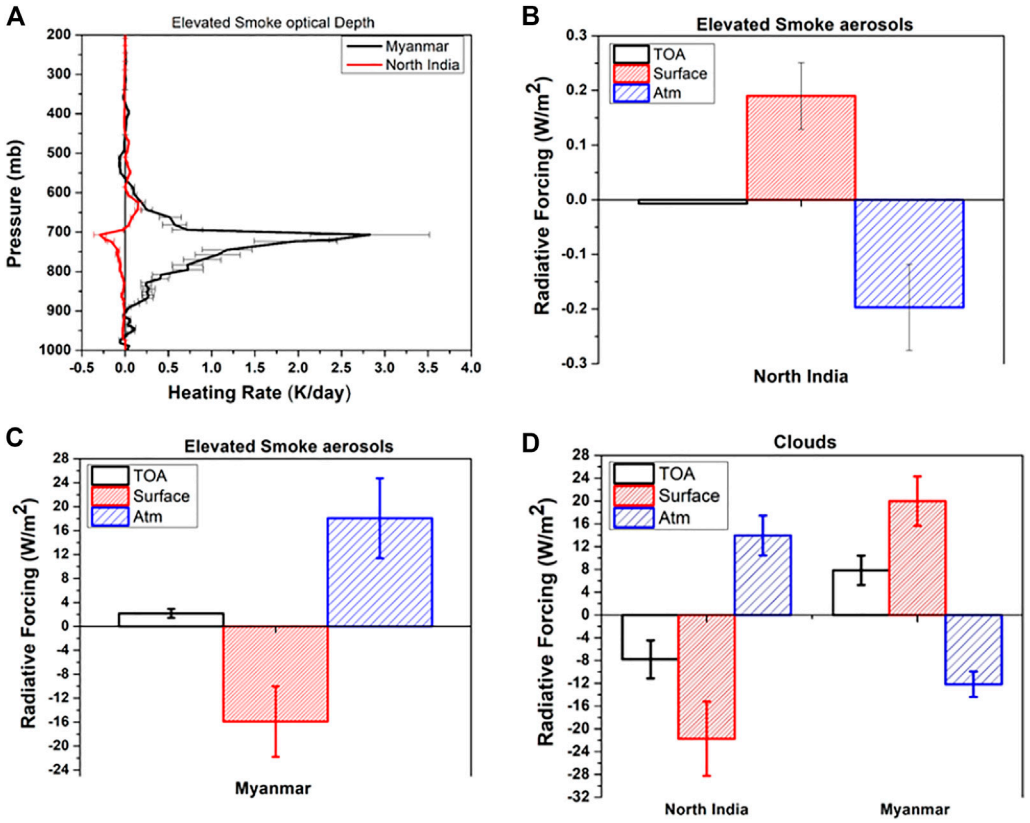

FIGURE 6 | (A) Anomaly of heating rate profile for elevated smoke optical depth-averaged for the period of April-May for the two regions. **(B)** Radiative forcing due to the elevated smoke aerosols at the top of atmosphere (TOA), atmosphere (ATM), and surface for North Indian region. **(C)** Radiative forcing due to the elevated smoke aerosols at the top of atmosphere (TOA), atmosphere (ATM), and surface for Myanmar region **(D)** Radiative forcing due to the clouds at the TOA, ATM, and surface for the two regions North India and Myanmar.

vice versa. Therefore, observed changes in cloud fraction may be the combined impact of carbonaceous aerosols and changes in dynamics. The high amount of biomass burning aerosols results in an increased amount of INP (Levin et al., 2016; Jahn et al., 2020). However, such analysis is out of the scope of this study. The impact of the suppressed/enhanced cloud fraction may affect the regional rainfall.

3.4 Heating Rate, Radiative Forcing, and Precipitation

Biomass burning aerosols are an important part of the Earth-atmosphere radiative budget. Absorbing the incoming solar radiation with consequent warming of the atmospheric layer, they cool the surface (Li et al., 2017; Zhang et al., 2020; Fadnavis et al., 2019). The lockdown of April–May 2020 was characterized by a higher number of fires over the Myanmar region and a lower number of fires over the North Indian region. It led to a differential biomass burning aerosol loading over these regions that might have affected heating and radiations. **Figure 6A** shows the anomaly of the heating rate profile for the elevated smoke aerosols observed by CALIPSO. The heating rate profiles over the Myanmar region show a significantly high amount of heating ~0.05–2.8 K/day in the levels from 900 to 600 hPa, whereas the North Indian region shows a small amount of heating ~0.05–0.2 K/day in the levels from 700 to 650 hPa. The strong heating in the Myanmar region coincides with the presence of elevated smoke aerosols. The North Indian region shows negative or no heating below 700 hPa during the lockdown period because of the absence of fires and anthropogenic aerosols, which used to otherwise contribute to heating. This high amount of heating may be responsible for cloud dissipation, affecting the precipitation over the Myanmar region. **Figures 6B,C** show the radiative forcing anomaly due to elevated smoke aerosols averaged for the lockdown period over the North Indian and Myanmar regions. It shows warming of ~2.17 W/m^2 the TOA over the Myanmar region and a slight cooling of ~0.01 W/m^2 over the North Indian region. The surface radiative forcing also shows slight warming of +0.19 W/m^2 over the North Indian region, which may be due to improved air quality and more solar radiation reaching the surface during the lockdown period. The surface radiative forcing over the Myanmar region showed a cooling of ~15.89 W/m^2 due to the presence of an elevated smoke layer over the region. This accounts for the atmospheric warming of ~18.06 W/m^2 over the Myanmar region but an atmospheric cooling of ~0.2 W/m^2 over the

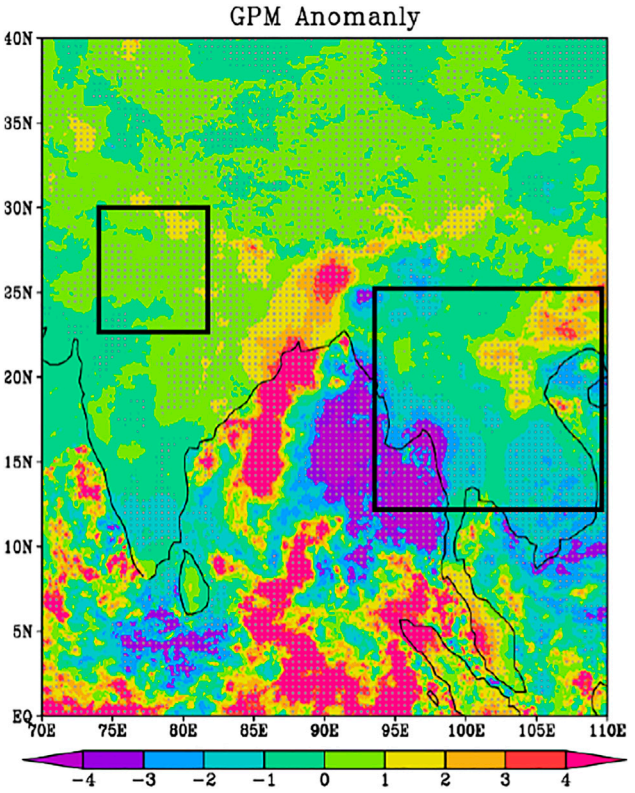

FIGURE 7 | GPM rainfall anomaly (2020-climatology) for the lockdown period of April-May. White dots indicate a 99% significance level. Boxes indicate North India and Myanmar regions.

North India region. This high atmospheric heating affects the cloud formation process and the stability of the atmosphere. Previous studies also showed warming in the TOA and cooling at the surface due to black carbon aerosols (Babu et al., 2002; Nair et al., 2017). The high surface cooling and atmospheric warming due to elevated smoke aerosols caused the burning of clouds and suppression of the precipitation. However, small surface warming due to less elevated smoke aerosols over the North Indian region might have caused an increase in liquid water content (as seen in **Figure 4**) to form clouds, giving rise to the enhanced precipitation over the North Indian region (see **Figure 7**).

Figure 6C indicates cloud radiative forcing anomaly averaged for the lockdown period over the two regions. The North Indian region shows negative radiative forcing of ~7.78 W/m^2 at the TOA and ~21.72 W/m^2 at the surface, −13.98 W/m^2 in atmosphere (TOA—surface) due to clouds. Myanmar regions show positive radiative forcing of ~7.84 W/m^2 at TOA and ~19.99 W/m^2 at the surface, and negative ~ −12.51 W/m^2 in atmosphere due to clouds. Thus, high atmospheric cloud warming (~+14 W/m^2) over the North Indian region may be conducive for rain formation processes in contrast to cloud atmospheric cooling (~−13 W/m^2) over the Myanmar region.

Figure 7 indicates the GPM rainfall anomaly for the lockdown period. An increase in the elevated smoke aerosols over the Myanmar region inhibited the cloud formation process leading to a high number of smaller cloud droplets, thereby suppressing rainfall over the Myanmar region. The North Indian region shows a reduction in elevated smoke during the lockdown period. The aerosol reduction has enhanced the cloud formation process resulting in enhanced rainfall over the North Indian region. In agreement with our results, Bhawar and Rahul 2013 showed that the absorbing aerosols had enhanced the microphysical and radiative effect, which reduced the cloud fraction by almost 30% and might have contributed to the drought-like conditions in the year 2009. It should be noted that the anomalies of cloud and rainfall might have been influenced by other drivers, such as convection and dynamics. As aerosols and these atmospheric drivers provide feedback on each other, the anomalies of cloud cover, atmospheric heating, and radiative forcing at the surface, rainfall, and so on agree with previous studies (**Table 1**).

4 CONCLUSION

This study explores variability in aerosols and clouds over South Asia using multiple datasets (MODIS, MERRA, CALIPSO, and ERA-5) during the COVID lockdown period (April-May 2020). Our analysis shows that the distribution of AOD with South Asia shows a dipole pattern, that is, an enhancement over Myanmar and reduction over North India, although there was a reduction in anthropogenic aerosols due to lockdown restriction. MODIS fire count, along with CALIPSO elevated smoke data, shows that aerosol enhancement (reduction) over the Myanmar region (North India) is due to enhancement (reduction) in fires during the lockdown period compared to climatology (10 years). The smoke aerosol formed a layer over the Myanmar region (900–600 hPa with a peak at 750 hPa). They

TABLE 1 | A comparison of cloud cover, atmospheric heating, radiative forcing at the surface and rainfall with previous studies.

Sr. No.	Result	Reference	Our finding
1	Cloud cover decreased by 7%	Huang et al. (2019)	Cloud fraction decreased by 10%
2	Atmospheric heating rate 4 K/day	Ningombam et al. (2020)	Atmospheric heating of ~2.8 K/day
3	Radiative forcing at the surface −42.76 W/m^2 over Myanmar region Surface radiative forcing of −30 to −40 W/m^2	Singh et al. (2020) Mallet et al. (2020)	Surface radiative forcing −15.89 W/m^2 over Myanmar region
4	Decrease in domain average rainfall by 25% Reduction in precipitation by 23% Precipitation reduces by 1.09 mm/day	Hodzic and Duvel (2018) Liu et al. (2020) Huang et al. (2019)	Precipitation reduces by 29% Precipitation reduces by 1–4 mm

produced atmospheric heating of 0–2.8 K/day leading to in-atmospheric warming of (radiative forcing ~18.06 W/m^2 and cooling of the surface (~15.89 W/m^2). This region is associated with a reduction in cloud cover and precipitation (−1 to −4 mm), indicating cloud dissipation/burning by the heating due to the smoke aerosols. The North Indian region is associated with an increase in cloud cover, a decrease in cloud liquid water content, and an enhancement in precipitation. Thus, reduction in aerosol over North India might have enhanced precipitation *via* the anti-Twomey effect. The clouds over North India have produced radiative forcing ~−21.72 W/m^2 at the surface and ~−7.78 W/m^2 at the TOA and ~ +14 W/m^2 in the atmosphere. Although other factors contribute to precipitation processes, for example, moisture convergence, temperature gradient, low-pressure zone, and convective process (Levy et al., 2013; Gryspeerdt et al., 2020; Guo et al., 2020; Liu et al., 2020; Lolli and Vivone, 2020), this study provides a clear signature of cloud dissipation/burning by the smoke aerosol over the Myanmar region leading to precipitation reduction. Also, the anti-Twomey effect due to aerosol reduction over North India led to precipitation enhancement during the lockdown period. It should be noted that the anomalies of cloud and rainfall might have been influenced by other drivers such as convection and dynamics.

DATA AVAILABILITY STATEMENT

The original contributions presented in the study are included in the article/Supplementary Material, further inquiries can be directed to the corresponding author.

AUTHOR CONTRIBUTIONS

This article is the combined efforts of all the authors. RB and SF formulated and wrote the article, with contributions from all co-authors. DL, SB, PR, PP, and SL contributed to the analysis. SL computed heating rates and radiative forcing using a radiative transfer model.

ACKNOWLEDGMENTS

RB and DL acknowledge with gratitude the Department of Science and Technology (DST), SERB, through which the work was initiated. RB also acknowledges UGC-FRP, CALIPSO, MODIS, MERRA, and ERA database teams and NASA websites from where data were downloaded.

REFERENCES

Ackerman, A. S., Toon, O. B., Stevens, D. E., Heymsfield, A. J., Ramanathan, V., and Welton, E. J. (2000). Reduction of Tropical Cloudiness by Soot. *Science* 288 (5468), 1042–1047. doi:10.1126/science.288.5468.1042

Albrecht, B. A. (1989). Aerosols, Cloud Microphysics, and Fractional Cloudiness. *Science* 245 (4923), 1227–1230. doi:10.1126/science.245.4923.1227

Andreae, M. O., and Rosenfeld, D. (2008). Aerosol-cloud-precipitation Interactions. Part 1. The Nature and Sources of Cloud-Active Aerosols. *Earth-Science Rev.* 89 (1-2), 13–41. doi:10.1016/j.earscirev.2008.03.001

Babu, S. S., Satheesh, S. K., and Moorthy, K. K. (2002). Aerosol Radiative Forcing due to Enhanced Black Carbon at an Urban Site in India. *Geophys. Res. Lett.* 29 (18), 1880. doi:10.1029/2002gl015826

Bhawar, R. L., Fadnavis, S., Kumar, V., Rahul, P. R. C., Sinha, T., and Lolli, S. (2021). Radiative Impacts of Aerosols during COVID-19 Lockdown Period over the Indian Region. *Front. Environ. Sci.* 9, 746090. doi:10.3389/fenvs.2021.746090

Bhawar, R. L., and Rahul, P. R. C. (2013). Aerosol-Cloud-Interaction Variability Induced by Atmospheric Brown Clouds during the 2009 Indian Summer Monsoon Drought. *Aerosol Air Qual. Res.* 13 (4), 1384–1391. doi:10.4209/aaqr.2012.11.0329

Biswas, S., Vadrevu, K. P., Lwin, Z. M., Lasko, K., and Justice, C. O. (2015). Factors Controlling Vegetation Fires in Protected and Non-protected Areas of Myanmar. *PLoS one* 10 (4), e0124346. doi:10.1371/journal.pone.0124346

Bréon, F.-M., Vermeulen, A., and Descloitres, J. (2011). An Evaluation of Satellite Aerosol Products against Sunphotometer Measurements. *Remote sensing Environ.* 115 (12), 3102–3111. doi:10.1016/j.rse.2011.06.017

Chavan, P., Fadnavis, S., Chakroborty, T., Sioris, C. E., Griessbach, S., and Müller, R. (2021). The Outflow of Asian Biomass Burning Carbonaceous Aerosol into the Upper Troposphere and Lower Stratosphere in spring: Radiative Effects Seen in a Global Model. *Atmos. Chem. Phys.* 21 (18), 14371–14384. doi:10.5194/acp-21-14371-2021

Derber, J. C., Purser, R. J., Wu, W. S., Treadon, R., Pondeca, M., Parrish, D., et al. (2003). "Flow-dependent Jb in a Global Grid-point 3D-Var," in Proceeding of the ECMWF annual seminar on recent developments in data assimilation for atmosphere and ocean, U.K., 2003 September, 125–134.

Fadnavis, S., Sabin, T. P., Roy, C., Rowlinson, M., Rap, A., Vernier, J.-P., et al. (2019). Elevated Aerosol Layer over South Asia Worsens the Indian Droughts. *Sci. Rep.* 9 (1), 1–11. doi:10.1038/s41598-019-46704-9

Fadnavis, S., Sabin, T. P., Rap, A., Müller, R., Kubin, A., and Heinold, B. (2021). The Impact of COVID-19 Lockdown Measures on the Indian Summer Monsoon. *Environ. Res. Lett.* 16 (7), 074054. doi:10.1088/1748-9326/ac109c

Feingold, G., Jiang, H., and Harrington, J. Y. (2005). On Smoke Suppression of Clouds in Amazonia. *Geophys. Res. Lett.* 32, L02804. doi:10.1029/2004GL021369

Flossmann, A. I., and Wobrock, W. (2019). Cloud Processing of Aerosol Particles in marine Stratocumulus Clouds. *Atmosphere* 10 (9), 520. doi:10.3390/atmos10090520

Fu, Q., and Liou, K. N. (1992). On the Correlatedk-Distribution Method for Radiative Transfer in Nonhomogeneous Atmospheres. *J. Atmos. Sci.* 49, 2139–2156. doi:10.1175/1520-0469(1992)049<2139:otcdmf>2.0.co;2

Fu, Q., and Liou, K. N. (1993). Parameterization of the Radiative Properties of Cirrus Clouds. *J. Atmos. Sci.* 50, 2008–2025. doi:10.1175/1520-0469(1993)050<2008:potrpo>2.0.co;2

Geng, G., Zhang, Q., Martin, R. V., van Donkelaar, A., Huo, H., Che, H., et al. (2015). Estimating Long-Term PM2.5 Concentrations in China Using Satellite-Based Aerosol Optical Depth and a Chemical Transport Model. *Remote sensing Environ.* 166, 262–270. doi:10.1016/j.rse.2015.05.016

Gryspeerdt, E., Mülmenstädt, J., Gettelman, A., Malavelle, F. F., Morrison, H., Neubauer, D., et al. (2020). Surprising Similarities in Model and Observational Aerosol Radiative Forcing Estimates. *Atmos. Chem. Phys.* 20 (1), 613–623. doi:10.5194/acp-20-613-2020

Gu, Y., Farrara, J., Liou, K. N., and Mechoso, C. R. (2003). Parameterization of Cloud-Radiation Processes in the UCLA General Circulation Model. *J. Clim.* 16, 3357–3370. doi:10.1175/1520-0442(2003)016<3357:pocpit>2.0.co;2

Gu, Y., Liou, K. N., Ou, S. C., and Fovell, R. (2011). Cirrus Cloud Simulations Using WRF with Improved Radiation Parameterization and Increased Vertical Resolution. *J. Geophys. Res.* 116, D06119. doi:10.1029/2010JD014574

Guo, Z. D., Wang, Z. Y., Zhang, S. F., Li, X., Li, L., Li, C., et al. (2020). Aerosol and Surface Distribution of Severe Acute Respiratory Syndrome Coronavirus 2 in Hospital Wards, Wuhan, China, 2020. *Emerg. Infect. Dis.* 26 (7), 1583–1591. doi:10.3201/eid2607.200885

Hodzic, A., and Duvel, J. P. (2018). Impact of Biomass Burning Aerosols on the Diurnal Cycle of Convective Clouds and Precipitation over a Tropical Island. *J. Geophys. Res. Atmos.* 123, 1017–1036. doi:10.1002/2017jd027521

Hsu, N. C., Gautam, R., Sayer, A. M., Bettenhausen, C., Li, C., Jeong, M. J., et al. (2012). Global and Regional Trends of Aerosol Optical Depth over Land and Ocean Using SeaWiFS Measurements from 1997 to 2010. *Atmos. Chem. Phys.* 12 (17), 8037–8053. doi:10.5194/acp-12-8037-2012

Huang, L., Lin, W., Li, F., Wang, Y., and Jiang, B. (2019). Climate Impacts of the Biomass Burning in Indochina on Atmospheric Conditions over Southern China. *Aerosol Air Qual. Res.* 9, 2707–2720. doi:10.4209/aaqr.2019.01.0028

Huffman, G. J., Bolvin, D. T., Nelkin, E. J., and Tan, J. (2015). Integrated Multi-satellitE Retrievals for GPM (IMERG) Technical Documentation. *NASA/GSFC Code* 612 (47), 2019.

Hunt, W. H., Winker, D. M., Vaughan, M. A., Powell, K. A., Lucker, P. L., and Weimer, C. (2009). CALIPSO Lidar Description and Performance Assessment. *J. Atmos. Oceanic Tech.* 26 (7), 1214–1228. doi:10.1175/2009jtecha1223.1

Ippc (2013). in *Climate Change 2013: The Physical Science Basis. Contribution of Working Group I to the Fifth Assessment Report of the Intergovernmental Panel on Climate Change*. Editors T. F. Stocker, D. Qin, G.-K. Plattner, M. Tignor, S. K. Allen, J. Boschung, et al. (Cambridge, United Kingdom and New York, NY, USA: Cambridge University Press), 1535.

Jahn, L. G., Polen, M. J., Jahl, L. G., Brubaker, T. A., Somers, J., and Sullivan, R. C. (2020). Biomass Combustion Produces Ice-Active Minerals in Biomass-Burning Aerosol and Bottom Ash. *Proc. Natl. Acad. Sci. USA* 117 (36), 21928–21937. doi:10.1073/pnas.1922128117

Jain, S., and Sharma, T. (2020). Social and Travel Lockdown Impact Considering Coronavirus Disease (COVID-19) on Air Quality in Megacities of India: Present Benefits, Future Challenges and Way Forward. *Aerosol Air Qual. Res.* 20 (6), 1222–1236. doi:10.4209/aaqr.2020.04.0171

Johnson, R. B., and Onwuegbuzie, A. J. (2004). Mixed Methods Research: A Research Paradigm Whose Time Has Come. *Educ. Res.* 33 (7), 14–26. doi:10.3102/0013189x033007014

Jones, A., Haywood, J. M., and Boucher, O. (2007). Aerosol Forcing, Climate Response and Climate Sensitivity in the Hadley Centre Climate Model. *J. Geophys. Res. Atmospheres* 112, D20211. doi:10.1029/2007jd008688

Kaskaoutis, D. G., Kumar Kharol, S., Sinha, P. R., Singh, R. P., Kambezidis, H. D., Rani Sharma, A., et al. (2011). Extremely Large Anthropogenic-Aerosol Contribution to Total Aerosol Load over the Bay of Bengal during winter Season. *Atmos. Chem. Phys.* 11 (14), 7097–7117. doi:10.5194/acp-11-7097-2011

Kaufman, Y. J., Koren, I., Remer, L. A., Rosenfeld, D., and Rudich, Y. (2005). The Effect of Smoke, Dust, and Pollution Aerosol on Shallow Cloud Development over the Atlantic Ocean. *Proc. Natl. Acad. Sci.* 102 (32), 11207–11212. doi:10.1073/pnas.0505191102

Kim, M.-H., Omar, A. H., Tackett, J. L., Vaughan, M. A., Winker, D. M., Trepte, C. R., et al. (2018). The CALIPSO Version 4 Automated Aerosol Classification and Lidar Ratio Selection Algorithm. *Atmos. Meas. Tech.* 11 (11), 6107–6135. doi:10.5194/amt-11-6107-2018

Koren, I., Martins, J. V., Remer, L. A., and Afargan, H. (2008). Smoke Invigoration versus Inhibition of Clouds over the Amazon. *science* 321 (5891), 946–949. doi:10.1126/science.1159185

Levin, E. J. T., McMeeking, G. R., DeMott, P. J., McCluskey, C. S., Carrico, C. M., Nakao, S., et al. (2016). Ice-nucleating Particle Emissions from Biomass Combustion and the Potential Importance of Soot Aerosol. *J. Geophys. Res. Atmos.* 121, 5888–5903. doi:10.1002/2016JD024879

Levy, R. C., Remer, L. A., Kleidman, R. G., Mattoo, S., Ichoku, C., Kahn, R., et al. (2010). Global Evaluation of the Collection 5 MODIS Dark-Target Aerosol Products over Land. *Atmos. Chem. Phys.* 10 (21), 10399–10420. doi:10.5194/acp-10-10399-2010

Levy, H., Horowitz, L. W., Schwarzkopf, M. D., Ming, Y., Golaz, J.-C., Naik, V., et al. (2013). The Roles of Aerosol Direct and Indirect Effects in Past and Future Climate Change. *J. Geophys. Res. Atmos.* 118 (10), 4521–4532. doi:10.1002/jgrd.50192

Li, Z., Guo, J., Ding, A., Liao, H., Liu, J., Sun, Y., et al. (2017). Aerosol and Boundary-Layer Interactions and Impact on Air Quality. *Natl. Sci. Rev.* 4 (6), 810–833. doi:10.1093/nsr/nwx117

Li, J., Jiang, Y., Xia, X., and Hu, Y. (2018). Increase of Surface Solar Irradiance across East China Related to Changes in Aerosol Properties during the Past Decade. *Environ. Res. Lett.* 13 (3), 034006. doi:10.1088/1748-9326/aaa35a

Lin, C.-Y., Hsu, H.-m., Lee, Y. H., Kuo, C. H., Sheng, Y.-F., and Chu, D. A. (2009). A New Transport Mechanism of Biomass Burning from Indochina as Identified by Modeling Studies. *Atmos. Chem. Phys.* 9 (20), 7901–7911. doi:10.5194/acp-9-7901-2009

Liu, S., Aiken, A. C., Arata, C., Dubey, M. K., Stockwell, C. E., Yokelson, R. J., et al. (2014). Aerosol Single Scattering Albedo Dependence on Biomass Combustion Efficiency: Laboratory and Field Studies. *Geophys. Res. Lett.* 41 (2), 742–748. doi:10.1002/2013gl058392

Liu, L., Cheng, Y., Wang, S., Wei, C., Pöhlker, M. L., Pöhlker, C., et al. (2020). Impact of Biomass Burning Aerosols on Radiation, Clouds, and Precipitation over the Amazon: Relative Importance of Aerosol-Cloud and Aerosol-Radiation Interactions. *Atmos. Chem. Phys.* 20, 13283–13301. doi:10.5194/acp-20-13283-2020

Lolli, S. (2021). Is the Air Too Polluted for Outdoor Activities? Check by Using Your Photovoltaic System as an Air-Quality Monitoring Device. *Sensors* 21 (19), 6342. doi:10.3390/s21196342

Lolli, S., Khor, W. Y., Matjafri, M. Z., and Lim, H. S. (2019). Monsoon Season Quantitative Assessment of Biomass Burning clear-sky Aerosol Radiative Effect at Surface by Ground-Based Lidar Observations in Pulau Pinang, Malaysia in 2014. *Remote Sensing* 11 (22), 2660. doi:10.3390/rs11222660

Lolli, S., Chen, Y. C., Wang, S. H., and Vivone, G. (2020). Impact of Meteorological Conditions and Air Pollution on COVID-19 Pandemic Transmission in Italy. *Sci. Rep.* 10 (1), 16213–16215. doi:10.1038/s41598-020-73197-8

Lolli, S., and Vivone, G. (2020). The Role of Tropospheric Ozone in Flagging COVID-19 Pandemic Transmission. *Bull. Atmos. Sci. Technol.* 1 (3), 551–555. doi:10.1007/s42865-020-00026-1

Ma, X., Yu, F., and Luo, G. (2012). Aerosol Direct Radiative Forcing Based on GEOS-Chem-APM and Uncertainties. *Atmos. Chem. Phys.* 12 (12), 5563–5581. doi:10.5194/acp-12-5563-2012

Mallet, M., Solmon, F., Nabat, P., Elguindi, N., Waquet, F., Bouniol, D., et al. (2020). Direct and Semi-direct Radiative Forcing of Biomass-Burning Aerosols over the Southeast Atlantic (SEA) and its Sensitivity to Absorbing Properties: a Regional Climate Modeling Study. *Atmos. Chem. Phys.* 20, 13191–13216. doi:10.5194/acp-20-13191-2020

McGrath-Spangler, E. L., and Denning, A. S. (2013). Global Seasonal Variations of Midday Planetary Boundary Layer Depth from CALIPSO Space-Borne LIDAR. *J. Geophys. Res. Atmos.* 118 (3), 1226–1233. doi:10.1002/jgrd.50198

Mishra, M. K., and Rathore, P. S. (2021). Impact of Nationwide COVID-19 Lockdown on Indian Air Quality in Terms of Aerosols as Observed from the Space. *Aerosol Air Qual. Res.* 21, 200461. doi:10.4209/aaqr.2020.07.0461

Morrison, H., van Lier-Walqui, M., Fridlind, A. M., Grabowski, W. W., Harrington, J. Y., Hoose, C., et al. (2020). Confronting the Challenge of Modeling Cloud and Precipitation Microphysics. *J. adv. model. earth syst.* 12. doi:10.1029/2019MS001689

Muhammad, S., Long, X., and Salman, M. (2020). COVID-19 Pandemic and Environmental Pollution: A Blessing in Disguise? *Sci. total Environ.* 728, 138820. doi:10.1016/j.scitotenv.2020.138820

Nair, V. S., Babu, S. S., Manoj, M. R., Moorthy, K. K., and Chin, M. (2017). Direct Radiative Effects of Aerosols over South Asia from Observations and Modeling. *Clim. Dyn.* 49 (4), 1411–1428. doi:10.1007/s00382-016-3384-0

Ningombam, S. S., Chandra Dumka, U., Srivastava, A. K., and Song, H.-J. (2020). Optical and Physical Properties of Aerosols during Active Fire Events Occurring in the Indo-Gangetic Plains: Implications for Aerosol Radiative Forcing. *Atmos. Environ.* 223, 17225. doi:10.1016/j.atmosenv.2019.117225

Paital, B. (2020). Nurture to Nature via COVID-19, a Self-Regenerating Environmental Strategy of Environment in Global Context. *Sci. Total Environ.* 729, 139088. doi:10.1016/j.scitotenv.2020.139088

Pandey, S. K., and Vinoj, V. (2021). Surprising Changes in Aerosol Loading over India amid COVID-19 Lockdown. *Aerosol Air Qual. Res.* 21, 200466. doi:10.4209/aaqr.2020.07.0466

Pathakoti, M., Muppalla, A., Hazra, S., D. Venkata, M., A. Lakshmi, K., K. Sagar, V., et al. (2021). Measurement Report: An Assessment of the Impact of a Nationwide Lockdown on Air Pollution - a Remote Sensing Perspective over India. *Atmos. Chem. Phys.* 21 (11), 9047–9064. doi:10.5194/acp-21-9047-2021

Pincus, R., and Baker, M. B. (1994). Effect of Precipitation on the Albedo Susceptibility of Clouds in the marine Boundary Layer. *Nature* 372 (6503), 250–252. doi:10.1038/372250a0

Poli, P., Hersbach, H., Dee, D. P., Berrisford, P., Simmons, A. J., Vitart, F., et al. (2016). ERA-20C: An Atmospheric Reanalysis of the Twentieth century. *J. Clim.* 29 (11), 4083–4097. doi:10.1175/jcli-d-15-0556.1

Posselt, R., and Lohmann, U. (2008). Influence of Giant CCN on Warm Rain Processes in the ECHAM5 GCM. *Atmos. Chem. Phys.* 8 (14), 3769–3788. doi:10.5194/acp-8-3769-2008

Reddy, B. S. K., Kumar, K. R., Balakrishnaiah, G., Gopal, K. R., Reddy, R. R., Reddy, L. S. S., et al. (2012). Potential Source Regions Contributing to Seasonal Variations of Black Carbon Aerosols over Anantapur in Southeast India. *Aerosol Air Qual. Res.*, 12(3), 344–358. doi:10.4209/aaqr.2011.10.0159

Remer, L. A., Kaufman, Y. J., Tanré, D., Mattoo, S., Chu, D. A., Martins, J. V., et al. (2005). The MODIS Aerosol Algorithm, Products, and Validation. *J. Atmos. Sci.* 62 (4), 947–973. doi:10.1175/jas3385.1

Remer, L. A., Kleidman, R. G., Levy, R. C., Kaufman, Y. J., Tanré, D., Mattoo, S., et al. (2008). Global Aerosol Climatology from the MODIS Satellite Sensors. *J. Geophys. Res. Atmospheres* 113, D14S07. doi:10.1029/2007jd009661

Rienecker, M. M., Suarez, M. J., Gelaro, R., Todling, R., Bacmeister, J., Liu, E., et al. (2011). MERRA: NASA's Modern-Era Retrospective Analysis for Research and Applications. *J. Clim.* 24 (14), 3624–3648. doi:10.1175/jcli-d-11-00015.1

Sanap, S. D. (2021). Global and Regional Variations in Aerosol Loading during COVID-19 Imposed Lockdown. *Atmos. Environ.* 246, 118132. doi:10.1016/j.atmosenv.2020.118132

Seinfeld, J. H., Bretherton, C., Carslaw, K. S., Coe, H., DeMott, P. J., Dunlea, E. J., et al. (2016). Improving Our Fundamental Understanding of the Role of Aerosol–cloud Interactions in the Climate System. *Proc. Natl. Acad. Sci. USA* 113 (21), 5781–5790. doi:10.1073/pnas.1514043113

Shepherd, R. H., King, M. D., Marks, A. A., Brough, N., and Ward, A. D. (2018). Determination of the Refractive index of Insoluble Organic Extracts from Atmospheric Aerosol over the Visible Wavelength Range Using Optical Tweezers. *Atmos. Chem. Phys.* 18 (8), 5235–5252. doi:10.5194/acp-18-5235-2018

Shi, Y., Zhang, J., Reid, J. S., Liu, B., and Hyer, E. J. (2014). Critical Evaluation of Cloud Contamination in the MISR Aerosol Products Using MODIS Cloud Mask Products. *Atmos. Meas. Tech.* 7 (6), 1791–1801. doi:10.5194/amt-7-1791-2014

Singh, P., Sarawade, P., and Adhikary, B. (2020). Carbonaceous Aerosol from Open Burning and its Impact on Regional Weather in South Asia. *Aerosol Air Qual. Res.* 20, 419–431. doi:10.4209/aaqr.2019.03.0146

Singh, R. P., and Chauhan, A. (2020). Impact of Lockdown on Air Quality in India during COVID-19 Pandemic. *Air Qual. Atmos. Health* 13 (8), 921–928. doi:10.1007/s11869-020-00863-1

Song, M., Marcolli, C., Krieger, U. K., Zuend, A., and Peter, T. (2012). Liquid-liquid Phase Separation in Aerosol Particles: Dependence on O: C, Organic Functionalities, and Compositional Complexity. *Geophys. Res. Lett.* 39, L19801. doi:10.1029/2012gl052807

Thomas, A., Kanawade, V. P., Sarangi, C., and Srivastava, A. K. (2021). Effect of COVID-19 Shutdown on Aerosol Direct Radiative Forcing over the Indo-Gangetic Plain Outflow Region of the Bay of Bengal. *Sci. Total Environ.* 782, 146918. doi:10.1016/j.scitotenv.2021.146918

Tosca, M. G., Randerson, J. T., and Zender, C. S. (2013). Global Impact of Smoke Aerosols from Landscape Fires on Climate and the Hadley Circulation. *Atmos. Chem. Phys.* 13 (10), 5227–5241. doi:10.5194/acp-13-5227-2013

Twomey, S. (1977). The Influence of Pollution on the Shortwave Albedo of Clouds. *J. Atmos. Sci.* 34 (7), 1149–1152. doi:10.1175/1520-0469(1977)034<1149:tiopot>2.0.co;2

Vadrevu, K. P., Lasko, K., Giglio, L., and Justice, C. (2015). Vegetation Fires, Absorbing Aerosols and Smoke Plume Characteristics in Diverse Biomass Burning Regions of Asia. *Environ. Res. Lett.* 10 (10), 105003. doi:10.1088/1748-9326/10/10/105003

Wagh, S., Singh, P., Ghude, S. D., Safai, P., Prabhakaran, T., and Kumar, P. P. (2021). Study of Ice Nucleating Particles in Fog-Haze Weather at New Delhi, India: A Case of Polluted Environment. *Atmos. Res.* 259 (2021), 105693. doi:10.1016/j.atmosres.2021.105693

Wu, W.-S., Purser, R. J., and Parrish, D. F. (2002). Three-dimensional Variational Analysis with Spatially Inhomogeneous Covariances. *Mon. Wea. Rev.* 130 (12), 2905–2916. doi:10.1175/1520-0493(2002)130<2905:tdvaws>2.0.co;2

Young, S. A., and Vaughan, M. A. (2009). The Retrieval of Profiles of Particulate Extinction from Cloud-Aerosol Lidar Infrared Pathfinder Satellite Observations (CALIPSO) Data: Algorithm Description. *J. Atmos. Oceanic Tech.* 26 (6), 1105–1119. doi:10.1175/2008jtecha1221.1

Yunus, A. P., Masago, Y., and Hijioka, Y. (2020). COVID-19 and Surface Water Quality: Improved lake Water Quality during the Lockdown. *Sci. Total Environ.* 731, 139012. doi:10.1016/j.scitotenv.2020.139012

Zhang, R., Khalizov, A. F., Pagels, J., Zhang, D., Xue, H., and McMurry, P. H. (2008). Variability in Morphology, Hygroscopicity, and Optical Properties of Soot Aerosols during Atmospheric Processing. *Proc. Natl. Acad. Sci.* 105 (30), 10291–10296. doi:10.1073/pnas.0804860105

Zhang, X., Ji, Z., Yue, Y., Liu, H., and Wang, J. (2020). Infection Risk Assessment of COVID-19 Through Aerosol Transmission: A Case Study of South China Seafood Market. *Environ. Sci. Technol.* 55 (7), 4123–4133. doi:10.1021/acs.est.0c02895

Zhang, Y. L., Huang, R. J., El Haddad, I., Ho, K. F., Cao, J. J., Han, Y., et al. (2015). Fossil vs. Non-Fossil Sources of Fine Carbonaceous Aerosols in Four Chinese Cities During the Extreme Winter Haze Episode of 2013. *Atmos. Chem. Phys.* 15 (3), 1299–1312. doi:10.5194/acp-15-1299-2015

Zheng, Z., Zhao, C., Lolli, S., Wang, X., Wang, Y., Ma, X., Li, Q., and Yang, Y. (2020). Diurnal Variation of Summer Precipitation Modulated by Air Pollution: Observational Evidences in the Beijing Metropolitan Area. *Environ. Res. Lett.* 15 (9), 094053. doi:10.1088/1748-9326/ab99fc

Conflict of Interest: The authors declare that the research was conducted in the absence of any commercial or financial relationships that could be construed as a potential conflict of interest.

Publisher's Note: All claims expressed in this article are solely those of the authors and do not necessarily represent those of their affiliated organizations or those of the publisher, the editors, and the reviewers. Any product that may be evaluated in this article, or claim that may be made by its manufacturer, is not guaranteed or endorsed by the publisher.

frontiers | Frontiers in Environmental Science

ORIGINAL RESEARCH
published: 04 April 2022
doi: 10.3389/fenvs.2022.826799

Phase-Resolved Lockdown Features of Pollution Parameters Over an Urban and Adjoining Rural Region During COVID-19

Sunil M. Sonbawne[1], *Suvarna Fadnavis*[1], *K. Vijayakumar*[2], *Panuganti C. S. Devara*[3]* *and Prashant Chavan*[1]

[1]Indian Institute of Tropical Meteorology (IITM), Pune, India, [2]Department of Physics, Sri Venkateswara University (SVU), Tirupati, India, [3]Centre of Excellence in Ocean-Atmospheric Science and Technology (ACOAST)/Environmental Science and Health (ACESH), Amity University Haryana (AUH), Gurugram, India

OPEN ACCESS

Edited by:
Sabine Griessbach,
Helmholtz Association of German Research Centres (HZ), Germany

Reviewed by:
Eduardo Landulfo,
Instituto de Pesquisas Energéticas e Nucleares (IPEN), Brazil
Chinmay Mallik,
Central University of Rajasthan, India

***Correspondence:**
Panuganti C. S. Devara
pcsdevara@ggn.amity.edu

Specialty section:
This article was submitted to Atmosphere and Climate, a section of the journal Frontiers in Environmental Science

Received: 01 December 2021
Accepted: 04 March 2022
Published: 04 April 2022

Citation:
Sonbawne SM, Fadnavis S, Vijayakumar K, Devara PCS and Chavan P (2022) Phase-Resolved Lockdown Features of Pollution Parameters Over an Urban and Adjoining Rural Region During COVID-19. Front. Environ. Sci. 10:826799. doi: 10.3389/fenvs.2022.826799

In this study, we investigate the temporal variations in columnar aerosol pollutants and their possible association with the simultaneously measured black carbon (BC) aerosol mass concentration and associated biomass burning (BB) over urban (Delhi) and rural (Panchgaon) sites during the lockdown phases of the COVID-19 pandemic. We also show the impact of lockdown measures on boundary layer ozone and its primary precursors, NO_2, and water vapor (H_2O), potent greenhouse gases that destroy protective ozone. For this purpose, we used multiple datasets, namely, black carbon (BC) aerosol mass concentration and biomass burning (BB) aerosols using an aethalometer at Amity University Haryana (AUH), Panchgaon, India, and satellite retrievals from NASA's MODIS and OMI at both the stations. The analysis was conducted during the pre-lockdown period (1–25 March), lockdown 1st phase (25 March–14 April), lockdown 2nd phase (15 April–3 May), lockdown 3rd phase (4–17 May), lockdown 4th phase (18–31 May), and post-lockdown (1–30 June) period in 2020. Our diagnostic analysis shows a substantial reduction in AOD (Delhi: −20% to −80%, Panchgaon: −20% to −80%) and NO_2 (Delhi: −10% to −42.03%, Panchgaon −10% to −46.54%) in comparison with climatology (2010–2019) during all four phases of lockdown. The reduction in AOD is attributed to lockdown measures and less transport of dust from west Asia than climatology. Despite a reduction in NO_2, there is an increase in the ozone amount (Delhi: 1% to 8% and Panchgaon: 1% to 10%) during lockdown I, II, and III phases. The observed enhancement in ozone may be resultant from the complex photochemical processes that involve the presence of NO_2, CO, volatile organic compounds (VOCs), and water vapor. The reduction in AOD and NO_2 and enhancement in ozone are stronger at the rural site, Panchgaon than that at the urban site, Delhi.

Keywords: aerosol pollution, MODIS, OMI, aethalometer, COVID-19 lockdown, AOD, TCO

INTRODUCTION

The novel coronavirus first detected in late December 2019 in Wuhan, China, has eventually become a deadly virus, which is highly transmissible, along with a high mortality rate (Suresh et al., 2020). Due to its rapid spread and deadly nature, several people were affected within a month (Bull et al., 2020; He et al., 2020); it is considered as one of the major disasters, which has affected the whole world. In early March 2020, the World Health Organization (WHO) named the coronavirus as COVID-19 and declared this COVID-19 as a pandemic. After the outbreak of this COVID-19, it affected the world in a gradual manner (Raibhandari et al., 2020) mainly through cross-border travels. As the numbers of COVID-19 cases were increasing, the Prime Minister of India asked all citizens across the country to observe a 14-h public curfew on 22 March 2020. Following this, the government of India ordered a complete nationwide lockdown for 21 days, starting from midnight of 24 March 2020. To handle the worsening of the pandemic in the country, the government urged the Indian states and citizens to strictly follow the social distancing measures as a preventive strategy (https://www.mha.gov.in/).

After detecting the cases of COVID-19 in late January 2020 in India, the COVID-19 was found significantly spared in various states of India. According to the Ministry of Health and Family Welfare (MoHFW), present situation on 13 October 2020, total infected cases were 35,985,920, mortality was 450,963, and the recovery cases of 33,320,057 were reported in entire India on https://www.mygov.in/covid-19/, translating into a case fatality rate of 1.33% (MoHFW, 2020). Maharashtra, Tamil Nadu, Delhi, and Gujarat reported 50% of India's cases, and the number of cases increased in the northeast states. In order to respond to this novel threat and to limit the spread of a virus, the Indian government has taken various precautionary measures, such as large scale COVID-19 screening tests, quarantine, social distancing, wearing of a mask, and sanitization of hands. Furthermore, considering the seriousness of the disease, the measures were taken to impose a nationwide lockdown in entire India, which was not the case for other countries (Rimesh and Urmila, 2020).

Tocontrol the transmission of COVID-19 and to measure the outcome from the precautionary measures, initially, on 22 March 2020 a 1-day Janata (people's) curfew, followed by a 21-day nationwide lockdown (25 March 2020 to 14 April 2020: lockdown phase (LDP)-1) was announced and thereafter in succession LDP-II: 15 April to 3 May 2020, LDP-II: 4 May to 17 May 2020, and LDP-IV: 18 May to 31 May 2020 have been imposed. As a result, many industries, transport, economic, and social activity were shut down. After that, to restart the economy, two unlock phases have also been announced, respectively, on ULP-I: 1 June 2020 to 30 June 2020, and ULP-II: 1 July 2020 to 31 July 2020. These various lockdown phases reduced the mortality rate of COVID-19, improved the environment and air quality in the country. Various researchers from the world have focused on finding the effects of COVID-19 lockdown on the atmosphere. Recent studies have reported the improvement in air quality due to restrictions placed during the lockdown.

Research from other countries, namely, Germany, France, Italy, and Spain, reported a drastic decrease in concentration levels of GHGs, NO_2, $PM_{2.5}$, and PM_{10} but spikes in ozone concentration. The researchers, all over the world, have indicated a significant reduction in greenhouse gases, PM_{10}, $PM_{2.5}$, CO, NO, NO_2, NH_3, NOx, and SO_2 concentrations dropped during the lockdown period (for example, Devara et al., 2020). Ghosh and Ghosh (2020), Srivastava (2020) reviewed various studies and concluded the improvement in the air quality due to lockdown. Gautam (2020a), Fadnavis et al. (2021) analyzed NO_2 data, derived from the satellite (Sentinel–5P) and reported a significant reduction in Asian (Kanniah et al., 2020) and European countries. In another study, Gautam (2020b) analyzed the data from the National Aeronautics and Space Administration (NASA) and reported a 50% reduction in the air quality of the Indian region. Gupta et al. (2020) reported a reduction in the concentration of that influenced the a in 40 $\mu g/m^3$ in particulate matter ($PM_{2.5}$ and 10 ppm in CO over New Delhi, India. Mahato et al. (2020) reported a 40–50% improvement in the air quality over New Delhi. Jain and Sharma (2020) reported a ~30–80% reduction in pollutants levels in all the major cities of India. Bera et al. (2020) found a positive correlation between $PM_{2.5}$ and the lethality related to COVID-19 in Kolkata. Ranjan et al. (2020), Ranjan et al. (2021) reported from their studies of aerosol optical depth (AOD) using MODIS data, a 45% reduction in AOD during the lockdown period as compared to 19-year (2000–2019) AOD long-term mean.

The northern part of India normally experiences a poor air quality and high levels of atmospheric pollution due to various reasons, such as vehicular emissions, industrial activity, brick-kilns, and crop-residue burning (Singh et al., 2004; Prasad et al., 2006; Srivastava et al., 2021). Correlations between deviations in different pollutant mass concentrations, the spread of COVID-19, social distancing, indoor pollution, trends in morbidity, and mortality during 2020 have been derived from studies of air pollution and synchronous local and long-range meteorological parameters (Devara et al., 2020, 2021).

During this complete lockdown, there was an improvement in the air quality and a reduction in pollutant parameters in this area too (Sonbawne et al., 2021). The present study deals with such pollution scenarios, lockdown episodes in Panchgaon (Manesar) and New Delhi (Noida), situated about 50 km apart in the northern part of India.

DATA AND METHODOLOGY

MODIS Satellite Measurements

The moderate-resolution imaging spectroradiometer (MODIS) is a scientific instrument (radiometer) onboarded the NASA Terra and Aqua satellite platforms. Both Terra and Aqua satellite platforms were launched in 1999 and 2002, respectively. These instruments offer a look at terrestrial, atmospheric, and ocean phenomenology for a wide and various communities of users throughout the world. Terra and Aqua satellites with MODIS instruments attached fly on the sun-synchronous orbits at

705 km altitude and pass over the same spot of the Earth at about the same local time every day, that is, 10:30 a.m. in the case of Terra and 1:30 p.m. for Aqua. MODIS measures reflected solar and emitted thermal radiation in a total of 36 bands ranging at a wavelength from 0.4 to 14.4 μm and at varying spatial resolutions (2 bands at 250 m, 5 bands at 500 m, and 29 bands at 1 km).

The MODIS radiance data are inverted into nearly 40 different products having applications in various fields of considerable interest and importance in the Earth's system to study global dynamics of the Earth's atmosphere, land, ice, clouds, and oceans (for example, King et al., 1999; Devara, 2017; Zambrano-Monserrate et al., 2020). In this study, a deep blue product of AOD at 550 nm and water vapor observations were used.

OMI Satellite Measurements

The ozone monitoring instrument (OMI) was launched in 2004 on a 705 km sun-synchronous polar orbit on the AURA satellite with an ascending node equator crossing time of 1:45 p.m. The OMI measures the solar radiation backscattered by the Earth's atmosphere and surface over the entire wavelength range from 270 to 500 nm with a spectral resolution of about 0.5 nm. The wavelength ranges (ultraviolet: 270–365 nm and visible: 365–500 nm) are used to retrieve total column gases such as O_3 and NO_2. Furthermore, OMI gives ultraviolet aerosol index (AI) parameters (Torres et al., 2007). NO_2, ozone, and AI data were used for OMI version 3 data, which has daily temporal with a minimum grid of 0.25 × 0.25 spatial resolution. However, for the anomaly study, we have considered a grid of 1 × 1. The details of the OMI data and retrieval methods can be found in Krotkov et al. (2019). The data are downloaded using the NASA Giovanni portal (https://giovanni.gsfc.nasa.gov/).

Aethalometer Measurements

The aethalometer used in the present study is an advanced (next-generation) multi-beam instrument, being operated at AUH, Panchgaon, in collaboration with IITM, Pune, for the 24 × 7 measurement of black carbon (BC) aerosol mass concentration and biomass burning (Sonbawne et al., 2021). This instrument uses the latest "Dual Spot" technology that eliminates data contamination due to filter loading (Drinovec et al., 2015) A unique feature of this instrument is that it provides a simultaneous measurement of biomass burning (BB) contribution (in percentage) to the measured BC mass concentration (μgm^{-3}). The seven operating wavelengths permit the identification of biomass emissions. More details of the instrument and its wide applications to the studies of carbonaceous (most absorbing) aerosol influence on human health and climate have been reported in the literature (for example, Bond et al., 2013; Devara et al., 2017; Dumka et al., 2019; Sonbawne et al., 2021).

The total column aerosol optical depth (AOD), from MODIS, and columnar AI (aerosol index, representative of columnar aerosol size distribution) and water vapor; total column ozone (TCO) and total column nitrogen dioxide from OMI during the period from 01 March to 30 June 2020, which encompasses the pre-lockdown (1–24 March), phase I (25 March–14 April), phase II (15 April–3 May), phase III (4–17 May), phase IV (18–31 May), and post-lockdown (1–30 June) periods have been retrieved. The simultaneous ground-based data using an aethalometer at 370 nm (brown carbon or wood-burning aerosol emissions) and at 880 nm (black carbon emissions from the burning of fossil fuel) have also been archived. These datasets have been analyzed to examine the inter-relationship between the pollutant variations and their resultant influence at two contrasting locations, one situated in the urban and the other in the rural environment, during different lockdown phases of COVID-19. It may be noted here that the norms introduced by the government during different phases affected the pollution levels in different manners (Chen et al., 2020). During phase I, nearly all the industrial and mass transportation were suspended immediately except for some of the essential services. During phase II, conditional relaxation was imposed in the regions where the spread of COVID-19 had been slowed down. During phase III, conditional relaxation continued, and the entire country has been split into three zones as red zone (higher cases), orange zone (lower cases than the red zone), and green zone (no case in the past 21 days). Normal public movement is permitted in the green zones. Red zones were further divided into the "containment" and "buffer" zones and the local bodies were given the authority for this demarcation.

We estimate anomalies (daily values in 2020 minus daily climatology) of AOD, AI, H_2O, NO_2, and O_3. The daily climatology is obtained for the period 2010–2019 for all the species. Since biases are the same in observations in 2020 and climatology, the anomaly is benefited by the removal of systematic biases and examining the variations in relative NO_2, O_3, AI, H_2O, and AOD in 2020. The anomalies of NO_2, O_3, AI, and AOD represent reduction due to anthropogenic activities during the COVID-19 lockdown period, while anomalies of H_2O are mainly due to meteorology.

Trajectory Analysis

An approach to merge trajectories (driven by HYSPLIT) that are near each other and represent those groups, called clusters, by their mean trajectory (Su et al., 2015). Differences between trajectories within a cluster are minimized, while differences between clusters are maximized (Srivastava et al., 2021). Computationally, trajectories are combined until the total variance of the individual trajectories about their cluster mean starts to increase. Cluster analysis is a multivariate statistical technique increasingly used in air pollution research. This method involves splitting the data set into a number of groups that need to be as homogenous and as distinctly different from each other as possible. Generally, the result of the application of the cluster analysis technique to air trajectories is similar to a flow climatology in which trajectories are classified into groups according to certain criteria, but cluster analysis is more objective, and it accounts for variation in transport speed and direction simultaneously, yielding clusters of trajectories, which have similar length and curvature (Harris and Kahl, 1990).

In order to examine the sources that are responsible for the air masses at the study location (Panchgaon, a rural site in the

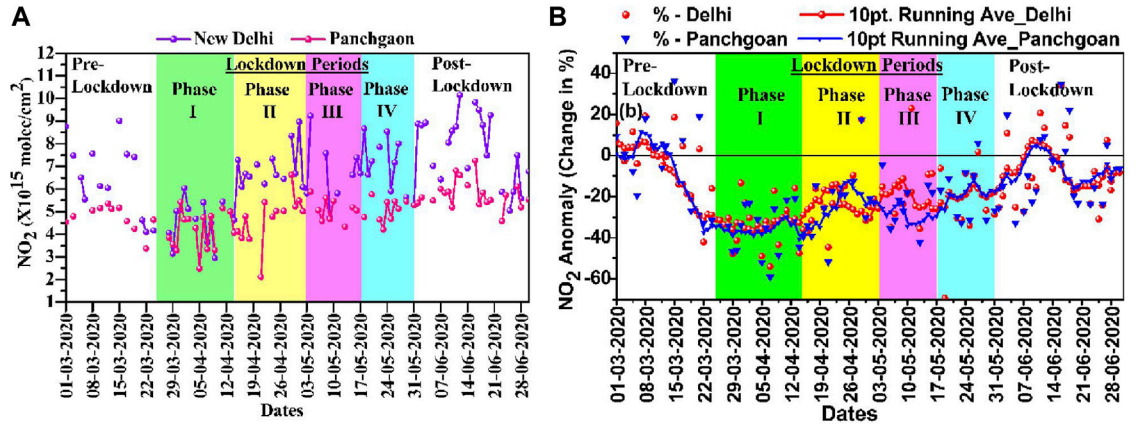

FIGURE 1 | (A) Daily variation in total column nitrogen dioxide (NO_2) (*10^{15} molecule/cm^2) obtained from OMI satellite retrievals at New Delhi and Panchgaon, **(B)** same as **(A)** but for anomalies (2020 minus climatology). Climatology is obtained for the period 2010–2019.

present case), cluster mean backward trajectories at the optimum level and the associated TSV (total spatial variance, in percent) during each phase of lockdown were calculated for the pre-lockdown, phases I, II, III, and IV, and post-lockdown periods. When the clustering is completed, the program calculates the total spatial variance (TSV) as the trajectories are merged into one cluster. In this study, the TSV is a measure of the degree to which the chosen clusters fit the data (Harris and Kahl, 1990; Draxler et al., 2020). In the present case, the change in TSV variance for only the last 30 clusters is considered. The maximum number of clusters in each case varied from two to three, and they are marked by red, dark blue, and green, respectively, for 1st, 2nd, and 3rd clusters. A **Supplementary File**, covering the details of the experimental location and the results of TSV analysis, is given separately.

RESULTS AND DISCUSSION

Variations in NO_2 in Delhi and Panchgaon

The daily variation of total column nitrogen dioxide (expressed in 10^{15} molecules/square centimeter) during the pre-lockdown; phases I, II, III, and IV; and post-lockdown periods over New Delhi and Panchgaon is plotted in **Figure 1A**. The most striking feature that can be seen from **Figure 1A** is that the NO_2 values over the urban station, New Delhi, are almost the double of the rural station, Panchgaon, throughout the study period. **Figure 1B** shows anomalies in NO_2 at these two stations during the study period. It shows a reduction in NO_2 column during phase I compared to the pre-lockdown period by −54% (5.4–2.5 × 10^{15} mol/cm^2) in Delhi and −59% (9.2–3.2 × 10^{15} mol/cm^2) at Panchgaon. This indicates a clear signal of reduced anthropogenic activity during the lockdown that has reduced the NO_2 column at both stations. The reduction at Panchgaon is higher than that at New Delhi by 3–10%.

Figure 1B shows an increasing trend in NOx during lockdown to the post-lockdown period at both stations. This could be due to relaxing the strict measures and slowly opening of the economy. However, an average reduction in NOx is by 42.03% in Delhi and by 46.54% at Panchgaon during phase I to IV lockdown periods. The positive anomaly in the pre-lockdown and post-lockdown period suggests the contribution from the anthropogenic activity that was restricted in the COVID lockdown. Previous studies have also reported a reduction in NO_2 over North India (in Delhi: −52.68% during phase I–II, by Mahato et al., 2020, at Lucknow: −54% during phase I, by Karuppasamy et al., 2020). These results agree with our findings. More importantly, New Delhi, the capital of India, showed less decrease in NOx compared to Panchgaon. Other stations in India also showed a reduction in NO_2 (Mumbai- 43.08%, Gandhinagar- 45.64%, Bangalore- 48.25%, and Nagpur 46.13%) (Vedrevu et al., 2020; Singh and Chauhan, 2020).

Variations in Total Column Ozone (TCO) at New Delhi and Panchgaon

The daily mean variations in total column ozone (TCO) in Dobson Unit (DU), over New Delhi and Panchgaon during the pre-lockdown; lockdown phases I, II, III, and IV; and post-lockdown periods are compared in **Figure 2**. It shows that most of the time the TCO values over New Delhi are larger than Panchgaon during the study periods.

Figure 2A shows a decrease in ozone amounts during lockdown periods in comparison to pre-lockdown phase I by 342 to 270 DU in Delhi and 334 to 274 DU at Panchgaon. The ozone concentration shows a decreasing trend over the period covering pre-lockdown to post-lockdown. Furthermore, we show ozone anomalies during the study period in **Figure 2B**. Its shows, positive anomalies during pre-lockdown to phase III with the range of ~+12% to +1%, this indicates that ozone concentrations at both stations are higher than the climatology, while ozone anomalies are negative anomalies during phase IV and in the post-lockdown period. This indicates that ozone amounts are less than the climatology during phase IV and in the post-lockdown period.

The positive anomalies of ozone during the pre-lockdown period may be due to a reduction in NO_2 (negative anomalies in

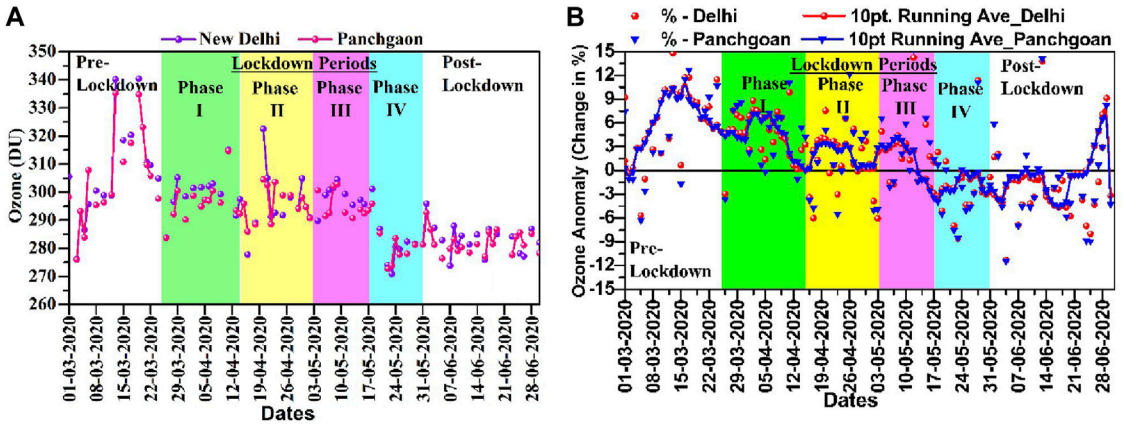

FIGURE 2 | (A) Daily variation in total column ozone (O_3) (DU) obtained from OMI satellite retrievals at New Delhi and Panchgaon, **(B)** same as **(A)** but for anomalies (2020 minus climatology). Climatology is obtained for the period 2010–2019.

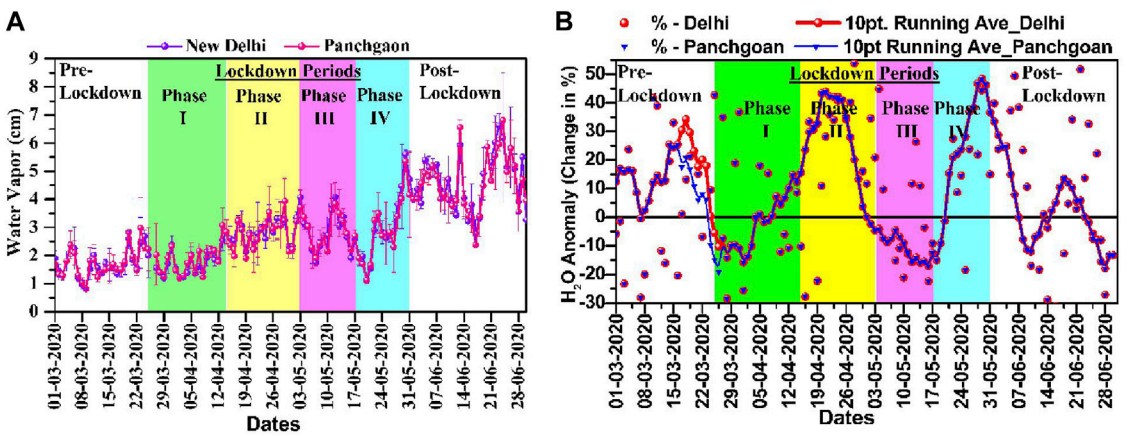

FIGURE 3 | (A) Daily variation in total column water vapor (TCW) obtained from MODIS satellite retrievals at New Delhi and Panchgaon, **(B)** same as **(A)** but for anomalies (2020 minus climatology). Climatology is obtained for the period 2010–2019.

for phase–IV and post-lockdown) during the same time at New Delhi and Panchgaon stations. A decrease in NO_2 has reduced O_3 destruction *via* the NO titration cycle that led to more ozone amounts. Ozone photochemistry is also affected by solar radiation. The reduction of aerosol pollution during the lockdown has increased the solar radiation reaching the ground (Devara et al., 2019; Fadnavis et al., 2019) that might have accelerated ozone formation. A feature of increase in ozone emphasizes the complex O_3 chemistry. The variation in other ozone precursors, for example, CO, volatile organic compounds and meteorological variability and solar irradiance (cloudiness) plays an important role in ozone heterogeneous chemistry (Sillman et al., 1990) under significant aerosol reduction conditions (Shi and Brasseur, 2020). Our results are also in agreement with the reported reduction in ozone by 36% during phase-I by Girach et al. (2021) and also with the other studies (Mahato et al., 2020; Soni et al., 2021; Dhaka et al., 2020; Singh et al., 2020).

Variations in Total Column Water Vapor (TCW) at New Delhi and Panchgaon

The daily mean variations in total column water vapor (TCW, in cm), derived from MODIS over New Delhi and Panchgaon are compared in **Figure 3A**. It is clear from the figure that TCW shows an increasing trend at both study sites. Furthermore, TCW values over New Delhi exhibit almost close to those over Panchgaon during the study period, while it varied from 1.10 to 6.62 cm for New Delhi and from 1.13 to 5.96 cm for Panchgaon during the pre-lockdown period. Phase II, III, and IV periods show the TCW values are slightly higher than those in phase I. However, these values are higher than those of the pre-lockdown period. The increase in the total column water content could also partly be due to the increase in ground-level temperature and change in local meteorological conditions. Increasing water vapor leads to a cooling of the stratosphere and modifies stratospheric chemical processes. Thus, the cooling of the stratosphere leads to stratospheric ozone depletion processes (Tian et al., 2009).

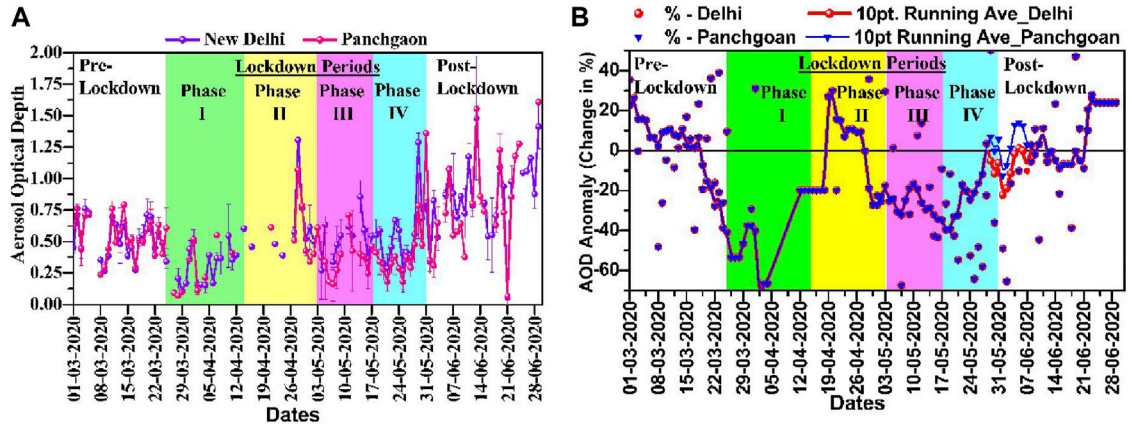

FIGURE 4 | (A) Daily variation in total column aerosol optical depth (AOD) obtained from MODIS satellite retrievals at New Delhi and Panchgaon, **(B)** same as **(A)** but for anomalies (2020 minus climatology). Climatology is obtained for the period 2010–2019.

On the whole, the variations in ozone/water vapor over both locations are found to be well correlated throughout the study period; and they exhibited a monotonic decreasing/increasing trend, which coincides with the fact that the increase in the water vapor content reduces the ozone content, as mentioned before. The variations in TCW during different phases of lockdown are attributed to the relaxations imposed by the government. Thus, the variations in TCW (affected by net radiation) are found to be unique as compared to those of other pollutants at both study regions.

The anomalies computed for MODIS-derived TCW over both study regions are also plotted in **Figure 3B**. Although the scatter is more in the anomaly, the values are almost coincident, except at the end-stage of the transition between pre-COVID and lockdown phase I over both study regions. Moreover, the TCW anomaly values are larger and positive during the pre-COVID than those in the post-COVID period. Overall, positive values during pre-, II, IV, and post-lockdown, and negative during I and III lockdown periods were shown. These variations could partly be due to the heterogeneous lockdown policy, involving strict and relaxed structures. During the lockdown period, because of the absence of anthropogenic activity, most of the solar radiation reaches the Earth's surface and hence there was an increase in ground level temperature which in turn causes warmer climate (Vargas et al., 2019). The warmer climate at the surface enhances the stratospheric water vapor. It may be mentioned here that, as explained before, the reduction in AOD during the phase I may be due to the combination of unusual rain and also due to the restrictions imposed by the government.

Variations in AOD in Delhi and Panchgaon

The daily mean variations in aerosol optical depth (AOD) from MODIS during pre-, I, II, III, and IV, and post-lockdown periods at New Delhi (28.35 N, 77.12 E, ~ 215 m amsl), and Panchgaon (28.32 N, 76.92 E, 285 m amsl) stations are shown in **Figure 4**. In general, **Figure 4A** shows higher AODs at New Delhi than Panchgaon during the study period. There is a reduction in AOD during lockdown phase I in Delhi (by 0.54 to 0.15) and Panchgaon (by 0.65 to 0.42) due to the lockdown restrictions imposed by the government. The AOD increase during phase I to the post-lockdown period indicates an increasing trend. The observed increase in AOD at these stations is associated with the partial opening of the economy during phases II, III, and IV. During these phases, the transportation continued to play a significant role since industrial, construction, and economical activities were active. During the post-lockdown phase, AOD values at New Delhi shoot up to 0.50 to 1.50 and at Panchgaon 0.1 to 1.50. These nearly doubled as compared to that during the pre-lockdown period.

Furthermore, we show anomalies of MODIS AOD in **Figure 4B**, over the New Delhi and Panchgaon obtained as the difference between the daily values of March to June 2020 with respect to climatology. It shows a sharp reduction in AOD by the same amount over New Delhi and Panchgaon (−20% to −80%) during phase I. But in phase II MODIS AOD shows a positive anomaly (5% to 30%). The increase in AOD compared to climatology is due to the higher amount of fires in the vicinity of both the stations. Furthermore, in phase III, IV AOD anomaly is negative over New Delhi (−10% to −40%) and Panchgaon (−10% to −40%). Earlier studies also showed that there is a reduction in AOD during the COVID-19 period over North India (e.g., Ranjan et al., 2020; Fadnavis et al., 2021; Ranjan et al., 2021), which agree with the present work.

Variations in Aerosol Index (AI) in Delhi and Panchgaon

The OMI aerosol index (AI) is an indicator of aerosol size distribution that has been deduced from the spectral dependence of AOD observations on each day. We analyzed the OMI aerosol index (AI) over New Delhi and Panchgaon during the pre-lockdown, lockdown phase I, II, III, and IV, and post-lockdown period. **Figure 5A** shows day-

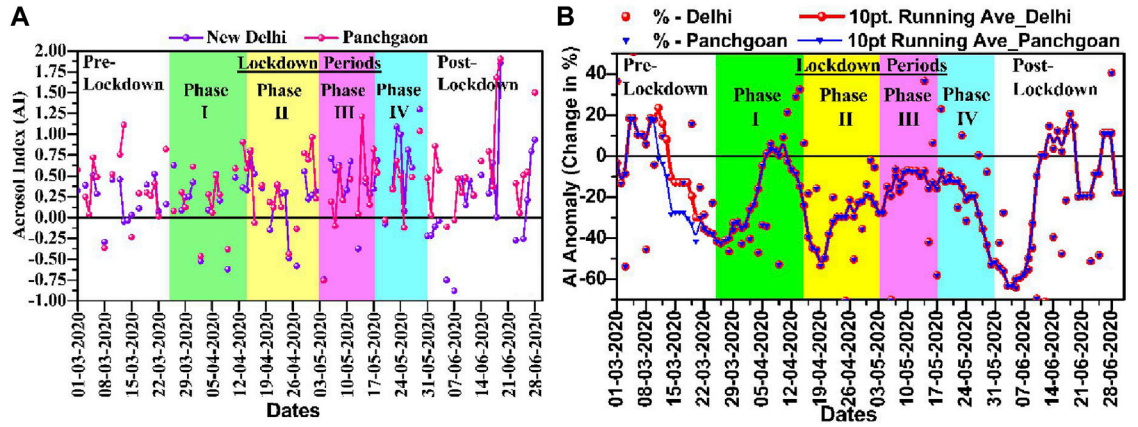

FIGURE 5 | (A) Daily variation in aerosol index (AI) obtained from OMI satellite retrievals at New Delhi and Panchgaon, **(B)** same as **(A)** but for anomalies (2020 minus climatology). Climatology is obtained for the period 2010–2019.

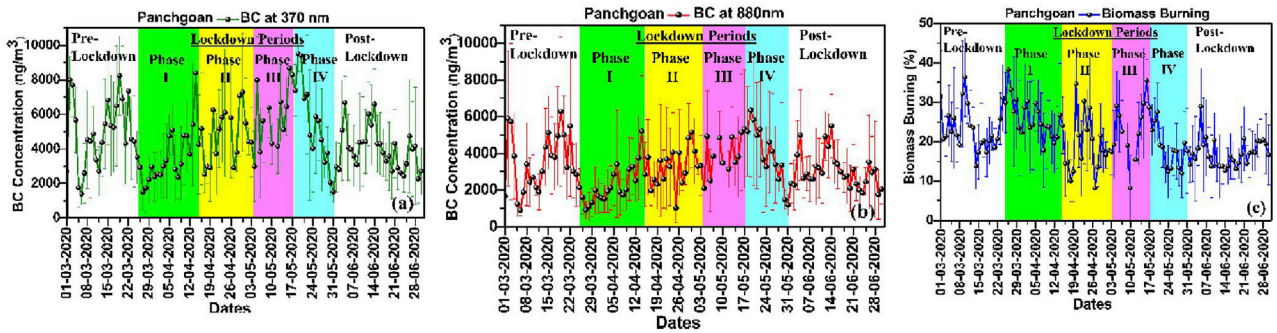

FIGURE 6 | Day-to-day marching of BC mass concentration and BB % obtained using multi-spectral aethalometer measurements **(A)** at 370 nm, **(B)** 880 nm, and **(C)** BB%.

to-day variation and **Figure 5B** anomaly of AI. It is clear from the figure that, overall, the AI values for Panchgaon (rural station) are larger (smaller size particles) and smaller (bigger particles) at New Delhi (Urban station). In general AI values are less than 1 at both stations indicating the presence of anthropogenic aerosols. The anomalies in AI (**Figure 5B**) show positive anomalies in the pre-lockdown and post-lockdown period. This is due to higher anthropogenic emissions. The negative anomalies of AI during lockdown phases are due to limited anthropogenic activity. The large grid of OMI (1 × 1) covers both Delhi and Panchgaon stations. Hence, variations in anomalies are the same at both stations. It also suggests the transport of dust is less than during the rest of the normal year (year not associated with any major ocean-atmospheric coupled phenomenon like El Nino, IOD etc.)., which is also shown by Fadnavis et al. (2021). The time-series patterns of AI at New Delhi and Panchgaon have been studied. The results show a substantial reduction in AOD (Delhi: −20% to −80%, and Panchgaon: −20% to −80%) in comparison with climatology (2010–2019) during all the four phases of lockdown. The observed reduction in AOD at both stations is attributed to lockdown measures and less transport of dust from west Asia than climatology.

Variations in BC and BB Over Panchgaon

Both black carbon (BC) aerosols and biomass burning (BB) have received particular attention around the world due to their impact on air quality and public health. Due to its fine size (size-mode 2.5 μm), large specific surface area, and irregular morphology, it is easily inhaled and can affect human health, causing cardiovascular, respiratory, and other diseases (Highwood and Kinnersley, 2006; Suglia et al., 2008; Cunha-Lopes et al., 2019). BC mass concentrations, measured using an aethalometer at 370 and 880 nm wavelengths during the pre-, phase I, II, III, IV, and post-lockdown periods are plotted in **Figures 6A,B**. The daily mean variation in black carbon (BC) mass concentration observed using a multi-spectral aethalometer at 370 and 880 nm wavelengths during the pre-, phase I, II, III, IV and post-lockdown periods is plotted in **Figures 6A,B**. The daily variation of the percentile of biomass burning (BB) aerosol contribution to BC is also plotted in

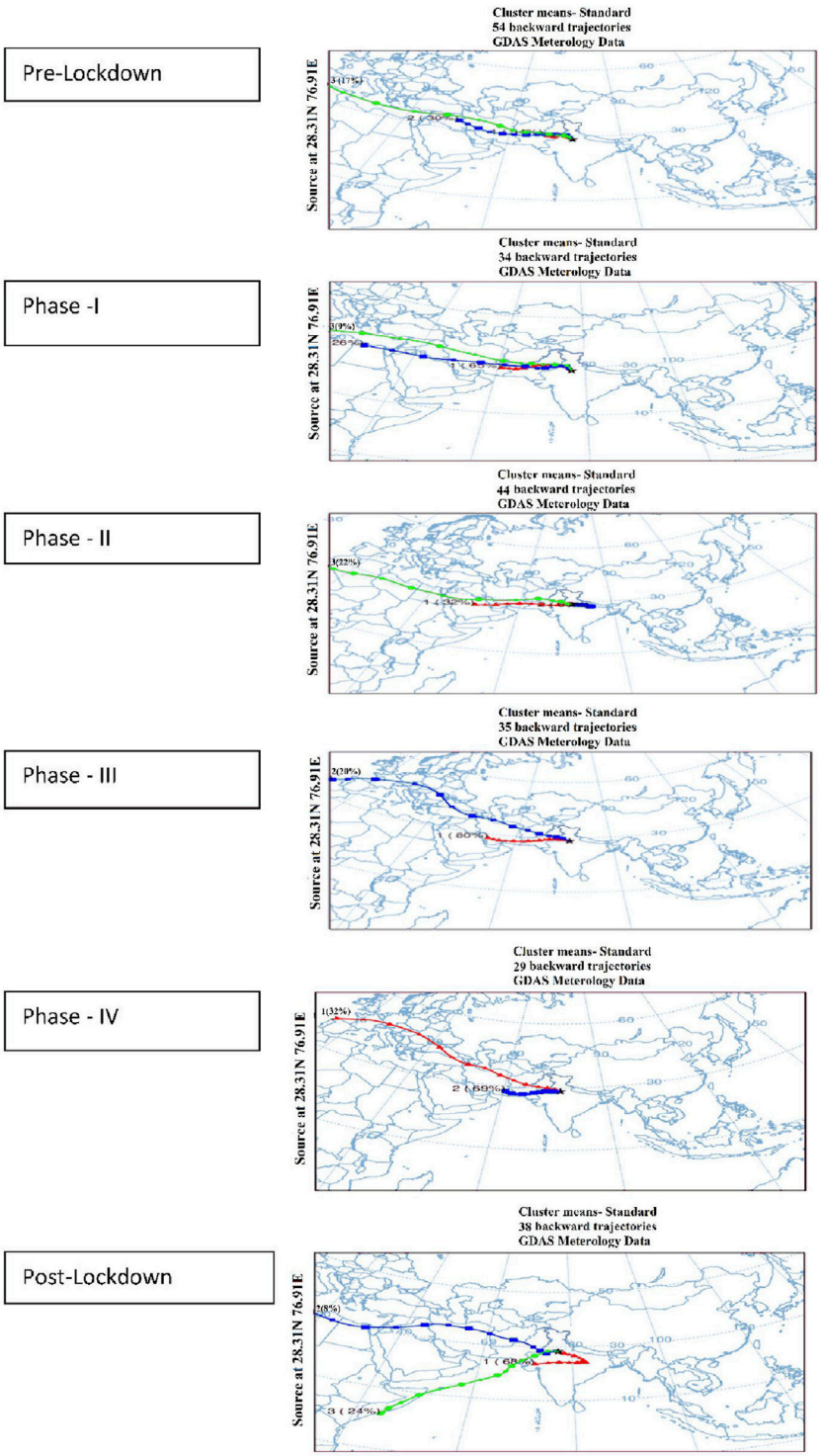

FIGURE 7 | Air mass backward trajectory (Source at 28.37N, 76.91E) cluster for the BC data of pre-, I, II, III, IV, and post-lockdown phases during 1 March–30 June 2020.

Figure 6B. As explained in Dumka et al. (2019), the major contribution to BC at 370 nm comes from the vehicular exhaust, while the contribution at 880 nm comes from industrial emissions. Since these estimations are mainly made by the property of absorption, the effects due to wavelength dependence are normalized in the calculations.

Figure 6A shows a reduction in the BC mass concentration during phase I as compared to the pre-lockdown period (370 nm: 8,241-1,510 ng/m^3; 880 nm:6,293-912 ng/m^3) at Panchgaon, The observed reduction is due to the total restriction on transportation and industrial operations. BC at 370 and 880 nm (**Figure 6B**) increases during phase I to IV, whereas the contribution of BB % shows a decline (**Figure 6C**) during lockdown phases. However, these observations are not available at New Delhi.

Variations in Transport Characteristics During Lockdown

During the pre-monsoon season when the lockdown was imposed over India, variation in aerosols is influenced by long-range transport of dust from west Asia (Lau, 2006; Fadnavis et al., 2017). However, the transport pattern may be different in spring 2020 due to variation in dynamics (Fadnavis et al., 2019). Hence, we show trajectory analysis during the lockdown period. While forward trajectories describe where a particle will go, backward trajectories indicate where it came from. Air trajectories are frequently used for the interpretation of individual flow situations for several decades, but statistical methods for large sets of trajectories have been developed more recently (Stohla et al., 2002; IPCC, 2017).

To examine the sources of air mass concentrations at the study location (New Delhi), we have shown cluster mean backward trajectories and the associated total spatial variance (TSV, in percent) during the pre-lockdown; phases I, II, III, and IV; and post-lockdown periods in **Figure 7**. It is to note that the number of trajectories available for forming the clusters during each phase of lockdown is different for different phases.

In the case of pre-lockdown (1st to 25th March 2020) the 54 backward trajectories of air masses come at the study location (New Delhi) from the Mediterranean Sea and desert region. However, cluster 2 contributes 30% of the air mass, which comes from the desert region. In the case of phase I lockdown (25th March–14th April 2020), 34 backward trajectories of air masses come from the Mediterranean Sea and desert region, however, maximum contribution (65%) by 1st cluster. 44 backward trajectories were averaged in the case of the phase II lockdown and formed three clusters; the 1st cluster contributed 32% of air mass from the desert region. In the case of the phase III lockdown period, 35 backward trajectories were averaged, and two clusters were formed. The 1st cluster contributed a maximum of 80% of air mass from the desert region. Similarly, in the case of the phase IV lockdown phase, a total of 29 backward air mass trajectories participated the formation of clusters; and two clusters were formed. The 2nd cluster contributed a maximum of 69% of air mass from the desert region. On the other hand, in the case of post-lockdown, a total of 38 backward trajectories have participated in the formation of clusters; and three clusters were formed. The 1st cluster contributed 68% to the air mass from a local transport and the 2nd cluster contributed 24% of air mass coming from the Arabian Sea. This trajectory analysis indicates a transport of dust from the Mediterranean Sea and desert region (Fadnavis et al., 2021).

SUMMARY AND CONCLUSION

The impact of lockdown concept of COVID-19 on the synchronous near-surface carbonaceous aerosols and satellite-derived columnar aerosol optical depth, size distribution, water vapor, ozone, and nitrogen peroxide over two contrasting environmental (urban and rural) conditions during 2020 has been reported in this study. The analysis of OMI NO_2 shows a substantial reduction in Delhi (−10% to −42.03%) and Panchgaon (−10% to −46.54%), while ozone amounts show enhancement in Delhi (1% to 8%) and Panchgaon (1% to 10%) than climatology during lockdown I—III phases. The observed enhancement in ozone, despite a reduction in NO_2, may be a resultant of the complex photochemical processes related to the ozone formation mechanisms that involve the presence of NO_2, CO, volatile organic carbon (VOC), and water vapor. The columnar density of pollutants over the urban station (New Delhi), especially in the case of columnar NO_2, is found to be higher than that over the rural (Panchgaon) station.

The variation of pollutant levels showed a positive trend in tropospheric column NO_2 and H_2O and a negative trend in tropospheric column ozone. The behavior of pollutant concentrations during both lockdown versus no-lockdown phase, and their comparison within the lockdown periods also exhibited interesting results. It is observed that the pollutant concentration scenarios are different not only between pre- and post-lockdown periods due to local meteorology and long-range transport processes but also within the four lockdown phases implemented by the government. The significant differences observed between certain phases are considered to be due to the nature of lockdown, imposed by the government. Overall, the concentration of pollutants is found to be lower during the lockdown phases than those observed either during the pre-lockdown or post-lockdown period. This aspect clearly indicates the positive impact of the lockdown concept, and it is found more helpful not only for curbing the regional pollution but also for improving the other requirements of maintaining the social distance to minimize the health hazards leading to morbidity and mortality during the COVID-19 period.

DATA AVAILABILITY STATEMENT

The raw data supporting the conclusions of this article will be made available by the authors, without undue reservation.

AUTHOR CONTRIBUTIONS

PD: conceptualization, investigation, methodology, project administration, supervision, and original manuscript. SS, SF, KV, and PC: data curation, formal analysis, validation, and visualization of the study.

ACKNOWLEDGMENTS

The research work reported in this article was carried out as a part of joint collaborative research project between Amity University Haryana (AUH), Gurugram, Indian Institute of Tropical Meteorology (IITM), Pune, and Sri Venkateswara University (SVU), Tirupati, India. The authors are thankful to Ashok K. Chauhan, founder president; Aseem Chauhan, chancellor and all other authorities of AUH for their continued support; and to the Director, IITM, and Head of Department of Physics, SVU, for their cooperation. We also acknowledge NASA for the MODIS and OMI satellite products and also NOAA-ERL for the HYSPLIT back-trajectory model analysis results for the study period. We thank the reviewers and the editor for their valuable suggestions toward the improvement of the manuscript.

SUPPLEMENTARY MATERIAL

The Supplementary Material for this article can be found online at: https://www.frontiersin.org/articles/10.3389/fenvs.2022.826799/full#supplementary-material

REFERENCES

Bera, B., Bhattacharjee, S., Shit, P. K., Sengupta, N., and Saha, S. (2020). Significant Impacts of COVID-19 Lockdown on Urban Air Pollution in Kolkata (India) and Amelioration of Environmental Health. *Environ. Dev. Sustain.* 28, 1–28. doi:10.1007/s10668-020-00898-5

Bond, T. C., Doherty, S. J., Fahey, D. W., Forster, P. M., Berntsen, T., DeAngelo, B. J., et al. (2013). Bounding the Role of Black Carbon in the Climate System: a Scientific Assessment. *J. Geophys. Res. Atmos.* 118, 5380–5552. doi:10.1002/jgrd.50171

Bull, F. C., Al-Ansari, S. S., Biddle, S., Borodulin, K., Buman, M. P., Cardon, G., et al. (20202020). World Health Organization 2020 Guidelines on Physical Activity and Sedentary Behaviour. *Br. J. Sports Med.* 54, 1451–1462. doi:10.1136/bjsports-2020-102955

Chen, L.-W. A., Chien, L.-C., Li, Y., and Lin, G. (2020). Nonuniform Impacts of COVID-19 Lockdown on Air Quality over the United States. *Sci. Total Environ.* 745, 141105. doi:10.1016/j.scitotenv.2020.141105

Cunha-Lopes, I., Martins, V., Faria, T., Correia, C., and Almeida, S. M. (2019). Children's Exposure to Sized-Fractioned Particulate Matter and Black Carbon in an Urban Environment. *Building Environ.* 155, 187–194. doi:10.1016/j.buildenv.2019.03.045

Devara, P. C. S., Alam, M. P., Dumka, U. C., Tiwari, S., and Srivastava, A. K. (2017). "Anomalous Features of Black Carbon Aerosols Observed over a Rural Station during Diwali Festival of 2015," *In; Book Titled "Environmental Pollution". Science* (Berlin, Germany: Springer).

Devara, P. C. S., Kumar, A., Sharma, P. B., Banerjee, P., Khan, A. A., Sonbawne, S. M., et al. (2021). Multi-Sensor Study of the Impact of Air Pollution on COVID-19. *J. Infect. Dis. Res. (Jidr)* 4 (1), 157–168.

Devara, P. C. S., Kumar, A., Sharma, P. B., Banerjee, P., Khan, A. A., Tripathi, A., et al. (2020). "Influence of Air Pollution on Coronavirus (COVID-19): Some Evidences from Studies at AUH, Gurugram, India," in *Open Research Communication in the Social Science Research Network (SSRN), USA*. doi:10.2139/ssrn.3588060

Devara, P. C. S. (2017). "Remote Sensing for Environment and Climate Diagnostics. Book Chapter," in *Environmental Science and Engineering* (Houston, TX: Studium Press LLC, USA), 287–312.

Dhaka, S. K., Chetna, K. V., Kumar, V., Panwar, V., Dimri, A. P., Singh, N., et al. (2020). PM2.5 Diminution and Haze Events over Delhi during the COVID-19 Lockdown Period: an Interplay between the Baseline Pollution and Meteorology. *Sci. Rep.* 10, 13442. doi:10.1038/s41598-020-70179-8

Draxler, R., Stunder, B., Rolph, G., Stein, A., and Taylor, A. (2020). *HYSPLIT User's Guide, Version 5*. Boulder, Colorado, USA: NOAA.

Drinovec, L., Močnik, G., Zotter, P., Prévôt, A. S. H., Ruckstuhl, C., Rupakheti, M., et al. (2015). The "Dual-Spot" Aethalometer: an Improved Measurement of Aerosol Black Carbon with Real-Time Loading Compensation. *Atmos. Meas. Tech.* 8, 1965–1979. doi:10.5194/amt-8-1965-2015

Dumka, U. C., Kaskaoutis, D. G., Devara, P. C. S., Kumar, R., Kumar, S., Tiwari, S., et al. (2019). Year-long Variability of the Fossil Fuel and wood Burning Black Carbon Components at a Rural Site in Southern Delhi Outskirts. *Atmos. Res.* 216, 11–25. doi:10.1016/j.atmosres.2018.09.016

Fadnavis, S., Kalita, G., Kumar, K. R., Gasparini, B., and Li, J.-L. F. (2017). Potential Impact of Carbonaceous Aerosol on the Upper Troposphere and Lower Stratosphere (UTLS) and Precipitation during Asian Summer Monsoon in a Global Model Simulation. *Atmos. Chem. Phys.* 17, 11637–11654. doi:10.5194/acp-17-11637-2017

Fadnavis, S., Sabin, T. P., Rap, A., Müller, R., Kubin, A., and Heinold., B. (2021). The Impact of COVID-19 Lockdown Measures on the Indian Summer Monsoon. *Environ. Res. Lett.* 16 (2021), 074054. doi:10.1088/1748-9326/ac109c

Gautam, S. (2020a). COVID-19: Air Pollution Remains Low as People Stay at home. *Air Qual. Atmos. Health* 13 (May), 853–857. doi:10.1007/s11869-020-00842-6

Gautam, S. (2020b). The Influence of COVID-19 on Air Quality in India: A Boon or Inutile. *Bull. Environ. Contam. Toxicol.* 104 (6), 724–726. doi:10.1007/s00128-020-02877-y

Ghosh, S., and Ghosh, S. (2020). Air Quality during Covid-19 Lockdown: Blessing in Disguise. *Indian J. Biochem. Biophys.* 57, 420–430.

Girach, I. A., Narendra, O., and Sureshbabu, S. (2021). Ozone Chemistry and Dynamics at a Tropical Coastal Site Impacted by the COVID-19 Lockdown. *J. Earth Syst. Sci.* 130, 158. doi:10.1007/s12040-021-01666-3

Gupta, N., Tomar, A., and Kumar, V. (2020). The Effect of Covid-19 Lockdown on the Air Environment in India. *Glob. J. Environ. Sci. Manage.* 6, 31–40.

Harris, J. M., and Kahl, J. D. (1990). A Descriptive Atmospheric Transport Climatology for the Mauna Loa Observatory, Using Clustered Trajectories. *J. Geophys. Res.* 95, 13651–13667. doi:10.1029/jd095id09p13651

He, G., Pan, Y., and Tanaka, T. (2020). The Short-Term Impacts of COVID-19 Lockdown on Urban Air Pollution in China. *Nat. Sustain.* 3, 1005. doi:10.1038/s41893-020-0581-y

Highwood, E. J., and Kinnersley, R. P. (2006). When Smoke Gets in Our Eyes: The Multiple Impacts of Atmospheric Black Carbon on Climate, Air Quality and Health. *Environ. Int.* 32, 560–566. doi:10.1016/j.envint.2005.12.003

IPCC (2017). *Synthesis Report. Contribution of Working Groups I, II and III to the Fourth Assessment Report of the Intergovernmental Panel on Climate Change [Core Writing Team, Pachauri, R.K and Reisinger, A. (eds.)]*. Geneva, Switzerland: IPCC, 104. IPCC 4th Assessment Report.

Jain, S., and Sharma, T. (2020). Social and Travel Lockdown Impact Considering Coronavirus Disease (COVID-19) on Air Quality in Megacities of India: Present Benefits, Future Challenges and Way Forward. *Aerosol Air Qual. Res.* 20, 1222–1236. doi:10.4209/aaqr.2020.04.0171

Kanniah, K. D., Kamarul Zaman, N. A. F., Kaskaoutis, D. G., and Latif, M. T. (2020). COVID-19's Impact on the Atmospheric Environment in the Southeast Asia Region. *Sci. Total Environ.* 736, 139658. doi:10.1016/j.scitotenv.2020.139658

Karuppasamy, M. B., Seshachalam, S., Natesan, U., Ayyamperumal, R., Karuppannan, S., Gopalakrishnan, G., et al. (2020). Air Pollution Improvement and Mortality Rate during COVID-19 Pandemic in India: Global Intersectional Study. *Air Qual. Atmos. Health* 13, 1375–1384. doi:10.1007/s11869-020-00892-w

King, M. D., Kaufman, Y. J., Tanre, D., and Nakajima, T. (1999). Remote Sensing of Tropospheric Aerosols from Space: Past, Present and Future. *Bull. Amer. Meteorol. Soc.* 80 (11). doi:10.1175/1520-0477(1999)080<2229:rsotaf>2.0.co;2

Krotkov, N. A., Lamsal, L. N., Marchenko, S. V., Celarier, E. A., Bucsela, E. J., Swartz, W. H., et al. OMI Core team (2019). *OMI/Aura NO2 Cloud-Screened Total and Tropospheric Column L3 Global Gridded 0.25° X 0.25 ° V3, NASA Goddard Space Flight Center, Goddard Earth Sciences Data and Information*

Services Center (GES DISC). Accessed:29/04/2020. doi:10.5067/Aura/OMI/DATA3007

Lau, K. M., Kim, M. K., and Kim, K. M. (2006). Asian Summer Monsoon Anomalies Induced by Aerosol Direct Forcing: the Role of the Tibetan Plateau. *Clim. Dyn.* 26, 855–864. doi:10.1007/s00382-006-0114-z

Mahato, S., Pal, S., and Ghosh, K. G. (2020). Effect of Lockdown amid COVID-19 Pandemic on Air Quality of the Megacity Delhi, India. *Sci. Total Environ.* 730, 139086. doi:10.1016/j.scitotenv.2020.139086

MoHFW (2020). Ministry of Health and Family Welfare (MoHFW), Government of India. COVID-19 India. Available at: https://www.mohfw.gov.in (Accessed June 9, 2020).

Prasad, A. K., Singh, R. P., and Kafatos, M. (2006). Influence of Coal Based thermal Power Plants on Aerosol Optical Properties in the Indo-Gangetic basin. *Geophys. Res. Lett.* 33 (5). doi:10.1029/2005gl023801

Rajbhandari, B., Phuyal, N., Shrestha, B., and Thapa, M. (2020). Air Medical Evacuation of Nepalese Citizen during Epidemic of COVID-19 from Wuhan to Nepal. *JNMA J. Nepal Med. Assoc.* 58 (222), 125–133. doi:10.31729/jnma.4857

Ranjan, A. K., Patra, A. K., and Gorai, A. K. (2021). A Review on Estimation of Particulate Matter from Satellite-Based Aerosol Optical Depth: Data, Methods, and Challenges. *Asia-pacific J. Atmos. Sci.* 57, 679–699. doi:10.1007/s13143-020-00215-0

Ranjan, A. K., Patra, A. K., Goraia, A. K., and Gorai, A. K. (2020). Effect of Lockdown Due to SARS COVID-19 on Aerosol Optical Depth (AOD) over Urban and Mining Regions in India. *Sci. Total Environ.* 745, 141024. doi:10.1016/j.scitotenv.2020.141024

Rimesh, P., and Urmila, Y. (2020). COVID-19 Pandemic in India: Present Scenario and a Steep Climb Ahead. *J. Prim. Care Community Health* 11, 1–4. doi:10.1177/2150132720939402

Shi, X., and Brasseur, G. P. (2020). The Response in Air Quality to the Reduction of Chinese Economic Activities during the COVID-19 Outbreak. *Geophys. Res. Lett.* 47, e2020GL088070. doi:10.1029/2020GL088070

Sillman, S., Logan, J. A., and Wofsy, S. C. (1990). The Sensitivity of Ozone to Nitrogen Oxides and Hydrocarbons in Regional Ozone Episodes. *J. Geophys. Res.* 95 (D2), 1837–1852. doi:10.1029/JD095iD02p01837

Singh, R. P., and Chauhan, A. (2020). Impact of Lockdown on Air Quality in India during COVID-19 Pandemic. *Air Qual. Atmos. Health* 13, 921–928. doi:10.1007/s11869-020-00863-1

Singh, R. P., Dey, S., Tripathi, S. N., Tare, V., and Holben, B. (2004). Variability of Aerosol Parameters over Kanpur, Northern India. *J. Geophys. Res-atmos.* 109 (D23). doi:10.1029/2004jd004966

Singh, V., Singh, S., Biswal, A., Kesarkar, A. P., Mor, S., and Ravindra, K. (2020). Diurnal and Temporal Changes in Air Pollution during COVID-19 Strict Lockdown over Different Regions of India. *Environ. Pollut.* 266, 115368. doi:10.1016/j.envpol.2020.115368

Sonbawne, S. M., Devara, P. C. S., and Bhoyar, P. D. (2021). Multisite Characterization of Concurrent Black Carbon and Biomass Burning Around COVID-19 Lockdown Period. *Urban Clim.* 39, 100929. doi:10.1016/j.uclim.2021.100929

Soni, M., Ojha, N., and Girach, I. (2021). Impact of COVID-19 Lockdown on Surface Ozone Build-Up at an Urban Site in Western India Based on Photochemical Box Modelling. *Curr. Sci.* 120, 376–381. doi:10.18520/cs/v120/i2/376-381

Srivastava, A. (2020). COVID-19 and Air Pollution and Meteorology-An Intricate Relationship: A Review. *Chemosphere* 263, 128297. doi:10.1016/j.chemosphere.2020.128297

Srivastava, A. K., Bhoyar, P. D., Kanawade, V. P., Devara, P. C. S., Thomas, A., and Soni, V. K. (2021). Improved Air Quality during COVID-19 at an Urban Megacity over the Indo-Gangetic Basin: From Stringent to Relaxed Lockdown Phases. *Urban Clim.* 36, 100791. doi:10.1016/j.uclim.2021.100791

Stohl, A., Eckhardt, S., Forster, C., James, P., Spichtinger, N., and Seibert, P. (2002). A Replacement for Simple Back Trajectory Calculations in the Interpretation of Atmospheric Trace Substance Measurements. *Atmos. Environ.* 36, 4635–4648. doi:10.1016/s1352-2310(02)00416-8

Su, L., Yuan, Z., Fung, J. C. H., and Lau, A. K. H. (2015). A Comparison of HYSPLIT Backward Trajectories Generated from Two GDAS Datasets. *Sci. Total Environ.* 506, 527–537. doi:10.1016/j.scitotenv.2014.11.072

Suglia, S. F., Gryparis, A., Schwartz, J., and Wright, R. J. (2008). Association between Traffic-Related Black Carbon Exposure and Lung Function Among Urban Women. *Environ. Health Perspect.* 16 (10), 1333–1337. doi:10.1289/ehp.11223

Suresh, A., Chauhan, D., Othmani, A., Bhadauria, N., S, A., Jose, J., et al. (2020). Diagnostic Comparison of Changes in Air Quality over China before and during the COVID-19 Pandemic. *Res. Square*. doi:10.21203/rs.3.rs-30482/v1

Tian, W., Chipperfield, P. M., and Lu, D. (2009). Science of the Total Environment. *Adv. Atmos. Sci.* 506-507 (3), 423–437. doi:10.1016/j.scitotenv.2014.11.072

Torres, O., Tanskanen, A., Veihelmann, B., Ahn, C., Braak, R., Bhartia, P. K., et al. (2007). Aerosols and Surface UV Products from Ozone Monitoring Instrument Observations: An Overview. *J. Geophys. Res.* 112, D24S47. doi:10.1029/2007JD008809

Vadrevu, K. P., Eaturu, A., Biswas, S., Lasko, K., Sahu, S., Garg, J. K., et al. (2020). Spatial and Temporal Variations of Air Pollution over 41 Cities of India during the COVID-19 Lockdown Period. *Sci. Rep.* 10, 16574. doi:10.1038/s41598-020-72271-5

Vargas, L. R. Z., Donohoe, A., and Battisti, D. S. (2019). Does Surface Temperature Respond to or Determine Downwelling Longwave Radiation? *Geophys. Res. Lett.* 46, 2781. doi:10.1029/2019gl082220

Zambrano-Monserrate, M. A., Ruano, M. A., and Sanchez-Alcalde, L. (2020). Indirect Effects of COVID-19 on the Environment. *Sci. Total Environ.* 728, 138813. doi:10.1016/j.scitotenv.2020.138813

Conflict of Interest: The authors declare that the research was conducted in the absence of any commercial or financial relationships that could be construed as a potential conflict of interest.

Publisher's Note: All claims expressed in this article are solely those of the authors and do not necessarily represent those of their affiliated organizations, or those of the publisher, the editors, and the reviewers. Any product that may be evaluated in this article, or claim that may be made by its manufacturer, is not guaranteed or endorsed by the publisher.

frontiers | Frontiers in Environmental Science

ORIGINAL RESEARCH
published: 28 April 2022
doi: 10.3389/fenvs.2022.877268

Impact of Meteorological Conditions and Human Activities on Air Quality During the COVID-19 Lockdown in Northeast China

Taihao Wang[1], *Huadong Du*[1], *Zezheng Zhao*[1], *Jiping Zhang*[2] *and Chengjun Zhou*[1,3]*

[1]College of Meteorology and Oceanology, National University of Defense Technology, Changsha, China, [2]Institute of Atmospheric Physics, Chinese Academy Sciences, Beijing, China, [3]Bureau of Audit of Foshan Municipality, Foshan, China

During the lockdown implemented to curb the spread of COVID-19, human activities have drastically reduced, providing a valuable opportunity to study and compare the impact of meteorological conditions and human activities on air quality. In this study, large-scale weather circulation, local meteorological conditions, and the impact of human activities are comprehensively considered, and changes in the concentration of major air pollutants in the northeast during this period are systematically studied. The large-scale weather circulation patterns that mainly affect the northeast region are divided into nine types by using the T-mode Principal components analysis objective circulation classification method. It is found that the northeast region is located at the edge of weak high pressure (Types 1, 2, and 7) and at the rear of high pressure (Type 4) and has higher concentrations of PM2.5, NO_2, SO_2, and CO; in cyclonic weather systems, low vortices (Types 3 and 5) and under the influence of the updraft (Type 6) in front of the trough, the ozone concentration is higher. The changes in the concentrations of PM2.5, NO_2, CO, SO_2, and O_3 in the three cities, namely Shenyang, Changchun, and Harbin, during the lockdown period are compared, and it is found that the concentrations of PM2.5, NO_2, CO, and SO_2 have a tendency to first decrease and then increase, while the changes of O_3 concentration are cyclical and increased significantly during this period. This demonstrates that pollutants such as PM2.5, NO_2, CO, and SO_2 are more susceptible to human activities and local meteorological conditions, and changes in O_3 concentration are more closely related to changes in weather circulation types. Finally, the FLEXPART-WRF model is used to simulate the pollution process of nine circulation types, which confirms that particulate pollution in the northeast is mainly affected by local emissions and local westward sinking airflow.

Keywords: north east China, meteorological condition, t-mode PCA, air pollutants, human activies, FLEXPART-WRF

OPEN ACCESS

Edited by:
Suvarna Sanjeev Fadnavis, Indian Institute of Tropical Meteorology (IITM), India

Reviewed by:
Daniele Contini, Institute of Atmospheric Sciences and Climate (CNR-ISAC), Italy
Sudesh Yadav, Jawaharlal Nehru University, India

***Correspondence:**
Chengjun Zhou
nudt_zcj@foxmail.com

Specialty section:
This article was submitted to Atmosphere and Climate, a section of the journal Frontiers in Environmental Science

Received: *16 February 2022*
Accepted: *01 April 2022*
Published: *28 April 2022*

Citation:
Wang T, Du H, Zhao Z, Zhang J and Zhou C (2022) Impact of Meteorological Conditions and Human Activities on Air Quality During the COVID-19 Lockdown in Northeast China. Front. Environ. Sci. 10:877268. doi: 10.3389/fenvs.2022.877268

1 INTRODUCTION

Since 2020, COVID-19 has spread globally (Jiang and Xu, 2021). Since 23 January 2020, the Chinese government has implemented closed management of cities across the country (China State Council, 2020; Zhao et al., 2020; Sulaymon et al., 2021a). A series of strict control measures, such as reducing large-scale activities, restricting people's transportation, shutting down large factories and

enterprises, and closing schools, has been beneficial in constraining the rapid spread of the disease (Chen S. et al., 2020; Liu et al., 2020; Li et al., 2021; Tian et al., 2020; Zhang et al., 2020; Zhao et al., 2021a). Many studies have also found that these restrictions have greatly improved the local air quality (Chen H. et al., 2020; Mahato et al., 2020; Muhammad et al., 2020; Sulaymon et al., 2021a). Silver et al. (2020) found that the average concentration of pollutants such as NO_2, PM2.5, and PM10 in China during the lockdown period was significantly reduced by 27, 10.5, and 21.4%, respectively. The region with the largest decline was Hubei Province, with NO_2 concentration being 50.5% lower than that expected during the lockdown. Filonchyk et al. (2020) used satellites to monitor changes in the concentration of SO_2, NO_2, CO, and AOD (Aerosol Optical Depth) in Eastern China during this period and found that during the COVID-19 lockdown, CO and NO_2 concentrations in the region decreased by 20 and 30%, respectively, because of strict control of industrial and traffic emissions. Some countries in Europe, North America, and Africa also implemented strict lockdown measures, which reduced the concentration of local pollutants (Xiang et al., 2020; Zambrano-Monserrate et al., 2020; Filonchyk et al., 2021; Mostafa et al., 2021; Skirienė and Stasiškienė, 2021). Tobías et al. (2020) found that in Spain, the concentration of pollutants such as NO_2 and PM10 decreased considerably during the lockdown. Berman and Ebisu, (2020) showed that the PM2.5 concentrations declined in the counties in the United States that implemented strict lockdown measures. Venter and Kristin, (2020) showed that isolation measures reduced the concentration of NO_2 and particulate matter in 34 countries and regions by approximately 60 and 31%, respectively, and that the effect on ozone was mixed. Dinoi et al., 2021 showed that different percentage reductions in atmospheric nanoparticle concentrations are observed, −19% and −23% in Lecce and −7% and −4% in Lamezia Terme in southern Italy during lockdown and postlockdown, respectively. However, some studies have found that the concentration of pollutants sometimes increased abnormally during the lockdown (Broomandi et al., 2020; Dai et al., 2020; Liu et al., 2020; Wang et al., 2020; Zhao X. et al., 2021; Hong et al., 2021; Li et al., 2021). Sulaymon et al. (2021b) studied the changes in air quality during the pandemic in the Beijing-Tianjin-Hebei region of China and found that unfavourable weather conditions during the COVID-19 lockdown led to increasing PM2.5 pollution in this region. Hong et al. (2021) studied the changes in the concentration of pollutants along the southeast coast of China during this period and found that although traffic, dust, and industrial emissions decreased significantly by 9, 8.5, and 8%, respectively, the O_3 concentration increased by 28.1% compared with that during the same period in 2019. Liu et al. (2020) studied the changes in air quality during the pandemic in the Yangtze River Delta and found that a significant increase in ozone concentration during the lockdown was caused by emission reduction (29–52%) and changes in meteorological conditions (17–49%). The increase in ozone concentration accelerates the formation of secondary aerosols. Shen et al. (2021) studied the impact of meteorological conditions on air pollution changes in Hubei, China, during the COVID-19 lockdown and found that abnormal vertical wind divergence and northeasterly winds contributed to the serious PM2.5 pollution. Most studies have only considered changes in the concentration of pollutants during the pandemic caused by local meteorological conditions or human activities (Chang et al., 2020; Huang et al., 2020; Shi and Brasseur, 2020). However, a few studies have combined large-scale weather circulation, local meteorological conditions, and meteorological factors and comprehensively considered the effects of human activities.

Northeast China is China's heavy industry base (Li et al., 2015; Zhao et al., 2017), and biomass burning frequently occurs (Li et al., 2019; Cheng et al., 2021). This region witnesses a serious air pollution problem all year round (Ma et al., 2018; Li et al., 2019). The present study focuses on the relationship among air quality, weather conditions, and human activities in Northeast China during the lockdown implemented to control the pandemic. First, the T-PCA method is used to divide the synoptic circulation patterns in the northeast region into nine types, analyse the corresponding local meteorological conditions under each circulation type, and discuss the effects of circulation patterns and local weather conditions on changes in the concentration of main pollutants, namely PM2.5, O_3, NO_2, SO_2, and CO. Then, based on the proportion of circulation patterns in Northeast China from January to April during 2016–2020 (defined as specific period, SP, same below), the changes in pollutant concentration during the SP period are discussed. Further, the 2020 pandemic lockdown phase is divided into three periods, before control (BC) unblocked, under control (UC) strictly blocked, and after control (AC) restricted activity period. The main circulation patterns in the three periods are analysed and the causes of abnormal large-scale air pollution during the epidemic in Northeast China are discussed, combining the changes in pollutant concentrations in the three periods. Finally, nine severe pollution events with PM2.5 concentrations exceeding the national secondary standard (75 $\mu g/m^3$) under nine circulation patterns are screened, and the backward plume trajectory is simulated using the FLEXPART-WRF model to analyse the characteristics of pollutant transmission.

2 DATA, METHOD, AND MODEL

2.1 Data

2.1.1 Meteorological Data

In this study, we use the fifth-generation atmospheric reanalysis data ERA5 data set developed by ECMWF to perform circulation classification, with a horizontal resolution of 0.25 × 0.25. The sea level pressure field of 500 hPa, geopotential height field of 850 hPa, and wind field at 00:00 UTC time by day from 1979 to 2020 are used to determine the daily circulation pattern. The space range is 25–60° N, 105–140° E. To analyse the local meteorological conditions during the study period (2016–2020) in the northeast region, we use hourly wind field, humidity, and temperature data from meteorological observatories in Harbin, Changchun, and Shenyang to compare the local meteorological conditions, which are

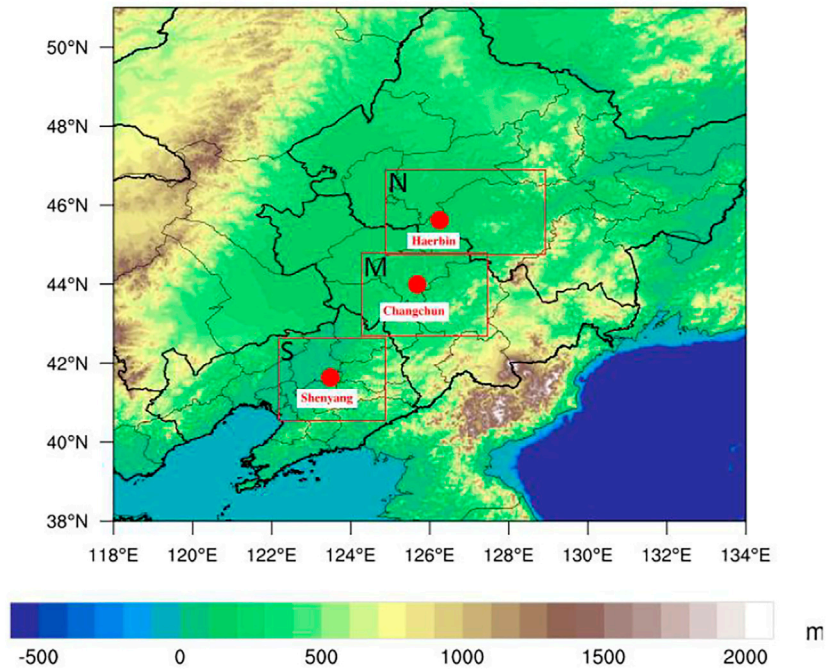

FIGURE 1 | Research area and surrounding terrain.

obtained from the National Climate Data Center (ftp://ftp.ncdc.noaa.gov/pub/data/noaa/) under the National Oceanic and Atmospheric Administration of the United States. The observatories are Harbin Taiping Airport, Changchun Longjia Airport and Shenyang Taoxian Airport, respectively.

2.1.2 Air Quality Data

Air pollution data are obtained from the China Environmental Monitoring website (http://www.cnemc.cn). Station-wise data are released after quality control by the environmental protection department. In this study, the 24 h average concentration data of PM2.5, NO_2, SO_2, and CO and the daily maximum 8 h average (MDA8) ozone concentration from 30 monitoring sites in Northeast China in Harbin, Changchun, and Shenyang are used. We also use the daily PM2.5 concentration data (Geng et al., 2021) in the near real-time tracking data set (TAP) of China's atmospheric composition (spatial range: 25–60° N, 105–140° E; horizontal resolution = 10 km) to reflect the spatial distribution characteristics of pollutants when serious pollution occurs under each circulation pattern during lockdown and to verify the results of the backward simulation of the pollutant particle trajectory. The data set incorporates ground observations, satellite remote sensing, emission inventories, model simulations, and other multi-source data (Xiao et al., 2021a, 2021b) that can more accurately reflect the pollution status of the study area.

2.1.3 Study Area

To study the temporal and spatial distribution and change characteristics of the concentration of major atmospheric pollutants during the epidemic blockade, in this study, the northeast region is divided into three regions, namely Harbin (Northern N), Changchun (Middle M), and Shenyang (Southern S). All three regions include elements such as mountains, industrial areas, major cities, villages, and grasslands, and thus can represent the local meteorological conditions and the characteristics of the temporal and spatial distribution of pollutants in the northeast. The scope of the three regions and the surrounding topography are shown in **Figure 1**.

2.2 Circulation Classification Method

To obtain an accurate and stable weather circulation pattern that affects Northeast China, we use the T-PCA method proposed by Huth et al. (2008) to classify the large-scale weather circulation in the northeast. Assuming that the parameter dependence is small, this method is widely used in the analysis of the impact of large-scale weather circulation on pollutants (Compagnucci and Richman, 2008; Zhou et al., 2018; Zhou et al., 2019; Zhao et al., 2019; Zhao et al., 2021b; Wang et al., 2022). Herein, sea level pressure field of 850 hPa and wind field and altitude field of 500 hPa are used to comprehensively and accurately explore the weather types that mainly affect this region. We use the COST733 mode software package based on the FORTRAN language, and the specific usage has been presented in detail in other studies (Yan et al., 2021; Zhang et al., 2018; Philipp et al., 2010; Philipp et al., 2014). Zhang et al. (2012) proved that circulation patterns are generally divided into nine types in the mid-high latitudes of the northern hemisphere; a similar classification method is adopted in this study.

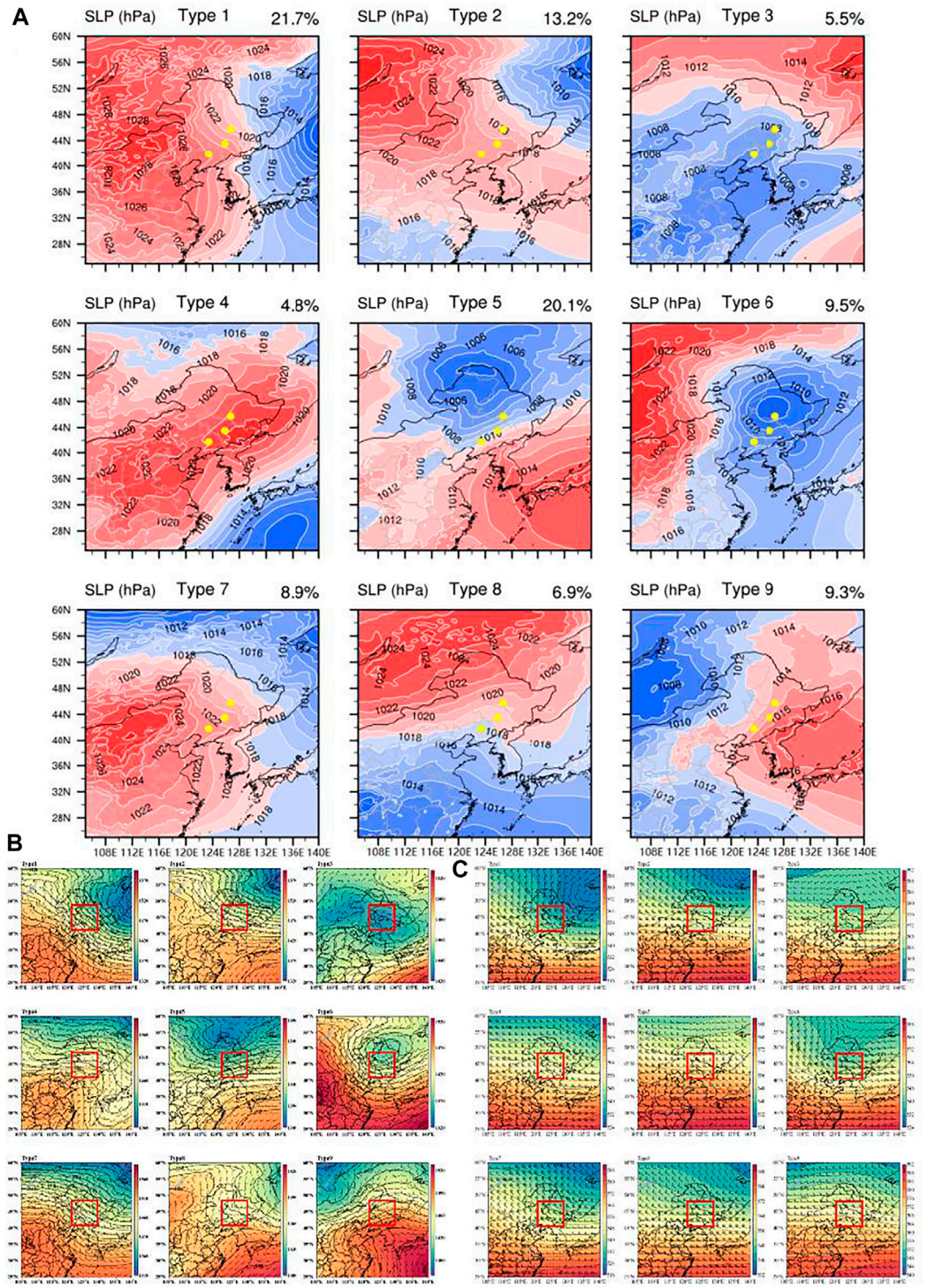

FIGURE 2 | (A–C) Nine main weather circulation types (SLP) affecting the northeast, 850 hPa geopotential height field and wind field, and 500 hPa geopotential height field and wind field.

2.3 Parameterisation Scheme of the WRF and FLEXPART-WRF Models

The WRF model can provide accurate weather field variables for the FLEXPART-WRF model in particle trajectory simulation. In this simulation, we use two nests; the first nesting is 15×15 km^2 in horizontal resolution, covering the entire eastern part of China, and the second nesting is 4×4 km^2, covering the entire northeast region. The main parameterisation schemes are Mellor-Yamada-

Janjic (Eta) TKE boundary layer parameterisation scheme, Noah land surface scheme (Chen et al., 2006), WSM 3-class simple ice scheme (Hong et al., 2004), Kain-Fritsch (new Eta) Cumulus convection parameterisation scheme (Kain, 2004), Monin-Obukhov (Janjic Eta) surface layer scheme (Nakanishi and Niino, 2006), RRTM longwave radiation scheme (Mlawer et al., 1997), and Dudhia shortwave radiation scheme (Dudhia, 1989). The initial and boundary conditions of the model use fnl (Final) Operational Global Analysis 6-h data per day (horizontal resolution 0.25°×0.25°) from the National Centers for Environmental Prediction (NCEP), and the model outputs the results every 30 min.

Furthermore, we use the FLEXPART-WRF version 3.3 of the Lagrangian particle diffusion model (Brioude et al., 2013) that uses the function of backward simulation of particle trajectory. Because Changchun is located in the middle of the northeast, it is more susceptible to pollution particles from the south, north, and surrounding areas; therefore, the Changchun area (143.35N, 43.88E) is selected as the particle release point. The model releases particles uniformly every 1 h during the nine types of simulation periods (24 h) in Changchun area; overall, 50,000 particles are released throughout the simulation period. A total of five layers of vertical stratification (10, 100, 500, 1,000, and 5,000 m) are set up. The release height of particle clusters is 10–1,000 m, and the horizontal resolution is 0.125 × 0.125. The model comprehensively considers the processes of release transmission, turbulent diffusion, and dry and wet sedimentation and simulates the dispersion and aggregation of particles, possible source distributions, and other conditions by calculating the backward transmission trajectory of large-scale particles. In this study, we superimpose the 48-h plume trajectories of particles under several circulation patterns (Zhang et al., 2012; Shen et al., 2021) to obtain a comprehensive distribution, which helps analyse the source of pollutants and factors affecting the diffusion of pollutants.

3 RELATIONSHIP BETWEEN CIRCULATION TYPES AND POLLUTANTS IN NORTHEAST CHINA

3.1 Circulation Classification Results

Figures 2A–C shows the nine main weather circulation patterns, with geopotential height fields and wind fields of 850 hPa and 500 hPa, respectively, that affect the northeast region of China. According to the ground circulation characteristics, the nine circulation types are classified as follows: Type 1 (western high-pressure type), Type 2 (northwest high-pressure type), Type 3 (northeast high-pressure type, weak pressure gradient), Type 4 (high-pressure type), Type 5 (northern low pressure, southeast high-pressure type), Type 6 (low pressure type), Type 7 (southwest high-pressure type), Type 8 (northern high-pressure type), and Type 9 (eastern high-pressure type). **Figure 2** shows that the main types of circulation affecting the study region are Type 1 (21.7%) and Type 5 (20.1%) followed by Type 2 (13.2%).

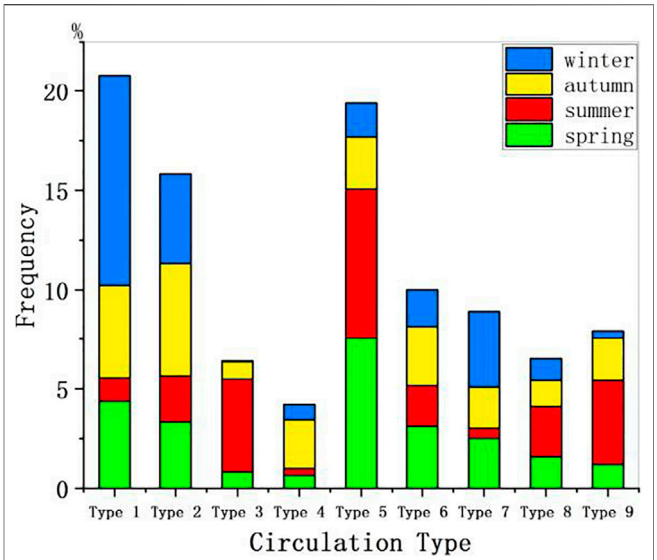

FIGURE 3 | Seasonal distribution of nine circulation patterns in Northeast China during 2016–2020.

Types 1, 2, 4, and 7 are mainly related to the activities of cold high pressure. Under Type 1 and 7 control, the high-pressure centre is located in the west of the northeast region. Under Type 2 control, cold high pressure has not yet entered the territory of China, which is far from the northeast region. Type 4 controls the lower northeast region and is located behind the cold high pressure; it is closest to the high-pressure centre. Under the control of Types 3, 5, and 9, the West Pacific subtropical high extends from the west to the north and affects most of China. At the same time, the lower northeast of Types 3 and 5 is also affected by the low vortex. Under Type 6, the northeast region is often affected by high-altitude troughs and cyclones. At this time, the northeast region is often in front of the trough. The northeast area under the control of Type 8 is affected by both cold high pressure and subtropical high; thus, cold high pressure has a considerable influence on the northeast area.

3.2 Seasonal Characteristics, Local Meteorological Characteristics of the Nine Circulation Types, and Their Relationship With the Concentration of Major Air Pollutants

Figures 3, **4** show the seasonal distribution of nine circulation types and the corresponding local wind fields in Northeast China. **Figure 5** shows the relationship between the concentration of five major pollutants (PM2.5, O_3, NO_2, CO, and SO_2) and the circulation types in Harbin, Changchun, and Shenyang. The distributions of the five air pollutants under the nine circulation types in Changchun, Harbin, and Shenyang are relatively consistent. **Table 1** shows the average values of the concentrations of these five pollutants under nine circulation types, as well as the average values of temperature, relative humidity, and wind speed, in these three cities. **Figures 3–5**

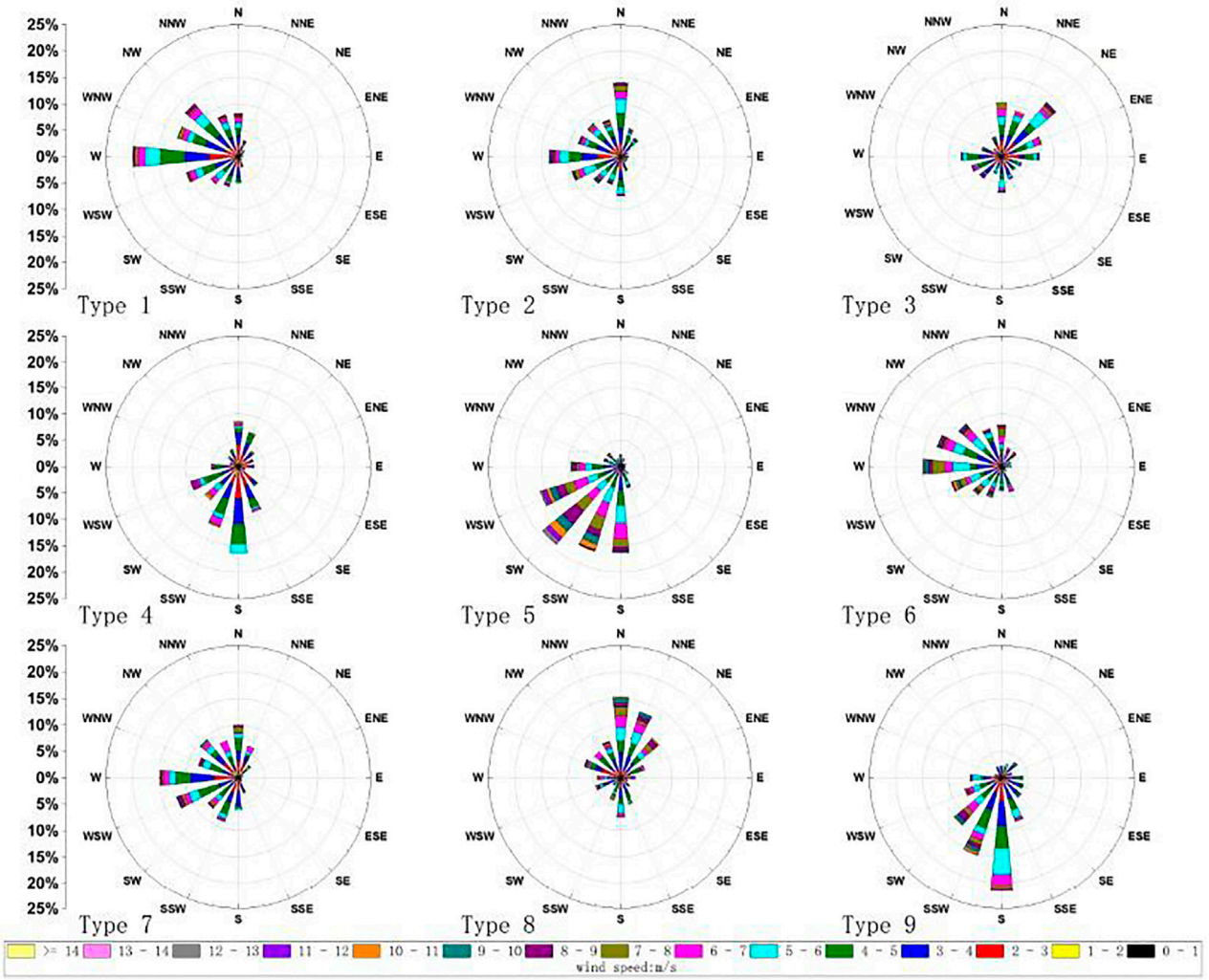

FIGURE 4 | A wind rose of the local wind field corresponding to the nine circulation types in Northeast China during 2016–2020.

and **Table 1** show that Types 1, 2, 4, and 7 mainly appear in winter and autumn. At this time, the northeast region is cold and dry (average temperatures are −0.26 , 7.35, 10.68, and 4.08 ˚C under Types 1, 2, 4 and 7 respectively, and the corresponding average relative humidity percentages are 40.65, 45.36, 43.74, and 42.25% under Types 1, 2, 4 and 7 respectively), the local wind field is characterised by weak southwesterly and northerly winds (average wind speed = 2.62 m/s, 2.77 m/s, 2.12 m/s, 2.12 m/s, and 2.59 m/s). In the meanwhile, Compared with summer, the atmosphere is more prone to static stability in autumn and winter (Zhou et al., 2019). Therefore, the diffusion conditions are poor, which is not conducive to the diffusion and transmission of pollutants, and the accumulation of pollutants is likely to occur under the control of Types 1, 2, 4, and 7. The concentrations of PM2.5, NO_2, SO_2, and CO under these types of circulation are relatively high (the average concentrations are as follows: PM2.5–47.8 μg/m^3, 51.5 μg/m^3, 56.3 μg/m^3, and 57.1 μg/m^3, NO_2 −39.4 μg/m^3, 38.8 μg/m^3, 46.6 μg/m^3, and 42.1 μg/m^3, SO_2 −33.01 μg/m^3, 30.07 μg/m^3, 31.58 μg/m^3, and 32.01 μg/m^3, and CO −0.92 mg/m^3, 0.93 mg/m^3, 1.15 mg/m^3, and 1.01 mg/m^3). Type 3 has obvious summer characteristics (high temperature and high humidity), with an average temperature of 23.85 ˚C and an average relative humidity of 57.29%. The region is dominated by strong northeast winds (average wind speed = 3.51 m/s), which is conducive to the diffusion and transmission of pollutants. PM2.5, NO_2, SO_2, and CO concentrations are extremely low (22.5 μg/m^3, 29.6 μg/m^3, 9.8 μg/m^3, and 0.635 mg/m^3, respectively), but at this time, O_3 concentration is very high (97.2 μg/m^3). Type 6 often occurs in spring and autumn. Due to the westerly wind (average wind speed = 4.58 m/s) in front of the trough, pollutants cannot accumulate easily. Simultaneously, the convection is prone to precipitation, which is conducive to the deposition of pollutants. At this time, the concentrations of PM2.5, NO_2, SO_2, and CO are relatively low (38.2 μg/m^3, 31.3 μg/m^3, 18.9 μg/m^3, and 0.86 mg/m^3), but O_3 concentration is high (86.9 μg/m^3). Types 5 and 9 mainly appear in summer and spring. The local wind field in the northeast under Type 5 is dominated by strong southwest wind (average wind speed =

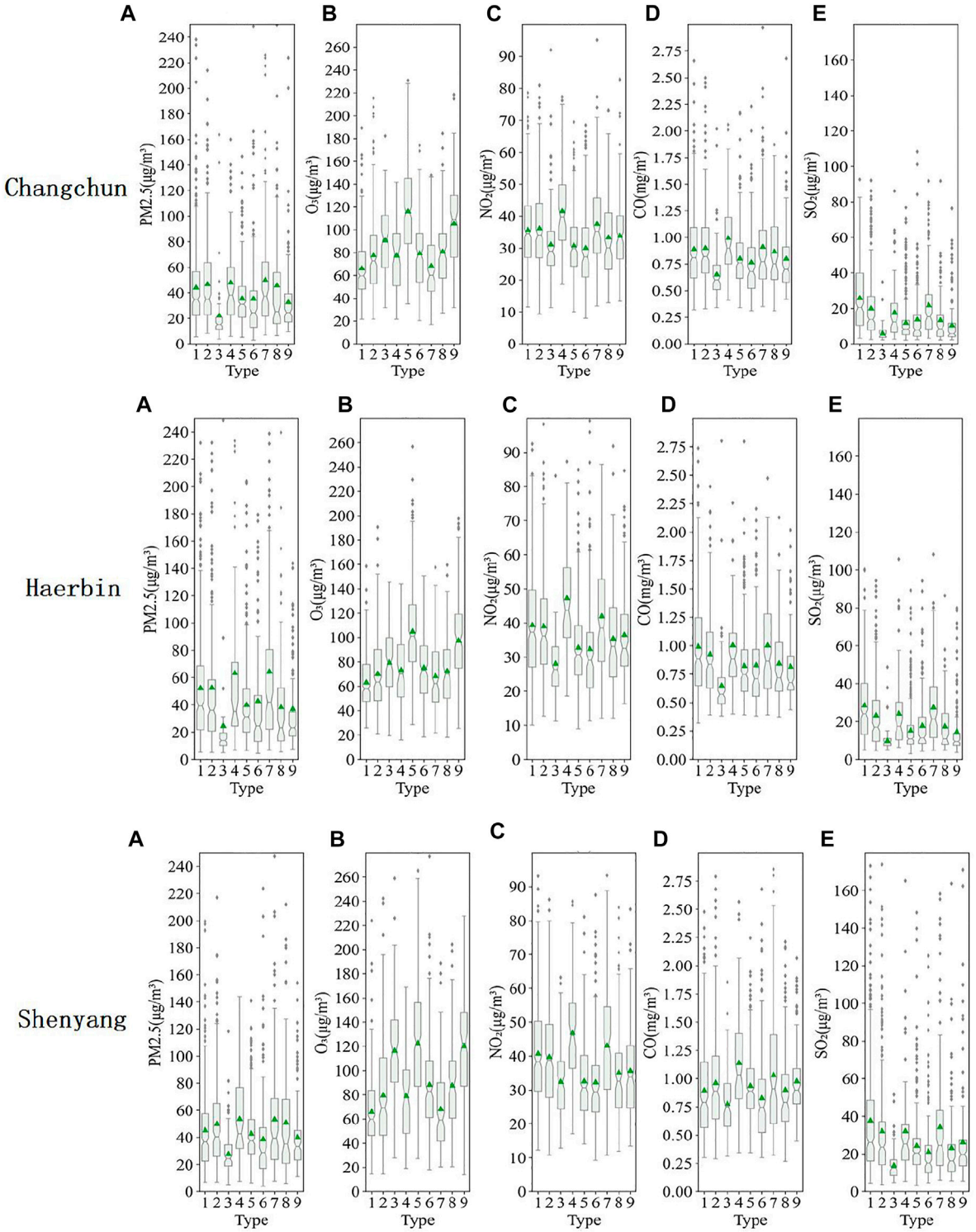

FIGURE 5 | Relationship between the nine circulation patterns and the concentration of major air pollutants in Changchun, Harbin, and Shenyang; the triangle represents the average concentration, the short line represents the median concentration of pollutants, the upper short line of the box represents the third-quarter value, and the lower short line of the box represents the quarter-quarter value.

TABLE 1 | Average concentrations of the five major atmospheric pollutants (PM2.5, O_3, NO_2, SO_2, and CO) of the nine circulation types in Northeast China, and values of local meteorological elements (temperature, relative humidity, and average wind speed) during 2016–2020.

Circulation Type	Concentration of Pollutants					Meteorological Factors		
	PM2.5 (μg/m^3)	O_3 (μg/m^3)	NO_2(μg/m^3)	SO_2(μg/m^3)	CO(mg/m^3)	Temperature (°C)	Relative Humidity (%)	Wind Speed (m/s)
Type 1	47.8	64.3	39.4	33.01	0.92	-0.26	40.65	2.62
Type 2	51.5	76.4	38.8	30.07	0.93	7.35	45.36	2.77
Type 3	22.5	97.2	29.6	9.80	0.64	23.85	57.29	3.51
Type 4	56.3	77.2	46.6	31.58	1.15	10.68	43.74	2.12
Type 5	40.1	113.4	31.5	18.10	0.85	20.17	47.13	5.40
Type 6	38.2	86.9	31.3	18.90	0.86	11.62	53.13	4.58
Type 7	57.1	71.1	42.1	32.01	1.01	4.08	42.25	2.59
Type 8	44.2	81.5	33.4	18.89	0.89	13.30	61.27	3.99
Type 9	39.2	108.9	34.5	17.8	0.84	22.06	51.91	3.84

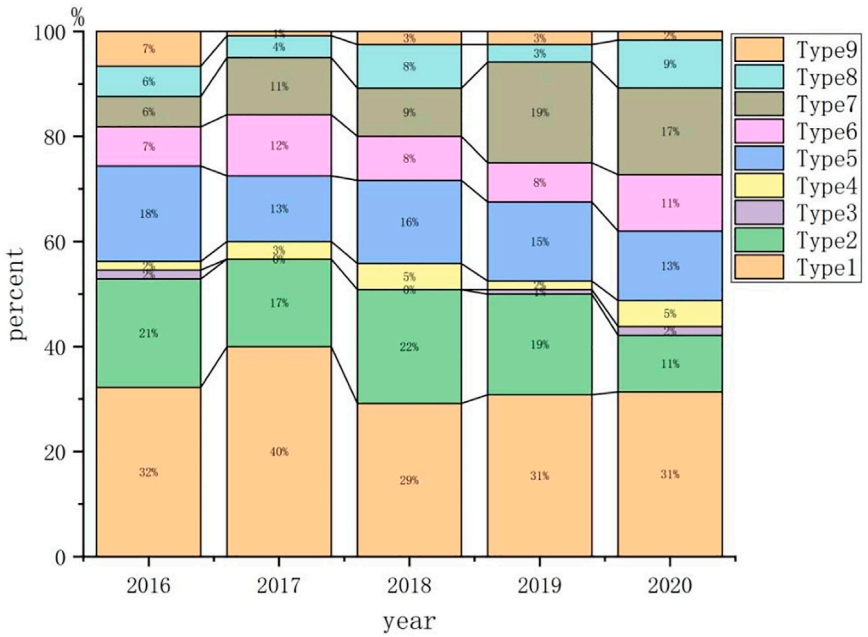

FIGURE 6 | Proportions and changing trends of the nine circulation patterns during the SP period.

5.4 m/s), with high temperature and humidity (20.17 °C and 47.13%, respectively) and convective development. Because of vigorous and good diffusion conditions, pollutants do not easily accumulate (the average concentrations of PM2.5, NO_2, SO_2, and CO are 40.1 μg/m^3, 31.5 μg/m^3, 18.1 μg/m^3, and 0.85 mg/m^3, respectively). The warm and humid airflow in the south brought by the subtropical high under Type 9 control is strong (average wind speed = 3.84 m/s), which is conducive to the diffusion of particulate pollutants, and the concentrations of PM2.5, NO_2, SO_2, and CO are relatively low (39.2 μg/m^3, 34.5 μg/m^3, 17.8 μg/m^3, and 0.84 mg/m^3), but O_3 concentration is higher under the above two types of circulations (113.4 μg/m^3 and 108.9 μg/m^3, respectively).

Based on the aforementioned analysis, we draw the following conclusions: under the control of Types 1, 2, 4, and 7, the concentrations of PM2.5, NO_2, SO_2, and CO in the northeast are all high, while under the control of Types 3, 5, 6, and 9, the concentrations of PM2.5, NO_2, SO_2, and CO are maintained at relatively low levels. O_3 concentration distribution is different from other that of pollutants. O_3 concentration is high under the control of Types 3, 5, 6, and 9, whereas it is low under the control of Types 1, 2, 4, and 7.

4 CHANGES IN THE CONCENTRATION OF POLLUTANTS IN NORTHEAST CHINA DURING COVID-19

4.1 Changes in Circulation Types and Air Quality During the SP

Figure 6 shows the proportions of the nine main circulation patterns during the SP, which were rather similar. The main

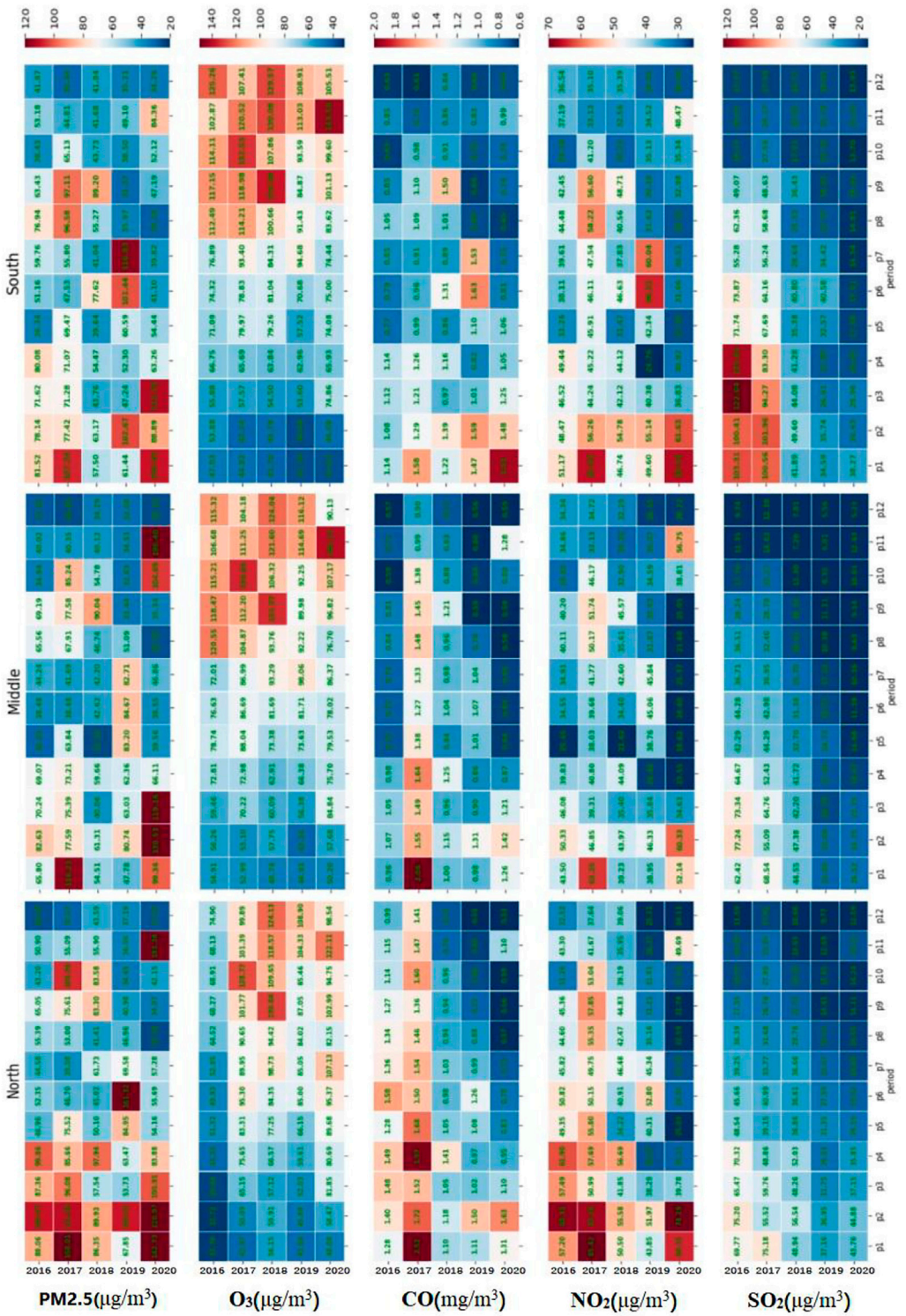

FIGURE 7 | Heat map of the changes in the concentration of the five main pollutants during the SP. The north is Harbin, the middle is Changchun, and the south is Shenyang. The green numbers indicate the average pollutant concentration.

circulation patterns are Type 1, 2, 5, and 7, indicating that the weather-scale circulation affecting the northeast region during January–April is relatively stable. Comparing the analysis in **Section 3.1**, we find that Types 1, 2, and 7 respectively represent the three locations of cold high pressure affecting the northeast region, which is more consistent with the

TABLE 2 | Change rate of PM2.5, NO_2, SO_2, CO, and O_3 pollutant concentrations during UC in 2020 compared with the same period in 2016–2019.

Pollutant	Change Ratio (UC)			
	Changchun	Shenyang	Harbin	Average
PM2.5	−29.70%	−31.39%	−23.70%	−28.24%
O_3	−5.70%	−8.04%	6.45%	−2.43%
NO_2	−40.54%	−31.49%	−45.90%	−39.31%
SO_2	−62.51%	−65.48%	−38.47%	−55.49%
CO	−37.50%	−19.42%	−43.20%	−33.37%

climatic characteristics of the northeast region during January–April. In spring (March–May), with the appearance of the northeast cold vortex and the northward uplift of the subtropical high, Type 5 appears more frequently (accounting for 13–18%).

Figure 7 shows the concentration changes of the five main pollutants during the SP. The abscissa p1–p12 indicate that the January–April period is divided into 12 periods. Among these, p1–p3 correspond to BC, p4–p9 correspond to UC, and p10–p12 correspond to AC. At the same time, the average concentration change rate (R) is defined as the ratio of the difference (between the average pollutant concentration in 2020 under each circulation pattern and the average pollutant concentration under the same circulation pattern during 2016–2019) and the average concentration of pollutants under the same circulation pattern during 2016–2019. $R > 0$ means increase, and $R < 0$ means decrease; a large absolute value of R implies an obvious change, and vice versa. In this study, the circulation type during the lockdown period is roughly the same as in the same period in 2016–2019, although the human activity is substantially reduced. Therefore, the average concentration change rate R can reflect the degree to which meteorological conditions and human activities affect air quality in the region. Greater absolute value of the average concentration change rate R implies greater impact of human activities on the concentration of these pollutants, and the converse, that is, greater impact of circulation conditions on the concentration of these pollutants is also true. **Table 2** shows the change rates of PM2.5, NO_2, SO_2, CO, and O_3 pollutant concentrations during UC in 2020 compared with the same period in 2016–2019. **Table 3** shows the average concentration change rate R of PM2.5 and O_3 under nine circulation patterns. **Figure 7**; **Table 2** show that the PM2.5 concentration of the three cities during the UC period decreased by 31.39, 29.7, and 23.7% from the average for the same period during 2016–2019 (average decrease of the three cities = 28.24%). The change trend of NO_2, CO, and SO_2 concentrations is similar to that of PM2.5, and their concentrations also declined significantly during the UC period (the average change rates are −39.31%, −33.37%, and −55.49%, respectively). This shows that the industrial, transportation, and agricultural emissions during the UC period decreased significantly compared with the same period during 2016–2019, resulting in a decrease in PM2.5, NO_2, SO_2, and CO concentrations. Human activities significantly impacted the concentration changes of these pollutants. **Table 3** shows that the absolute value of the change rate R of the average PM2.5 concentration under the nine circulation patterns is very large, indicating that the PM2.5 concentration responds more strongly to human activities. The change trend of O_3 concentration during the SP is almost the same and shows some regularity. During the UC period in 2020, the change rate of O_3 concentration during the same period during 2016–2019 is only −2.43%. Additionally, **Table 3** shows that the absolute value of the change rate R of the average O_3 concentration is relatively small, indicating that although O_3 concentration is affected by human activities and weather conditions, it is more susceptible to weather circulation conditions compared to PM2.5 concentration.

4.2 Changes of Air Quality in BC, UC, and AC Stages

Figure 8 shows the proportion of each circulation pattern under BC, UC, and AC. In the BC stage, the northeast region is mainly influenced by Types 1, 2, 4, and 7 (accounting for 32.3, 19.4, 12.9, and 22.6%, respectively), whereas in the UC stage, it is mainly influenced by Types 1, 2, 5, and 7 (accounting for 26.7, 11.7, 20, and 20%, respectively). The main circulation patterns of the BC and UC stages are not much different. In the AC phase, the circulation patterns affecting the northeast are Types 1, 5, 6, and 8 (40, 10, 30, and 10%, respectively), which are significantly different from the BC and UC phases. During the entire lockdown period, the total proportions of Types 1, 2, 4, and 7 gradually decrease over time (87.2, 61.2, and 43.3% in BC, UC, and AC, respectively). This shows that from winter to spring, the influence of cold high pressure on the northeast region gradually weakens. In the spring, the northeast cold vortex and cyclone systems frequently appear, and the subtropical high moves northward. Therefore, the total proportions of Types 3, 5, 6, and 9 related to these conditions during BC, UC, and AC also gradually increase (3.2, 30, and 46.7%, respectively). As mentioned in **Section 3.2**, the appearance of the aforementioned four circulation patterns is also related to the increase in O_3 concentration.

Figure 9 shows the changes in the concentration of the five major pollutants between BC and UC stages and between UC

TABLE 3 | Average concentration change rate R of PM2.5 and O_3 under nine circulation types.

Pollutant	Circulation Type								
	Type 1 (%)	Type 2	Type 3 (%)	Type 4	Type 5	Type 6	Type 7 (%)	Type 8	Type 9
PM2.5	11.54	4.36%	196.61	52.37%	−20.56%	−20.60%	8.19	12.87%	−17.28%
O_3	11.2	−8.3%	23.1	−12.8	-3.1%	8.6%	1.9	−6.3%	−4.5%

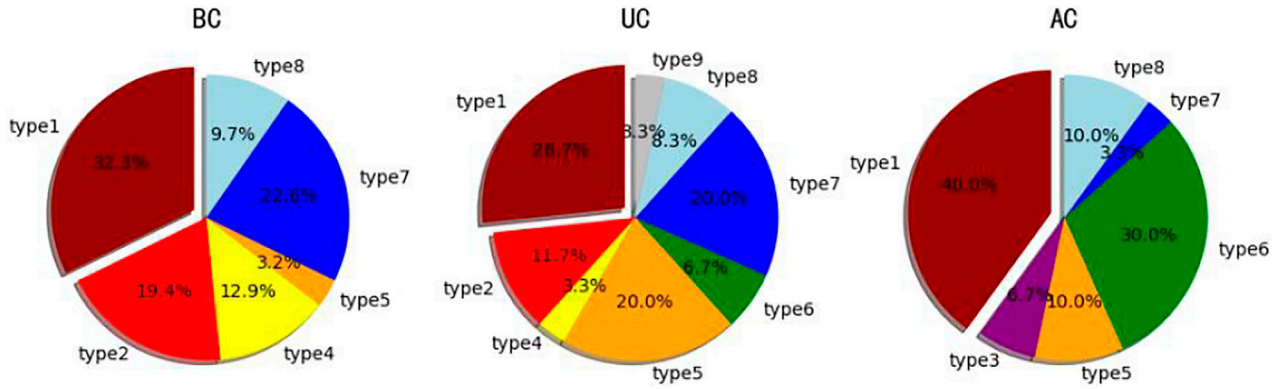

FIGURE 8 | Proportion of the nine circulation types in the BC, UC, and AC stages.

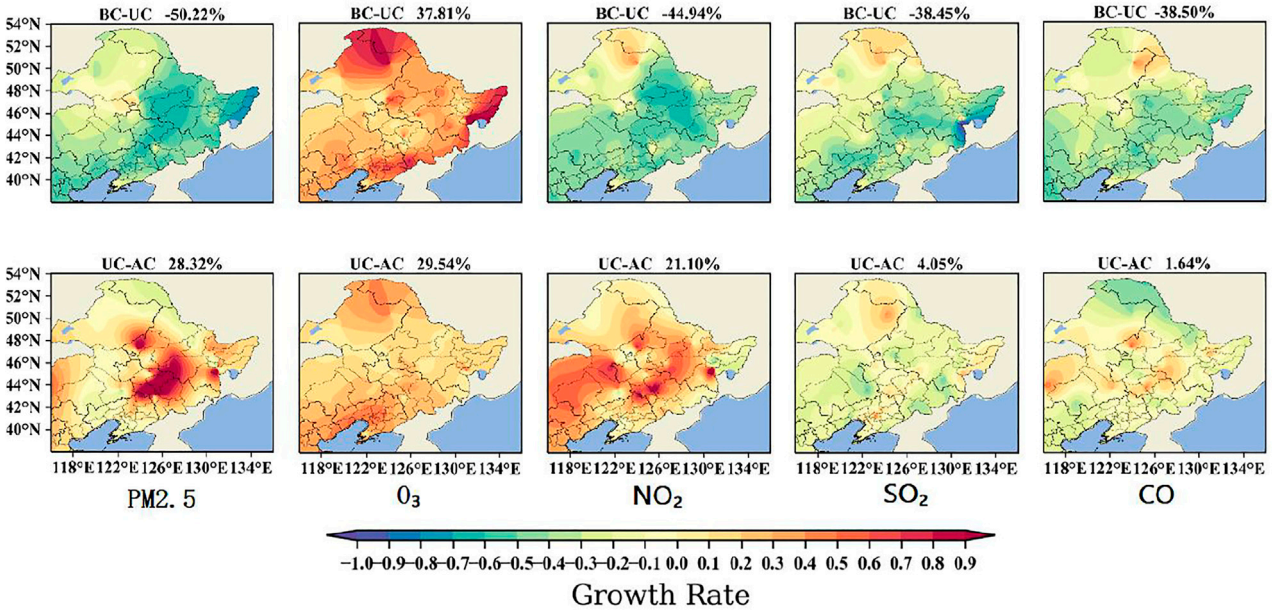

FIGURE 9 | Spatial distribution of the concentration change rates of the five main pollutants in the BC-UC and UC-AC phases during the lockdown period in 2020.

and AC stages in Northeast China in 2020. As illustrated in **Figures 8**, **9**, although the proportion of Types 1, 2, 4, and 7 decreased from 87 to 43.3% from the BC stage to the AC stage in 2020, the PM2.5 concentration did not consistently decrease; it first increased and then decrease, that is, due to curtailed human activities, the PM2.5 concentration considerably decreased from the BC stage to the UC stage (average rate of change = −50.22%). From the UC stage to the AC stage, some restrictions on human activities were lifted, and therefore, the PM2.5 concentration increased and showed a wide range (average rate of change = 28.32%). When the proportions of Types 3, 5, 6, and 9 corresponding to high ozone concentration increase, the O_3 concentration shows an increasing trend from the BC stage to the UC stage and from the UC stage to the AC stage (the change rates are 37.81 and 29.54%, respectively). However, the increase rate from the BC stage to the UC stage is significantly higher than the increase rate from the UC stage to the AC stage. This is because PM2.5 decreased from the BC stage to the UC stage, the shading rate decreased, and the radiation enhanced, which promoted the photochemical reactions, generating large amounts of O_3 while consuming large amounts of NO_2. The concentrations of NO_2, CO, and SO_2 showed similar trend as that of PM2.5, decreasing considerably during the UC stage (the change rates are −44.94%, −38.5% and −38.45%, respectively). However, during the AC stage, these values showed an increasing trend, with the average increase rates of 21.1, 4.05, and 1.64%, respectively.

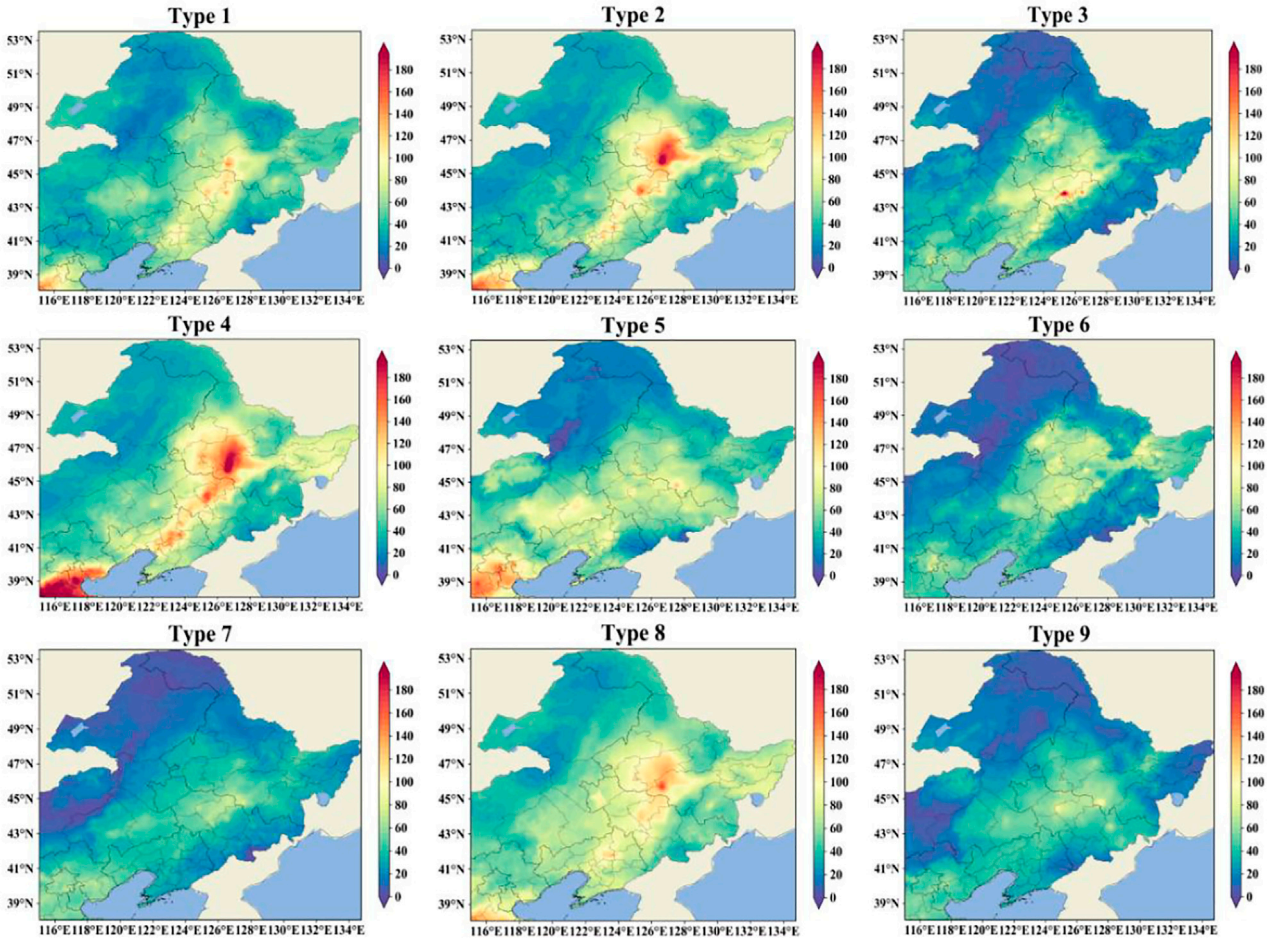

FIGURE 10 | Distribution characteristics of PM2.5 concentration during severe pollution periods under nine circulation types.

In summary, curtailing human activities during the lockdown only slightly impacted the concentration changes of O_3, and it was mainly affected by the large-scale circulation conditions. The concentrations of PM2.5, NO_2, SO_2, and CO, however, were greatly affected by the curtailed human activity during the lockdown.

4.3 Numerical Simulation Study on the Source of Particulate Matter During the Pandemic in Northeast China

To study the source and transmission path of the main pollutants during the lockdown period in 2020 in the northeast, Changchun City, located in the central part of this region, was selected for the simulation study of pollutant particle trajectory. The time periods when the average daily PM2.5 concentration during the lockdown period of COVID-19 was >75 μg/m^3 were determined, and these periods were classified according to the circulation type. A 24-h backward trajectory simulation analysis was carried out to characterise the pollutant trajectory of each period under each circulation pattern.

Figure 10 shows the distribution of PM2.5 concentration corresponding to heavy pollution periods under the nine circulation patterns based on TAP data. **Figure 11** shows the backward plume trajectory of pollutant particles in nine circulation patterns.

Figures 10, **11** show that under Type 1, pollutants exist in North China and the eastern part of Northeast China. However, the pollutants in Changchun are from the western part of Changchun. The heavily polluted areas under Type 2 are in Northeast and North China, and PM2.5 pollutants in Changchun come from the northwest mountains. The distribution of pollutants under Type 3 is concentrated around Changchun, and the pollutants transmitted over long distances mainly come from the mountainous areas in northern North Korea. The heavily polluted area under Type 4 appears on a heavily polluted zone in the northeast-southwest direction centred on the Harbin–Changchun–Shenyang region. The pollutants that affect Changchun mainly come from the surrounding areas such as southwest of Changchun. The particulate matter under Type 5 mainly travels long-distance from North China, Liaodong Peninsula, and northern Korean Peninsula. Under Type 6, there is considerable pollution in the northern part of Heilongjiang, and the particulate matter comes from the northwest part of Northeast China and the Liaodong

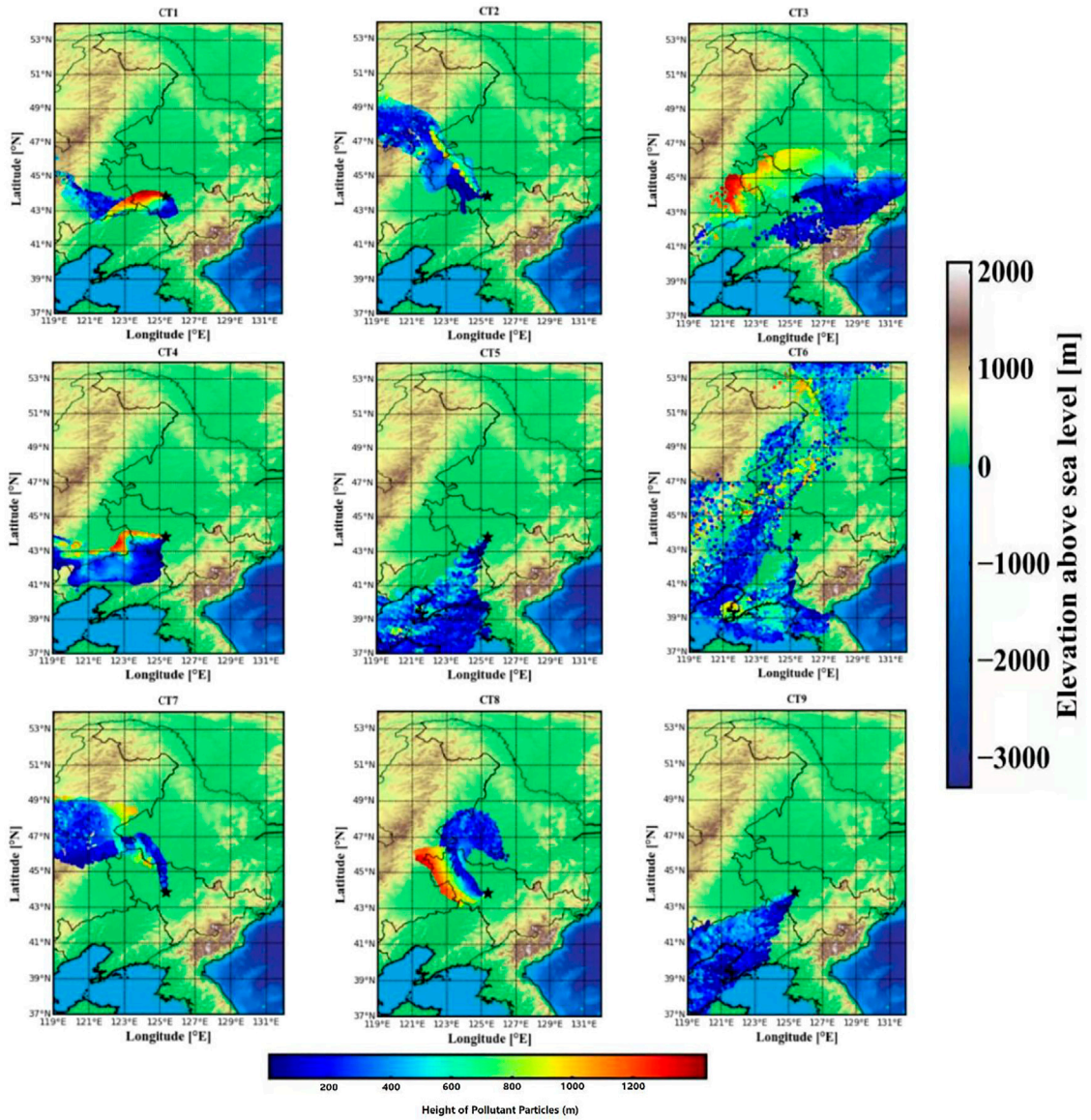

FIGURE 11 | Backward plume trajectory of particles during heavy pollution periods of PM2.5 under nine circulation types during the lockdown. The colour bar below indicates the height of the particles from surface and that on the right represents the terrain height.

Peninsula. The PM2.5 concentration under Type 7 is relatively low overall, and only a small area of polluted weather occurs around Changchun. Trajectory simulation shows that the pollution at this time mainly comes from local emissions, and some of the pollutants come from the Greater Xing'an Mountains in Inner Mongolia. Large-scale pollution occurs in the northern part of Northeast China under Type 8, and the pollutant particle trajectory shows that the particulate matter comes from near northwest Changchun. Under Type 9, the PM2.5 concentration in most areas of Northeast China is relatively small, and the pollution in Changchun area comes from the Bohai Bay in North China.

In summary, the particulate pollution in the severe pollution processes of Types 1, 2, 4, 7, and 8 is mainly from Changchun and surrounding area, and the particulate matter transmission height changes significantly. It indicates that the particulate matters are affected by sinking flow. However, particulate matter pollution of Types 3, 5, 6, and 9 in the lower northeast is mainly from North China, Liaodong Peninsula and other areas far away from Changchun.

5 CONCLUSION

This study investigates the effects of human activities and meteorological conditions on the changes in the concentrations of major pollutants (PM2.5, O_3, NO_2, SO_2, and CO) during the lockdown implemented for curbing the spread of COVID-19. First,

we classified the large-scale circulation in the northeast and obtained nine main weather circulation patterns (Type 1–Type 9) that affect this region. Analysis of sea level pressure field (500 hPa and 850 hPa) altitude and local meteorological conditions suggests that meteorological conditions are closely related to air quality in this region. Comparison of the concentrations of pollutants during the lockdown period in 2020 and the same period in previous years, as well as the changes in the concentrations of pollutants at different stages during the lockdown period suggests that human activities and meteorological conditions have different effects on the changes in the concentrations of different air pollutants. The specific research conclusions are as follows:

(1) Under Types 1, 2, 4, and 7, the concentrations of PM2.5, NO_2, SO_2, and CO in the northeast are high, while under Types 3, 5, 6, and 9, the concentrations of PM2.5, NO_2, SO_2, and CO are low. The O_3 concentration is high under Types 3, 5, and 9, while it is low under Types 1, 2, 4, and 7. Particulate pollution in Northeast China is related to the equalising field in the back of high-pressure regions and the front of weak-high-pressure regions, while O_3 pollution is closely related to the trough, low vortex, and surface cyclonic weather systems.
(2) Human activities and local meteorological conditions significantly impact the changes in PM2.5, NO_2, SO_2, and CO concentrations. Although O_3 is formed from NO_2 and VOC, O_3 concentration is more sensitive to the large-scale weather circulation situation compared to PM2.5.
(3) FLEXPART-WRF simulation results suggest that local emissions and southwest and northwest sinking airflows are the main causes of severe particulate pollution in the northeast during the lockdown period.

DATA AVAILABILITY STATEMENT

The original contributions presented in the study are included in the article/Supplementary Material, further inquiries can be directed to the corresponding author.

AUTHOR CONTRIBUTIONS

Data curation, JZ; Methodology, JZ; Project administration, CZ; Software, HD; Visualization, HD; Writing—original draft, TW; Writing—review and editing, CZ and ZZ.

FUNDING

This study was supported by the National Key Research and Development Program of China (Grant No. 2017YFC1501803), the National Natural Science Foundation Committee of China (41475021, 41375154, and 41405146), and the Chinese Prime Minister Fund (DQGG0104). We thank the authors and developers of the COST733 classification software.

REFERENCES

Berman, J. D., and Ebisu, K. (2020). Changes in U.S. Air Pollution during the COVID-19 Pandemic. *Sci. Total Environ.* 739, 139864. doi:10.1016/j.scitotenv.2020.139864

Brioude, J., Arnold, D., Stohl, A., Cassiani, M., Morton, D., Seibert, P., et al. (2013). The Lagrangian Particle Dispersion Model FLEXPART-WRF Version 3.1. *Geosci. Model. Dev.* 6 (6), 1889–1904. doi:10.5194/gmd-6-1889-2013

Broomandi, P., Karaca, F., Nikfal, A., Jahanbakhshi, A., Tamjidi, M., and Kim, J. R. (2020). Impact of COVID-19 Event on the Air Quality in Iran. *Aerosol Air Qual. Res.* 20 (8), 1793–1804. doi:10.4209/aaqr.2020.05.0205

Chang, Y., Huang, R. J., Ge, X., Huang, X., Hu, J., Duan, Y., et al. (2020). Puzzling Haze Events in China during the Coronavirus (COVID-19) Shutdown. *Geophys. Res. Lett.* 47, e2020GL088533. doi:10.1029/2020GL088533

Chen, F., Tewari, M., Kusaka, H., and Warner, T. (2006). "Current Status of Urban Modeling in the Community Weather Research and Forecast (WRF) Model," in paper presented at Joint Session with Sixth Symposium on the Urban Environment and AMS Forum: Managing our Physical and Natural Resources: Successes and Challenges, the 86th AMS Annual Meeting, 28 January–3 February (Atlanta, Georgia: AMS).

Chen, H., Guo, J., Wang, C., Luo, F., Yu, X., Zhang, W., et al. (2020). Clinical Characteristics and Intrauterine Vertical Transmission Potential of COVID-19 Infection in Nine Pregnant Women: a Retrospective Review of Medical Records. *Lancet.* doi:10.1016/s0140-6736(20)30360-3

Chen, S., Yang, J., Yang, W., Wang, C., and Bärnighausen, T. (2020). COVID-19 Control in China during Mass Population Movements at New Year. *The Lancet.* 395, 764–766. doi:10.1016/s0140-6736(20)30421-9

Cheng, Y., Cao, X., and Liu, J. (2022). New Open Burning Policy Reshaped the Aerosol Characteristics of Agricultural Fire Episodes in Northeast China. *Sci. Total Environ.* 810, 152272. doi:10.1016/j.scitotenv.2021.152272

China State Council (2020). The New Coronavirus Disease (Covid-19) Prevention and Control. Available at: http://news.xinhuanet.com/house/bj/2014-03-17/c_126274610.htm.

Compagnucci, R. H., and Richman, M. B. (2008). Can Principal Component Analysis Provide Atmospheric Circulation or Teleconnection Patterns? *Int. J. Climatol.* 28 (6), 703–726. doi:10.1002/joc.1574

Dai, Q., Liu, B., Bi, X., Wu, J., Liang, D., Zhang, Y., et al. (2020). Dispersion Normalized PMF Provides Insights into the Significant Changes in Source Contributions to PM2.5 after the COVID-19 Outbreak. *Environ. Sci. Technol.* 54 (16), 9917–9927. doi:10.1021/acs.est.0c02776

Dinoi, A., Gulli, D., Ammoscato, I., Calidonna, C. R., and Contini, D. (2021). Impact of the Coronavirus Pandemic Lockdown on Atmospheric Nanoparticle Concentrations in Two Sites of Southern Italy. *Atmosphere.* 12, 352. doi:10.3390/atmos12030352

Dudhia, J. (1989). Numerical Study of Convection Observed during the winter Monsoon experiment Using a Mesoscale Two-Dimensional Model. *J. Atmos. Sci.* 46, 3077–3107. doi:10.1175/1520-0469(1989)046<3077:nsocod>2.0.co;2

Filonchyk, M., Hurynovich, V., Yan, H., Gusev, A., and Shpilevskaya, N. (2020). Impact Assessment of COVID-19 on Variations of SO2, NO2, CO and AOD over East China. *Aerosol Air Qual. Res.* 20 (7), 1530–1540. doi:10.4209/aaqr.2020.05.0226

Filonchyk, M., Hurynovich, V., and Yan, H. (2021). Impact of Covid-19 Lockdown on Air Quality in the Poland, Eastern Europe. *Environ. Res.* 198, 110454. doi:10.1016/j.envres.2020.110454

Geng, G., Xiao, Q., Liu, S., Liu, X., Cheng, J., Zheng, Y., et al. (2021). Tracking Air Pollution in China: Near Real-Time PM2.5 Retrievals from Multisource Data Fusion. *Environ. Sci. Technol.* 55, 12106–12115. doi:10.1021/acs.est.1c01863

Hong, S.-Y., Dudhia, J., and Chen, S.-H. (2004). A Revised Approach to Ice Microphysical Processes for the Bulk Parameterization of Clouds and Precipitation. *Mon. Wea. Rev.* 132, 103–120. doi:10.1175/1520-0493(2004)132<0103:aratim>2.0.co;2

Hong, Y., Xu, X., Liao, D., Zheng, R., Ji, X., Chen, Y., et al. (2021). Source Apportionment of PM2.5 and Sulfate Formation during the COVID-19 Lockdown in a Coastal City of Southeast China. *Environ. Pollut.* 286, 117577. doi:10.1016/j.envpol.2021.117577

Huang, X., Ding, A., Gao, J., Zheng, B., Zhou, D., Qi, X., et al. (2020). Enhanced Secondary Pollution Offset Reduction of Primary Emissions during COVID-19 Lockdown in China. *Natl. Sci. Rev.* doi:10.1093/nsr/nwaa137

Huth, R., Beck, C., Philipp, A., Demuzere, M., Ustrnul, Z., Cahynová, M., et al. (2008). Classifications of Atmospheric Circulation Patterns. *Ann. N. Y. Acad. Sci.* 1146 (1), 105–152. doi:10.1196/annals.1446.019

Jiang, Y., and Xu, J. (2021). The Association between COVID-19 Deaths and Short-Term Ambient Air Pollution/meteorological Condition Exposure: a Retrospective Study from Wuhan, China. *Air Qual. Atmos. Health.* 14 (1), 1–5. doi:10.1007/s11869-020-00906-7

Kain, J. S. (2004). The Kain-Fritsch Convective Parameterization: An Update. *J. Appl. Meteorol.* 43, 170–181. doi:10.1175/1520-0450(2004)043<0170:tkcpau>2.0.co;2

Li, M., Wang, T., Xie, M., Li, S., Zhuang, B., Fu, Q., et al. (2021). Drivers for the Poor Air Quality Conditions in North China Plain during the COVID-19 Outbreak. *Atmos. Environ.* 246, 118103. doi:10.1016/j.atmosenv.2020.118103

Li, Y., Liu, J., Han, H., Zhao, T., Zhang, X., Zhuang, B., et al. (2019). Collective Impacts of Biomass Burning and Synoptic Weather on Surface PM2.5 and CO in Northeast China. *Atmos. Environ.* 213, 64–80. doi:10.1016/j.atmosenv.2019.05.062

Li, Y., Zhao, H., and Wu, Y. (2015). Characteristics of Particulate Matter during Haze and Fog (Pollution) Episodes over Northeast China, Autumn 2013. *Aerosol Air Qual. Res.* 15 (3), 853–864. doi:10.4209/aaqr.2014.08.0158

Liu, T., Wang, X., Hu, J., Wang, Q., An, J., Gong, K., et al. (2020). Driving Forces of Changes in Air Quality during the COVID-19 Lockdown Period in the Yangtze River Delta Region, China. *Environ. Sci. Technol. Lett.* doi:10.1021/acs.estlett.0c00511

Ma, Y., Zhao, H., Dong, Y., Che, H., Li, X., Hong, Y., et al. (2018). Comparison of Two Air Pollution Episodes over Northeast China in winter 2016/17 Using Ground-Based Lidar. *J. Meteorol. Res.* 32 (2), 313–323. doi:10.1007/s13351-018-7047-4

Mahato, S., Pal, S., and Ghosh, K. G. (2020). Effect of Lockdown amid COVID-19 Pandemic on Air Quality of the Megacity Delhi, India. *Sci. Total Environ.* 730, 139086. doi:10.1016/j.scitotenv.2020.139086

Mlawer, E. J., Taubman, S. J., Brown, P. D., Iacono, M. J., and Clough, S. A. (1997). Radiative Transfer for Inhomogeneous Atmospheres: RRTM, a Validated Correlated-K Model for the Longwave. *J. Geophys. Res.* 102, 16663–16682. doi:10.1029/97jd00237

Mostafa, M. K., Gamal, G., and Wafiq, A. (2021). The Impact of COVID 19 on Air Pollution Levels and Other Environmental Indicators - a Case Study of Egypt. *J. Environ. Manage.* 277, 111496. doi:10.1016/j.jenvman.2020.111496

Muhammad, S., Long, X., and Salman, M. (2020). COVID-19 Pandemic and Environmental Pollution: a Blessing in Disguise? *Sci. Total Environ.* 728, 138820. doi:10.1016/j.scitotenv.2020.138820

Nakanishi, M., and Niino, H. (2006). An Improved Mellor-Yamada Level-3 Model: Its Numerical Stability and Application to a Regional Prediction of Advection Fog. *Boundary-layer Meteorol.* 119 (2), 397–407. doi:10.1007/s10546-005-9030-8

Philipp, A., Bartholy, J., and Beck, C. (2010). Cost733cat – A Database of Weather and Circulation type Classifications. *Phys. Chem. Earth, Parts A/b/c* 35 (9–12), 360–373. doi:10.1016/j.pce.2009.12.010

Philipp, A., Beck, C., and Esteban, P. (2014). *cost733-class-1.2 User Guide*. Germany: Augsburg, 10–21.

Shen, L., Zhao, T., Wang, H., Liu, J., Bai, Y., Kong, S., et al. (2021). Importance of Meteorology in Air Pollution Events during the City Lockdown for COVID-19 in Hubei Province, Central China. *Sci. Total Environ.* 754, 142227. doi:10.1016/j.scitotenv.2020.142227

Shi, X., and Brasseur, G. P. (2020). The Response in Air Quality to the Reduction of Chinese Economic Activities during the COVID-19 Outbreak. *Geophys. Res. Lett.* 47 (11), e2020GL088070. doi:10.1029/2020GL088070

Silver, B., He, X., Arnold, S. R., and Spracklen, D. V. (2020). The Impact of COVID-19 Control Measures on Air Quality in China. *Environ. Res. Lett.* 15 (8), 084021. doi:10.1088/1748-9326/aba3a2

Skirienė, A. F., and Stasiškienė, Ž. (2021). COVID-19 and Air Pollution: Measuring Pandemic Impact to Air Quality in Five European Countries. *Atmosphere.* 12 (3), 290. doi:10.3390/atmos12030290

Sulaymon, I. D., Zhang, Y., Hopke, P. K., Zhang, Y., Hua, J., and Mei, X. (2021a). COVID-19 Pandemic in Wuhan: Ambient Air Quality and the Relationships between Criteria Air Pollutants and Meteorological Variables before, during, and after Lockdown. *Atmos. Res.* 250, 105362. doi:10.1016/j.atmosres.2020.105362

Sulaymon, I. D., Zhang, Y., Hopke, P. K., Hu, J., Zhang, Y., Li, L., et al. (2021b). Persistent High PM2.5 Pollution Driven by Unfavorable Meteorological Conditions during the COVID-19 Lockdown Period in the Beijing-Tianjin-Hebei Region, China. *Environ. Res.* 198, 111186. doi:10.1016/j.envres.2021.111186

Tian, H., Liu, Y., Li, Y., Wu, C.-H., Chen, B., Kraemer, M. U. G., et al. (2020). An Investigation of Transmission Control Measures during the First 50 Days of the COVID-19 Epidemic in China. *Science.* 368, 638–642. doi:10.1126/science.abb6105

Tobías, A., Carnerero, C., Reche, C., Massagué, J., Via, M., Minguillón, M. C., et al. (2020). Changes in Air Quality during the Lockdown in Barcelona (Spain) One Month into the SARS-CoV-2 Epidemic. *Sci. Total Environ.* 726, 138540. doi:10.1016/j.scitotenv.2020.138540

Venter, Z. S., Aunan, K., Chowdhury, S., and Lelieveld, J. (2020). COVID-19 Lockdowns Cause Global Air Pollution Declines. *Proc. Natl. Acad. Sci. U.S.A.* 117 (32), 18984–18990. doi:10.1073/pnas.2006853117

Wang, P., Chen, K., Zhu, S., Wang, P., and Zhang, H. (2020). Severe Air Pollution Events Not Avoided by Reduced Anthropogenic Activities during COVID-19 Outbreak. *Resour. Conservation Recycling.* 158, 104814. doi:10.1016/j.resconrec.2020.104814

Wang, T., Du, H., Zhao, Z., Russo, A., Zhang, J., and Zhou, C. (2022). The Impact of Potential Recirculation on the Air Quality of Bohai Bay in China. *Atmos. Pollut. Res.* 13 (1), 101268. doi:10.1016/j.apr.2021.101268

Xian, T., Li, Z., and Wei, J. (2021). Changes in Air Pollution Following the COVID-19 Epidemic in Northern China: The Role of Meteorology. *Front. Environ. Sci.* 9, 64. doi:10.3389/fenvs.2021.654651

Xiao, Q., Zheng, Y., Geng, G., Chen, C., Huang, X., Che, H., et al. (2021a). Separating Emission and Meteorological Contribution to PM2.5 Trends Over East China During 2000–2018. *Atmos. Chem. Phys.* 21, 9475–9496. doi:10.5194/acp-2021-28

Xiao, Q., Geng, G., Cheng, J., Liang, F., Li, R., Meng, X., et al. (2021b). Evaluation of Gap-Filling Approaches in Satellite-Based Daily PM2.5 Prediction Models. *Atmos. Environ.* 244, 117921. doi:10.1016/j.atmosenv.2020.117921

Xiang, J., Austin, E., Gould, T., Larson, T., Shirai, J., Liu, Y., et al. (2020). Impacts of the COVID-19 Responses on Traffic-Related Air Pollution in a Northwestern US City. *Sci. Total Environ.* 747, 141325. doi:10.1016/j.scitotenv.2020.141325

Yan, Y., Wang, X., Qu, K., Li, X., Shi, W., Peng, Z., et al. (2021). Impacts of Synoptic Circulations on Summertime Ozone Pollution in Guanzhong Basin, Northwestern China. *Atmos. Environ.* 262, 118660. doi:10.1016/j.atmosenv.2021.118660

Zambrano-Monserrate, M. A., Ruano, M. A., and Sanchez-Alcalde, L. (2020). Indirect Effects of COVID-19 on the Environment. *Sci. Total Environ.* 728, 138813. doi:10.1016/j.scitotenv.2020.138813

Zhang, J. P., Zhu, T., Zhang, Q. H., Li, C. C., Shu, H. L., Ying, Y., et al. (2012). The Impact of Circulation Patterns on Regional Transport Pathways and Air Quality over Beijing and its Surroundings. *Atmos. Chem. Phys.* 12, 5031–5053. doi:10.5194/acp-12-5031-2012

Zhang, R., Zhang, Y., Lin, H., Feng, X., Fu, T.-M., and Wang, Y. (2020). NOx Emission Reduction and Recovery during COVID-19 in East China. *Atmosphere.* 11, 433. doi:10.3390/atmos11040433

Zhang, Y., Wang, S., Jia, X., Lian, J., Zhang, X., and Xu, Y. (2018). Study on the Objective Classification of Air Pollution Weather in the winter Half Year in North China. *Acta Scientiae Circumstantiae.* 38 (10), 3826–3833. (in Chinese). doi:10.13671/j.hjkxxb.2018.0169

Zhao, H., Che, H., Ma, Y., Wang, Y., Yang, H., Liu, Y., et al. (2017). The Relationship of PM Variation with Visibility and Mixing-Layer Height under Hazy/Foggy Conditions in the Multi-Cities of Northeast China. *Int. J. Environ. Res. Public Health.* 14 (5), 471. doi:10.3390/ijerph14050471

Zhao, N., Wang, G., Li, G., Lang, J., and Zhang, H. (2020). Air Pollution Episodes during the COVID-19 Outbreak in the Beijing-Tianjin-Hebei Region of China:

An Insight into the Transport Pathways and Source Distribution. *Environ. Pollut.* 267, 115617. doi:10.1016/j.envpol.2020.115617

Zhao, Z., Xi, H., Russo, A., Du, H., Gong, Y., Xiang, J., et al. (2019). The Influence of Multi-Scale Atmospheric Circulation on Severe Haze Events in Autumn and Winter in Shanghai, China. *Sustainability.* 11 (21), 5979. doi:10.3390/su11215979

Zhao, Z., Zhou, Z., Russo, A., Xi, H., Zhang, J., Du, H., et al. (2021a). Comparative Analysis of the Impact of Weather Conditions and Human Activities on Air Quality in the Dongting and Poyang Lake Region during the COVID-19 Pandemic. *Atmos. Pollut. Res.* 12 (5), 101054. doi:10.1016/j.apr.2021.101054

Zhao, Z., Zhou, Z., Russo, A., Du, H., Xiang, J., Zhang, J., et al. (2021b). Impact of Meteorological Conditions at Multiple Scales on Ozone Concentration in the Yangtze River Delta. *Environ. Sci. Pollut. Res.* 28 (44), 62991–63007. doi:10.1007/s11356-021-15160-2

Zhao, X., Wang, G., Wang, S., Zhao, N., Zhang, M., and Yue, W. (2021). Impacts of COVID-19 on Air Quality in Mid-eastern China: An Insight into Meteorology and Emissions. *Atmos. Environ.* 266, 118750. doi:10.1016/j.atmosenv.2021.118750

Zhou, C. J., Wei, G., and Xiang, J. (2018). Effects of Synoptic Circulation Patterns on Air Quality in Nanjing and its Surrounding Areas during 2013–2015. *Atmos. Pollut. Res.* 9 (4), 723~734. doi:10.1016/j.apr.2018.01.015

Zhou, C., Wei, G., Zheng, H., Russo, A., Li, C., Du, H., et al. (2019). Effects of Potential Recirculation on Air Quality in Coastal Cities in the Yangtze River Delta. *Sci. Total Environ.* 651, 12–23. doi:10.1016/j.scitotenv.2018.08.423

Conflict of Interest: The authors declare that the research was conducted in the absence of any commercial or financial relationships that could be construed as a potential conflict of interest.

Publisher's Note: All claims expressed in this article are solely those of the authors and do not necessarily represent those of their affiliated organizations, or those of the publisher, the editors and the reviewers. Any product that may be evaluated in this article, or claim that may be made by its manufacturer, is not guaranteed or endorsed by the publisher.

frontiers | Frontiers in Environmental Science

ORIGINAL RESEARCH
published: 04 May 2022
doi: 10.3389/fenvs.2022.823973

Impact of the COVID-19 Restrictive Measures on Urban Traffic-Related Air Pollution in Serbia

Slavica Malinović-Milićević [1], Dejan Doljak [1], Gorica Stanojević [1] and Milan M. Radovanović [1,2]*

[1]Geographical Institute "Jovan Cvijić", Serbian Academy of Sciences and Arts, Belgrade, Serbia, [2]Institute of Sports, Tourism and Service, South Ural State University, Chelyabinsk, Russia

This study has analyzed the traffic-related change in atmospheric pollutants levels ($PM_{2.5}$, PM_{10}, CO, NO_2, SO_2, and O_3) caused by the COVID-19 restrictive measures, based on traffic ground-based stations data in urban areas in Serbia. The possible influence of several meteorological factors (temperature, wind, pressure, and humidity), and mobility on the pollutants' levels were also considered. The obtained results showed a positive correlation of daily NO_2 concentrations with mobility and its significant reduction during restrictive measures at all selected monitoring stations. The reduction of NO_2 was higher than in other countries (71.1–111.5% for measured, and 49.3–92.6% for "deweathered" data), indicating a high traffic impact on NO_2 levels in Serbia. The PM, CO, and SO_2 showed a weak correlation with mobility during the period with restrictive measures, which, besides traffic, indicates the significant influence of other sources of their concentration. The O_3 concentrations were increased at all measuring stations and are negatively correlated to mobility. Comparison of pollutant concentrations during restriction with the equivalent period in preceding years showed reductions in NO_2 and SO_2 concentrations. However, compared to previous years, the concentrations of $PM_{2.5}$, PM_{10}, and CO increased in the period with restrictive measures, indicating lower sensitivity to population mobility and higher dependence on other emission sources. The findings suggest the justification for the use of traffic reduction strategies to improve air quality.

Keywords: air pollution, traffic, COVID-19 restrictions, meteorology, mobility, Serbia

OPEN ACCESS

Edited by:
Suvarna Sanjeev Fadnavis, Indian Institute of Tropical Meteorology (IITM), India

Reviewed by:
Vijay Bhaskar Bojan, Madurai Kamaraj University, India
Ana Alebić-Juretić, University of Rijeka, Croatia
Predrag Ilić, PSRI Institute for Protection and Ecology of the Republic of Srpska, Bosnia and Herzegovina

****Correspondence:***
Slavica Malinović-Milićević
s.malinovic-milicevic@gi.sanu.ac.rs

Specialty section:
This article was submitted to Atmosphere and Climate, a section of the journal Frontiers in Environmental Science

Received: *28 November 2021*
Accepted: *20 April 2022*
Published: *04 May 2022*

Citation:
Malinović-Milićević S, Doljak D, Stanojević G and Radovanović MM (2022) Impact of the COVID-19 Restrictive Measures on Urban Traffic-Related Air Pollution in Serbia. Front. Environ. Sci. 10:823973. doi: 10.3389/fenvs.2022.823973

INTRODUCTION

Air quality is one of the dominant factors that affect health and quality of life. The harmful effects of air pollution on health are well documented, especially when it comes to pollutants such as particulate matter, nitrogen, and sulfur oxides, carbon monoxide, and ozone (Setton et al., 2011; Sujaritpong et al., 2014; Likhvar et al., 2015; WHO, 2021; etc). According to WHO (2018), air pollution is responsible for 26% of deaths from respiratory diseases, 25% of cases of chronic obstructive pulmonary disease, and 17% of cases of ischemic heart disease. Besides the influence on mortality and morbidity, several studies conducted in major cities around the world have proven the harmful effects of air pollutants on the course and prognosis of acute and chronic diseases in adults and children (Elliot et al., 2016; Weber et al., 2016; Xu et al., 2016).

During the Coronavirus Disease 2019 (COVID-19) pandemic restrictive measures, many human activities in the fields of transport, economy, and education were globally limited to prevent the

further spread of the virus. Restrictions on human activity have resulted in significant reductions in pollutant emissions and have given scientists a unique opportunity to assess the impact of limited anthropogenic emissions on air quality. Existing country-specific case studies have reported a reduction in air pollution during the implementation of restrictive measures, which may be the result of reduced transport. The majority of them showed that nitrogen oxide (NO_x) concentrations significantly decreased, while ground-level ozone (O_3) concentrations increased (Baldasano, 2020; Bekbulat et al., 2021; Briz-Redón et al., 2021; Chen et al., 2021; Munir et al., 2021; Prats et al., 2021; etc). Lockdown had a positive effect on particle concentrations ($PM_{2.5}$, PM_{10}) in many countries but with a less pronounced effect (Menut et al., 2020; Betancourt-Odio et al., 2021; Ropkins and Tate, 2021; Shi et al., 2021). Some studies also found an increase in particulate matter (PM) concentration due to unfavorable meteorological conditions, the contribution from other sources, and transport from remote areas (Munir et al., 2021; Song et al., 2021). Sulfur dioxide (SO_2) and carbon monoxide (CO) also showed a decrease during the lockdown, but it has not been consistent (Grivas et al., 2020; Briz-Redón et al., 2021; Chen et al., 2021; Filonchyk et al., 2021). Lenzen et al. (2020) and Venter et al. (2020) examined the pandemic impacts on global air quality levels. Lenzen et al. (2020) found a reduction in greenhouse gases, $PM_{2.5}$, and gaseous air pollutants (SO_2 and NO_2) by 4.6, 3.8, and 2.9% of the global annual levels, respectively, while Venter et al. (2020) reported a decrease of NO_2 and $PM_{2.5}$ by approximately 60 and 31%.

The first case of coronavirus in Serbia was confirmed on March 6, 2020. On March 15, 2020, the Serbian Government declared a state of emergency (from midnight on March 16). From then on, a series of partial and strict restrictive measures were successively undertaken to limit the spread of COVID-19, including the closure of schools and universities, travel restrictions, working at home, closure of catering and sales facilities, and ban on public gatherings. During the holidays and the majority of weekends, starting from Friday afternoon, a full weekend curfew was imposed on the entire territory of Serbia. After seven and a half weeks of measures, and obtaining successful outcomes, the state of emergency was lifted on May 6, 2020.

Studies on the impact caused by the COVID-19 outbreak on air pollution in Serbia are quite limited. So far, the effects of the lockdown on the level of air pollutants have been investigated in one city (Novi Sad), only for April 2020. Davidović et al. (2021) showed that $PM_{2.5}$, PM_{10}, and SO_2 levels during restrictive measures, did not change noticeably, compared to the pre-restrictive measures period. Having in mind the fact that the impact of restrictive measures on air pollution has not been analyzed in other cities in Serbia, and that measures have mostly affected traffic reduction, the following study aimed to assess the changes in the air quality at traffic air pollution stations linked to COVID-19 lockdown restrictions. In particular, the study focuses on the several criteria air pollutants ($PM_{2.5}$, PM_{10}, NO_2, SO_2, CO, and O_3), evaluating: 1) effect of meteorological factors and population mobility on air pollution levels; 2) variation in daily concentrations between February 1 and June 30, 2020 (before, during, and after restrictive measures), and 3) difference in the mean concentration in 2020 compared to average concentration during the equivalent period in previous years.

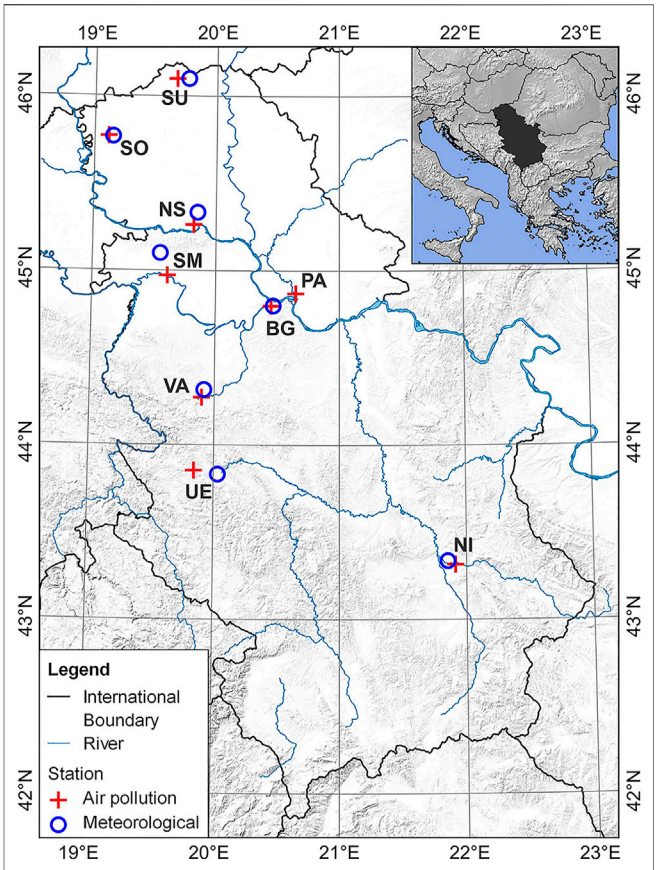

FIGURE 1 | Location of the traffic air pollution monitoring and meteorological stations in Serbia used in the study.

MATERIAL AND METHODS

Study Area

The Republic of Serbia is positioned in Southeast Europe on the Balkan Peninsula, between latitudes 41°and 47° N and longitudes 18° and 23° E. The country covers an area of 88,499 km^2 (Statistical Office of the Republic of Serbia, 2020). The northern part of the country is lowland, while the altitude increases to the south. The estimated population in Serbia in 2020 was 6,899,126 (Statistical Office of the Republic of Serbia, 2021). The population is mainly concentrated at lower altitudes in northern and central areas and along the river valleys. Nearly 60% of Serbia's population lives in urban areas (Drobnjaković and Spalević, 2017).

This study covers urban areas with traffic stations for measuring air quality, which have different sizes and population densities (**Figure 1**). The largest by far is the nation's capital, Belgrade (BG), with a population of 1.7

million in the total city area (1.2 million in the urban city area). Novi Sad (NS) is the second, while Niš (NI) is the third-largest city in Serbia, with a population of 360,000 and 260,000, respectively. Subotica (SU) and Pančevo (PA) are cities with populations ranging from 100,000 to 150,000 inhabitants, while the population of other cities covered by the study (Valjevo (VA), Sremska Mitrovica (SM), Sombor (SO), and Užice (UE)) is between 70,000 and 85,000 (Statistical Office of the Republic of Serbia, 2020).

The main sources of outdoor air pollution in Serbia comprise the energy production sector, industrial activities, and mining. In almost every urban municipality, traffic and individual domestic heating additionally pollute the air. In some cities, such as UE and VA, the unfavorable geographical position, such as valleys and gorges, further, makes air quality even worse. The major sources of air pollution in BG are electricity production, heating, and industry, while for NO_x, the major source is traffic (Serbian Environmental Protection Agency, Ministry of Environmental Protection, Republic of Serbia, 2012; Serbian Environmental Protection Agency, Ministry of Environmental Protection, Republic of Serbia, 2013). The specific sources of air pollution in NS are the petrochemical industry and growing vehicle traffic (WHO, 2019), while in NI dominate boiler rooms, individual furnaces, traffic, and industry. In the UE, the metallurgical industry is responsible for the emission of SO_2 and NO_x. In PA, the chemical industry is a source of SO_2, and NO_x, while traffic and individual heating are the sources of PM. In VA, the use of wood and coal for heating households and the frequent occurrence of temperature inversion in the cold part of the year lead to a large excess of PM concentrations (Stanojević et al., 2019). In SU, SO, and SM the main sources of PM are domestic heating and traffic.

Collection and Selection of Data on Air Quality, Meteorology, and Mobility

To analyze the impact of COVID-19 lockdown on air quality, we used air pollution, meteorology, and mobility data. For that purpose, we divided all datasets into three periods: 1) before restrictive measures (BRM), from February 1 to March 14, 2020; 2) during restrictive measures (RM), from March 15 to May 5, 2020, and 3) after restrictive measures (ARM), from May 6 to June 30, 2020. In addition, we extracted and analyzed data for the curfew subperiod inside of the RM period.

Air pollutant concentrations including NO_2, SO_2, CO, $PM_{2.5}$, PM_{10}, and O_3 for the period 2015–2020 were obtained from the national network of automatic stations for air quality monitoring managed by the Serbian Environmental Protection Agency (SEPA, 2021). All measurements were performed using precision air quality monitoring equipment with quality assurance and quality control protocols for sampling and analysis. According to Regulation on monitoring conditions and air quality requirements (2013) checking the quality of measurements, method of processing, display of results, and assessment of their reliability, as well as adjustment and calibration of measuring instruments is carried out according to the prescribed measurement methods and requirements of SRPS ISO/IEC 17025 (Institute for standardization of Serbia, 2021). The maximum measurement uncertainty of the measured data was within the limits prescribed in the Regulation on monitoring conditions and air quality requirements (2013). For a 95% confidence interval, the maximum measurement uncertainty was 15% for NO_2, SO_2, CO, and O_3, and 25% for PM_{10} and $PM_{2.5}$. Uncertainty evaluation was done according to the methodology described in the European Committee for Standardization (CEN, French: Comité Européen de Normalisation) report "Approach to uncertainty estimation for ambient air reference measurement methods" (CEN, 2002) following the European Framework Directive10 on Ambient Air Quality and the associated Daughters Directives. The national network consists of samplers/analyzers that detect and analyze the concentration of air pollutants 24 h/day throughout the year according to reference technical standards (SRPS EN 14211, SRPS EN 14212, SRPS EN 14626, SRPS EN 14907, SRPS EN 12,341, SRPS EN 14625) (Institute for standardization of Serbia, 2021). The air sampling takes place hourly, using TELEDYNE API Model 200A for NO_2, TELEDYNE API Model 100E for SO_2, TELEDYNE API Model 300A for CO, GRIMM EDM 180 for $PM_{2.5}$, TCR TECORA Skypost HV for PM_{10}, and TELEDYNE API Model 400A for O_3. Measurements and data processing were identical at all stations. We downloaded data for the period 2015–2020 and restricted them to consider a specific window of days each year between February 1 and June 30 (150 or 151 days). Before processing, to remove faulty data and inaccurate measurements resulting from the response error of the sensor, each data was subject to quality control by using different control tests similar to those described by Dunn et al. (2012): the existence of gaps in data series, occurrences of physically impossible values and long consecutive, and occurrences of the same value. All data (each monitoring station and each year) were verified to determine if they will be included in the study. If any monitoring station in each year contains <70% of data in the specified window (70% × 150 days × 24 h = 2520 data) it is excluded from further analysis. Each period (before, during, and after the restrictive measures) was checked whether it contained more than 70% of the data and if not, it was excluded from further analysis. The monitoring stations with a sufficient number of years before 2020 were further processed to calculate base averages. Each station with less than 3 years of measurements in the period 2015–2019 is excluded from the analysis. After a completeness check, data from three $PM_{2.5}$ (BG, NS, NI), three PM_{10} (BG, NS, NI), six NO_2 (BG, NS, NI, VA, UE, SM), five SO_2 (BG, NS, NI, UE, PA), seven CO (BG, NS, VA, UE, SU, SO, SM), and three O_3 (PA, SU, SO) traffic urban air pollution monitoring stations were used.

Meteorology data including wind speed (ws), wind direction (wd), air temperature (T), air pressure (P), and relative humidity (RH) for each city were downloaded from the National Oceanic and Atmospheric Administration Integrated Surface Database (NOAA, 1901—present). Meteorological data were used to deweather air quality data and estimate the impact of meteorological conditions on air quality during the analyzed period.

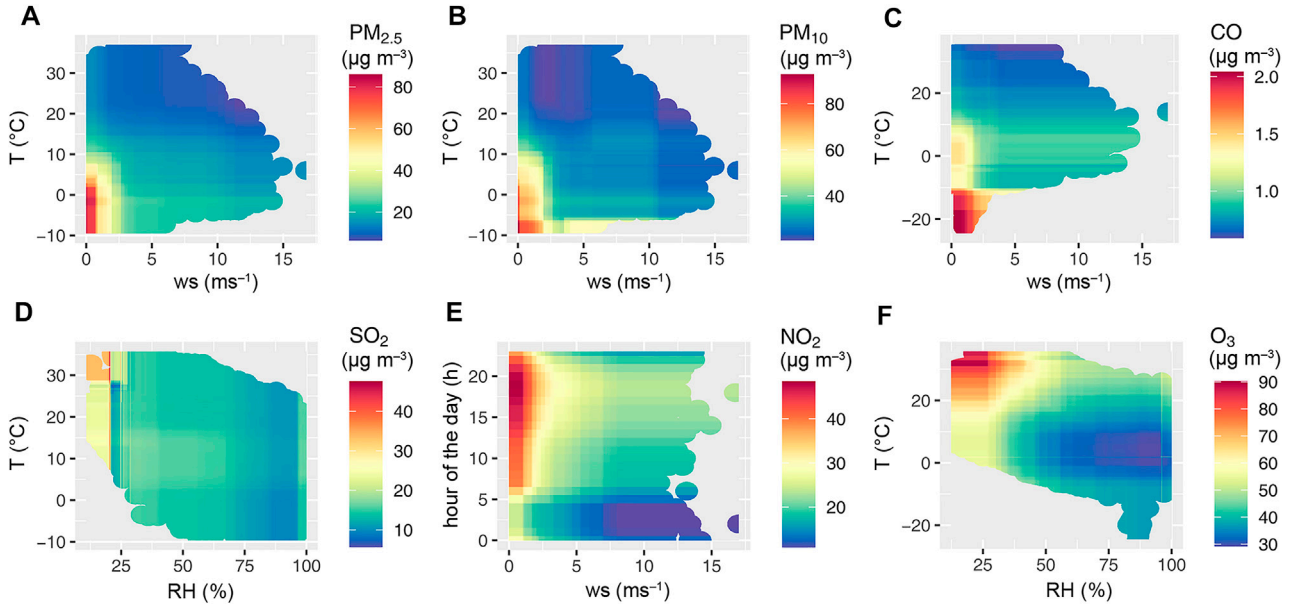

FIGURE 2 | Two-way interactions between the most influential covariates: **(A)** PM2.5 - air temperature (T) and wind speed (ws); **(B)** PM10 - air temperature (T) and wind speed (ws); **(C)** CO- air temperature (T) and wind speed (ws); **(D)** SO_2 - air temperature (T) and relative humidity (RH); **(E)** NO_2 -hour of the day (h) and wind speed (ws); and **(F)** O_3 - air temperature (T) and relative humidity (RH).

TABLE 1 | Differences between measured and "deweathered" mean concentrations were shown as percentages (%) before (BRM), during (RM), and after the restrictive measures (ARM). '/' means that there is no measurement of a specific air pollutant at this particular station.

		BG	NS	NI	VA	UE	PA	SU	SO	SM
$PM_{2.5}$	BRM	0.9	−1.7	0.9	/	/	/	/	/	/
	RM	2.7	2.5	2.5	/	/	/	/	/	/
	ARM	−1.6	0.7	−2.5	/	/	/	/	/	/
PM_{10}	BRM	2.0	0.4	1.0	/	/	/	/	/	/
	RM	1.6	1.4	1.3	/	/	/	/	/	/
	ARM	0.3	0.8	0.2	/	/	/	/	/	/
CO	BRM	3.5	0.7	/	3.6	3.8	/	−12.6	−0.7	5.1
	RM	−1.4	1.5	/	0.3	0.9	/	−3.7	−0.2	−3.7
	ARM	1.7	−3.1	/	1.1	−8.0	/	3.8	0.8	3.1
NO_2	BRM	0.3	3.3	7.2	3.1	2.8	/	/	/	1.3
	RM	−9.8	−8.6	−11.6	−7.8	−10.0	/	/	/	−2.3
	ARM	3.8	4.1	4.6	1.9	4.0	/	/	/	2.1
SO_2	BRM	3.9	3.0	1.2	/	1.6	−0.4	/	/	/
	RM	−3.7	2.0	−2.4	/	−3.2	2.5	/	/	/
	ARM	−1.9	−3.2	−6.3	/	1.8	0.1	/	/	/
O_3	BRM	/	/	/	/	/	−3.8	−5.4	0.7	/
	RM	/	/	/	/	/	1.3	2.0	1.1	/
	ARM	/	/	/	/	/	−0.5	−0.8	−0.6	/

Serbia's community mobility data were downloaded from the Google Community Mobility Reports (Google, 2021) and Apple's COVID-19 mobility trend (Apple Inc, 2020). Google datasets show daily changes in the number of visitors to specific locations (e.g., grocery stores; parks; transit stations) relative to the median baseline level before the pandemic outbreak, where the baseline level represents a normal value for that day of the week, given as median value over the five weeks from January 3 to February 6, 2020. Google reports usually contain data for the period February 15 - December 31, 2020, however, the report for Serbia lacks data for the period May 19– July 3, 2020. Apple's mobility trend reports show how human mobility has changed relative to January 13, 2020. Google transit station data and Apple driving data were used in this analysis.

Deweathering of Air Quality Data and Statistical Analysis

Meteorology plays an important role in air pollutant concentrations. Considering trends, it is difficult to know whether a change in concentration is a consequence of emissions or meteorology. Therefore, this analysis included

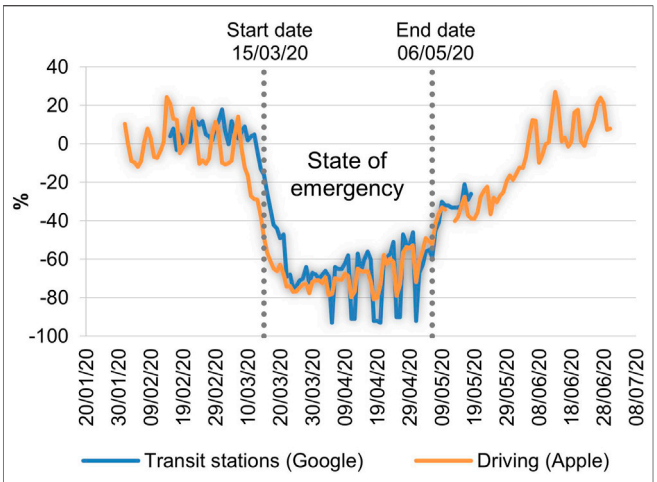

FIGURE 3 | Changes in mobility data (%) in Serbia during the period February–June 2020. The vertical lines show the start and end of the restrictive measures period.

measured and 'deweathered' data. The 'deweather' package in the R programing language (Carslaw, 2020) was used to remove the influence of meteorology from air quality time series. This package is based on boosted regression trees statistical technique using the gbm package (Ridgeway, 2017). It takes into account the complex interactions and non-linear relationships between the variables. Without the need for prior data transformation or elimination of outliers, it is possible to select relevant variables, fit accurate functions and automatically identify and model interactions (Elith et al., 2008). The advantage of the technique is to assess how a dependent variable reacts to individual model variables, the relative importance of different variables for prediction, and the possibility to determine, rank, and visualize interactions between variables (Carslaw and Taylor, 2009). Five meteorological (T, ws, wd, P, and RH) and two temporal (hour of the day-h and day of the week-wdy) predictors were used to develop models for each air pollutant and each measuring station. Each model was built using 80% of the random data, while the rest of the data was used for validation. This resulted in the "deweathered" data showing the changes in the concentrations of air pollutants as emission products. The boosted regression tree technique is also used to examine the effect of meteorological conditions on air pollutants by exploring partial dependencies. The partial dependencies show the relationship between the pollutant and the covariates used in the model while keeping the value of the other covariates at their mean level.

Statistical data analysis was performed using R programming language and Rstudio software (R Core Team, 2013; RStudio Team, 2015). Plots of pollutant time variations and correlations between air pollutants and meteorological parameters were developed using a purpose-built for air quality analysis—openair (Carslaw and Ropkins, 2012). To determine the statistical significance of differences in 2020 air pollutant levels versus concentration during the same period in previous years, both observed and 'deweathered' data were compared using a *t*-test. Values of $p < 0.05$ were considered statistically significant.

TABLE 2 | Correlation analysis between Google mobility data and air pollutant concentrations at different monitoring stations in the restrictive measures period (RM).

$PM_{2.5}$	PM_{10}	CO	NO_2	SO_2	O_3
−0.16	0.07	0.35[a]	0.60[a]	−0.01	−0.52[a]

[a]*significant for* $p < 0.05$.

RESULTS AND DISCUSSION

Influence of Meteorological Factors and Population Mobility on Air Pollution

The interactions between the most influential covariates and air pollutants are shown in **Figure 2**. The air temperature and wind speed were the most important variables affecting $PM_{2.5}$, PM_{10}, and CO concentrations and show a negative correlation. The concentrations of SO_2 were the most affected by low relative humidity and high temperatures, while the concentrations of NO_2 are closely related to traffic flows and tend to be higher during the afternoon traffic peak. Concentrations of O_3 concentrations are strongly positively correlated with air temperature, and also inversely correlated with relative humidity.

The overall effects of the weather conditions on air pollution levels before, during, and after the restrictive measures (BRM, RM, ARM) were shown in **Table 1**. Differences between measured and "deweathered" mean concentrations were shown as percentages (%). The negative signs show a reduction in measured air pollutant concentrations due to favorable weather conditions, while positive signs indicate an increase in the measured concentration caused by unfavorable weather conditions. During the BRM period, weather conditions were slightly unfavorable in most places, resulting in a slight deterioration in air quality. The exceptions were the stations in the north of the country (SU, SO, and PA), where the weather conditions led to the purification of the air. During the RM period, the weather conditions were the most unfavorable for PM and O_3 at all stations. However, the weather had a positive impact on the levels of NO_2 in all cases, and on SO_2 at the majority of stations (except in NS and PA). When it comes to CO, weather conditions have worsened the air quality in the central and southwestern parts of the country, while in places in the north and northwest (SU, SO, and SM) it had a positive effect. In the ARM period, the weather had the most unfavorable effect on NO_2 concentrations in all places.

A significant reduction in mobility over the RM period is expected to reduce vehicle emissions and lead to an improvement in air quality. Changes in mobility data as a percentage for the whole of Serbia for the period February 1—June 30, 2020 are shown in **Figure 3**. Both sets of mobility data, Google and Apple, showed a sharp decline from the weekend before the start of the implementation of the restrictive measures, which began on March 15, 2020. Later, mobility data showed a slightly growing trend from the second week of April 2020 until the end of the RM. There is a noticeable decline in mobility during curfew on weekends, preceded by a slight increase on Fridays. After the RM period, mobility was constantly growing until the second week of June, when it returned to the BRM level.

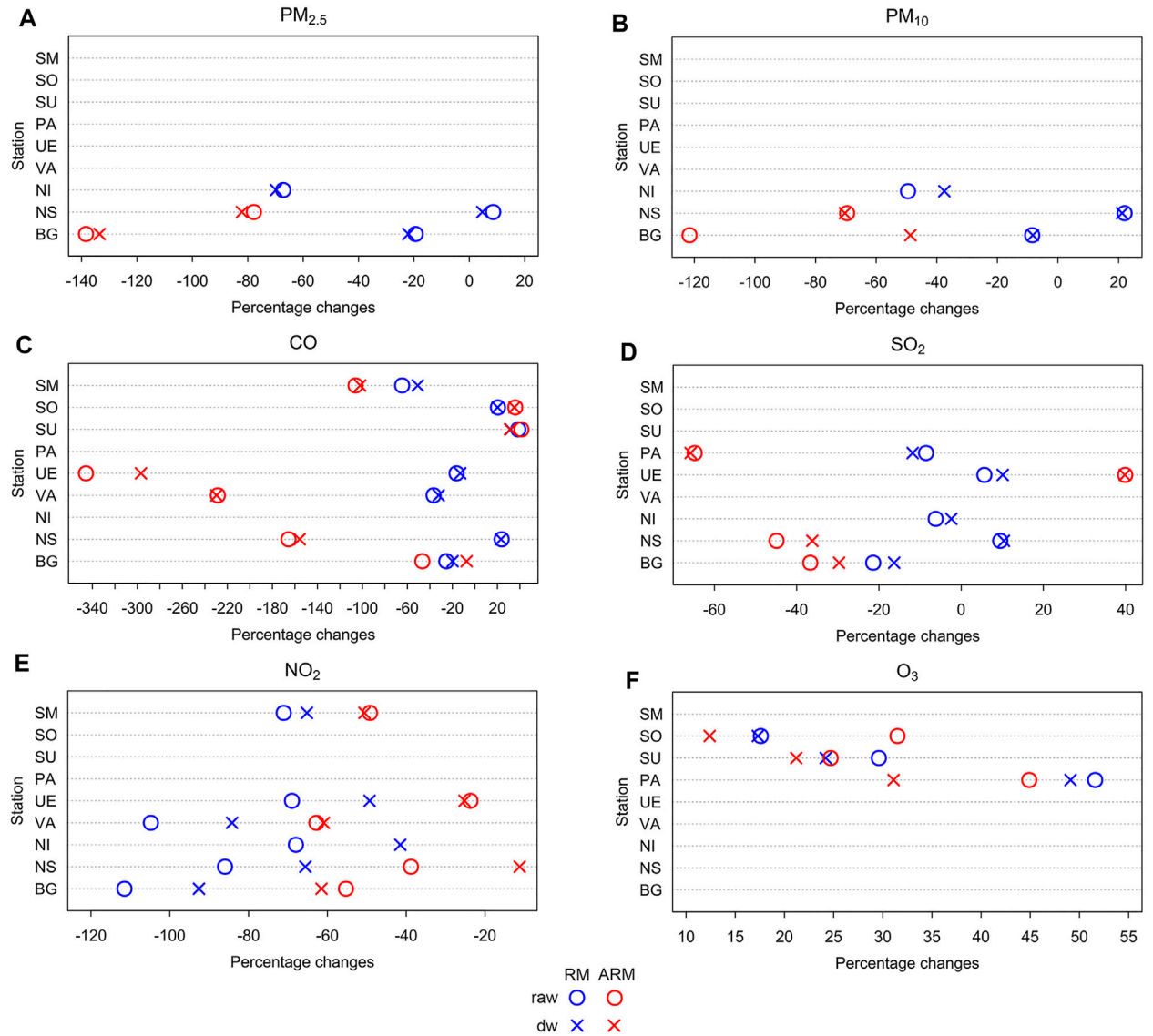

FIGURE 4 | Percentage changes of city-specific pollutant concentrations in restrictive measures (RM) and after the restrictive measures (ARM) periods compared to before restrictive measures (BRM) periods for raw and "deweathered" data for **(A)** PM2.5, **(B)** PM10, **(C)** CO, **(D)** SO_2, **(E)** NO_2, and **(F)** O_3.

To investigate the strength of the linear relationship a correlation between the average mobility trend (Google data) and "deweathered" air pollution levels was performed (**Table 2**). The Pearson correlation coefficients are presented in **Table 2**, whereby values lower than 0.40 are considered weak, while values higher than 0.70 are considered a strong correlation.

The highest positive correlation with mobility had NO_2 concentrations, with a moderate statistically significant R-value of 0.60. This was expected as NO_x is mostly emitted from traffic in urban areas. The percentage of the mobility and NO_2 concentrations reduction was similar (−67% *vs.* −61%, respectively) indicating a close cause-and-effect relationship. The correlations between PM and SO_2 on the one hand and mobility, on the other hand, were low and statistically insignificant, so they can be considered negligible indicating the higher effect of other emission sources, such as individual heating. A statistically significant positive correlation between CO and mobility was expected because CO is an important component of traffic exhaust fumes. O_3 concentrations had a weak, but statistically significant, negative correlation with mobility. A negative correlation of O_3 was expected because lower NO_x emissions from motor vehicles cause an increase in the ratio of volatile organic compounds (VOC) to NO_x, which leads to higher surface O_3 concentrations.

Changes in Air Pollutant Concentrations in BRM, RM, and ARM Periods

Variations of the measured and 'deweathered' concentrations of air pollutants in percent (%) for the RM and ARM periods

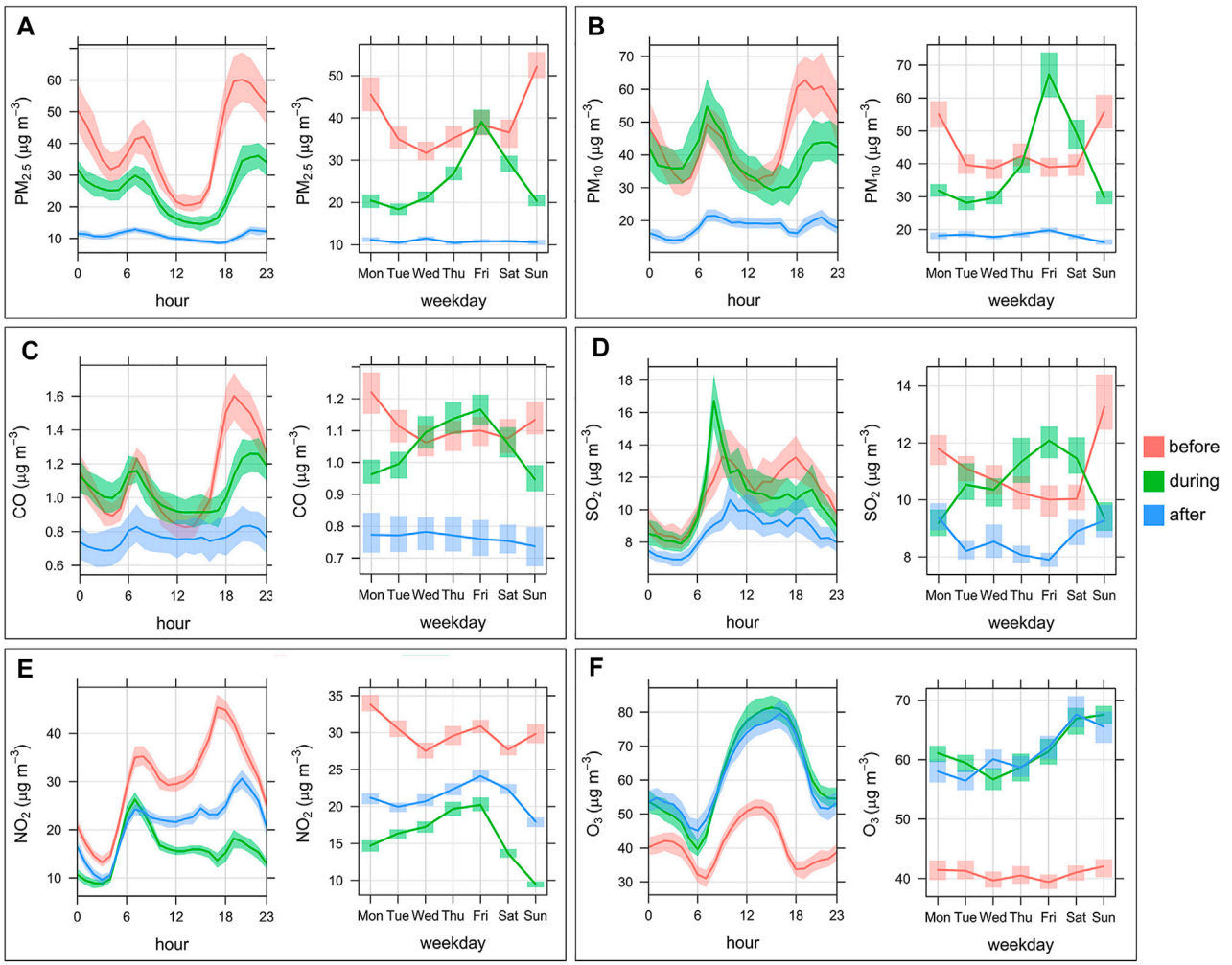

FIGURE 5 | Hourly and weekly cycles of pollutants concentrations in Serbia before (BRM), during (RM), and after the restrictive measures (ARM) periods for **(A)** PM2.5, **(B)** PM10, **(C)** CO, **(D)** $_2$, **(E)** NO_2, and **(F)** O_3.

compared to the BRM period are presented in **Figure 4**. The hourly and weekly cycles of all measured pollutants for BRM, RM, and ARM periods are given in **Figure 5**.

Measured and 'deweathered' NO_2 concentrations decreased significantly at all measurement sites during the RM period (71.1–111.5%, and 49.3–92.6%, respectively). The percentage of decrease was higher than those reported in the other studies (Grivas et al., 2020; Donzelli et al., 2021; Fenech et al., 2021; Shi et al., 2021), indicating that the impact of traffic on NO_2 levels in Serbia is greater than in other countries. The substantial impact of traffic on air pollution in Serbia is due to the fact that vehicles in Serbia (and in groups in Southeast Europe in general) emit significantly more air pollutants than in the rest of Europe. Although Serbia has solved the problem of importing vehicles with particularly high air pollutants by prohibiting imports of old vehicles and vehicles with low European emission standards, the vehicle stocks in Serbia consist of vehicles with an average age of more than 11 years and a low proportion of new vehicles (Velten et al., 2020). Serbia imports low-cost vehicles, which have a substantial impact on air pollution due to excessive kilometers traveled or other shortcomings of vehicles that lower their price. In the ARM period, NO_2 levels increased relative to the RM period (10–30% for raw, and 9–20% for "deveathered" data), but concentrations remained below those in the BRM period (23.7–62.8% for raw, and 11.2–61.5% for "deveathered" data). This was expected because population mobility during the ARM period was still lower than during the BRM period. Changes in O_3 concentrations were also uniform through all measuring stations. Similar to other studies (Chen et al., 2021; Fenech et al., 2021; Hernández-Paniagua et al., 2021; Song et al., 2021), during the RM and ARM periods, there is an increase in O_3 levels (**Figure 4F**). Being a secondary pollutant, the production of O_3 is associated with the changes in meteorological conditions and NO_2 and VOCs concentrations. The decrease in NO_x from motor vehicles in the RM period, while the amount drop of VOC is not as large as NO_x, is linked to a reduced titration effect of O_3 by NO, and leads to higher O_3 concentrations. An increase in O_3 in the late spring and early summer ARM period is associated with higher insolation and temperatures.

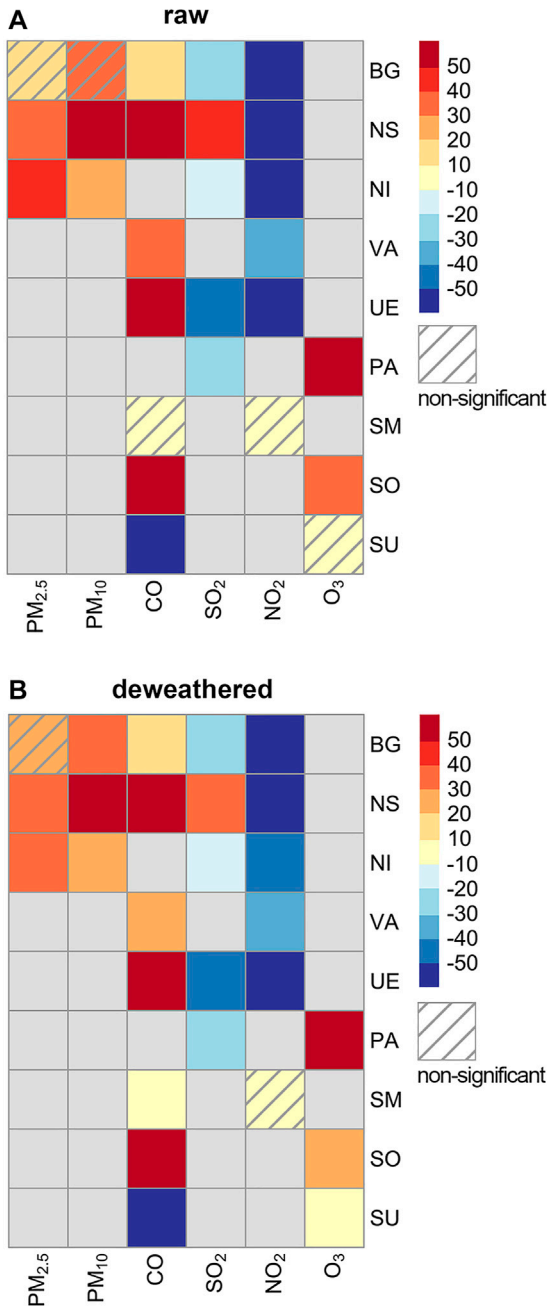

FIGURE 6 | Percentage of variations in raw **(A)** and "deweathered" **(B)** pollutant levels in each city under the study between 2020 and average concentrations in the period 2015–2019.

For PM, the relationship between the decrease in PM_{10} and $PM_{2.5}$ concentration and restrictive measures was unclear and inconsistent (**Figures 4A,B**). A moderate reduction was observed in BG and NI in comparison to the BRM period, followed by a significant reduction during the ARM period, while NS experienced an increase in $PM_{2.5}$ and PM_{10}. An increase in PM in NS may indicate the presence of local sources emitting particles that were active in the RM period. According to Davidović et al. (2021), in the period March 26th–28th the transport of particles from the Aralkum Desert in Asia additionally contributed to the increased concentrations in NS. The raw and "deweathered" data variations (%) for $PM_{2.5}$ ranged from −67.5 to +8.6% and −69.8 to +4.7%, respectively which is within the range of values reported by Gao et al. (2021). Similar to the PM, changes in SO_2 and CO levels in the RM period were uneven and city-specific. At most measuring stations, the changes of SO_2 during the RM period compared to the BRM period were relatively small, up to 11%, except in BG (**Figure 4D**). The levels of CO (both, raw and "deweathered") showed a significant decrease in the RM period at stations in the central and southern part of the country (from −16.3% to −64.7%, and from −13.0% to −50.0%, for measured and "deweathered" data, respectively), while at stations in the north levels of CO increased (SU, SO, and NS).

Hourly and weekly profiles of pollutants in the BRM, RM, and ARM periods contribute to the understanding of the effect of traffic on air pollution (**Figure 5**). Hourly profiles of NO_2 and SO_2 showed two peaks, in the morning (7–9 h) and afternoon (16–19 h), which is expected as the levels of traffic flows are the highest during those periods. It also showed a reduction in the afternoon peaks NO_2 and SO_2 during the RM period indicating a link with reduced mobility. During all three periods, the hourly and weekly variations of $PM_{2.5}$, PM_{10}, and CO showed a similar trend, which is to be expected (**Figures 5A–C**). Measured hourly concentrations during BRM and RM periods revealed a decrease throughout the night (between 00 and 06 h), then an increase between 06 and 10 h, and a drop between 10 and 15 h. During the afternoon, concentrations increase, and the highest peak of the day was achieved between about 19 and 22 h. The late evening peak is linked to both daily changes in the thickness of the atmosphere's boundary layer, which thins during the night, and an increase in emissions from households, such as heating (Vicente et al., 2015; Gama et al., 2018). Higher temperatures, a thicker boundary layer, and lower emissions due to heating during the warmer half of the year result in lower concentrations during the ARM. The same hourly and weekly CO to PM trends, as well as similar daily CO profiles during the BRM and RM periods, indicate that individual residential heating is the primary source of this pollutant. During the RM period, a weekly pattern of all pollutant values revealed an increase in concentrations on Fridays. It can be explained by the fact that every weekend during the RM period, a curfew was in force, therefore on Fridays, a large percentage of the population went shopping and traveled to the countryside.

Changes in Air Pollutant Concentrations During the RM Period in 2020 *Vs.* Average Concentration During the Same Period in Previous Years

For each city, percentage variations in pollutant levels between 2020 and average values in the corresponding period 2015–2019 were calculated to see if pollution concentrations during the RM period were different from those in previous years. **Figure 6** presents variations of raw (**Figure 6A**) and "deweathered" data (**Figure 6B**).

In the majority of cities, PM, CO, and O_3 levels increased, while NO_2 and SO_2 levels decreased in 2020 compared to previous years' averages. Although a decrease in concentrations of $PM_{2.5}$ and PM_{10} compared to previous years' average can be expected, a consistent reduction cannot be seen across all cities, as is the case in Serbia. Similar to finding in Serbian cities, Briz-Redón et al. (2021) reported an increase in PM_{10} levels compared to the year 2019 in several Spanish cities by more than 35%, while Bar et al. (2021) reported higher $PM_{2.5}$ concentrations in Springfield, Lincoln, and Bismarck in 2020 than in 2019. Higher concentrations of PM and CO in Serbian cities during the RM period in 2020 compared to the same period 2015–2020 can be attributed to an increased contribution of emissions from household heating given that the average temperature in cities during the RM period 2020 was lower between 10.5 and 16.9% than in previous years. The high levels of PM during the RM period can also be attributed to the unusually dry period in April 2020 (Republic Hydrometeorological Service of Serbia, 2021). The highest reduction relative to previous years was in NO_2 concentrations, up to above 40%. Those results are similar to findings in the other studies (Baldasano, 2020; Bekbulat et al., 2021; Collivignarelli et al., 2020; Lovrić et al., 2021; etc.). For example, Munir et al. (2021) reported a decrease of 37.3–55.5% in NO_2 levels in three urban areas in Northern England during the lockdown period compared to values in 2019. When compared to the same dates in 2018 and 2019, NO_2 concentrations in urban areas of Poland decreased in the range of 5.3–38.7% in April and May 2020 (Filonchyk et al., 2021). These findings indicate that atmospheric NO_2 is much more sensitive than PM and CO to population mobility.

CONCLUSION

This study focuses on the effects of the restrictive measures due to the COVID-19 pandemic on air pollutants levels at traffic measuring stations in Serbia. The influence of meteorological factors and reduced mobility on the levels of pollutants has been quantified. The analysis of pollutants concentrations was performed for the RM in comparison to BRM and ARM, as well as against the averages in preceding years.

Obtained results showed that the daily concentrations of NO_2 (a primary pollutant produced directly by vehicle emissions) were significantly reduced at all the selected monitoring stations. A percentage reduction of NO_2 was higher than in other countries, indicating a high impact of traffic on NO_2 levels in Serbia. Unlike NO_2, the relationship between particulate matters, CO and SO_2 concentrations, and restrictive measures was unclear and inconsistent. The PM, CO, and SO_2 showed a weak correlation with mobility during the RM period, indicating that, in addition to traffic, their concentrations are also strongly influenced by other sources. When comparing the pollution levels to previous years' average it was discovered that PM and CO concentrations were, confirming a strong link between these pollutants and seasonal variations, and regional and cross-border transport. All together indicate that in the absence of restrictive measures the levels would have been even higher. Also, the traffic reduction during restrictive measures negatively influenced O_3 levels as expected due to NO_2 reduction.

This study confirmed that even a short-term reduction in traffic can significantly improve air quality, especially when it comes to NO_2 concentrations. These findings are encouraging and they should encourage policymakers to limit mobility as a way to enhance air quality. Other sources such as domestic heating, industry, and transportation from other locations also contribute significantly to the increase of pollutant levels, particularly PM and CO concentrations. Therefore, further research will need to better understand the impact of individual sectors.

DATA AVAILABILITY STATEMENT

Publicly available datasets were analyzed in this study. This data can be found here: (https://data.gov.rs/sr/datasets/?q = vazduh&tag = verifikovane-vrednosti (air quality data), https://covid19.apple.com/mobility, https://www.google.com/covid19/mobility/(mobility data), https://www.ncdc.noaa.gov/isd (meteorology data)).

AUTHOR CONTRIBUTIONS

SM-M: Conceptualization, Data curation, Methodology, Software, Writing—original draft. DD: Conceptualization, Visualization, Writing—review and editing. GS: Conceptualization, Data curation, Investigation, Writing—review and editing. MM: Supervision, Writing—review and editing.

REFERENCES

Apple Inc (2020). COVID-19–Mobility Trends Reports. Available at: https://covid19.apple.com/mobility (Accessed August 15, 2021).

Baldasano, J. M. (2020). COVID-19 Lockdown Effects on Air Quality by NO_2 in the Cities of Barcelona and Madrid (Spain). *Sci. Total Environ.* 741, 140353. doi:10.1016/j.scitotenv.2020.140353

Bar, S., Parida, B. R., Mandal, S. P., Pandey, A. C., Kumar, N., and Mishra, B. (2021). Impacts of Partial to Complete COVID-19 Lockdown on NO_2 and $PM_{2.5}$ Levels in Major Urban Cities of Europe and USA. *Cities* 117, 103308. doi:10.1016/j.cities.2021.103308

Bekbulat, B., Apte, J. S., Millet, D. B., Robinson, A. L., Wells, K. C., Presto, A. A., et al. (2021). Changes in Criteria Air Pollution Levels in the US before, during, and after Covid-19 Stay-At-Home Orders: Evidence from Regulatory Monitors. *Sci. Total Environ.* 769, 144693. doi:10.1016/j.scitotenv.2020.144693

Betancourt-Odio, M. A., Martínez-de-Ibarreta, C., Budría-Rodríguez, S., and Wirth, E. (2021). Local Analysis of Air Quality Changes in the Community of Madrid Before and During the COVID-19 Induced Lockdown. *Atmosphere* 12, 659. doi:10.3390/atmos12060659

Briz-Redón, Á., Belenguer-Sapiña, C., and Serrano-Aroca, Á. (2021). Changes in Air Pollution during COVID-19 Lockdown in Spain: A Multi-City Study. *J. Environ. Sci.* 101, 16–26. doi:10.1016/j.jes.2020.07.029

Carslaw, D. C. (2020). *Deweather: An R Package to Remove Meteorological Variation from Air Quality Data*. New York, NY, USA: University of York. Available at: https://github.com/davidcarslaw/deweather (Accessed June 1, 2021).Version 0.6

Carslaw, D. C., and Ropkins, K. (2012). Openair - an R Package for Air Quality Data Analysis. *Environ. Model. Softw.* 27-28, 52–61. doi:10.1016/j.envsoft.2011.09.008

Carslaw, D. C., and Taylor, P. J. (2009). Analysis of Air Pollution Data at a Mixed Source Location Using Boosted Regression Trees. *Atmos. Environ.* 43, 3563–3570. doi:10.1016/j.atmosenv.2009.04.001

CEN (2002). Air Quality – Approach to Uncertainty Estimation for Ambient Air Reference Measurement Methods. *CR*, 14377.

Chen, G., Tao, J., Wang, J., Dong, M., Li, X., Sun, X., et al. (2021). Reduction of Air Pollutants and Associated Mortality During and After the COVID-19 Lockdown in China: Impacts and Implications. *Environ. Res.* 200, 111457. doi:10.1016/j.envres.2021.111457

Collivignarelli, M. C., Abbà, A., Bertanza, G., Pedrazzani, R., Ricciardi, P., and Carnevale Miino, M. (2020). Lockdown for CoViD-2019 in Milan: What Are the Effects on Air Quality? *Sci. Total Environ.* 732, 139280. doi:10.1016/j.scitotenv.2020.139280

Davidović, M., Dmitrašinovic, S., Jovanovic, M., Radonić, J., and Jovaševic-Stojanović, M. (2021). Diurnal, Temporal and Spatial Variations of Main Air Pollutants Before and during Emergency Lockdown in the City of Novi Sad (Serbia). *Appl. Sci.* 11, 1212. doi:10.3390/app11031212

Donzelli, G., Cioni, L., Cancellieri, M., Llopis Morales, A., and Morales Suárez-Varela, M. M. (2021). The Effect of the Covid-19 Lockdown on Air Quality in Three Italian Medium-Sized Cities. *Atmosphere* 11, 1118. doi:10.3390/atmos11101118

Drobnjaković, M., and Spalević, A. (2017). "Naselja Srbije (The Settlements in Serbia)," in *Geografija Srbije (Geography of Serbia)*. Editor M. Radovanović (Belgrade, Serbia): Geografski institut "Jovan Cvijić" SANU), 566–613.

Dunn, R. J. H., Willett, K. M., Thorne, P. W., Woolley, E. V., Durre, I., Dai, A., et al. (2012). Hadisd: A Quality-Controlled Global Synoptic Report Database for Selected Variables at Long-Term Stations From 1973–2011. *Clim. Past.* 8, 1649–1679. doi:10.5194/cp-8-1649-2012

Elith, J., Leathwick, J. R., and Hastie, T. (2008). A Working Guide to Boosted Regression Trees. *J. Anim. Ecol.* 77 (4), 802–813. doi:10.1111/j.1365-2656.2008.01390.x

Elliot, A. J., Smith, S., Dobney, A., Thornes, J., Smith, G. E., and Vardoulakis, S. (2016). Monitoring the Effect of Air Pollution Episodes on Health Care Consultations and Ambulance Call-Outs in England during March/April 2014: A Retrospective Observational Analysis. *Environ. Pollut.* 214, 903–911. doi:10.1016/j.envpol.2016.04.026

Fenech, S., Aquilina, N. J., and Vella, R. (2021). COVID-19-Related Changes in NO2 and O3 Concentrations and Associated Health Effects in Malta. *Front. Sustain. Cities* 3, 631280. doi:10.3389/frsc.2021.631280

Filonchyk, M., Hurynovich, V., and Yan, H. (2021). Impact of Covid-19 Lockdown on Air Quality in the Poland, Eastern Europe. *Environ. Res.* 198, 110454. doi:10.1016/j.envres.2020.110454

Gama, C., Monteiro, A., Pio, C., Miranda, A. I., Baldasano, J. M., and Tchepel, O. (2018). Temporal Patterns and Trends of Particulate Matter over Portugal: a Long-Term Analysis of Background Concentrations. *Air. Qual. Atmos. Health.* 11, 397–407. doi:10.1007/s11869-018-0546-8

Gao, C., Li, S., Liu, M., Zhang, F., Achal, V., Tu, Y., et al. (2021). Impact of the COVID-19 Pandemic on Air Pollution in Chinese Megacities from the Perspective of Traffic Volume and Meteorological Factors. *Sci. Total Environ.* 773, 145545. doi:10.1016/j.scitotenv.2021.145545

Google (2021). Google Community Mobility Reports. Available at: https://www.google.com/covid19/mobility/(Accessed August 15, 2021).

Grivas, G., Athanasopoulou, E., Kakouri, A., Bailey, J., Liakakou, E., Stavroulas, I., et al. (2020). Integrating *In Situ* Measurements and City Scale Modelling to Assess the COVID-19 Lockdown Effects on Emissions and Air Quality in Athens, Greece. *Atmosphere* 11, 1174. doi:10.3390/atmos11111174

Hernández-Paniagua, I. Y., Valdez, S. I., Almanza, V., Rivera-Cárdenas, C., Grutter, M., Stremme, W., et al. (2021). Impact of the COVID-19 Lockdown on Air Quality and Resulting Public Health Benefits in the Mexico City Metropolitan Area. *Front. Public. Health* 9, 642630. doi:10.3389/fpubh.2021.642630

Institute for standardization of Serbia (2021). Draft Serbian Standards on Public Enquiry. Available at: https://195.178.42.116/en/project/advanced-search (Accessed October 22th, 2021).

Lenzen, M., Li, M., Malik, A., Pomponi, F., Sun, Y.-Y., Wiedmann, T., et al. (2020). Global Socio-Economic Losses and Environmental Gains from the Coronavirus Pandemic. *Plos One* 15 (7), e0235654. doi:10.1371/journal.pone.0235654

Likhvar, V. N., Pascal, M., Markakis, K., Colette, A., Hauglustaine, D., Valari, M., et al. (2015). A Multi-Scale Health Impact Assessment of Air Pollution over the 21st Century. *Sci. Total Environ.* 514, 439–449. doi:10.1016/j.scitotenv.2015.02.002

Lovrić, M., Pavlović, K., Vuković, M., Grange, S. K., Haberl, M., and Kern, R. (2021). Understanding the True Effects of the COVID-19 Lockdown on Air Pollution by Means of Machine Learning. *Environ. Pollut.* 274, 115900. doi:10.1016/j.envpol.2020.115900

Menut, L., Bessagnet, B., Siour, G., Mailler, S., Pennel, R., and Cholakian, A. (2020). Impact of Lockdown Measures to Combat Covid-19 on Air Quality over Western Europe. *Sci. Total Environ.* 741, 140426. doi:10.1016/j.scitotenv.2020.140426

Munir, S., Coskuner, G., Jassim, M. S., Aina, Y. A., Ali, A., and Mayfield, M. (2021). Changes in Air Quality Associated with Mobility Trends and Meteorological Conditions during COVID-19 Lockdown in Northern England, UK. *Atmosphere* 12, 504. doi:10.3390/atmos12040504

NOAA (National Oceanic and Atmospheric Administration) (1901—present). Integrated Surface Database. Available at: https://www.ncdc.noaa.gov/isd (Accessed August 18, 2021).

Prats, R. M., van Drooge, B. L., Fernández, P., Marco, E., and Grimalt, J. O. (2021). Changes in Urban Gas-Phase Persistent Organic Pollutants During the COVID-19 Lockdown in Barcelona. *Front. Environ. Sci.* 9, 650539. doi:10.3389/fenvs.2021.650539

R Core Team (2013). *R: A Language and Environment for Statistical Computing*. Vienna, Austria: R Foundation for Statistical Computing. Available at: http://www.R-project.org/(Accessed June 1, 2021).

Regulation on monitoring conditions and air quality requirements (2013). This Regulation Enters into Force Eight Days after its Publication in the Official Gazette. Available at: http://www.pravno-informacioni-sistem.rs.

Republic Hydrometeorological Service of Serbia (2021). Annual Bulletin for Serbia the Year of 2020. Available at: http://www.hidmet.gov.rs/data/klimatologija/eng/2020.pdf (Accessed August 18, 2021).

Ridgeway, R. with contributions from others (2017). Gbm: Generalized Boosted Regression Models. R Package. Version 2.1.3. Available at: https://CRAN.R-project.org/package=gbm.

Ropkins, K., and Tate, J. E. (2021). Early Observations on the Impact of the COVID-19 Lockdown on Air Quality Trends across the UK. *Sci. Total Environ.* 754, 142374. doi:10.1016/j.scitotenv.2020.142374

RStudio Team (2015). *RStudio*. Boston, MA: Integrated Development Environment for R. Available at: http://www.rstudio.com/(Accessed June 1, 2021).

Serbian Environmental Protection Agency (SEPA) (2021). Combined Review of Automatic Air Quality Monitoring in the Republic of Serbia. Available at: http://www.amskv.sepa.gov.rs/(Accessed May 26, 2021).

Serbian Environmental Protection Agency (SEPA), Ministry of Environmental Protection, Republic of Serbia (2012). Environment Report in the Republic of Serbia for the 2011 Year (In Serbian). Available at: http://www.sepa.gov.rs/download/Izvestaj2011.pdf (Accessed August 15, 2021).

Serbian Environmental Protection Agency (SEPA), Ministry of Environmental Protection, Republic of Serbia (2013). Environment Report in the Republic of Serbia for the 2012 Year (In Serbian). Available at: http://www.sepa.gov.rs/download/Izvestaj_2012.pdf (Accessed August 15, 2021).

Setton, E., Marshall, J. D., Brauer, M., Lundquist, K. R., Hystad, P., Keller, P., et al. (2011). The Impact of Daily Mobility on Exposure to Traffic-Related Air Pollution and Health Effect Estimates. *J. Expo. Sci. Environ. Epidemiol.* 21, 42–48. doi:10.1038/jes.2010.14

Shi, Z., Song, C., Liu, B., Lu, G., Xu, J., Van Vu, T., et al. (2021). Abrupt but Smaller Than Expected Changes in Surface Air Quality Attributable to COVID-19 Lockdowns. *Sci. Adv.* 7, eabd6696. doi:10.1126/sciadv.abd6696

Song, Y., Lin, C., Li, Y., Lau, A. K. H., Fung, J. C. H., Lu, X., et al. (2021). An Improved Decomposition Method to Differentiate Meteorological and Anthropogenic Effects on Air Pollution: A National Study in China during

the COVID-19 Lockdown Period. *Atmos. Environ.* 250, 118270. doi:10.1016/j.atmosenv.2021.118270

Stanojevic, G., Miljanovic, D., Doljak, D., Curcic, N., Radovanovic, M., Malinovic-Milicevic, S., et al. (2019). Spatio-Temporal Variability of Annual $PM_{2.5}$ Concentrations and Population Exposure Assessment in Serbia for the Period 2001-2016. *J. Geogr. Inst. Cvijic* 69 (3), 197–211. doi:10.2298/IJGI1903197S

Statistical Office of the Republic of Serbia (2020). Municipalities and Regions of the Republic of Serbia, 2020. Available at: https://publikacije.stat.gov.rs/G2020/PdfE/G202013047.pdf (Accessed July 30, 2021).

Statistical Office of the Republic of Serbia (2021). Statistical Release. Available at: https://publikacije.stat.gov.rs/G2021/PdfE/G20211181.pdf (Accessed July 30, 2021).

Sujaritpong, S., Dear, K., Cope, M., Walsh, S., and Kjellstrom, T. (2014). Quantifying the Health Impacts of Air Pollution under a Changing Climate-A Review of Approaches and Methodology. *Int. J. Biometeorol.* 58, 149–160. doi:10.1007/s00484-012-0625-8

Velten, E. K., Brauer, C., and Thie, J. E. (2020). *Used Vehicle Trade and Fleet Composition in EuropeFinal Report of the Project "Used Vehicle Trade and Fleet Composition in Europe" on Behalf of the EEA*. Berlin, Karlsruhe: Ecologic Institute and Fraunhofer Institute for Systems and Innovation Research ISI.

Venter, Z. S., Aunan, K., Chowdhury, S., and Lelieveld, J. (2020). COVID-19 Lockdowns Cause Global Air Pollution Declines. *Proc. Natl. Acad. Sci. U.S.A.* 117, 18984–18990. doi:10.1073/pnas.2006853117

Vicente, E. D., Duarte, M. A., Calvo, A. I., Nunes, T. F., Tarelho, L., and Alves, C. A. (2015). Emission of Carbon Monoxide, Total Hydrocarbons and Particulate Matter during Wood Combustion in a Stove Operating under Distinct Conditions. *Fuel Process. Technol.* 131, 182–192. doi:10.1016/j.fuproc.2014.11.021

Weber, S. A., Insaf, T. Z., Hall, E. S., Talbot, T. O., and Huff, A. K. (2016). Assessing the Impact of Fine Particulate Matter ($PM_{2.5}$) on Respiratory-Cardiovascular Chronic Diseases in the New York City Metropolitan Area Using Hierarchical Bayesian Model Estimates. *Environ. Res.* 151, 399–409. doi:10.1016/j.envres.2016.07.012

WHO (World Health Organization) (2018). WHO Ambient (Outdoor) Air Quality Database, Summary Results, Update 2018. Available at: https://www.who.int/airpollution/data/AAP_database_summary_results_2018_final2.pdf (Accessed June 1, 2021).

WHO (World Health Organization) Regional Office for Europe (2019). Health Impact of Ambient Air Pollution in Serbia, A Call to Action. Available at: https://serbia.un.org/en/22141-health-impact-ambient-air-pollution-serbia-call-action (Accessed June 1, 2021).

WHO (World Health Organization) Regional Office for Europe (2021). *Review of Evidence on Health Aspects of Air Pollution: REVIHAAP Project: Technical Report*. Copenhagen: World Health Organization. Available at: https://apps.who.int/iris/handle/10665/341712 (Accessed June 1, 2021).

Xu, Q., Li, X., Wang, S., Wang, C., Huang, F., Gao, Q., et al. (2016). Fine Particulate Air Pollution and Hospital Emergency Room Visits for Respiratory Disease in Urban Areas in Beijing, China, in 2013. *Plos One* 11, e0153099. doi:10.1371/journal.pone.0153099

Conflict of Interest: The authors declare that the research was conducted in the absence of any commercial or financial relationships that could be construed as a potential conflict of interest.

Publisher's Note: All claims expressed in this article are solely those of the authors and do not necessarily represent those of their affiliated organizations, or those of the publisher, the editors and the reviewers. Any product that may be evaluated in this article, or claim that may be made by its manufacturer, is not guaranteed or endorsed by the publisher.

frontiers | Frontiers in Environmental Science

TYPE Original Research
PUBLISHED 24 August 2022
DOI 10.3389/fenvs.2022.911363

OPEN ACCESS

EDITED BY
Yang Gao,
Ocean University of China, China

REVIEWED BY
Pinya Wang,
Nanjing University of Information Science and Technology, China
Chenghai Wang,
Lanzhou University, China

*CORRESPONDENCE
S. Fadnavis,
suvarna@tropmet.res.in

SPECIALTY SECTION
This article was submitted to Atmosphere and Climate, a section of the journal Frontiers in Environmental Science

RECEIVED 02 April 2022
ACCEPTED 27 July 2022
PUBLISHED 24 August 2022

CITATION
Asutosh A, Fadnavis S, Chavan P, Sabin TP and Müller R (2022), Abrupt emission reduction during COVID-19 intensified the spring 2020 rainfall over India.
Front. Environ. Sci. 10:911363.
doi: 10.3389/fenvs.2022.911363

Abrupt emission reduction during COVID-19 intensified the spring 2020 rainfall over India

A. Asutosh[1], S. Fadnavis[2]*, Prashant Chavan[2], T. P. Sabin[2] and Rolf Müller[3]

[1]Indian Institute of Technology Bhubaneswar, Bhubaneswar, OD, India, [2]Indian Institutes of Tropical Meteorology, Ministry of Earth Sciences, Pune, India, [3]Forschungszentrum Jülich GmbH, IEK-7, Jülich, Germany

The high level of aerosol pollution in South Asia has a measurable impact on clouds, radiation, and precipitation. Here, exploring multiple observational data sets and simulations of the state-of-the-art ECHAM6-HAMMOZ chemistry-climate model, we report that the reduction in anthropogenic emissions during the COVID-19 lockdown period has enhanced precipitation by 5–25% over India. This precipitation enhancement is the result of the combined effect of an enhancement in cloud cover, a reduction in aerosol induced cloud invigoration and dynamical changes. We observed that the increase in cloud cover was associated with a reduction in cloud base height and an increase in the effective radius of cloud particles which led to an increase in cloud water content. In response to sudden emission reduction, an anomalous northward moisture transport was observed adding convection and precipitation over the Indian region. Importantly, we show that there is an advantage of anthropogenic pollution reduction for water availability in addition to benefits of air quality, human health, and crop yield.

KEYWORDS

COVID-19, emission reduction, regional climate, precipitation enhancement, cloud properties

1 Introduction

Environmental deterioration in the South Asian region as a result of rising levels of air pollution has harmed people's health (Chowdhury et al., 2018; Balakrishnan et al., 2019; Manisalidis et al., 2020), reduced crop yield, and hence has damaged the economy (Gu et al., 2018). Ground-level pollutants are known to cause serious impacts on people's health (Ghude et al., 2016). Additionally, the elevated level of aerosol pollution is prone to impact the hydrological cycle (Ramanathan et al., 2005; Lau et al., 2006; Fadnavis et al., 2019, Fadnavis et al.,2013). However, the lockdown restrictions imposed to control the transmission of the Corona-Virus Disease 2019 (COVID-19) caused a drastic reduction in emissions of pollutants globally (Isaifan, 2020; Navinya et al., 2020; Sanap, 2021).

On 11 January 2020, the World Health Organization (WHO) declared a worldwide health emergency due to the COVID-19. The disease was initially discovered in late December 2019 in China (Muhammad et al., 2020; Pandey et al., 2020). To prevent

widespread transmission and an increase in the death toll, countries around the world imposed a complete or partial shutdown of human activities, starting primarily in March 2020. From March 23 until 31 May 2020, South Asia (including India) and south-east Asian countries implemented the first lockdown phase. As a result, anthropogenic emissions from transportation, urban areas, and industries were reduced significantly during this period (Zhang et al., 2021). According to past studies, the lockdown induced less human activity, which indirectly helped in improving air quality around the planet (Zhang et al., 2021; Menut et al., 2020; Lou et al., 2022). Over a large part of the globe, concentrations of major pollutants were found to be lower compared to their long-term mean (past 10 years), in particular NO_2 (nitrogen dioxide) (by −30% to −50%), SO_2 (sulphur dioxide) (by −20% to −35%), CO (carbon monoxide) (−15% to −20%), and particulate matter $PM_{2.5}$ and PM_{10} (by up to 49%). Several studies have documented a decrease in aerosol and other gaseous concentrations over China (Bao and Zhang, 2020; Bauwens et al., 2020) as well as over India (Gautam, 2020; Mahato et al., 2020; Navinya et al., 2020)

Anthropogenic emissions from various sources, including transportation, industry, and other commercial sectors, as well as agriculture, contribute to South Asia's long-standing air pollution problem. Restrictions imposed during the COVID-19 lockdown period resulted in reducing high levels of pollution in Asia, particularly over hotspot regions such as East Asia, the Indo Gangetic Plains (IGP), the Indonesian region, and eastern China, according to in-situ and satellite observations (Liu et al., 2021, Venter et al., 2020). A recent population density estimate shows the high population density over IGP (Supplementary Figure S1). Even if only for a short time during the lockdown period (April–May 2020), reduced pollution levels may pause (or even temporally reverse) increasing trend in anthropogenic aerosol emissions over South Asia.

Atmospheric aerosols interact with the earth's radiation directly and through clouds via the indirect effect. The aerosol over South Asia attenuates solar radiation by 10–25 W m^{-2} (Li et al., 2016). Changes in anthropogenic aerosol emissions contribute to changes in surface air temperature, low-level humidity, atmospheric circulation, Upper Troposphere and Lower Stratosphere (UTLS) processes, and even rainfall patterns (Ramanathan et al., 2005; Bollasina et al., 2014; Vinoj et al., 2014; Li et al., 2016; Fadnavis et al., 2018). Aerosol particles act as cloud condensation and ice nuclei, therefore, modulating the nature of the cloud by changing cloud brightness, thickness, and lifetime (Twomey, 1977; Albrecht, 1989; Zhao et al., 2018). These cloud properties further interact with cloud radiation features and indirectly with circulation and precipitation. However, our scientific understanding of aerosol-climate interactions is still incomplete (Stocker et al., 2013; Li et al., 2016). Due to the complex nature of aerosol-cloud interactions, there is large uncertainty in estimating the cloud susceptibility for aerosol emission changes and quantifying radiative impacts of aerosols in varying emission and meteorological scenarios (Stocker et al., 2013; Li et al., 2016). It is crucial to resolve such uncertainty to understand the future global and regional climate responses to the combination of emissions of greenhouse gases and aerosols (Samset et al., 2016; Myhre et al., 2017).

The first phase of the COVID-19 lockdown provides us with a unique opportunity to study the possible regional climate response to short-term reductions of atmospheric gases and pollutants. Here, we investigate the effects of the reductions in regional atmospheric concentrations of several gases and anthropogenic aerosol on rainfall, clouds, water vapour, and consequently on rainfall over South Asia during the lockdown period April–May 2020. For this purpose, we use the state-of-art ECHAM6.3-HAM2.3-MOZ1.0 aerosol-chemistry climate model (Schultz et al., 2018; Tegen et al., 2019). The goal of our study is to isolate the effect of the Asian anthropogenic pollution on clouds and precipitation during April-May caused by the COVID-19 restrictions. There is a large volume of COVID-19 related studies, but most of them are mainly focused on air quality improvements (Navinya et al., 2020; Dumka et al., 2021; Manchanda et al., 2021). A recent study by Yang et al. (2022) showed that the COVID-19 induced substantial reduction in anthgropogenic aerosols and greenhouse gases (GHGs) strengthened the summer atmospheric convection over eastern China and further intensified rainfall. The study also highlighted that the impact of aerosol are stonger over GHGs on change in precipitation. Hence, we suggest detailed modelling studies, which may shed further light on the link between aerosol reduction and associated regional climatic effects (Khatri et al., 2021).

While a few studies investigated the associations between rainfall during monsoon season and COVID-19 lockdown (Fadnavis et al., 2021; Kripalani et al., 2022), those are mostly linked to the change in atmospheric dynamics and not to the roles of clouds for the observed changes in rainfall. Additionally, accurate aerosol-climate impact assessments are essential in implementing future national and international air pollution mitigation strategies.

This paper is organised as follows. Section 2 explains the details of the model experiments and datasets used in this study. Major findings from the analysis are presented in Section 3, a mechanism for rainfall enhancement is proposed in Section 4, followed by a summary and conclusion in Section 5.

2 Material and methods

2.1 The model description and the experimental set-up

We adopt the reductions in anthropogenic emission due to the COVID-19 restrictions based on the activity decline in

mobility data from Google and Apple following Forster et al. (2020) (Supplementary Table S1 and see Fadnavis et al., 2021 for details). The model comprises of three sub-modules 1) the ECHAM6 (Stevens et al., 2013) atmospheric general circulation module, 2) the MOZ tropospheric chemistry module (Schultz et al., 2018; Tegen et al., 2019), and 3) the Hamburg Aerosol Model (HAM). The HAM submodule predicts nucleation, growth, evolution, and sinks of sulphate (SO_4^{2-}), black carbon (BC), particulate organic matter (POM), sea salt (SS), and mineral dust (DU) aerosols (Stier et al., 2005; Zhang et al., 2012). The MOZ submodule describes the trace gas chemistry from the troposphere to the lower thermosphere, including 108 species, 71 photolytic processes, 218 gas-phase reactions, and 18 heterogeneous reactions with aerosol (Schultz et al., 2018). We performed the model simulations at the T63 spectral resolution i.e., 1.875°× 1.875° in the horizontal and 47 levels in the vertical from the surface to 0.01 hPa (corresponding to approximately 80 km), with a time step of 20 min. Details of emissions (anthropogenic, biomass burning, biogenic, fossil fuel, etc.) are reported by Fadnavis et al. (2021). The ECHAM6-HAMMOZ model experimental set-up and simulations details are as described by Fadnavis et al. (2021). While Fadnavis et al. (2021) report the impact of COVID lockdown emission reduction on the Indian summer monsoon precipitation, here, we show the effect of emission reductions on clouds during spring 2020 (April-May).

The simulation consists of two sets of ten-member ensemble simulations 1) the control experiment, referred to as CTRL hereafter, and 2) the sensitivity experiment for the reductions in anthropogenic emission due to the COVID-19, referred to as C19, hereafter. Other sets were created from initial conditions with the start time shifted by 1 day from March 1–10 and then simulated for a year to obtain stabilized fields. The initial and boundary conditions for both sets of simulations were set to the year 2016. The year 2016 was chosen because the El Nino-Southern Oscillation (ENSO) and the Indian Ocean Dipole (IOD) were both in a neutral phase, making it perfect for isolating COVID-19 emission influences. This way we avoid interference of impacts COVID emission changes with of ENSO or the Indian Ocean dipole. Both tests use the same dust emission parameterization based on Tegen et al. (2002).

2.2 Observational datasets

To evaluate the model aerosol optical depth (AOD), we have used the Level 3 AOD from the Moderate Resolution Imaging Spectroradiometer (MODIS). MODIS is onboard the Terra/Aqua satellites and provides daily aerosol products (Levy et al., 2010; Namdari et al., 2018). MODIS has a view scan of ±55° and an orbit of 700 km above the ground. MODIS AOD is extensively used in aerosol related studies. More information is available at http://modis.gsfc.nasa.gov/. Additionally, to add confidence to the modelled AOD, we have compared MODIS with Modern-Era Retrospective Analysis Research and Applications, Version 2 (MERRA-2) aerosol data assimilated from Goddard Earth Observing System-5 (GEOS-5) atmospheric general circulation Model (Gelaro et al., 2017). The GEOS-5 coupled with Goddard Chemistry Aerosol Radiation and Transport (GOCART) model and aerosol observations from space for better representation of aerosols in the model (Buchard et al., 2014).

The NOAA Interpolated Outgoing Longwave Radiation (OLR) data are used as a proxy of cloud cover/water vapour during the study period (April–May 2020). OLR values are often used as a proxy for convection/cloud in tropical and subtropical regions. In addition, the ERA-5 reanalysis datasets (Hersbach et al., 2020) are used for cloud cover, cloud base height, and precipitation information. The horizontal resolution of ERA5 is ~31 km, and there are 137 model levels (from the ground up to 0.01 hPa). ERA5 uses the IFS Cy41r2 4D-Var assimilation system. The India Meteorological Department (IMD) gridded rainfall datasets (Dash et al., 2006; Srinivas et al., 2013) have also been used to compare the observed IMD precipitation with the model derived precipitation. It should be noted that the analysis is performed for the national lockdown period across India in 2020, i.e., for April and May (lockdown period hereafter). For variables using observational data, the anomalies and percentage changes are determined by comparing mean of April-May 2020 to the mean of April-May for five-years 2016–2019. On the other hand, we employ the C19 and CTRL simulations for similar computations from the model (averaged over 10 ensemble members).

3 Results and discussions

3.1 AOD changes due to anthropogenic aerosol reduction over South Asia

The simulated aerosol optical depth (AOD) anomaly is evaluated against the MODIS satellite observation and MERRA-2 during the lockdown period (Figure 1). When AOD is compared to its five-year mean, both MERRA and MODIS reveal a significant reduction in AOD over India (between 10% and 40%). Polluted areas, such as the IGP, show a significant decline in AOD (MODIS: 30–40%, Model: 5%–25%, MERRA: 10%–30%). The drop in AOD across the Bay of Bengal (MODIS: 10%–40%, MERRA: 10%–25% MODEL: 10%–30%), on the other hand, could be related to a weaker aerosol outflow from the IGP. Every spring, aerosol pollution is transported from the IGP to the Bay of Bengal (Thomas et al., 2021). The reduction in anthropogenic pollution over the IGP during the lockdown period resulted in the transport of less aerosol to the Bay of Bengal than in prior years (five-year mean). The slight enhancement in AOD

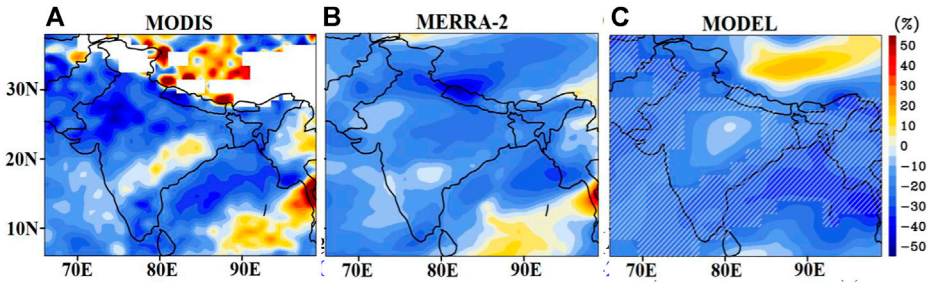

FIGURE 1
(A) Percentage change in aerosol optical depth (AOD) averaged for the lockdown period (mean of April-May 2020 - mean of April-May 2016–2019) calculated from **(A)** MODIS satellite observation, **(B)** MERRA-2 reanalysis, **(C)** ECHAM6-HAMMOZ simulated AOD anomalies (C19—CTRL) averaged over 10 members. Hatching shows the area where mean differences between C19 and CTRL are statistically significant at a 95% confidence level.

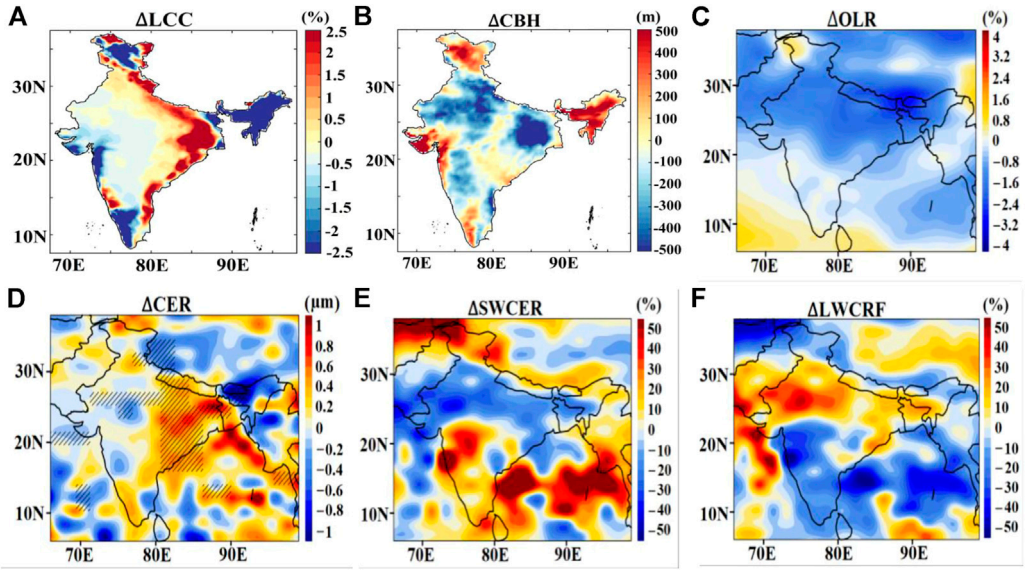

FIGURE 2
Spatial distribution of anomalies (2020—mean of 2016–2019) averaged for the lockdown period for **(A)** Low Cloud Cover (ΔLCC) and **(B)** Cloud Base Height from ERA5 (ΔCBH). The rest of the figures are for simulated anomalies (C19—CTRL) averaged over 10 members and for the lockdown period, **(C)** outgoing longwave radiation (ΔOLR, %), **(D)** Cloud Effective Radius (Δ CER, μm), **(E)** Short Wave Cloud Radiative Forcing (ΔSWCRF, %), **(F)** Longwave Cloud Radiative Forcing (Δ LWCRF, %). Hatching shows the area where mean differences between C19 and CTRL are statistically significant at a 90% confidence level.

anomalies over central and southern India (both in MODIS and MERRA-2) could be attributed to particle growth in response to changes in relative humidity, atmospheric background conditions, or agricultural fires (Pandey and Vinoj, 2021; Sanap, 2021). It is worth noting that the simulated ensemble mean AOD may qualitatively approximate the spatial pattern of AOD from MERRA-2 and MODIS. Anomalies of simulated AOD show fair agreement with Aerosol Robotic Network (AERONET) ground based observations at Kanpur Lon: 80.23°E, Lat: 26.51°N), Lahore (Lon:74.26°E, Lat:31.48°N) and Gandhi Collage (Lon: 84.12°E, Lat: 25.87°N) in the Indo-Gangetic Plain during the lockdown period (mean of April-May 2020- mean April-May during 2016–2019) (Fig. S2a). As a result, the model may be used to analyze the response of emission reductions that may have occurred as a result of the COVID-19 lockdownMany previous studies (Fadnavis et al., 2021, 2018) reported satisfactory model performance versus multiple observations for AOD, absorbing aerosol index, precipitation, mixing ratio black carbon aerosol, cloud ice, etc.

3.2 Cloud response to the reduction in anthropogenic aerosol emissions

Changes in aerosol field emission caused by the lockdown could have had an impact on radiation and cloud characteristics (Timmermann et al., 2020; Khatri and Hayasaka, 2021). Here, we show changes in cloud parameters in response to aerosol changes during the lockdown period. The ERA5 reanalysis revealed an unusual increase in the low cloud (>5%) and a drop in cloud base height (CBH) (>500 m) during the lockdown period in 2020 (Figure 2A,B). These characteristics are particularly noticeable over the IGP and adjacent regions, where the most significant reduction in aerosols was observed (Figure 1).

The anthropogenic changes during the lockdown period may be reflected in the shift in cloud microphysical features and accompanying atmospheric conditions. The model simulations show the response of cloud properties to the anthropogenic aerosol reduction (Figure 2). There is an unusual drop in outgoing longwave radiation in model simulations and an increase in cloud effective radius (Figures 2C,D). NOAA's outgoing longwave radiation anomalies have also shown a similar reduction (1.6%–4%) as observational evidence (Supplementary Figure S2b).

The locations of maximum decrease in outgoing longwave radiation are co-located with the location of maximum increase in low clouds (Figure 2C) and maximum reduction of aerosol optical depths (Figure 1). Additionally, a decrease in aerosol loading over the IGP has resulted in a decrease in shortwave (−10% to −40%) and an increase in longwave (10%–50%) cloud radiative forcing anomalies (Figure 2 e-f). These results also support the increase in cloud cover. The strong negative short wave cloud radiative forcing over the IGP is partly compensated by the longwave induced warming (Figures 2E,F). It is known that both droplet size and cloud cover are reduced in the presence of absorbing aerosols (Hansen et al., 1997). There is a reduction in simulated absorbing AOD (BC) by 10–30% over the Indian region. As a result of reduced AOD resulting in an enhancement in cloud cover (Figures 2A,B) and a higher cloud effective radius (Figure 2D), such cloud burning (reducing) efficiency (also known as aerosol semi-direct effect) could have been reduced over the Indian region (strong decrease over the IGP) in 2020, as seen in C19 simulation as a response to reduced AOD, resulting in large cloud cover.

From our model simulations, the changes in cloud parameters in 2020 (C19—CTL) indicate the response of clouds to anthropogenic emission reduction (Figure 2). It is well known that in the presence of an anomalous increase in aerosol loading, cloud invigoration may take place, i.e., in response to increased aerosol number concentration; there can be a decrease in cloud-droplet size (Rosenfeld et al., 2014; Zhao et al., 2018; Khatri et al., 2021). This may further lead to vertical cloud growth and conversion of a water cloud into an ice cloud. Since, large amounts of aerosol in the atmosphere help in enhancing cloud vertical movement that leads to an increase in the conversion of water clouds to ice clouds due to the combination of rain inhibition and vertical growth (Rosenfeld et al., 2014; Khatri et al., 2021).

The model simulations (an increase of effective radius as a proxy for cloud droplet size, Figure 2D) and ERA5 indicate that this aerosol invigoration impact may have been suppressed because of the aerosol reduction in 2020 (COVID condition) (reduction in cloud base height). An increase in cloud effective radius further results in larger cloud droplets, which leads to less droplet evaporation and further modulation of precipitation (discussed in Section 4).

We also present the averaged vertical distribution of aerosol extinction and cloud parameters over the IGP region (78–90°E, 18–27°N, where the greatest aerosol reduction occurred (Figure 3). Figure 3A shows negative anomalies in aerosol extinction with a maximum decrease near the surface. Interestingly, there is an increase in cloud droplet effective radius between 1,000–400 hPa (Figure 3B, max up to 0.6 ± 0.2 microns at 800 hPa). Consistent with our results, Khatri et al., 2021, also observed an increase (in the range of 10 – 20%) in cloud effective radius values over the IGP in 2020 compared to previous years. Furthermore, anomalous lower-level circulation/meteorological feedbacks may be responsible for a large increase in low level (below 500 hPa) relative and specific humidity profiles (Figures 3C,F) (discussed in Section 3.3). In the reduction aerosol emission/pristine scenario (Like the C19 case), features are conducive to the enhancement in cloud effective radius/droplet size (Jayaraman, 2001). The reduction in cloud droplet evaporation further helps in increasing cloud cover (Figure 3D) and precipitation. A recent study of the conditions over China (Yang et al., 2022) shows an enhancement in cloud cover at all the levels of the atmosphere in response to COVID-19 aerosol emission reduction, in support of our findings.

3.3 Possible response of atmospheric conditions to emission changes

This section covers the possible effects of reduced anthropogenic emissions on atmospheric conditions. The response of near-surface air temperature is shown in Figure 4A. The eastern part of the IGP and the southeast Indian regions have experienced significant warming. This increased temperature could be explained in part by the reduction of aerosol pollution in the atmosphere, which increases incoming solar radiation and thus short-wave warming (Fadnavis et al., 2021). The east-west dipolar temperature response (Figure 4A) (warming over North East

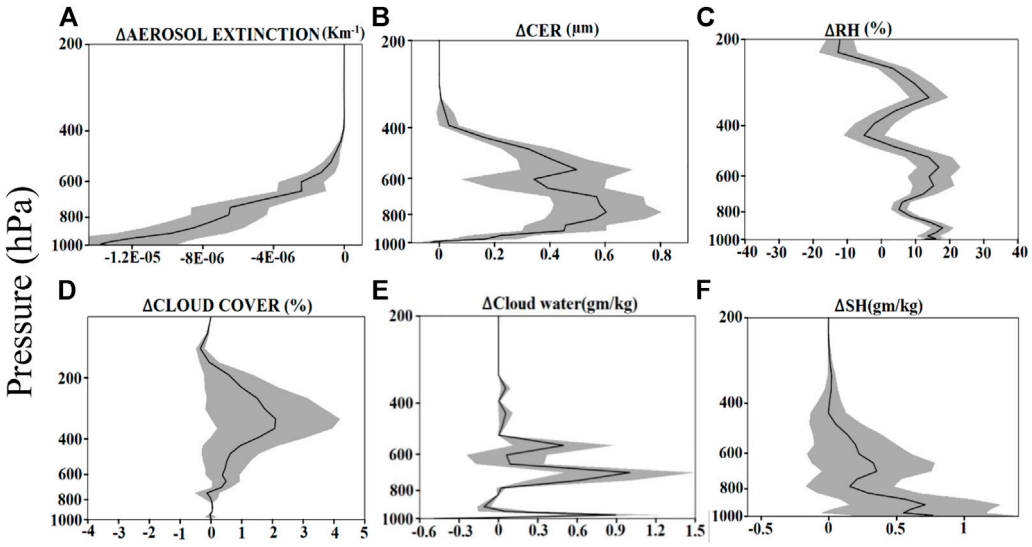

FIGURE 3
Area averaged (78:90°E, 18–27°N) ECHAM6-HAMMOZ simulated anomalies (C19—CTRL) averaged over 10 members and for the lockdown period for **(A)** Aerosol extinction coefficient (km^{-1}), **(B)** cloud effective radius (ΔCER, μm), **(C)** relative humidity (ΔRH, %), and **(D)** cloud cover (%), **(E)** cloud water (gm kg^{-1}), **(F)** specific humidity (gm kg^{-1}). The shading represents the standard error of the difference of the means.

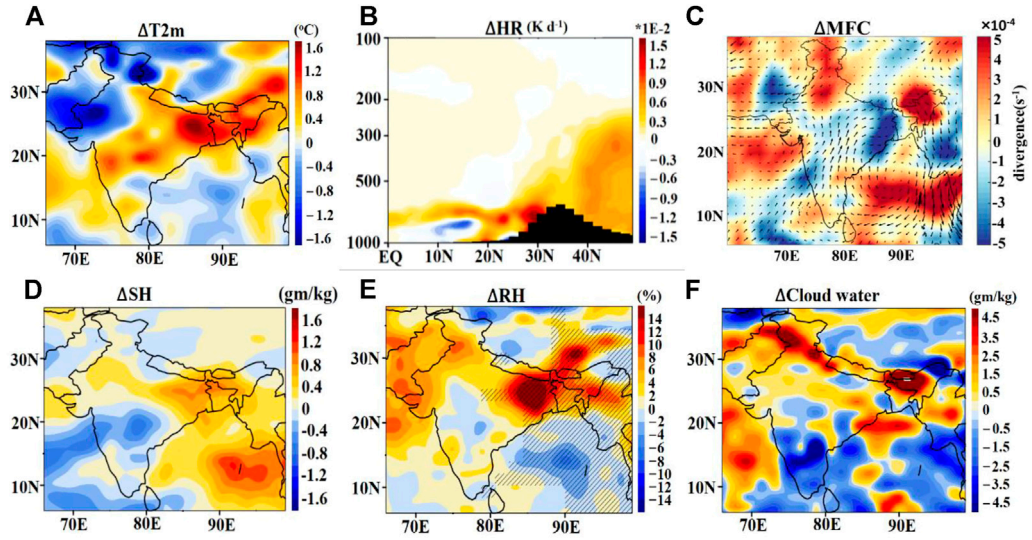

FIGURE 4
Spatial distribution of ECHAM6-HAMMOZ simulated anomalies (C19—CTRL) averaged over 10 members and for lockdown period for **(A)** 2 m air temperature (ΔT2m, °C) **(B)** heating rate (averaged over 70–90°E, ΔHR, K d^{-1}) **(C)** column integrated moisture flux divergence (1,000–300 hPa), arrows indicate column integrated moisture flux (kg m^{-1} s^{-1}), **(D)** specific humidity (averaged for 1,000–500 hPa, gm kg^{-1}),**(E)** relative humidity (averaged for 1,000–500 hPa, %) and **(F)** cloud water (averaged over the surface to 500 hPa, gm/kg).

India and cooling over the North-West India and Pakistan region), however, does not precisely follow the regions of pollution reductions (Figure 1). The cooling over the North-West India and Pakistan region is due to subsidence in return to the ascent over North India - Tibetan Plateau region (80–90°E, 20–30°N) (Supplementary Figure S3). These circulation

changes are the response to changes in convection, cloud, and associated cloud radiative forcing (Figure 2). Additionally, the heating rates (averaged over 70–90°E, Figure 4B) show warming (>0.015 K d^{-1}) in the lower troposphere over northern India and at the foothills of the Himalayas. The high elevated Tibetan Plateau region (TP) also shows moderate heating (~0.005 K d^{-1}) that has further extended vertically to the 200 hPa level (Figure 4B). The heating over these regions is conducive to the early onset of the monsoon (during May–June) and enhanced rainfall over north India, as suggested by previous studies (Lau et al., 2008, 2006; Lau, 2016). The mechanism proposed by Lau et al. (2006) mainly points to the presence of absorbing aerosols (dust and BC) as the reason behind elevated heating and rainfall enhancement (known as an elevated heat pump or EHP). A recent study showed that there is anomalous dust transport towards Tibetan Plateau regions from Taklamakan (North-Western Asian desert regions) as a response to COVID-19 induced circulation changes during April-May 2020 (Fadnavis et al., 2021). Another recent modelling study by Yang et al. (2022) also discussed COVID-19 emission induced enhancement in atmospheric heating rates. Supplementary Figure S3b depicts dust migration from the Taklamakan desert to the Tibetan Plateau. Dust AOD is anomalously enhanced by 20%–40% in the Tibetan Plateau region. The total warming in the North India-TP regions occurs because of the combined effect of anthropogenic emission reduction as well as elevated natural aerosol (dust) induced warming (EHP).

Moisture flux convergence (MFC) is a popular matrix to study precipitation by linking it to both moisture and precipitation (Fasullo & Webster 2003). The detailed theory and mathematical calculation of MFC are provided in Appendix A. A negative divergence (convergence) correlates well with the area of maximum precipitation (Chansaengkrachang et al., 2018). A response to anthropogenic pollution reduction is an overall moisture flux convergence observed over a large part of the north and central Indian region (Figure 4C), (moisture sink). Both Bay of Bengal and the Northern Arabian Sea act as a moisture sources with strong positive MFC (divergence).

In response to sudden emissions reductions, the aerosol effects were mainly mediated through fast climate responses including changes in large scale atmospheric circulation (Wang et al., 2017; Lin et al., 2018; Wing et al., 2017; Lin et al., 2018). A change in surface circulation pattern is also observed in response to anthropogenic pollution reduction (Supplementary Figure S3c). The dynamic changes induced by the reduction in anthropogenic emissions have produced an anomalous cyclonic circulation over the Bay of Bengal region. In a different context, Vinoj and Swain (2020), observed enhancement of the atmospheric circulation related to a cyclone during the COVID-19 lockdown's low emission phase. Our model simulations show that significant surface heating as a response to emission reduction resulted in an anomalous low-pressure zone over the Indian region with two high-pressure zones to India's east and west sides (Supplementary Figure S3c). Such blocking high patterns control the surface level moisture transport (Fadnavis et al., 2021). Moderately strong wind flow from the oceanic regions (the Bay of Bengal and Northern Arabian Sea regions) towards the Indian mainland (Figure 4D; Supplementary Figure S3C) enhances moisture/specific humidity and clouds over the IGP and North West regions of India (Figures 4E,F) eventually conducive for rainfall enhancement.

3.4 Observed and simulated changes in rainfall

According to the India Meteorological Department (IMD), India had 158.5 mm of rainfall during the pre-monsoon 2020 season, which was 20% more than the long-term average (1961–2010). In observed datasets e.g., Global Precipitation Climatology Project (GPCP) (Figure 5A) and IMD, positive rainfall anomalies can be noted (Figure 5B). Both the GPCP and IMD datasets agree rather well with the simulated rainfall anomaly (C19 minus CTRL).

Both observation and simulated rainfall, anomalies show a north-east enhancement and south-west reduction, forming a dipolar rainfall pattern. It is also worth noting that the rise in rainfall in all datasets corresponds to places with significant decreases in anthropogenic pollution (Timmermann et al., 2020; Lee et al., 2021; Kripalani et al., 2022; Yang et al., 2022). The ERA5 reanalysis results also show a comparable spatial increase in rainfall (Figure S4), justifying the model results. All data sets and model simulations show an increase in rainfall by 0.04–2 mm/day (5%–25%) over the eastern IGP and nearby regions.

4 Possible mechanism behind enhanced rainfall

Precipitation can be influenced by both scattering and absorbing aerosols through microphysical and dynamical processes A simple schematic is shown in Figure 6 to highlight the links between the emission reduction due to the COVID-19 lockdown and the observed increase in cloud and precipitation. Over a wide region within South Asia, there was a more than 40% drop in atmospheric aerosol loading (AOD) during the lockdown period, April-May 2020 (Figure 1), compared to its long-term mean (2016–2019). A recent modelling study for the conditions in China shows that the reduction in aerosols had a stronger impact on precipitation than the decrease of greenhouse gases during the COVID-19 lockdown (Yang et al., 2022).

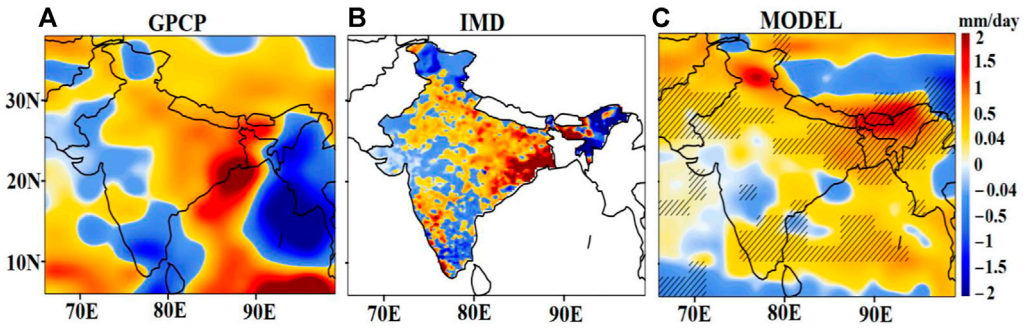

FIGURE 5
(A) Spatial distribution of anomalies in rainfall (2020—mean of 2016–2019) averaged for the lockdown period from **(A)** Global Precipitation Climatology Project (GPCP), **(B)** India Meteorological Department (IMD), and **(C)** ECHAM6-HAMMOZ simulations averaged over 10 members (C19 - CTRL). The hatching shows the area where mean differences between C19 and CTRL are statistically significant at a 90% confidence level.

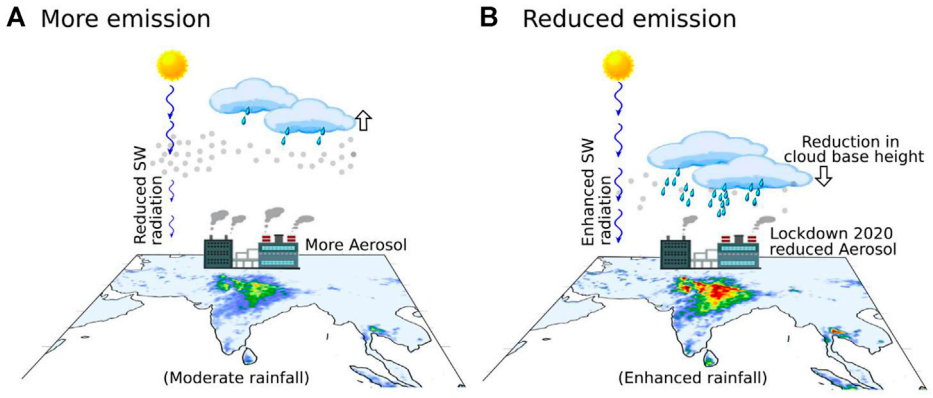

FIGURE 6
Schematic of the possible mechanism behind the COVID-19 pollution reduction and observed changes in cloud and precipitation over South Asia. **(A)** shows a normal emission condition and **(B)** explains the reduced emission (COVID-19) condition.

The cloud base height dropped by more than 500 m over the IGP and neighbouring regions, and low cloud cover increased significantly (C19—CTRL) (Figures 2A,B). Over the regions of cloud cover enhancement, there was warming effect caused by longwave cloud radiative forcing. However, there is cooling effect due to short wave radiative forcing which is due to cloud enhancement (Figures 2E,F). Furthermore, positive moisture feedback from the Bay of Bengal, Northern Arabian Sea to the Indian peninsula, combined with a reduction in cloud invigoration, favours low clouds with larger cloud droplets (Figure 4). Such situations are conducive to the enhancement of rainfall activity (Figure 5). The enhanced pre-monsoon rainfall during lockdown may further increase the latent heat release (not shown) and help in trapping more moisture in the lower atmosphere, allowing for more low clouds to develop (Timmermann et al., 2020; Yang et al., 2022), and resulting in increased precipitation. Thus, observed rainfall enhancement over India during the lockdown period may be due to the combined effect of the following:

(1) Anthropogenic forcing (emission reduction during the COVID-19) imposed changes in cloud parameters, atmospheric dynamics, and thermodynamical feedback.
(2) As a response to the emission reductions, favourable conditions for cloud augmentation (Khatri et al., 2021) and a decrease in the aerosol invigoration effect have emerged.
(3) The reduction in COVID-19 emissions altered atmospheric circulation, enhancing the low-pressure band over the Bay of Bengal and blocking high patterns on India's west and east

sides. It played a crucial role in amplifying the northward transport of moisture.

(4) All these lead to enhanced convective activity that increased rainfall over India by 0.04–2 mm day^{-1} (5%–25%) during the lockdown period.

5 Summary and conclusion

COVID-19 lockdown has been shown to improve air quality over the planet and alter the climate system in various ways that are still uncertain. The lockdown also provides a good opportunity to revisit a less polluted atmosphere to determine how human activity influences the environment and climate. It is interesting to note that due to the sudden emergence of the COVID-19 pandemic in early 2020, emissions were reduced notably causing an immediate and abrupt change in various components of the climate and earth system. Such sudden changes in emission could be significantly different from gradual policy-driven emission changes (Yang et al., 2022). It is important to mention that aerosol induced changes to the climate system are significantly different from GHG induced changes as the former possesses strong non-uniformity and non-linearity (Deng et al., 2020). This points to the fact that even small aerosol reductions (40%) during the pandemic could potentially impact and create a dramatic change in the earth system.

Quantifying the regional climate response in terms of cloud and precipitation changes in connection with emission/aerosol changes has always been challenging (Xie et al., 2020). Also, these are important processes to consider in weather and climate predictions. In this study, using the ECHAM6-HAMMOZ state-of-the-art aerosol-chemistry-climate model, we have investigated the possible reasons behind the observed enhancement in rainfall witnessed during the lockdown period over the Indian regions. The mean rainfall enhancement was found to be 5%–25% (0.04–2 mm/day) and is consistent in both observations and the C19 model simulation. We propose two supporting paths for the observed rainfall changes during the pre-monsoon of 2020. During the lockdown period, an increase in surface warming of 1°C was seen over broad swaths of the Indian landmass due to roughly 40% reductions in aerosol over the South Asian regions. Dust enhancement and reduction of anthropogenic aerosols resulted in increased heat across North India, the Himalayan foothills, and the TP areas. This might have led to the EHP amplification that is conducive to enhanced precipitation. Furthermore, the COVID-19 emission reduction induced a cyclonic circulation over the Bay of Bengal, resulting in increased moisture convergence to the Indian mainland, contributing to the observed rainfall enhancement. Besides this, lockdown-induced changes can be seen in cloud parameters and are discernible in the model simulations and ERA5 reanalysis. The cloud invigoration caused by aerosols may have been hampered due to the reduction in aerosols. As a result, we saw an increase in cloud cover (Yang et al., 2022), cloud effective radius and a cloud base height reduction, which could have translated to an increase in cloud water content and droplet size (Chakraborty and Maitra, 2013; Timmermann et al., 2020). Such circumstances may aid in increasing the likelihood of precipitation (Timmermann et al., 2020; Lee et al., 2021; Yang et al., 2022).

Aside from natural and anthropogenic aerosols, natural oscillations (El Nino, PDO, IOD, etc.) and remote drivers (e.g., Arctic Sea ice melting, Chatterjee et al., 2021) may potentially play an important and complex role in modulating cloud and rainfall over India. It's worth noting that the link between air pollution/emission forcing anomalies and cloud responses isn't limited to the forcing regions. A generalization of our results is limited due to the use of a single model and our results are specific to the regional emission perturbations. As society evolves and adopts policy measures gradually, regional and temporary emission reduction may continue to occur in the future. In this context, our study lends opportunities to enhance scientific understanding of how extreme weather and climate may respond to short-term emission perturbations like those that took place during the COVID-19 pandemic. Nonetheless, we can re-confirm the importance of anthropogenic pollution reduction for enhanced water availability across the Indian subcontinent and comprehend the robustness of its climatic implications. This will aid in understanding the necessity of improved emission management policies for a brighter future.

Data availability statement

The raw data supporting the conclusions of this article will be made available by the authors, without undue reservation.

Author contributions

This manuscript is the combined effort of all the co-authors. AA, SF, and RM formulated the manuscript. SF performed the model simulations. PC and TS analyzed the data. All co-authors contributed to writing the manuscript.

Acknowledgments

AA is thankful to the Department of Science and Technology Government of India for providing INSPIRE fellowship for doctoral research. The authors thank the staff of the High-Power Computing Centre (HPC) in IITM, Pune, India, for providing computer resources and the team members of MODIS, MERRA, and ERA5 for providing data.

Conflict of interest

The authors declare that the research was conducted in the absence of any commercial or financial relationships that could be construed as a potential conflict of interest.

Publisher's note

All claims expressed in this article are solely those of the authors and do not necessarily represent those of their affiliated organizations, or those of the publisher, the editors and the reviewers. Any product that may be evaluated in this article, or claim that may be made by its manufacturer, is not guaranteed or endorsed by the publisher.

Supplementary material

The Supplementary Material for this article can be found online at: https://www.frontiersin.org/articles/10.3389/fenvs.2022.911363/full#supplementary-material

References

Albrecht, B. A. (1989). Aerosols, cloud microphysics, and fractional cloudiness. *Science* 245 (4923), 1227–1230.

Balakrishnan, K., Dey, S., Gupta, T., Dhaliwal, R. S., Brauer, M., Cohen, A. J., et al. (2019). The impact of air pollution on deaths, disease burden, and life expectancy across the states of India: The global burden of disease study 2017. *Lancet Planet. heal.* 3. e26–e39. doi:10.1016/S2542-5196(18)30261-4/ATTACHMENT/EFB4D915-C39A-480A-A176-C311C2B3F1F3/MMC1

Bao, R., and Zhang, A. (2020). Does lockdown reduce air pollution? Evidence from 44 cities in northern China. *Sci. Total Environ.* 731. 139052, ttps://doi.org/doi:10.1016/J.SCITOTENV.2020.139052

Bauwens, M., Compernolle, S., Stavrakou, T., Müller, J. F., van Gent, J., Eskes, H., et al. (2020). Impact of coronavirus outbreak on NO2 pollution assessed using TROPOMI and OMI observations. *Geophys. Res. Lett.* 47, e2020GL087978. doi:10.1029/2020GL087978

Bollasina, M. A., Ming, Y., Ramaswamy, V., Schwarzkopf, M. D., and Naik, V. (2014). Contribution of local and remote anthropogenic aerosols to the twentieth century weakening of the South Asian Monsoon. *Geophys. Res. Lett.* 41, 680–687. doi:10.1002/2013GL058183

Buchard, V., Da Silva, A. M., Colarco, P., Krotkov, N., Dickerson, R. R., Stehr, J. W., et al. (2014). Evaluation of GEOS-5 sulfur dioxide simulations during the Frostburg, MD 2010 field campaign. *Atmos. Chem. Phys.* 14, 1929–1941. doi:10.5194/acp-14-1929-2014

Chakraborty, S., and Maitra, A. (2013). Interrelation between microphysical and optical properties of cloud and rainfall in the Indian region. *IJRSP* 42 (42), 105–112.

Chansaengkrachang, K., Luadsong, A., and Aschariyaphotha, N. (2018). Vertically integrated moisture flux convergence over southeast Asia and its relation to rainfall over Thailand. *Pertanika J. Sci. Technol.* 26, 235–246.

Chatterjee, S., Ravichandran, M., Murukesh, N., Raj, R. P., and Johannessen, O. M. (2021). A possible relation between Arctic sea ice and late season Indian Summer Monsoon Rainfall extremes. *npj Clim. Atmos. Sci.* 4, 36–6. doi:10.1038/s41612-021-00191-w

Chowdhury, S., Dey, S., and Smith, K. R. (2018). Ambient PM2.5 exposure and expected premature mortality to 2100 in India under climate change scenarios. *Nat. Commun.* 9, 318. doi:10.1038/s41467-017-02755-y

Dash, S. K., Shekhar, M. S., and Singh, G. P. (2006). Simulation of Indian summer monsoon circulation and rainfall using RegCM3. *Theor. Appl. Climatol.* 86, 161–172. doi:10.1007/s00704-006-0204-1

Deng, J., Dai, A., and Xu, H. (2020). Nonlinear climate responses to increasing CO2 and anthropogenic aerosols simulated by CESM1. *J. Clim.* 33, 281–301. doi:10.1175/JCLI-D-19-0195.1

Dumka, U. C., Kaskaoutis, D. G., Verma, S., Ningombam, S. S., Kumar, S., and Ghosh, S. (2021). Silver linings in the dark clouds of COVID-19: Improvement of air quality over India and Delhi metropolitan area from measurements and WRF-CHIMERE model simulations. *Atmos. Pollut. Res.* 12, 225–242. doi:10.1016/J.APR.2020.11.005

Fadnavis, S., Müller, R., Kalita, G., Rowlinson, M., Rap, A., Li, J.-L. F., et al. (2019). The impact of recent changes in Asian anthropogenic emissions of SO₂ on sulfate loading in the upper troposphere and lower stratosphere and the associated radiative changes. *Atmos. Chem. Phys.* 19, 9989–10008. doi:10.5194/acp-19-9989-2019

Fadnavis, S., Roy, C., Chattopadhyay, R., Sioris, C. E., Rap, A., Müller, R., et al. (2018). Transport of trace gases via eddy shedding from the Asian summer monsoon anticyclone and associated impacts on ozone heating rates. *Atmos. Chem. Phys.* 18, 11493–11506. doi:10.5194/ACP-18-11493-2018

Fadnavis, S., Sabin, T. P., Rap, A., Müller, R., Kubin, A., and Heinold, B. (2021). The impact of COVID-19 lockdown measures on the Indian summer monsoon. *Environ. Res. Lett.* 16, 074054. doi:10.1088/1748-9326/AC109C

Fadnavis, S., Semeniuk, K., Pozzoli, L., Schultz, M. G., Ghude, S. D., Das, S., et al. (2013). Transport of aerosols into the UTLS and their impact on the Asian monsoon region as seen in a global model simulation. *Atmos. Chem. Phys.* 13, 8771–8786. doi:10.5194/acp-13-8771-2013

Fasullo, J., and Webster, P. J. (2003)., A hydrological definition of Indian Monsoon onset and withdrawal. *J. Clim.* 16. 3200–3211. doi:10.1175/1520-0442(2003)016<3200a:AHDOIM>2.0

Forster, P. M., Forster, H. I., Evans, M. J., Gidden, M. J., Jones, C. D., Keller, C. A., et al. (2020). Current and future global climate impacts resulting from COVID-19. *Nat. Clim. Chang.* 10, 913–919. doi:10.1038/s41558-020-0883-0

Gautam, S. (2020). The influence of COVID-19 on air quality in India: A boon or inutile. *Bull. Environ. Contam. Toxicol.* 104, 724–726. doi:10.1007/S00128-020-02877-Y

Gelaro, R., McCarty, W., Suárez, M. J., Todling, R., Molod, A., Takacs, L., et al. (2017). The modern-era retrospective analysis for research and applications, version 2 (MERRA-2). *J. Clim.* 30, 5419–5454. doi:10.1175/JCLI-D-16-0758.1

Ghude, S. D., Chate, D. M., Jena, C., Beig, G., Kumar, R., Barth, M. C., et al. (2016). Premature mortality in India due to PM2.5 and ozone exposure. *Geophys. Res. Lett.* 43, 4650–4658. doi:10.1002/2016GL068949

Gu, Y., Wong, T. W., Law, C. K., Dong, G. H., Ho, K. F., Yang, Y., et al. (2018). Impacts of sectoral emissions in China and the implications: Air quality, public health, crop production, and economic costs. *Environ. Res. Lett.* 13, 084008. doi:10.1088/1748-9326/AAD138

Hansen, J., Sato, M., and Ruedy, R. (1997). Radiative forcing and climate response. *J. Geophys. Res.* 102, 6831–6864. doi:10.1029/96JD03436

Hersbach, H., Bell, B., Berrisford, P., Hirahara, S., Horányi, A., Muñoz-Sabater, J., et al. (2020). The ERA5 global reanalysis. *Q. J. R. Meteorol. Soc.* 146, 1999–2049. doi:10.1002/QJ.3803

Isaifan, R. J. (2020). The dramatic impact of coronavirus outbreak on air quality: Has it saved as much as it has killed so far? *Glob. J. Environ. Sci. Manag.* 6, 275–288. doi:10.22034/GJESM.2020.03.01

Jayaraman, A. (2001). Aerosol radiation cloud interactions over the tropical Indian Ocean prior to the onset of the summer monsoon. *Curr. Sci.* 81, 1437–1445. https://www.jstor.org/stable/24106568.

Khatri, P., Hayasaka, T., Holben, B., Tripathi, S. N., Misra, P., Patra, P. K., et al. (2021). Aerosol loading and radiation budget perturbations in densely populated and highly polluted Indo-Gangetic Plain by COVID-19: Influences on cloud properties and air temperature. *Geophys. Res. Lett.* 48, e2021GL093796–9. doi:10.1029/2021GL093796

Khatri, P., and Hayasaka, T. (2021). Impacts of Covid-19 on air quality over China: Links with meteorological factors and energy consumption. *Aerosol Air Qual. Res.* 21, 200668. doi:10.4209/AAQR.200668

Kripalani, R., Ha, K. J., Ho, C. H., Oh, J. H., Preethi, B., Mujumdar, M., et al. (2022). Erratic asian summer monsoon 2020: COVID-19 lockdown initiatives possible cause for these episodes? *Clim. Dyn.*, 1–14. doi:10.1007/s00382-021-06042-x

Lau, K. M., Kim, M. K., and Kim, K. M. (2006). Asian summer monsoon anomalies induced by aerosol direct forcing: The role of the Tibetan Plateau. *Clim. Dyn.* 26, 855–864. doi:10.1007/s00382-006-0114-z

Lau, K. M., Ramanathan, V., Wu, G. X., Li, Z., Tsay, S. C., Hsu, C., et al. (2008). The joint aerosol–monsoon experiment: A new challenge for monsoon climate research. *Bull. Am. Meteorol. Soc.* 89, 369–384. doi:10.1175/BAMS-89-3-369

Lau, W. K. M. (2016). The aerosol-monsoon climate system of Asia: A new paradigm. *J. Meteorol. Res.* 30, 1–11. doi:10.1007/s13351-015-5999-1

Le Quéré, C., Jackson, R. B., Jones, M. W., Smith, A. J. P., Abernethy, S., Andrew, R. M., et al. (2020). Temporary reduction in daily global CO2 emissions during the COVID-19 forced confinement. *Nat. Clim. Chang.* 107 (10), 647–653. doi:10.1038/s41558-020-0797-x

Lee, S. S., Chu, J. E., Timmermann, A., Chung, E. S., Lee, J. Y., et al. (2021). East Asian climate response to COVID-19 lockdown measures in China. *Sci. Rep.* 11, 16852. doi:10.1038/s41598-021-96007-1

Levy, R. C., Remer, L. A., Kleidman, R. G., Mattoo, S., Ichoku, C., Kahn, R., et al. (2010). Global evaluation of the Collection 5 MODIS dark-target aerosol products over land. *Atmos. Chem. Phys.* 10, 10399–10420. doi:10.5194/acp-10-10399-2010

Li, Z., Lau, W. K.-M., Ramanathan, V., Wu, G., Ding, Y., Manoj, M. G., et al. (2016). Aerosol and monsoon climate interactions over Asia. *Rev. Geophys.* 54, 866–929. doi:10.1002/2015RG000500

Lin, L., Xu, Y., Wang, Z., Diao, C., Dong, W., and Xie, S. P. (2018). Changes in extreme rainfall over India and China attributed to regional aerosol-cloud interaction during the late 20th century rapid industrialization. *Geophys. Res. Lett.* 45, 7857–7865. doi:10.1029/2018GL078308

Liu, F., Wang, M., and Zheng, M. (2021). Effects of COVID-19 lockdown on global air quality and health. *Sci. Total Environ.* 755, 142533. doi:10.1016/j.scitotenv.2020.142533

Lou, B., Barbieri, D. M., Passavanti, M., Hui, C., Gupta, A., Hoff, I., et al. (2022). Air pollution perception in ten countries during the COVID-19 pandemic. *Ambio* 51, 531–545. doi:10.1007/s13280-021-01574-2

Mahato, S., Pal, S., and Ghosh, K. G. (2020). Effect of lockdown amid COVID-19 pandemic on air quality of the megacity Delhi, India. *Sci. Total Environ.* 730, 139086. doi:10.1016/j.scitotenv.2020.139086

Manchanda, C., Kumar, M., Singh, V., Faisal, M., Hazarika, N., Shukla, A., et al. (2021). Variation in chemical composition and sources of PM2.5 during the COVID-19 lockdown in Delhi. *Environ. Int.* 153, 106541. doi:10.1016/j.envint.2021.106541

Manisalidis, I., Stavropoulou, E., Stavropoulos, A., and Bezirtzoglou, E. (2020). Environmental and health impacts of air pollution: A review. *Front. Public Health* 8, 14–13. doi:10.3389/fpubh.2020.00014

Menut, L., Bessagnet, B., Siour, G., Mailler, S., Pennel, R., and Cholakian, A. (2020). Impact of lockdown measures to combat Covid-19 on air quality over Western Europe. *Sci. Total Environ.* 741, 140426. doi:10.1016/j.scitotenv.2020.140426

Muhammad, S., Long, X., and Salman, M. (2020). COVID-19 pandemic and environmental pollution: A blessing in disguise? *Sci. Total Environ.* 728, 138820. doi:10.1016/j.scitotenv.2020.138820

Myhre, G., Forster, P. M., Samset, B. H., Hodnebrog, Ø., Sillmann, J., Aalbergsj, S. G., et al. (2017). Pdrmip: A precipitation driver and response model intercomparison project-protocol and preliminary results. *Bull. Am. Meteorol. Soc.* 98, 1185–1198. doi:10.1175/BAMS-D-16-0019.1

Namdari, S., Karimi, N., Sorooshian, A., Mohammadi, G. H., and Sehatkashani, S. (2018). Impacts of climate and synoptic fluctuations on dust storm activity over the Middle East. *Atmos. Environ. X.* 173, 265–276. doi:10.1016/j.atmosenv.2017.11.016

Navinya, C., Patidar, G., and Phuleria, H. C. (2020). Examining effects of the COVID-19 national lockdown on ambient air quality across urban India. *Aerosol Air Qual. Res.* 20, 1759–1771. doi:10.4209/AAQR.2020.05.0256

Pandey, S. K., Vinoj, V., and Panwar, A. (2020). The short-term variability of aerosols and their impact on cloud properties and radiative effect over the Indo-Gangetic Plain. *Atmos. Pollut. Res.* 11, 630–638. doi:10.1016/j.apr.2019.12.017

Pandey, S. K., and Vinoj, V. (2021). Surprising changes in aerosol loading over India amid Covid-19 lockdown. *Aerosol Air Qual. Res.* 21, 200466–200512. doi:10.4209/AAQR.2020.07.0466

Ramanathan, V., Chung, C., Kim, D., Bettge, T., Buja, L., Kiehl, J. T., et al. (2005). Atmospheric Brown clouds: Impacts on South Asian climate and hydrological cycle. *Proc. Natl. Acad. Sci. U. S. A.* 102, 5326–5333. doi:10.1073/pnas.0500656102

Rosenfeld, D., Andreae, M. O., Asmi, A., Chin, M., Leeuw, G., Donovan, D. P., et al. (2014). Global observations of aerosol-cloud-precipitationclimate interactions. *Rev. Geophys.* 52, 750–808. doi:10.1002/2013RG000441

Samset, B. H., Myhre, G., Forster, P. M., Hodnebrog, Ø., Andrews, T., Faluvegi, G., et al. (2016). Fast and slow precipitation responses to individual climate forcers: A pdrmip multimodel study. *Geophys. Res. Lett.* 43, 2782–2791. doi:10.1002/2016GL068064

Sanap, S. D. (2021). Global and regional variations in aerosol loading during COVID-19 imposed lockdown. *Atmos. Environ. X.* 246, 118132. doi:10.1016/j.atmosenv.2020.118132

Schultz, M. G., Stadtler, S., Schröder, S., Taraborrelli, D., Franco, B., Krefting, J., et al. (2018). The chemistry–climate model ECHAM6.3-HAM2.3-MOZ1.0. *Geosci. Model Dev.* 11, 1695–1723. doi:10.5194/gmd-11-1695-2018

Srinivas, C. V., Hariprasad, D., Bhaskar Rao, D. V., Anjaneyulu, Y., Baskaran, R., and Venkatraman, B. (2013). Simulation of the Indian summer monsoon regional climate using advanced research WRF model. *Int. J. Climatol.* 33, 1195–1210. doi:10.1002/joc.3505

Stevens, B., Giorgetta, M., Esch, M., Mauritsen, T., Crueger, T., Rast, S., et al. (2013). Atmospheric component of the MPI-M earth system model: ECHAM6. *J. Adv. Model. Earth Syst.* 5, 146–172. doi:10.1002/JAME.20015

Stier, P., Feichter, J., Kinne, S., Kloster, S., Vignati, E., Wilson, J., et al. (2005). The aerosol-climate model ECHAM5-HAM. *Atmos. Chem. Phys.* 5, 1125–1156. doi:10.5194/acp-5-1125-2005

Stocker, T. F., Qin, D., Plattner, G. K., Tignor, M. M. B., Allen, S. K., Boschung, J., et al. (2013). *Climate change 2013 the physical science basis: Working group I contribution to the fifth assessment report of the intergovernmental panel on climate change*. Cambridge University Press. doi:10.1017/CBO9781107415324

Tegen, I., Harrison, S. P., Kohfeld, K., Prentice, I. C., Coe, M., and Heimann, M. (2002). Impact of vegetation and preferential source areas on global dust aerosol: Results from a model study. *J. Geophys. Res.* 107 (D21), AAC-14. doi:10.1029/2001JD000963

Tegen, I., Neubauer, D., Ferrachat, S., Drian, C. S., Bey, I., Schutgens, N., et al. (2019). The global aerosol-climate model echam6.3-ham2.3—Part 1: Aerosol evaluation. *Geosci. Model Dev.* 12, 1643–1677. doi:10.5194/gmd-12-1643-2019

Thomas, A., Kanawade, V. P., Sarangi, C., and Srivastava, A. K. (2021). Effect of COVID-19 shutdown on aerosol direct radiative forcing over the Indo-Gangetic Plain outflow region of the Bay of Bengal. *Sci. Total Environ.* 782, 146918. doi:10.1016/j.scitotenv.2021.146918

Timmermann, A., Lee, S.-S., Chu, J.-E., Chung, E.-S., and Lee, J.-Y. (2020). COVID-19-related drop in anthropogenic aerosol emissions in China and corresponding cloud and climate effects. doi:10.31223/osf.io/z5dm8

Twomey, S. (1977). Pollution on the shortwave albedo of clouds. *J. Atmos. Sci.* 34, 1149–1152.

Vinoj, V., Rasch, P. J., Wang, H., Yoon, J. H., Ma, P. L., Landu, K., et al. (2014). Short-term modulation of Indian summer monsoon rainfall by West Asian dust. *Nat. Geosci.* 7, 308–313. doi:10.1038/ngeo2107

Vinoj, V., and Swain, D. (2020). Did COVID-19 lockdown brew "amphan" into a super cyclone? doi:10.20944/PREPRINTS202007.0033.V1

Wang, Z., Lin, L., Yang, M., Xu, Y., and Li, J. (2017). Disentangling fast and slow responses of the East Asian summer monsoon to reflecting and absorbing aerosol forcings. *Atmos. Chem. Phys.* 17, 11075–11088. doi:10.5194/acp-17-11075-2017

Wing, A. A., Emanuel, K., Holloway, C. E. , and Muller, C. (2018). Convective self-aggregation in numerical simulations: A review. *Shallow clouds, water vapor, circulation, and climate sensitivity*, 1–15.

Xie, X., Myhre, G., Liu, X., Li, X., Shi, Z., Wang, H., et al. (2020). Distinct responses of Asian summer monsoon to black carbon aerosols and greenhouse gases. *Atmos. Chem. Phys.* 20, 11823–11839. doi:10.5194/acp-20-11823-2020

Yang, Y., Ren, L., Wu, M., Wang, H., Song, F., Leung, L. R., et al. (2022). Abrupt emissions reductions during COVID-19 contributed to record summer rainfall in China. *Nat. Commun.* 13, 959. doi:10.1038/s41467-022-28537-9

Zhang, K., O'Donnell, D., Kazil, J., Stier, P., Kinne, S., Lohmann, U., et al. (2012). The global aerosol-climate model ECHAM-HAM, version 2: Sensitivity to improvements in process representations. *Atmos. Chem. Phys.* 12, 8911–8949. doi:10.5194/acp-12-8911-2012

Zhang, M., Katiyar, A., Zhu, S., Shen, J., Xia, M., Ma, J., et al. (2021). Impact of reduced anthropogenic emissions during COVID-19 on air quality in India. *Atmos. Chem. Phys.* 21, 4025–4037. doi:10.5194/acp-21-4025-2021

Zhao, C., Qiu, Y., Dong, X., Wang, Z., Peng, Y., Li, B., et al. (2018). Negative aerosol-cloud re relationship from aircraft observations over Hebei, China. *Earth and Space Science* 5 (1), 19–29.

Appendix A: Calculation of moisture flux convergence

The moisture conservation equation in flux form of vertical integration suggested by Trenberth et al. (2011). Vertical integrated Moisture flux/Transport (VMIT) and its convergence (moisture flux convergence, MFC) are important proxies to understand the source and sink of moisture and hence the precipitation (Chansaengkrachang et al., 2018). Especially, the moisture flux convergence (MFC) has been considered to directly characterize the behaviour of extreme precipitation.

The wind vector, V, is defined by V = (u, v), where u and v are the east-west and north- south components of wind. The vertically integrated moisture transport (VIMT) improved from Fasullo and Webster, 2003 from Fasullo and Webster (2003) is calculated as follows

$$VMIT = \int_{300}^{ps} Vdp/g \tag{A1}$$

and the vertically integrated moisture fluxes of u and v components are calculated as $\int_{300}^{ps} udp/g$ and $\int_{300}^{ps} vdp/g$ respectively. Where g is the acceleration due to gravity and ps is the surface atmospheric pressure in hPa.

Specific humidity is very small above the 300 hPa level and is not an effect to vertically integrated moisture transport (Fasullo & Webster, 2003).

Finally, Finally, the moisture flux divergence (convergence) is calculated by calculating the divergence of VMIT as follows

$$\mathrm{MFC} = \nabla.VMIT \tag{A2}$$

$$MFC = \frac{1}{g}\nabla.\int_{300}^{ps} Vdp \tag{A3}$$

Advantages of publishing in Frontiers

OPEN ACCESS
Articles are free to read for greatest visibility and readership

FAST PUBLICATION
Around 90 days from submission to decision

HIGH QUALITY PEER-REVIEW
Rigorous, collaborative, and constructive peer-review

TRANSPARENT PEER-REVIEW
Editors and reviewers acknowledged by name on published articles

Frontiers
Avenue du Tribunal-Fédéral 34
1005 Lausanne | Switzerland

Visit us: www.frontiersin.org
Contact us: frontiersin.org/about/contact

REPRODUCIBILITY OF RESEARCH
Support open data and methods to enhance research reproducibility

DIGITAL PUBLISHING
Articles designed for optimal readership across devices

FOLLOW US
@frontiersin

IMPACT METRICS
Advanced article metrics track visibility across digital media

EXTENSIVE PROMOTION
Marketing and promotion of impactful research

LOOP RESEARCH NETWORK
Our network increases your article's readership